



University
of Glasgow

Pino, Monica (2010) *Apatite deposition on NaOH-treated HDPE, PEEK and UHMWPE films for sclera materials in artificial cornea implants*. PhD thesis.

<http://theses.gla.ac.uk/1896/>

Copyright and moral rights for this thesis are retained by the author

A copy can be downloaded for personal non-commercial research or study, without prior permission or charge

This thesis cannot be reproduced or quoted extensively from without first obtaining permission in writing from the Author

The content must not be changed in any way or sold commercially in any format or medium without the formal permission of the Author

When referring to this work, full bibliographic details including the author, title, awarding institution and date of the thesis must be given.

**Apatite Deposition on NaOH-treated HDPE, PEEK and
UHMWPE films for Sclera Materials in Artificial
Cornea Implants**

Monica Pino

A thesis for the degree of Doctor of Philosophy (PhD)

Submitted to the Faculty of Engineering,
University of Glasgow

February 2010

ABSTRACT

Corneal disease is the second most common cause of blindness in the world. It is estimated that 45 million people worldwide are bilaterally blind and 10 million are affected by corneal blindness. Corneal blindness mostly affects the population in the equatorial zone, due to the high exposure to UV light. Corneal grafting presents complications such as rejections and the lack of donor material and resources. Conventional cornea grafting (keratoplasty) is not advised for patients with bilateral corneal blindness or for those who suffer from a range of clinical problems including tear deficiency, chemical burns and uncontrollable intraocular pressure. At present, an artificial cornea, i.e. a keratoprosthesis (KRPO), is the only alternative to keratoplasty (corneal donor transplantation).

Cornea implants consist of a clear optic part and a surrounding ring known as the skirt, which needs to integrate with the sclera of the eye. Currently used skirt materials lead to poor tissue integration, a major failure of cornea implants. Better integration may be achieved when using a bioactive skirt material, which adapts to the metabolic activity of the cornea. For this purpose, high density polyethylene (HDPE), polyether ether ketone (PEEK) and ultra-high molecular weight polyethylene (UHMWPE) films provide interesting possible alternatives, if they can be rendered bioactive. This study investigated the potential of using surface modified polymer films to fabricate the skirt. To improve bioactivity of the materials a two-step treatment using chemical surface modification (immersion in NaOH) and formation of apatite layers from Simulated Body Fluid (SBF) was applied. The effectiveness of the different molarity of the NaOH on the formation of the bioactive layer was investigated. Results showed that with an increase in NaOH concentration the wettability improved but also some changes to the topography (increase/decrease of roughness) of the polymers were observed. Moreover, 10M NaOH treatments resulted in more rapid formation of the apatite layer when compared with a non-treated and lower molarity solution. As immersion time in SBF increased, further nucleation and growth produced a thicker apatite layer which can be expected to be highly bioactive. Interestingly, the apatite growth is dependent on both the concentration of NaOH solution and the structure of the polymer surface. It was concluded that hydroxyapatite layers were formed on HDPE, PEEK and UHMWPE films after they were incubated in 1.5 SBF, which promises to render such thin-film structures bioactive – a necessity if they are to be integrated into artificial cornea. The Ca/P molar ratio of the apatite deposited on the

polymers increases with NaOH strength and SBF incubation time. The favourable effect of NaOH on apatite formation may at least partly be attributed to an increased wettability of the polymer films after such treatment, as well as to the modified topography. The apatite layer contained phosphate and carbonates ions, providing potentially good *in vitro* bioactivity on polymeric films. The inorganic layers are chemically stable as the calcium deposited on the films did not dissolve fully when immersed in water for one week. This demonstrates that polymer films can be rendered bioactive, using the described approach, hence providing potential materials suitable for artificial cornea implants.

ABBREVIATIONS

AAS	Atomic Absorption Spectroscopy
AFM	Atomic Force Microscopy
B	Bright side of PEEK film
CA	Contact angle
Ca/P	Calcium/phosphorus molar ratio
CaHA	Calcium hydroxyapatite
CDHA	Calcium-deficient hydroxyapatite
CHA	Carbonate hydroxyapatite
DCPD	Di-calcium phosphate dihydrate
EDX	Energy dispersive X-ray spectroscopy
ePTFE	expanded Polytetrafluoroethylene
FACIT	Fibril Associated Collagens with Interrupted Triple Helices
FCI	France Chirurgie Industries
FTIR	Fourier transform infrared spectroscopy
HA	Hydroxyapatite
HDPE	High density polyethylene
KP	Penetrating keratoplasty
KPRO	Keratoprosthesis
LK	Lamellar keratoplasty
M	Matt side of PEEK film
MCPM	Mono-calcium phosphate monohydrate
NaOH	Sodium hydroxyl

OCP	Octa-calcium phosphate
OOKP	Osteo-odonto-keratoprosthesis
PDMS	Polydimethylsiloxane
PEEK	Polyether ether ketone
PET	Polyethylene terephthalate
PHEMA	Poly(2-hydroxyethyl methacrylate)
PMMA	Poly(methyl methacrylate)
PTFE	Polytetrafluoroethylene
PVP	Polyvinylpyrrolidone
R _a	Roughness (a) value
SAMs	self-assembled monolayers
SBF	Simulated Body Fluid
SD	Standard Deviation
SEM	Scanning electron microscopy
TCP	Tricalcium phosphate
UHMWPE	Ultra-high molecular weight polyethylene
WAXD	Wide-angle X-ray diffraction

CONTENTS

Abstract	2
Abbreviations	4
Contents	6
List of Tables	9
List of Figures	10
Acknowledgements	13
Publications	18
Journal Publications	18
Peer Reviewed Conference Abstracts	19
Chapter 1 Introduction	20
1.1 Ideal Artificial Cornea	22
1.2 Biocompatibility and Bioactivity	23
1.3 Aims and Objectives	25
1.4 Overview and Structure of this Thesis	26
Chapter 2 Literature Survey	27
2.1 Introduction	27
2.2 The Cornea	29
2.3 The Sclera	33
2.4 The Conjunctiva	35
2.5 The Tears and Aqueous Humour Fluids	37
2.6 Diseases and trauma of the cornea	38
2.7 Treatments of corneal damage	40
2.7.1 Keratoplasty (donor corneal implant)	42
2.7.2 Artificial endothelium	42
2.7.3 Epikerotoprosthesis (artificial epithelium)	43
2.8 Biomaterial	43
2.9 Materials used in artificial cornea implants	46
2.9.1 Polymers	48
2.9.2 Poly(methyl methacrylate) (PMMA)	50
2.9.3 Poly(2-hydroxyethyl methacrylate) (PHEMA)	51
2.9.4 Polytetrafluoroethylene (PTFE)	52

2.9.5	Polyethylene terephthalate (PET)	53
2.9.6	High density polyethylene (HDPE)	54
2.9.7	Ultra high molecular weight polyethylene (UHMWPE)	54
2.9.8	Polyether ether ketone (PEEK)	55
2.9.9	Apatites	57
2.9.10	Simulated body fluid (SBF)	62
2.10	Artificial Cornea Implants	67
2.10.1	Keratoprosthesis (KPRO)	67
2.10.2	Osteo-odonto-keratoprosthesis (OOKP)	76
2.11	Present complications of artificial cornea designs	80
Chapter 3 Materials and Methods		82
3.1	Introduction	82
3.2	Materials	84
3.2.1	High Density Polyethylene (HDPE)	84
3.2.2	Ultra High Molecular Weight Polyethylene (UHMWPE)	85
3.2.3	Polyether Ether Ketone (PEEK)	86
3.2.4	Sodium Hydroxide (NaOH)	87
3.2.5	Simulated Body Fluid (SBF)	88
3.3	Methods to produce the bioactive layers	91
3.3.1	Production of HDPE, UHMWPE and PEEK films	92
3.3.2	NaOH pre-treatments	94
3.3.3	1.5 SBF treatment	95
3.4	Characterisation techniques	96
3.4.1	Scanning Electron Microscopy (SEM) and Energy Dispersive X-ray Spectroscopy (EDX)	96
3.4.2	Laser Raman Spectroscopy	98
3.4.3	Fourier Transform Infrared Spectroscopy (FTIR)	99
3.4.4	Atomic Absorption Spectroscopy (AAS)	100
3.4.5	Atomic Force Microscopy (AFM)	102
3.4.6	Water Contact Angle (CA)	104
3.4.7	Reflected Light Differential Contrast Microscopy (DIC)	106
3.4.8	Thin Film X-Ray Diffraction (TF-XRD) and Wide-angle X-ray Diffraction (WAXD)	107
3.4.9	Scratch test	108
3.4.10	Statistical Analysis	110

Chapter 4	Results	111
4.1	Introduction	111
4.2	Water Contact Angle (CA)	112
4.3	Atomic Force Microscopy (AFM)	114
4.4	Scanning Electron Microscopy (SEM)	120
4.4.1	Initial screening of polymers with NaOH activation	120
4.4.2	Assessment of Activation of PEEK and UHMWPE with high NaOH concentration and protracted SBF incubation	125
4.5	Energy Dispersive X-Ray Spectroscopy (EDX)	129
4.5.1	Initial screening of polymers with NaOH activation	129
4.5.2	Assessment of Activation of PEEK and UHMWPE with high NaOH concentration and protracted SBF incubation	134
4.6	Laser Raman Spectroscopy	142
4.7	Fourier Transform Infrared Spectroscopy (FTIR)	145
4.8	Reflected Light Differential Contrast Microscopy (DIC)	148
4.9	Thin Film X-Ray Diffraction (TF-XRD) and Wide-angle X-ray Diffraction (WAXD)	153
4.10	Scratch test	160
4.11	Atomic Absorption Spectroscopy (AAS)	160
Chapter 5	Discussion	162
5.1.	Introduction	162
5.2	Effectiveness of NaOH pre-treatment	163
5.3	Influence of the Immersion Time in 1.5 SBF treatment	168
5.4	Apatite formation	170
5.5	Application for Skirt Materials in Cornea Implants	172
Chapter 6	Conclusions and Future Work	174
6.1	Conclusions	174
6.2	Future Work	176
	References	178

LIST OF TABLES

- 2.2.1 Cornea layers functions (data from Hodge, 1995; Hicks *et al.*, 1997; IPAC, 2004; Refojo, 2004; NEI 2006; NHS, 2006)
- 2.3.1 Composition of the sclera in percentage of wet weight (from Meek, 2008)
- 2.9.1 Calcium phosphate compounds that can be deposited from aqueous solutions (data from Dorozhkin, 2007; Dorozhkin 2009)
- 2.10.1 Keratoprosthesis used in human clinical trials (data from Cardona, 1962; Strampelli, 1963; Cardona, 1969; Dohlman and Doane, 1994; Legeais *et al.*, 1997; Legeais and Renard, 1998; Hicks *et al.*, 2000; Crawford *et al.*, 2002; Allan, 2002; Albon, 2003; Falcinelli *et al.*, 2005; Bleckmann and Holak, 2006; Hollick *et al.*, 2006; Viitala *et al.* 2009)
- 3.2.1 Physical properties of HDPE (data from Sabic – Europe Ltd. Belgium)
- 3.2.2 Physical properties of UHMWPE (data from Himont, USA)
- 3.2.3 Physical properties of PEEK (data from Invibio Ltd. Lancashire, UK)
- 3.2.4 Physical and chemical properties of NaOH
- 3.2.5 Reagent grade chemicals to prepare 1 litre of 1.5 SBF
- 3.2.6 Ion concentration of SBF and human blood plasma (from Kokubo *et al.*, 1990; Kokubo and Takadama, 2006)
- 3.3.1 Experimental procedure and characterisation tests for batch I and batch II
- 4.3.1 Roughness (Ra) in nanometres (nm) from the Atomic Force Microscope (AFM) using scan sizes of 25 x 25 or 5 x 5 microns (μm) of PEEK (bright and matt) non-treated samples and pre-treated samples with NaOH (B= bright, M= matt, S.D.= standard deviation)
- 4.3.2 Roughness (Ra) in nanometres (nm) from the Atomic Force Microscope (AFM) using scan sizes of 45 x 45, 25 x 25 or 5 x 5 microns (μm) of UHMWPE(UH) non-treated samples and pre-treated samples with 5M or 10M NaOH (S.D = Standard Deviation)
- 4.5.1 The average calcium (Ca) phosphorous (P) and Ca/P molar ratio from the EDX of PEEK and UHMWPE films pre-treated with 5M or 10M NaOH and immersed in 1.5 SBF for 3, 7, 15 and 30 days (S.D = standard deviation)
- 4.8.1 Percentage of area/image area from the reflected light Differential Contrast (DIC) microscope pictures of PEEK (bright and matt sides) and UHMWPE films pre-treated with 5M or 10M NaOH and incubated in 1.5 SBF treatments for 3, 7, 15 and 30 days (B= bright, M= matt, S.D.= standard deviation)
- 4.11.1 Total (Ca) present in the samples after the NaOH pre-treatments followed by 1.5 SBF for 30 days and the Ca released in water of PEEK and UHMWPE after pre-treated with 5M or 10M NaOH and 1.5 SBF for 30 days. (S.D = standard deviation)

LIST OF FIGURES

- 2.2.1 Structure of the eye (from Martini, 1995)
- 2.2.2 Structure of the cornea (from James *et al.*, 2003)
- 2.9.1 Part of polyethylene chain (from Ward *et al.*, 2005)
- 2.9.2 Polymethyl methacrylate (PMMA) (from Smith and Javad, 2006)
- 2.9.3 Poly(2-hydroxyethyl methacrylate) (PHEMA) (from Ratner, 2004)
- 2.9.4 Polytetrafluoroethylene (PTFE) (from Houde *et al.*, 2006)
- 2.9.5 Polyethylene terephthalate (PET) (from Fakirov, 2002)
- 2.9.6 High density polyethylene (HDPE) (from Ward *et al.*, 2005)
- 2.9.7 Polyether ether ketone (PEEK) (from Sakamoto, 2003)
- 2.10.1 Central optic-and-skirt keratoprosthesis (from Ilhan-Sarar, 2005)
- 2.10.2 Collar-button keratoprosthesis (from Dohlman and Harissi-Dagher, 2007)
- 2.10.3 The Legeais BioKpro III before implantation (from Hollick *et al.*, 2006)
- 2.10.4 AphaCor™ keratoprosthesis (from Chirila *et al.*; 1995)
- 2.10.5 Schematic representation of the OOKP design (from Tan *et al.*, 2005)
- 2.10.6 Dentil lamina used a skirt in the OOKP (from Liu *et al.*, 2007)
- 2.10.7 Schematic representation of cross section of a normal teeth (from Shah, 2009)
- 2.10.8 Schematic representation of the cross section of an OOKP (from Liu *et al.*, 2008)
- 3.3.1 Experimental coating procedure and tests
- 4.2.1 Averaged water contact angle and the Standard Deviation (error bar) of the non-treated films, PEEK (bright and matt sides) and UHMWPE, and 5M or 10M NaOH pre-treated samples, PEEK (bright and matt sides) and UHMWPE (B= bright, M= matt)
- 4.2.2 Pictures of the water contact angle of the non-treated films, PEEK (bright and matt) and UHMWPE and 5M or 10M NaOH pre-treated PEEK (bright and matt) and UHMWPE
- 4.3.1 Example of Atomic Force Microscope (AFM) line profiles of PEEK (matt) pre-treated with 5M NaOH using a scan size of 25 microns (μm). The profiles for two different lines are shown (red, green), with arrows indicating the analysis range.
- 4.3.2 3D topography from the Atomic Force Microscope (AFM) using scan sizes of 25 x 25 and 5 x 5 μm of the non-treated PEEK and UHMWPE films

- 4.3.3 3D topography from the Atomic Force Microscope (AFM) using scan sizes of 25 x 25 and 5 x 5 μm of the 5 or 10M NaOH pre-treated PEEK (bright and matt)
- 4.3.4 3D topography from the Atomic Force Microscope (AFM) using scan sizes of 45 x 45, 25 x 25 and 5 x 5 microns (μm) of the 5M or 10M NaOH pre-treated UHMWPE films
- 4.4.1 SEM micrographs of the PEEK films pre-treated with 1, 5 and 10M NaOH and soaked in 1.5 SBF for 1,3, 7 and 15 days. (Scale bars= 40 μm)
- 4.4.2 SEM micrographs of the HDPE films pre-treated with 1M NaOH and 1.5 SBF for 3 and 7 days (top); HDPE films in 5M NaOH and 1.5 SBF for 3 and 15 days (middle); and HDPE films in 10M NaOH and 1.5 SBF for 1 and 7days (bottom). (Scale bars=40 μm)
- 4.4.3 SEM micrographs of the UHMWPE films pre-treated with 1, 5, and 10M NaOH and soaked in 1.5 SBF for 1 day and 7 days. (Scale bars= 40 μm for 1M NaOH for at 1 day and 7 days, 5M NaOH at 7 days and 10M NaOH at 1 day. Scale bars= 3 mm for 5M NaOH at 1 day and 10M NaOH at 7 days)
- 4.4.4 Spectra of the shadowing technique under EDX of the cross section of the polymer film pre-treated with NaOH and soaked in 1.5 SBF for 18 days. Dark shadow represents the thickness of the apatite layer. (Scale bar= 20 μm)
- 4.4.5 SEM micrographs of the PEEK films (bright and matt) pre-treated with 5M NaOH and soaked in 1.5 SBF for up to 30 days. (Scale bars= 50 μm)
- 4.4.6 SEM micrographs of the PEEK films (bright and matt) pre-treated with 10M NaOH and soaked in 1.5 SBF for up to 30 days. (Scale bars= 20 μm for PEEK bright at 7 and 15 days and PEEK matt at 15 and 30 days. Scale bars= 50 μm for PEEK matt side at 3 and 7 days. Scale bars= 100 μm for PEEK bright side at 3 and 30 days)
- 4.4.7 SEM micrographs of the UHMWPE films pre-treated with 5 or 10M NaOH and soaked in 1.5 SBF for up to 30 days. (Scale bars= 50 μm)
- 4.5.1 EDX spectra of PEEK pre-treated with 1, 5, and 10M NaOH and soaked in 1.5 SBF for 3, 7 and 15 days
- 4.5.2 EDX spectra of HDPE pre-treated with 1M NaOH and soaked in 1.5 SBF for 3 and 7 days (top); HDPE with 5M NaOH and 1.5 SBF for 3 and 15 days (middle); and HDPE with 10M NaOH and 1.5 SBF for 1 and 7 days (bottom)
- 4.5.3 EDX spectra of UHMWPE pre-treated with 1, 5, and 10M NaOH and soaked in 1.5 SBF for 1 and 7 days
- 4.5.4 EDX spectra of the bright and matt sides of PEEK pre-treated with 5M NaOH and soaked in 1.5 SBF for 3, 7, 15 and 30 days
- 4.5.5 EDX spectra of the bright and matt sides of PEEK pre-treated with 10M NaOH and soaked in 1.5 SBF for 3, 7, 15 and 30 days
- 4.5.6 EDX spectra of UHMWPE pre-treated with 5M or 10M NaOH and soaked in 1.5 SBF for 3, 7, 15 and 30 days
- 4.5.7 Average calcium (Ca) and phosphorous (P) in atomic % deposited on PEEK (PK) and UHMWPE (UH) films pre-treated with 5M or 10 M NaOH and immersed in 1.5 SBF for 3, 7, 15 and 30 day, obtained from the EDX test (B= bright, M= matt)

- 4.5.8 Average Ca/P molar ratio of PEEK and UHMWPE films pre-treated with 5 or 10M NaOH and immersed in 1.5 SBF for 3, 7, 15 and 30 days, obtained from the EDX test (B= bright, M= matt) (bar error=standard deviation)
- 4.6.1 Raman spectra of non-treated HDPE (top) and HDPE pre-treated with 5M NaOH and soaked in 1.5 SBF for 18 days (bottom)
- 4.6.2 Raman spectra of non-treated UHMWPE (top) and UHMWPE pre-treated with 5M NaOH and soaked in SBF for 18 days (bottom)
- 4.6.3 Raman spectrum of the layer scraped from PEEK, HDPE and UHMWPE pre-treated with 5M NaOH then the immersed in SBF for 18 days
- 4.7.1 FTIR of non-treated HDPE and pre-treated HDPE with 5M NaOH and SBF for 18 days
- 4.7.2 FTIR of non-treated UHMWPE and pre-treated UHMWPE with 5M NaOH and SBF for 18 days
- 4.7.3 FTIR of non-treated PEEK and pre-treated PEEK with 5M NaOH and SBF for 18 days
- 4.8.1 Reflected light Differential Contrast (DIC) microscope images of PEEK (bright and matt sides) films pre-treated with 5M NaOH and incubated in 1.5 SBF treatments for 3, 7, 15 and 30 days
- 4.8.2 Reflected light Differential Contrast (DIC) microscope images of PEEK (bright and matt sides) films pre-treated with 10M NaOH and incubated in 1.5 SBF treatments for 3, 7, 15 and 30 days
- 4.8.3 Reflected light Differential Contrast (DIC) microscope images of UHMWPE films pre-treated with 5 or 10M NaOH and incubated in 1.5 SBF treatments for 3, 7, 15 and 30 days
- 4.9.1 WAXD patterns of non-treated PEEK and PEEK treated only with 1.5 SBF for 15 and 30 days
- 4.9.2 WAXD patterns of non-treated UHMWPE and UHMWPE treated only with 1.5 SBF for 15 and 30 days
- 4.9.3 WAXD patterns of non-treated PEEK and PEEK pre-treated with 5M or 10M NaOH followed by 1.5 SBF for 15 days
- 4.9.4 WAXD patters of non-treated PEEK and PEEK pre-treated with 5M or 10M NaOH followed by 1.5 SBF for 30 days
- 4.9.5 WAXD patterns of non-treated UHMWPE and UHMWPE pre-treated with 5M or 10M NaOH followed by 1.5 SBF for 15 days
- 4.9.6 WAXD patterns of non-treated UHMWPE and UHMWPE pre-treated with 5M or 10M NaOH followed by 1.5 SBF for 30 days
- 5.2.1 Water contact angle (CA, coloured bars) vs. R_a from the whole image (scan size = 25 x 25 μm) (grey bars) of PEEK and UHMWPE specimens. (B= bright, M= matt, error bar= standard deviation)
- 5.2.2 Water contact angle (CA, coloured bars) vs. Ca/P from EDX (grey bars) of PEEK and UHMWPE specimens. (B= bright, M= matt, error bar= standard deviation)

ACKNOWLEDGEMENTS

I would like to thank everyone involved scientifically and as friends during this journey. Those are things in life that you can not do on your own despite of my need for freedom and independence. I appreciate immensely your time, effort, and kindness. I am very happy to know more and more lovely and clever people around me.

I would like to thank Prof. Elizabeth Tanner for initiating this project at Queen Mary University of London, and for the great freedom she gave me to take my own decisions in the course of this research which has brought me to the University of Glasgow. It was lovely to live in beautiful Scotland for a change!

Immense thanks to Dr. Natalie Stingelin for teaching me how to do science systematically and consistently and how to write the story beautifully. Science, music and dance were amazing, and you were always available even when I moved into Glasgow!

Very special thanks to Dr. Wojciech Chrzanowski for being the best college I've had, always ready to help. I learnt great science from you and a lot for my professional and personal life. It was a pleasure to work with you and to get to know and appreciate your qualities – cleverness, kindness, sense of humour, caring, sporty and positive.

Thanks to Dr. Chris Pearce for encouraging me to finish my work and for listening to me and counselling me, and to Prof. Frank Coton for financial advice and great moral support. It was nice to have someone ready to help and listen any time. I would also like to thank Dr. Donald Balance for his advice and the financial support from the Department. It was great to count on you all the time.

This research wouldn't have been possible without advice and support from lots of people at different institutions. Many thanks to: Dr. Karin Hing for access to her chemistry lab and chemicals, where Dr. Manuela Russo helped me until I became an expert at making solutions; Prof. Ton Peijs for access to his materials lab with the assistance of Dr. Emiliano Bilotti - it was fun to work with your group; Dr. Joseph Gargiuli for all the kindness and help with microscopes and lab assessment; Dr. Zofia Luklinska, Dr. Nima

Monica Pino

Roohpour, Dr. Rory Wilson and Dr. Monisha Philips for the SEM, EDX and TF-XR. Your kindness and time were much appreciated. Thanks also to Dr. Lucia Carassiti, Mr. Jim Gallagher for the help with SEM and EDX; Dr. Derek Fabel for the AAS equipment (great discussion and science were amazing); Dr. Mathis Riehle and Dr. Matt Dalby for accessing your fabulous labs - it was delightful to work there around you; Dr. Mohammed Baklar for help with the WAXD test a week before submitting a paper; Dr. Tomasz Liskiewicz for the scratch test and great discussion.

A big thank to Mr. Ian Peden for his help with optical microscopy, with the occasion assistance of Dr. Takashi Mine. You also taught me amazing things about history, science, culture and geography. Thanks to Dr. Phil Harrison for letting me use the hot press, with the assistant of Mr. John Davidson, for all the teaching labs jobs, plus the administrative duties of the Harrison Hotel, and for supporting my running races, and all the fun in Scotland. Thanks to Mrs. Fiona Downie for giving me a PC to write my thesis on, and for the support for my running races; Mr. Stephen Wicks, Mr. Kenny McLaren and Mr. Walter Robinson, for sorting out all the mess I managed to do with my computers; Mr. John Taylor, Mrs. Evelyn Love and Ms. Jane Livingston for the lovely help and advice; and Mrs. Marilyn Dunlop for counting how many coffees and glasses of water I took each day and keeping the record so precisely - thanks for all your kindness and care towards me.

Organising the viva date sometimes seemed a mission impossible, and it might have been unachievable without the help from Mrs. Elaine McNamara and Prof Matthew Cartmell. Thank you for all your help and kindness towards me.

Special thanks to Mr. Vince Ford for being the loveliest person around, doing all my moulds. Learning English and very useful skills from you were crazily cheerful.

A big thanks to Dr. Manuel Romero for all the counselling during this journey – your great support was always appreciated. Thanks to Dr. Sofia Paredez for all advices and adventures post-conference in Sardinia. Running has kept me balanced during this research, and it's been great fun in Scotland. Thanks to all my supporters.

This journey would have been impossible without my family, most of the time far away, but I'm always feeling close to them. Thank you, Dr. Maria Pino, for your support, advice and love. Thanks for teaching me science and all the fun on our California trip, the

Monica Pino

wee visit to Glasgow, and for the amazing trip to Egypt with all your enthusiasm as a business woman. Most importantly, I can't thank enough Prof. Mercedes Jaimes de Pino for your immense love and support. I learnt from you that science, honesty and fun must be together to live happy and looking young. Thanks for being with me when I moved to Glasgow. All your sweet words are always with me. Thanks for the much needed break in Egypt.

Vielen Dank, Dr. Henrik Gollee for your great patience and for being an excellent sub-editor and a great proof-reader of all my writing. Being there when I needed your help was and will be immensely appreciated. It was amazing travelling around Scotland, Germany, the Netherlands and Egypt. I hope this has prepared you for the challenges in Colombia. Classical concerts and books were great, and running most of the races with you was a good fun. My knowledge of Scotch whisky became so exquisite thanks to the samples you provided!

Prof. Tom McLiesh, Prof. Aldo Boccaccini, Dr. Manuela Russo, Dr. Javier Orono, Dr. Gillian Tweddell, Dr. Francesca Scrinzi, Dr. Mariangela Palladino, Dr. Paola Vacca, Miss Eleanor Champness, Dr. Giuseppe Pellegrini, Dr. Paola Ciselli and family, Mrs. Laleh Boyhan, Mrs. Clarte Bermejo, Dr. Suneel Kunamaneni, Mr. Grant Macaulay and family, Dr. Angelica de Izquierdo and family, Dr. Antonio Scherillo, Dr. Bostjan Bezensek, Mrs Rita Pennisi, Dr. Cristy Kazanidis, Dr. Fuad Shareef, Dr. Noelia Diaz, Dr. Domenico Gallipoli, Dr. Carlos Cruz, Mrs. Mari-Carmen Perez, Dr. Paolo Gallipoli, Miss Audrey Roman , Dr. Raquel Arevalo, Dr. Andrea Cardoni, Mr. Daniel Gonzalez, Miss Maria Gonzalez, Mr. Francesco Maggiolo, Dr. Monika Schoenleber , Dr. Marc Sorel, Mr. Mitesh Visaria, Dr. Nils Becht, Mr. Arnaud Robert, Mr. Carlos Martinez, Dr. Giovanni Circella, Dr. Rob Froud, Mr. Dong Wang, Dr. David Forehand, Dr. Andrew Mathieson, Dr. Aleksandra Vuckovic. Thanks to all of you for your kindness, friendship and support. I think without all of you and my family this journey would not being that nice. Especially without all the hill-walking and Ceilidh parties in Scotland!

Finally, I would like to acknowledge the generosity of Queen Mary University of London, the University of Glasgow, The Thomas and Margaret Roddan Trust, the IOM³ and the Royal Academy of Engineering for financial support, and Invibio Ltd for supplying the PEEK films.

In memory of my beloved father, Pedro Nel Pino Santiago, who sadly left this world just before I started this journey

And

My cousin and brother, Carlos Julian Duarte Jaimes, who passed to the other world when this journey commenced

Thanks for all the happy moments we shared and the strength I gained to do this work with love and patience

Monica Pino

*I dedicate this thesis to those who make a lovely difference in my life,
especially
Mercedes Jaimes de Pino
Maria Pino*

PUBLICATIONS

JOURNAL PUBLICATIONS

M. Pino, N. Stingelin, K. E. Tanner. Nucleation and growth of NaOH-treated PEEK, HDPE and UHMEPW for artificial cornea materials. *Acta Biomaterialia* 2008, 4, 1827-1836.

This paper contains the results of the first part of the experimental work done in batch I (Table 3.3.1).

M. Pino, W. Chrzanowski, D. Fabel, M. Baklar, N. Stingelin, K. E. Tanner. Apatite Deposition on NaOH-treated PEEK and UHMWPE Films for Sclera Materials in Artificial Cornea Implants. *Advanced Engineering Materials: Advanced Biomaterials* 2010 (in press).

This paper contains the outcomes of the second part of this research done in batch II (Table 3.3.1).

PEER REVIEWED CONFERENCE ABSTRACTS

M. Pino, W. Chrzanowski, D. Fabel, M. Baklar, N. Stingelin, K. E. Tanner. Apatite Phases on Alkali-treated PEEK and UHMWPE for Sclera Materials of Artificial Cornea Implants. 23rd European Society on Biomaterials Conference, September 2010, Tampere, Finland.

M. Pino, N. Stingelin, K. E. Tanner. Nucleation and Growth of Apatite on NaOH treated PEEK, HDPE and UHMWPE for Artificial Cornea Materials. European Congress on Advanced Materials and Processes, September 2009, Glasgow, UK.

M. Pino, N. Stingelin, K. E. Tanner. Nucleation and Growth of Apatite on NaOH treated PEEK, HDPE and UHMWPE for Corneal Materials. Annual Conference of the UK Society of Biomaterials, July 2009, University of Ulster, Jordanstown, Northern Ireland.

M. Pino, N. Stingelin, K. E. Tanner. Apatite on NaOH-treated PEEK and UHMWPE Films for Artificial Sclera Materials of Cornea Implant. Annual Conference of the Tissue and Cell Engineering Society, July 2009, University of Glasgow, Glasgow, UK.

M. Pino, N. Stingelin, K. E. Tanner. Nucleation and Growth of Apatite on NaOH treated PEEK, HDPE and UHMWPE for Corneal Materials. 8th World Biomaterials Congress, June 2008, Amsterdam, The Netherlands.

M. Pino, N. Stingelin, K. E. Tanner. Nucleation and Growth of Apatite on NaOH treated PEEK, HDPE and UHMWPE for Corneal Materials. 21st European Society on Biomaterials Conference, June 2007, Brighton, UK.

CHAPTER 1

INTRODUCTION

Corneal blindness is the second most common cause of blindness in the world. It is estimated that 45 million people worldwide are bilaterally blind and 10 million are affected by corneal blindness (WHO, 2001). Corneal blindness affects children and those of a younger age than those who suffer from cataracts (Sinha *et al.*, 2005). From this perspective, corneal blindness presents a greater impact in total blindness in number of years. In addition, corneal blindness mostly affects the population in the equatorial zone, due to the high exposure to UV light (Biswell, 1995; WHO, 1998).

A simple option to address corneal blindness is keratoplasty, a surgical intervention in which the damaged cornea is replaced by corneal tissue from a human donor, frequently donated by an eye bank. However, this corneal grafting presents complications such as rejection and post-astigmatism and there is also a lack of donor materials and resources (Biswell, 1995). The rejection rate has been lowered to 20% in the last decade by ensuring that the blood type between the donor and the recipient patient corresponds. Besides this improvement, allografts (collagen-base implants) still exhibit problems with the supply of corneas and disease transmissions. Approximately 20,000 corneas (eyes) are available annually, but about 40,000 new patients a year are added to the waiting list. It is clear that corneal blindness is not fully solved by this approach. Moreover, conventional corneal grafting is not advised for patients with bilateral corneal blindness who suffer from tear deficiency, chemical burns, trachoma, vascularization, Stevens-Johnson syndrome, ocular cicatricial pemphigoid, or uncontrollable intraocular pressure (Hicks *et al.*, 1997; Legeais and Renard, 1998; Kim *et al.*, 2002; Falcinelli *et al.*, 2005).

At present, an artificial cornea, i.e. a keratoprosthesis (KPRO) possibly provides an alternative to keratoplasty, and there is an urgent necessity to meet the demand.

KPROs consist of a clear optic portion and a surrounding ring known as the skirt, which needs to integrate with the sclera of the eye to anchor the implant. However, the current failure rate of the commercially-available artificial corneas is unacceptably high (40% at one year) due to the non-integration of the “skirt” used to hold the implant *in situ*. The skirt is implanted between the sclera and the ocular conjunctive, and it must be bioactive to encourage the metabolic nourishment of the cornea and to be firmly integrated (Legeais *et al.*, 1992; Chirila *et al.*, 1993; Legeais and Renard, 1998; Kim *et al.*, 2002; Albon, 2003; Hicks *et al.*, 2003; Hollick *et al.*, 2006; Meek, 2008). Integration may be improved by using a bioactive skirt material, which adapts to the metabolic activity of the cornea.

A few promising routes for the fabrication of keratoprotheses have been proposed. The Osteo-Odonto-KPro (OOKP) uses tooth enamel for the production of the skirt, that is an hydroxyapatite of biological origin. A central polymethyl methacrylate (PMMA) optic is glued into the enamel tooth. OOKP has been implanted since the 1960s. Falcinelli *et al.* (Falcinelli *et al.*, 2005) found excellent long term retention results (85% survival in 18 years) with 75% of patients seeing 6/12 or better. Liu *et al.* (2007) reported an 80% improvement of vision. However, poor tissue integration results in failure of the devices. Furthermore, it should be noted that, it would be desirable to restore the metabolic activity of the cornea by use of a more bioactive material.

Besides keratoprotheses based on biological hydroxyapatite, which need to be obtained from tooth enamel – a procedure that requires the donation of one of the patient’s teeth – synthetic devices have been investigated as they promise easier fabrication. In addition, clinically, it is easier to implant a polymeric skirt than rigid skirts, such as OOKP. Furthermore, one can expect the mechanical compatibility to be improved between the sclera and polymers compared to the sclera and tooth enamel.

Thus, it is clear that there is a strong desire to develop an artificial skirt material that can adapt to the sclera of the eye, but which is also bioactive. Polymer films such as HDPE, PEEK and UHMWPE could provide the basis for ophthalmic biomaterials related to KPROs, primarily because clinically, it is easier to implant a polymeric skirt than rigid skirts, such as OOKP and secondly because the mechanical compatibility could be

improved between the sclera and polymers compared to the sclera and osteo-odonto lamina (dental lamina).

These polymers, UHMWPE, PEEK and HDPE, have a clinical history as successful biomaterials for other medical implants (Kurtz, 2004; Roeder *et al.*, 2009) and, in a few cases, for ophthalmological implants (Allan, 1999) but none for the sclera implants. Therefore, from this perspective, these polymers are promising candidates to tackle at least some of the problems with current KPRO technologies. In addition, these materials can be engineered with a wide range of physical, mechanical and surface properties. However, the bioactivity of these polymers has to be significantly improved for them to be used as skirt materials for artificial cornea implants.

The skirt materials for the corneal implants should also be porous, which is required for good fixation *in vivo*, to allow fibroblast in-growth and collagen deposition to provide adequate anchorage of the skirt into the sclera. The porosity of polymer films therefore may need to be enhanced, e.g. by expanding the films biaxially during the production, or by perforating the films after production.

1.1 IDEAL ARTIFICIAL CORNEA

A KPRO must perform the functions of the cornea that is: be transparent, have a refractive surface to transmit and refract light, produce protection to give globe integrity, be non-immunogenic (Albon, 2003), and to allow the nourishment mechanism to carry out the normal metabolic process of the cornea. Also, a KPRO must secure long term fixation that is be able to withstand trauma, and for a wet eye requires an epithelialized surface (Hicks *et al.*, 1997). Therefore, the ideal KPRO should be coated with an epithelial layer, flexible, clear, and most important to be jointed permanently to the surrounding tissues, especially to the sclera (Li *et al.*, 2008; Meek, 2008; Deng *et al.*, 2010). The most feasible solution for the artificial cornea implant would be the development of a material that would accept growth and attachment of transparent epithelium on its surface (Refojo, 2005), in other words, a bioactive material. Also, a biomaterial that would heal into the recipient's corneal tissue would be desirable.

The successful integration of the KPRO with the cornea depends in part on peripheral host keratocyte adhesion to anchor the implant in place and prevent epithelial downgrowth (Sandeman *et al.*, 2000). Therefore, the skirt must be porous, to allow fibroblast ingrowth, and collagen deposition to provide good anchorage. Also, the anterior surface should allow epithelialization, be free from inflammation or mutagenesis, and be implantable without extensive surgery. The posterior surface should inhibit cellular attachment and proliferation to prevent the formation of opaque retro-prosthesis membranes. The optic must act as an UV filter (Hicks *et al.*, 1997).

The fundamental key for an ideal artificial cornea is to construct a one-piece device with similar layers of the normal cornea, which interact with each other to fulfill the functions of the cornea.

Consequently, the corneal material should allow the keratocytes to adapt and grow, and the cells should be re-shape the material into a cornea equivalent stroma, which is allowed to be colonized with layers of endothelial and epithelial cells on its surface. Therefore, the corneal materials must accept growth and bond of clear and transparent layers of epithelium on its outer surface. The ideal artificial cornea must allow examination of the retina and checking the ocular pressure. Lastly and less important, the ideal artificial cornea should be aesthetically acceptable and have a reasonable cost.

1.2 BIOCOMPATIBILITY AND BIOACTIVITY

Biocompatibility was recently defined by Ratner (Ratner and Bryant, 2004) as: „the ability of materials to locally trigger and guide normal wound healing, reconstruction and tissue regeneration“. The earlier definition of biocompatibility was as: „A biocompatible material is one that has the ability to perform with an appropriate host response in a specific application“ (Williams, 1999). Amongst various materials used to produce implants, which are supposed to satisfy these definitions, are polymers. Thus, HDPE, PEEK and UHMWPE polymer films have been used in the biomedical field for many years and have proved that they are biocompatible (Bonfield *et al.*, 1984; Allan, 1999; Kurtz, 2004; Kurtz and Devine, 2007; Roeder *et al.*, 2009). They might therefore provide

interesting alternatives, specifically in an ophthalmological implant if they can be made bioactive and fulfil the mechanical compatibility of the skirt of the artificial cornea.

The term bioactivity was defined in the early 70s as: „A bioactive materials is one that elicits a specific biological response at the interface of the materials which results in the formation of a bond between the tissue and the material“ (Hench *et al.*, 1972). This term was also defined by Williams as: „A bioactive material is one which has been designed to induce specific biological activity“ (Williams, 1987).

Accordingly, the concept of bioactivity relates strictly to the biological interactions of materials with the surrounding environment in a body or a simulated body environment. Bioactivity can be defined as generation of positive response of the tissue in contact with another material which is not biological in origin. On the other hand, more commonly, bioactivity is understood as inducing biologically associated reactions on the surface of the materials; for instance, formation of apatite layers from body fluids (Kokubo, 1998; Ryhänen, 2000; Abou-Neel *et al.*, 2007; Yousefpour, 2007; Chrzanowski *et al.*, 2008), which enable the prediction of bone bonding ability of the materials. Thus, Kokubo and Takadama (2006) consider bioactive materials as bone bonding materials (Bohner and Lemaitre, 2009). In other biomaterial applications different definitions of bioactivity will apply.

This study has not intended to develop a material which triggers bone bonding ability. The main purpose of this study is to find a material which will produce a similar response as tooth dentine, which is the bioactive material, known as the dentin lamina used successfully as skirt in the osteo-odonto-keratoprothesis (OOKP), the KRPO that demonstrated good retention of the implant due to its non-rejection issue from the host eye because the patient's own tooth is used to make the skirt of the semi-artificial cornea implant. Interestingly, the Ca/P molar ratio of dentine is 1.61 and the Ca/P molar ratio of dental enamel is 1.63 (Legeros, 1991; Daculsi *et al.*, 1997). The apatite contained in dentine, enamel and bone mineral is calcium deficient biological apatite related to hydroxyapatite (Legeros *et al.*, 2003). The tooth enamel is the most highly mineralized tissue of human body (Tadic *et al.*, 2001; Gutierrez-Salazar and Reyes-Gasga, 2003).

Finally, *in vitro* and *in vivo* testing has shown that the common characteristic of bioactive implant materials is that a layer of biologically active carbonate hydroxyapatite (CHA) forms on the implant surface after soaking in physiological fluids (Cao and Hench, 1996). Additionally, the mineral phase of calcified tissue (enamel, dentine and bone) is biological apatite, which is carbonate hydroxyapatite (CHA) (Cao and Hench, 1996).

To produce a CHA on the surface of polymers, 1.5 SBF can be used as a treatment to make them bioactive, before implantation; rather than to evaluate bioactivity (Tiffany et al., 1989; Renke-Gluszko and Fray, 2004). Thus, 1.5 SBF solution is part of the process to form a HA layer, and such supersaturated concentration can be used to accelerate the precipitation of HA.

1.3 AIMS AND OBJECTIVES

The main aim of this research was to increase the bioactivity of polymer materials which may be suitable for the design of skirt implants in artificial corneas. For this purpose, polyether ether ketone (PEEK), high-density polyethylene (HDPE) and ultra-high molecular weight polyethylene (UHMWPE) films have been investigated. In order to improve the bioactivity of the polymer films a two-step treatment using chemical surface modification (immersion in NaOH) and the formation of apatite layers from supersaturated Simulated Body Fluid (1.5 SBF) was applied.

The objectives of the present study were therefore to investigate the effect of different molarities of the NaOH pre-treatments on the polymer film structures and to determine the optimum NaOH concentration for stimulating apatite deposition from SBF, to get better understanding of the apatite nucleation and growth on polymer surfaces and to identify the apatite deposited (composition and crystalline phase) over the immersion time in SBF, as well as the morphology and dispersion of apatite on the films. Finally, to examine the stability of the apatite in a common medium such water, the release of calcium from the specimens was evaluated.

1.4 OVERVIEW AND STRUCTURE OF THIS THESIS

This thesis is divided into six chapters as follows:

Chapter one is the introduction, which explains the motivations of this work, and considerations for an ideal artificial cornea. Also, the concept of Biomaterial is explained in detail. Finally the aims and objectives of this research is given together with the structure of this thesis.

Chapter two is a literature survey, covering the physiology and pathology of the cornea and its surrounding structures such as conjunctive, tears and aqueous humor fluids, treatments of corneal damage, materials used in artificial cornea implants and the current complications of the artificial cornea devices.

Chapter three describes the materials and methods, the properties of the materials used to produce the polymer films, the preparation of the NaOH and SBF solutions and finally the characterisation techniques employed to study the morphology and the composition of the layers deposited on the films.

Chapter four describes the results, showing the outcomes of the assessment of the skirt materials with a view to evaluating the bioactivity on the layers formed on the polymers.

Chapter five is the discussion, which examines the implications of bioactivity in an implant, the effectiveness of NaOH and the influence of immersion time in SBF, the apatite phase formed on our polymers and lastly the applications for skirt materials in cornea implants.

Chapter six contains the conclusions drawn from this work and a summary of future work.

The peer-reviewed publications which have resulted from this research are listed prior chapter one.

CHAPTER 2

LITERATURE SURVEY

2.1 INTRODUCTION

The cornea is the transparent portion of the eye; it covers the iris and the pupil and it is continuous with the sclera. The cornea is a highly specialized avascular (without blood vessels) tissue that is nourished by the tears. For vision, the cornea must remain transparent. Thus, all layers of the cornea must be free of any cloudy or opaque areas and refract light correctly. The cornea can become opaque due to corneal diseases and trauma to the extent of causing corneal blindness, one major type of which mostly affects the population of the equatorial zone, due to their high exposure to UV light. To restore vision, the cornea can be replaced either by a donor corneal graft (keratoplasty) or by an artificial cornea. At the present time, an artificial cornea implant (keratoprosthesis) is the only alternative to cornea transplantation (keratoplasty) for patients with corneal blindness that can not under go keratoplasty due to other eye disorders such as dry eye (Hicks *et al.*, 1997; Falcinelli *et al.*, 2005). On the other hand, the current failure rate of the available artificial cornea is unacceptably high due to non-integration of the “skirt” used to hold the implant *in situ* (Legeais and Renard, 1998; Kim *et al.*, 2002; Albon, 2003; Meek, 2008). The skirt is placed between the sclera and the ocular conjunctive, and in addition to being biocompatible must be bioactive to maintain the metabolic activity of the cornea and to be firmly integrated. A biocompatible material by definition has “the ability to perform with an appropriate host response in a specific application” (Williams, 1999). A bioactive material is defined as “a material that elicits a specific biological response at the interface of the material, which results in the formation of a bond between the tissue and the materials” (Hench, 1998). The use of bioactive materials that allow colonization of the optic by host keratocytes and epithelial cells has shown that it is possible to integrate

alloplastic materials into the recipient cornea (Legeais *et al.*, 1992; Legeais and Renard, 1998; Chirila *et al.*, 1993; Hicks *et al.*, 2003). Thus, an understanding of the structure, functions and properties of the cornea and its surrounding tissues (the sclera and the conjunctiva) and also reasons for the failure of the artificial cornea helps in the development of the skirt materials.

In this chapter, the cornea physiology, together with its associated structures, such as the sclera, the conjunctiva, and the tears and aqueous humour fluids are described. The cornea pathology is outlined as well as the different treatments for the corneal damage. The materials used in the corneal implants are also detailed together with the materials used in this research for the skirts of the artificial cornea devices, high density polyethylene (HDPE), ultra high molecular weight polyethylene (UHMPE), polyether ether ketone (PEEK), apatites and Simulated Body Fluid (SBF). Then, the artificial cornea implants are reviewed, including the results from the artificial cornea in human clinical trials since the 1960s. Finally, the current complications of the artificial cornea devices are recounted.

2.2 THE CORNEA

The cornea is the transparent circular tissue of the external part of the eyeball (NHS, 2006) that covers the iris and the pupil, and admits light to the interior of the eye (IPAC, 2004) (Figure 2.2.1). Therefore, the main functions of the cornea are: 1) Globe integrity and protection, 2) transmission and refraction of the light, and 3) UV screening (Hicks *et al.*, 1997). The cornea is avascular (Refojo, 2005), that is there are no blood vessels to nourish or protect it against infection; instead, the cornea receives its nourishment from the tears and aqueous humour (NEI, 2006). The average adult cornea is 0.54 mm thick at the centre, gradually increasing to 0.65 mm thick at the periphery and 11.5 mm in diameter (Hodge, 1995).

Figure 2.2.1 has been removed due to the Copyright restrictions

Figure 2.2.1 Structure of the eye (from Martini, 1995)

The transparency of the cornea is due to its uniform and avascular structure and relatively dehydrated state of the corneal tissue (Hodge, 1995). The collagen contained in some layers of the cornea gives the cornea its strength, elasticity and form. Collagen's unique shape, arrangement and spacing are essential in producing the cornea's light-conducting transparency. The structure of the cornea consists of five layers (Figure 2.2.2): the epithelium, Bowman's layer, the stroma, Descemet's membrane, and the endothelium (NMP, 2003; Hodge, 1995). The description and functions of the cornea layers are detailed in the following paragraphs, and the main characteristics and composition are summarised in Table 2.2.1.

Figure 2.2.2 has been removed due to the Copyright restrictions

Figure 2.2.2 Structure of the cornea (from James et al., 2003)

Table 2.2.1 Cornea layers functions (data from Hodge, 1995; Hicks et al., 1997; IPAC, 2004; Refojo, 2005; NEI 2006; NHS, 2006)

Layer name	Characteristics	Composition	Functions
<i>Epithelium</i>	5 or 6 layers of cells, filled with thousands of tiny nerve endings that make the cornea extremely sensitive to pain when rubbed or scratched.	Keratinocytes (Epithelial cells)	Block the passage of foreign material (dust, water, bacteria) into the eye. Provide a smooth surface that absorbs oxygen and cell nutrients from tears.
<i>Bowman's membrane</i>	A clear acellular layer, a modified portion of the stroma.	Collagen type I (Protein fibres)	Protects the stroma. Once injured, this membrane can form a scar if it heals.
<i>Stroma</i>	A thick, transparent middle layer, approximate 200 layers of type I collagen fibrils. This layer is responsible for most of the focusing that occurs in the cornea.	3-5% Keratocytes, 16% type I collagen, 78% water, and 1%proteoglycans	Collagen gives the cornea its strength, elasticity, and form. The collagen's unique shape, arrangement and spacing are essential in producing the cornea's light-conducting transparency.
<i>Descemet's membrane</i>	A clear elastic membrane, which regenerates readily after injury.	Collagen	Serves as a protective barrier against infection and injuries.
<i>Endothelium</i>	Only one thin layer of cells. Once the endothelial cells are destroyed by diseases or trauma, they are lost for ever; if too many are destroyed, corneal oedema and blindness ensue.	Endothelial cells	The stroma tends to absorb water; the endothelium's primary task is to pump this excess fluid out of the stroma. Without this pumping action, the stroma would swell with water, become hazy and opaque.

The epithelium occupies about 10% of the overall thickness of the cornea, and is a thin multicellular tissue layer. The epithelial cells have the ability to regenerate when the cornea suffers from minor injuries. The functions of the corneal epithelium include: 1) blocking of the passage of foreign materials (dust, water or bacteria) inside the eye; 2) absorbing oxygen and nourishing from the tears and distributing these nutrients to the rest of the cornea. From a mechanical point of view, the most important function of the epithelium is for the cells to anchor and organize themselves in a manner that creates the basement membrane, which covers the surface of the cornea (Sanhermelando *et al.*, 2002).

Bowman's layer is composed of fine collagen type I layers in a random orientation, but very compact form which makes it a tough layer providing good protection for the stroma (Fratzl and Daxer, 1993). There is also a transition zone between the Bowman's layer and the stroma, where these two layers are joined, which is part of the Bowman's layer. It is composed of collagen fibrils arranged obliquely to be attached to the collagenous lamellae of the superficial stroma (James *et al.*, 2003). The acellular Bowman's layer is about 10 μm thick.

The stroma is the middle and major layer of the cornea, about 90% of the thickness of the cornea (Sanhermelando *et al.*, 2002). The stroma is composed of collagen fibres arranged regularly along with sparsely distributed keratocytes. Indeed, the collagen fibrils are obliquely oriented and bounded tightly forming a lamellae embedded in a cellular matrix mostly composed by sulphate glycosaminoglycans, and between the lamellae are the sparse keratocytes (fibrocytes). This structure makes the stroma a thick layer of approximately 200 layers of collagen type I fibrils, and the direction of the collagen fibrils differs in each layer providing high mechanical strength (Sanchis-Gimeno *et al.*, 2006).

Descemet's membrane is a thin acellular layer, very similar to the endothelium, since it is a sort of modified epithelial membrane. Descemet's membrane is composed of collagen fibres (different from those in the stroma) and is generated by the endothelial cells that lie below it, explaining why Descemet's membrane can be regenerated readily after a minor injury. Apart from this regenerating function, one of the main functions of Descemet's membrane is to serve as a protective barrier against infection and injuries.

Descemet's membrane is thin in infancy, increases in thickness to approximately 5 μm in childhood, and then to 8 to 10 μm in adulthood (Merindano-Encima *et al.*, 2002).

The endothelium is a single layer of mitochondrial cells, 5 to 6 μm thick arranged hexagonally in a very flattened manner. These cells are responsible for regulating fluid between the aqueous humour and the stroma; these endothelial cells do not regenerate, on the contrary they tend to stretch in order to compensate for dead cells reducing the overall cell density of the endothelium, which ultimately will have an impact on fluid regulation. When the endothelium can no longer maintain a proper fluid balance, the stroma starts to swell due to excess fluids and subsequent loss of transparency will occur (Sanchis-Gimeno *et al.*, 2006). Thus, the main function of the endothelium is to pump this excess fluid out of the stroma. If too many endothelial cells die, corneal edema and blindness will occur, and the only available procedure is corneal transplantation (Sanhermelando *et al.*, 2002).

2.3 THE SCLERA

The sclera is the opaque outer layer of the eye. It is a continuation of the cornea to the optic nerve at the back of the eye, and it is covered by the conjunctiva (Fig. 2.2.1). The sclera is a tough tissue that contains collagen and elastic fibres. The connective tissue present in the sclera as well as in the cornea contains the collagen fibrils embedded in a proteoglycan fibrillar matrix. This tissue therefore requires strength to maintain the internal pressure in the eye and to resist external knocks or any rubbing or other forces applied when the eyes are moved by the extraocular muscles. The mechanical strength is given by the deposition of collagen in a lamellar structure, where the lamellae lie parallel to the surface of the tissue rather than through its thickness (Meek, 2008). The fibrous connective tissue in the sclera give the eye its unique shape, and also serves as an attachment for the extraocular muscles (intrinsic muscles), which move the eye. Thus, providing attachment for the extraocular muscles of the eye is one of the most important function of the sclera (McBrien *et al.*, 2009). The sclera provides support for the retina on the posterior part of the eye and has essential physiological functions such as containing fluid outflow channels to prevent excessive pressure in the eye; and provided for the mechanical functions including maintaining eye shape during any movement of the eye (Meek, 2008).

The sclera starts at the limbus (Fig.2.2.1) as a contiguous tissue of the cornea, constituting the major part of the eye globe. It is connected to the conjunctiva and continues until it attaches to Tenon's capsule (McBrien and Gentle, 2003). The sclera is about 0.1-1.0 mm thick (Edwards and Prausnitz, 1998), with an average diameter of 24 mm; however, its thickness varies from 0.53 mm at the limbus, 0.39 mm at the equator, to 0.9 mm near to the optic nerve (Olsen *et al.*, 1998).

The constituents of the sclera are shown in Table 2.3.1 as wet weight percentages. The sclera is composed mainly of collagen, interfibrillar proteoglycans, glycoproteins, and the tissue is populated by fibroblasts (Meek, 2008). It also contains about 2% elastin (Watson and Young, 2004). The collagen is mostly type I (75% of the dry weight), plus 10% non-collagen protein, and 1% glycosaminoglycans (Montgomery, 2008). The sclera also contains a small number of isolated fibroblast cells (Montgomery, 2008).

Table 2.3.1 Composition of the sclera in percentage of wet weight (from Meek, 2008)

Constituent	Wet weight (%)
Collagen	30
Elastin	0.7
Other proteins	< 3
Proteoglycans	<1
Water	68

The hydration of the sclera is as important as that of the cornea; however, in the case of the sclera, this activity is governed by the hydrophilic proteoglycans only, since there are no epithelial or endothelial barriers as in the cornea (Meek, 2008). On the contrary, the cornea is dehydrated, so the corneal endothelium acts as a pump to keep the fluid out of the tissue, retaining the clarity of the cornea. The sclera tissue, on the other hand, is opaque because it is hydrated (Nemeth and Shea, 2007).

Both cornea and sclera have similar collagen content, however differences in

collagen types and their distribution between the two tissues results in radically different optical properties (Meek and Fullwood, 2001). There are around 20 different collagen types currently known and these can be classified into three super families:

1) Class 1 or banded fibrillar collagens have the classic D-period fibril appearance and include Types I, III and V (Meek and Fullwood, 2001). In both corneal and scleral collagen, Type I is the major component, comprising some 68% of the dry weight in cornea (Maurice, 1984) and 50–70% in sclera (Keely *et al.*, 1984).

2) Class 2 or FACIT (Fibril Associated Collagens with Interrupted Triple Helices) do not form fibrils by themselves, but do interact with fibrillar collagens and include Types XII and XIV (Meek and Fullwood, 2001).

3) Class 3 collagens have fibrous structures which are different from the structure of Class I collagens and include Type VI (Meek and Fullwood, 2001).

In addition, collagen Types III, V, VI, XII and XIV have all been detected in the corneal stroma and Types III, V and VI in the scleral stroma (Panjwani, 1997).

The collagen fibrils are surrounded by a matrix containing proteoglycans (sulphated glycosaminoglycans attached to a protein core) and various other proteins (Meek and Fullwood, 2001). The collagen fibrils are arranged in lamellae that lie roughly parallel to the surface of the eye (Meek and Fullwood, 2001).

2.4 THE CONJUNCTIVA

The conjunctiva is the vascular mucous membrane (transparent layer of cells) that covers the inner surface of the eye lids and the anterior part of the sclera to the cornea (Fig. 2.2.1). Over the lids it is thick and highly vascular and called the palpebral conjunctiva. Over the sclera it is known as the ocular or bulbar conjunctiva and is much thinner while over the cornea it is reduced to a single layer of epithelium (Ellis, 1977). At the junction between the posterior eyelid and the eyeball, there is a transition portion, which links the palpebral conjunctiva and the ocular (bulbar) conjunctiva, known as the fornix (Fig. 2.2.1)

which is considered part of the overall conjunctiva.

Basically, the conjunctiva is nourished by small blood vessels, and it also secretes oils and mucous, which add moisture to and lubricate the eye; this process is part of the corneal metabolic activity. Moreover, the sclera also contributes to immune surveillance and helps to prevent the entrance of microbes into the eye.

The palpebral conjunctiva is firmly attached to the eyelids (Nemeth and Shea, 2007), and forms the lines of the eyelid. The palpebral conjunctiva is thick and opaque. It is red, especially at the lower eye lid in its normal stage.

The bulbar (ocular) conjunctiva is loosely attached and is composed of a modified non-keratinized, staggered scaly epithelium. The bulbar conjunctiva has certain levels of mobility, for instance sliding back and forth over the front of the eyeball that it covers. Within the bulbar, conjunctivae are composed by the so-called goblet cells that secrete an important component of the pre-corneal tear layer, which protects and nourishes the cornea. The superficial bulbar conjunctival epithelium is continuous with the corneal epithelium. When the corneal epithelium is debrided, it may be resurfacing by limbal conjunctival epithelial cells „sliding“ over it (Nemeth and Shea, 2007).

The fornix is a loose pocket of conjunctiva that permits the eyeball to rotate freely. The fornix conjunctiva is coated by a staggered cubical to columnar epithelium of different thickness. This particular epithelium has a very uneven surface since it retains some scale-like features and many adhering spots, and has a hairy structure.

All three parts of conjunctiva (palpebral, bulbar and fornix) produce a viscous fluid (mucous), which lubricates the ocular surface, and they also produce some tears, which help to keep the eye clean. However, most of the tears are produced by the lacrimal glands, which are located at the upper outer corners of each orbit, and spread a thin layer of mucous and tears over the eye every time blinking occurs. After blinking, the fluid spreads over the eye and then flows into narrow canals in the lids that lead to the lacrimal sac, a pouch at the lower corner of each orbit. The mucous and tears from the lacrimal glands and the conjunctiva eventually drain through a passage into the nose.

Mucus is an excellent lubricant and it is believed to contain infection-fighting cells (Nemeth and Shea, 2007). Thus, the conjunctiva plays an important role in the immunological defense system of the eye and produces mucus that is critically needed for tear film stability. In tear film without this mucin layer, the tear layers destabilize, and then the cornea metabolic system is severely affected (Nemeth and Shea, 2007).

2.5 TEARS AND AQUEOUS HUMOUR FLUIDS

Tears are composed of lacrimal fluid produced in the lacrimal glands normally at 1 ml day⁻¹. Tears reduce friction on eyelids over the eye, remove debris from the cornea, prevent infection entering the eye, and provide nutrients and oxygen to the cornea. Tears are composed of a lipid layer and an aqueous/mucin gel layer that contains a complex mix of electrolytes, proteins and mucins. The lipid layer protects the tear film against evaporation while the mucins allow the wetting of the epithelial surface of the cornea, despite its natural hydrophobic state. The electrolytes (Na⁺, Cl⁻, Ca²⁺ and K⁺) help to increase the solubility of all the proteins and mucins found in the aqueous phase of the tear film, and also to maintain a constant osmolarity (295-300 mOsm L⁻¹) and pH (7.4). The proteins resist invasion by infectious agents, promote growth and healing of the epithelium (Tiffany *et al.*, 1989).

The aqueous humour is the liquid that occupies the anterior and posterior chambers of the eye (Fig. 2.2.1), i.e. it fills the space between the cornea and the iris (anterior chamber) and the part of the eye that lies just behind the iris (posterior chamber) since the aqueous humour fluid flows from the ciliary body. The aqueous humour fluid resembles blood plasma in composition, but contains less protein and glucose and more lactic acid and ascorbic acid because the aqueous humour is formed from blood by filtration, secretion and diffusion through the ciliary body. Thus, the aqueous humour is a filtrate of plasma secreted by the vessels of the iris and ciliary body into the posterior chamber of the eye; from here it passes through the pupil into the anterior chamber and is re-absorbed into the ciliary veins by way of the sinus venous sclera or canal of Schlemm (Nagyova and Tiffany, 1999). Therefore, the functions of the aqueous humour are: to provide substrates (glucose, oxygen, electrolytes) for the metabolic requirements of the cornea, remove metabolic

products (carbon dioxide, lactate, pyruvate) and maintain intraocular pressure.

2.6 DISEASES AND TRAUMA OF THE CORNEA

The corneal layers contribute to the function of the cornea. A healthy tear film and eyelids are vital to maintain corneal integrity and clarity. Disturbance of the eyelids, conjunctiva or tear film may lead to corneal problems.

Bilateral corneal blindness: Loss of sight in both eyes due to corneal diseases. The definition of blindness is a visual acuity of 3/60 or less, according to the World Health Organisation (WHO, 1998), and it is estimated that 45 million people worldwide are bilaterally blind, and in 10 million of these people the cause is primarily corneal diseases and secondly cataract (Whitcher *et al.*, 2001).

Climatic droplet keratopathy: Corneal degeneration caused by exposure to UV light. It is characterised in the early stages by fine sub-epithelial yellow droplets in the peripheral cornea. As the disease advances, the droplets become central, with subsequent corneal clouding causing blurred vision (Biswell, 1995).

Corneal dystrophies: These are hereditary and occur at any level in the epithelium, stroma and endothelium. They include conditions in which there is defective development or degeneration of corneal tissue, such as fingerprint and map-dot, keratoconus, and Fuch's (Langley and Ledford, 2007). ***Fingerprint and map-dot epithelial dystrophies*** may cause corneal erosion. ***Keratoconus*** (conical cornea) is the most common corneal dystrophy, and leads to corneal thinning, cone formation, and irregular myopic astigmatism; it causes painless visual distortion and loss (Langley and Ledford, 2007). ***Fuchs's endothelial dystrophy*** results in corneal clouding (Olver and Cassidy, 2005).

Corneal Injuries: Corneal abrasion, chemical burn, and corneal penetrating injury can all arise accidentally (Olver and Cassidy, 2005). ***Corneal abrasion*** occurs when tissues are scraped from the corneal surface, commonly involving the corneal epithelium but possibly extending more deeply (Langley and Ledford, 2007). ***Chemical burns*** can be produced by substances such as alkalis (lime, cement, plaster or ammonia), acids, solvents,

detergents, irritants and super-glue. Alkali in high concentrations causes subsequent scarring and blindness.

Dry eye: A disorder of the tear film due to *tear deficiency* or *excessive tear evaporation*. If untreated dry eye may lead to dry epithelium, corneal ulceration and perforation, and blindness (AET, 2006).

Infiltrates: Appearance of white or yellow particles in the cornea, commonly rounded in shape and cloudy, makes the cornea partially cloudy. Excessive contact lens wear and/or infections are the cause of these infiltrates (Langley and Ledford, 2007).

Keratitis: Inflammation of the cornea resulting from infection caused by bacteria, fungi, virus, exposure, or injury among others causes (Langley and Ledford, 2007). **Bacterial keratitis** can cause corneal abrasion, opacification, melt, perforation, endophthalmitis, and loss of vision. **Acanthamoeba keratitis** can induce cornea scarring. **Viral keratitis** can originate ulcers and stromal necrosis that is scarring with vascularization reducing cornea sensation, clarity and vision (Olver and Cassidy, 2005).

Oedema: Refers to hydration of the corneal tissue, presenting swelling and cloudiness, usually indicates a dysfunction in the endothelium. If corneal swelling is greater than 15%, a gross separation of the collagen fibres of the stroma occurs, results in a hazy or cloudy appearance of the cornea (Langley and Ledford, 2007). The corneal swelling is 4% under normal conditions.

Ocular cicatricial pemphigoid: A rare inflammatory conjunctival disease, whose early signs are redness, painful, tearing, and photophobia eyes. Later it may result in dry eye, corneal scarring and opacity (Olver and Cassidy, 2005).

Pterygium: A triangular growth of tissue that extends from the conjunctiva over the cornea (Vaughan *et al.*, 1995). It leads to inflammation and blurred vision due to obstruction of the visual axis or to astigmatism (Olver and Cassidy, 2005). Pterygium can be surgically removed especially if it blockes the optic axis (Langley and Ledford, 2007). The cornea may become scarred before or after the surgical intervention.

Stevens-Johnson syndrome: Inflammatory disorder of the skin and mucous membranes. The ocular disease can result in bilateral blindness. Prognosis of the corneal transplantation in the acute phase is poor because of the difficulty of overcoming the severe inflammation and allograft rejection (Kiozumi *et al.*, 2001).

Trachoma: A serious form of infection of the eye such as keratoconjunctivitis (Vaughan *et al.*, 1995). When the infection is repeated it leads to trachoma, which is contagious, and frequently passes from child to child, and develops into a chronic stage during the adulthood. Trachoma occurs in areas with shortage of water, large number of flies and crowded living conditions (Whitcher *et al.*, 2001). This chronic infection can lead to further symptoms: swollen eye lid, eye discharge, scarring in the eye lid, and corneal scarring (Taylor, 1999).

Vascularization: Growth of blood vessels into the cornea from limbus (Fig.2.2.1) into the normally avascular tissues (Langley and Ledford, 2007). This is produced as a physiological response to long term low oxygen leads in the cornea in contact lens wearers (EyeMD, 2006).

A consequence of these corneal diseases and trauma as well as eye surgery, glaucoma can develop. **Glaucoma** is an ocular condition in which the fluid pressure inside the eye is too high due to slow fluid drainage from the eye.

2.7 TREATMENTS OF CORNEAL DAMAGE

The healthy cornea is clear and avascular. Corneal clarity depends on the normal functioning of its layers. Of particular importance is the endothelium that maintains the cornea in a state of partial dehydration and hence transparency by means of a „pump-leak“ mechanism. Swelling, tissue proliferation and vascularization may compromise the transparency of the cornea (Olver and Cassidy, 2005; Refojo, 2005). However, the major causes of corneal blindness are: climatic droplet keratopathy, corneal injuries (corneal abrasion, chemical burn and corneal penetrating injury), failed corneal grafting, keratitis, ocular cicatricial pemphigoid, post-irradiation injury (Skelton *et al.*, 2000), Stevens-

Johnson syndrome and trachoma.

Patients who suffer from corneal conditions such as corneal injuries (corneal abrasion, chemical burns), oedema, vascularization and corneal dystrophies (keratoconus) when a contact lens can no longer be effective for keratoconus, are advised to undergo keratoplasty (donor corneal transplantation).

Patients with corneal blindness in whom the epithelium or endothelium diseases and trauma are the cause of the blindness, are suitable for a partial cornea replacement such as artificial endothelium or epikeratoprosthesis (artificial epithelium).

On the other hand, patients with bilateral corneal blindness in whom donor corneal transplantation (keratoplasty) has failed or keratoplasty is not advised for their specific health circumstances, are potential subjects for keratoprosthesis (KPRO) surgery, assuming the optic nerve and the retina are functioning normally. A KPRO is a type of artificial cornea containing an optical implant. One such procedure is described in detail in section 2.10.2.

In addition, some complications such as rejection and post-astigmatism are reported in keratoplasty (Biswell, 1995) which might be due to the collagen based implants in corneal allograft material, which may fail to sustain normal corneal epithelial or stromal tissues in the hostile ocular surface environment (Hollick *et al.*, 2006). Additionally with allograft there are problems with the supply of cornea and disease transmission. Keratoplasty is not advised for patients with bilateral corneal blindness or who suffer from a range of clinical problems including dry eye, corneal injuries (chemical burn, corneal abrasion or corneal penetrating injury) and uncontrollable intraocular pressure (Hicks *et al.*, 1997; Legeais and Renard, 1998; Kim *et al.*, 2002; Falcinelli *et al.*, 2005). At present, an artificial cornea that is a keratoprosthesis (KPRO), is the only alternative to keratoplasty.

The three main approaches to treat cornea blindness, keratoplasty, artificial endothelium and epikeratoprosthesis, are briefly described below.

2.7.1 KERATOPLASTY (DONOR CORNEAL TRANSPLANT)

Keratoplasty is indicated for corneal conditions such as opacity, scarring, oedema, thinning and corneal dystrophies, and when a contact lens can no longer be effective for keratoconus. There are two types of keratoplasty: 1) *Penetrating keratoplasty (PK)*, which is the transplantation of the full-thickness of the cornea, and 2) *lamellar keratoplasty (LK)*, which is a partial-thickness procedure. The donor cornea may be of human (homograft), or another species (heterograft) origin (Biswell, 1995).

For PK, a cornea from younger donors is preferred because of the direct correlation between age and number of the endothelial cells. The donor eyes should be enucleated soon after the death and refrigerated, and should be used within 24 to 48 hours. Cornea-scleral caps are stored in nutrient media and used within 6 days, or with preservation in tissue culture media used for up to 6 weeks. For LK, cornea can be frozen for several weeks as the endothelial cells are not important (Biswell, 1995).

In PK, the cornea-scleral cap is placed endothelium up on a Teflon block; a trephine is pressed down into the cornea, and a full-thickness button is punched out. In LK, a partial-thickness trephine incision is made in the cornea and the lamellar button is dissected free. Fine sutures are used to sew the transplant in position (Biswell, 1995).

Corneal graft rejection and controlling post-graft astigmatism are the major problems with keratoplasty (Biswell, 1995). There are additional problems with the supply of cornea and there are concerns over disease transmission as HIV or the hepatitis viruses can be transferred with the transplant.

2.7.2 ARTIFICIAL ENDOTHELIUM

The endothelium can be replaced by a silicone-rubber membrane. However, this procedure is not very successful because of the barrier properties of the membranes which do not allow the cornea to get nutrients from the aqueous humour (Refojo, 2005).

2.7.3 EPIKERATOPROSTHESIS (ARTIFICIAL EPITHELIUM)

An epithelium which has become irregular through swelling and proliferation may be replaced by an artificial epithelium made of a hard PMMA (poly methyl methacrylate) contact lens glued to the stroma using a cyanoacrylate adhesive. However, commonly this technique is not successful due to failure of the glue and penetration of the epithelium between the prosthesis and the cornea (Refojo, 2005).

2.8 BIOMATERIALS

The term biomaterial was defined in the 1980s as “a non-viable material used in a medical device, intended to interact with biological systems” (Williams, 1987). This definition was very exclusive to the medical field. In the more inclusive applications the term biomaterial refers to the interactions between synthetic materials and modified natural materials. Biomaterials involve interactions with chemistry, chemical engineering, material science, mechanics, surface modifications, bioengineering, biology and medicine (Ratner and Bryant, 2004). Thus, the definition of a biomaterial has overtime with the so-called third-generation (Hench and Polak, 2002) and other new terms having been developed (Williams, 2008), which are beyond the scope of this thesis (e.g. biotolerability – Ratner and Bryand, 2004).

The first generation of biomaterials was materials that “achieve a suitable combination of physical properties to match those of the replaced tissue with a minimal toxic response in the host” (Hench, 1980). A common feature of most of the biomaterials was their biological “inertness” (Hench and Polak, 2002). The principle underlying the biomaterials development was to minimise the immune response to the foreign body (Hench and Polak, 2002) and to an extend this is still valid.

The second generation of biomaterials was designed to be either resorbable or bioactive (Hench and Polak, 2002). This concept involved biomaterials interactions occurring on the surface of the materials and for bone bioactive materials in certain applications involved rapid ion exchange of Na^+ with H^+ and H_3O^+ , which provided a large

number of sites for nucleation and crystallisation of carbonate hydroxyapatite (CHA) layer similar to the inorganic mineral phase of bone (Hench and Polak, 2002). The growing CHA layer on the surface of the materials provided an ideal environment for cellular reactions to form new bone once implanted (Hench and Polak, 2002) and relates also to the broad extension of cellular growth in other fields such as dental, spinal and ophthalmological applications.

First and second generations biomaterials are limited because living tissues respond to changes in physiological loads or biomechanical stimuli; however synthetic materials are not capable of responding to the environment (Hench, 1980).

Third generation of biomaterials is being designed to stimulate specific cellular responses at the molecular level (Hench and Polak, 2002). Therefore, these biomaterials are referred to as cell and gene-activating materials, which combine the two properties: bioactive and resorbable, with the aim of developing materials that, once implanted, will help the body to heal itself (Hench and Polak, 2002). Toxicology is therefore implicit in the definition of biocompatibility (Ratner and Bryant, 2004).

The most important factor which differentiates a biomaterial of any generation from any other material is its ability to exist in contact with tissues of the body without causing an unacceptable degree of harm to the body (Williams, 2008). The mutual acceptance and co-existence of biomaterials and tissue interactions, are in essence called biocompatibility. Thus, these interactions are involved in any of the situations where biomaterials are used such as tissue engineering, invasive sensors, drug delivery and gene transfection systems, medically oriented nanotechnology and biotechnology in general (Williams, 2008).

A biocompatible material is a material that should not harm the patient. Thus, the definition of biocompatibility was given in the 1980s as “Biocompatibility refers to the ability of a material to perform with an appropriate host response in a specific situation” (Williams, 1987). By default, biocompatible materials are those that are non-toxic, non-immunogenic, non-thrombogenic, non-carcinogenic, non-irritant, etc. This early definition and its default status led to a later definition of biocompatibility as:

“Biocompatibility is the ability of materials to locally trigger and guide normal wound healing, reconstruction and tissue regeneration” (Ratner, 2004).

The second and third generations of biomaterials refer to their bioactivity. Bioactivity was defined as: “A bioactive material is one that elicits a specific biological response at the interface of the material which results in the formation of a bond between the tissue and the material” (Hench *et al.*, 1972). This definition lies somewhere between resorbable and bioinert material (Hench and Ethridge, 1982; Hench, 1988; Gross *et al.*, 1988).

The most important issue about bioactivity is that all the *in vitro* and *in vivo* test results showed that the only common characteristic of the known bioactive implant materials is that a layer of biologically active hydroxyl carbonates apatite forms on the implant surface (Cao and Hench, 1996).

Resorbable implants are designed to degrade gradually with time and be replaced with natural host tissues (Cao and Hench, 1996). For instance, tricalcium phosphate (TCP) ceramics degrade to calcium and phosphate salts. Large quantities of material must be handled by cells; the constituents of a resorbable implant must be metabolically acceptable (Cao and Hench, 1996). Another requirement for a resorbable implant is that the resorption rate must be matched to the repair rates of body tissues (de Groot, 1983). A good example are resorbable sutures.

Focusing on the specific field of ophthalmology there are several devices with a reasonable long record of use, including intraocular lenses and artificial cornea (keratoprosthesis), the main focus of this thesis. Thus, functionality is mainly determined by the optical properties, the physical compatibility with the scleral and corneal tissues and the insertion into and retention within the cornea location. Interestingly, biocompatibility is determined by the need to minimise the tissue reaction in order to avoid compromising the light transmission (Williams, 2008). So far, bioactive transparent and non-transparent polymers appeared to give good results, but the anchorage of the artificial corneal implant is still a challenge (Hick *et al.*, 2003; Steinert, 2003), which is one of the problems that is tackled in this thesis.

2.9 MATERIALS USED IN ARTIFICIAL CORNEA IMPLANTS

The materials used for either full-thickness or partial replacement of cornea must meet the needs of metabolic activity requirements of the cornea and the mechanical and optical properties of the corneal surface. Furthermore, the material used for any corneal implant must not be degraded by host proteases and have sufficient porosity to support optimal nutrient flow, and the right pore size to allow diffusion of low-and high molecular weight molecules. More over, the ability of the cornea to tolerate synthetic materials depends on the pore size and porosity of the material to accommodate stromal fibroblasts (Hicks *et al.*, 2000; Sweeney, 2006).

Most of the implants produced, starting from the most frequently applied synthetic biomaterials, do not possess functional groups on the surface to attach any coating on their surface (i.e apatite layer) (Desmet *et al.*, 2009). Therefore polymers are usually modified in order to enhance the biological response, i.e. apatite deposited from SBF is attached to the polymer surface after an initial surface modification. There are different methods that have been used to modify substrates for this approach, such as wet chemical treatment (e.g. immersion in NaOH, (Stancu *et al.* 2004; Chirila *et al.* 2007), and as used in this thesis), and plasma techniques. Oehr (2003) detail surface modification by plasma polymerization, with retention of the functional groups of the monomers used and listed some possible applications of plasma-modified polymers.

Plasma treatment can be used to directly, or indirectly introduce different functionalities on inert surfaces. Direct modification includes the reactive NH₃ plasma, which is known to introduce, among others, amines, where O₂ plasmas introduces a mixture of mainly COOH and OH functionalities. Argon plasmas are typically used to introduce free radicals (Desmet *et al.*, 2009).

The use of plasma modification techniques has some major advantages. First of all, some techniques will influence the mechanical properties of the outer layer of an implant. It is clear that wet chemical treatment of a surface (such as immersion in NaOH) will cause a partial degradation and scissions of the polymers at the surface, leading to a decrease of mechanical strength and to a faster degradation (Desmet *et al.*, 2009).

Interestingly, a comprehensive study showed that the structural and chemical integrity of PLGA 3D scaffolds was adversely affected by wet chemical methods (Djordjevic *et al.*, 2008).

Another advantage is that plasma enables uniform surface modification, regardless of their geometry (Deesmet *et al.*, 2009). The plasma technique can therefore be used on complex objects such as 3D components for tissue engineering or artificial organs (Lee *et al.*, 1996), nano-particles, and films (Ryu *et al.*, 2005). In addition, the use of hazardous solvents might be avoided, as plasma is a solvent-free method.

Despite the advantages of plasma treatment, NaOH-treatment is relatively easy and straightforward to apply, without the need for specialized equipment. For these reasons, NaOH was used to achieve chemical surface modification of the polymers.

2.9.1 POLYMERS

Artificial cornea materials are usually polymer based. In this section an overview is therefore given of polymer materials such as polymethyl methacrylate (PMMA), poly(2-hydroxyethyl methacrylate) (PHEMA), polytetrafluoroethylene (PTFE), polyethylene terephthalate (PET) and those used in this research (HDPE, PEEK and UHMWPE). Finally, apatites and Simulated Body Fluids (SBFs) used to make the polymer films bioactive are introduced.

Polymers or macromolecules have two basic „shapes“, each possessing its own characteristic properties. They may be linear (or branched) or crosslinked. Linear or branched polymers consist of an assembly of chains. Each chain consists of a number of similar units. Figure 2.9.1 shows a small section of a polyethylene chain, the simplest of all polymers.

Figure 2.9.1 has been removed due to the Copyright restrictions

Figure 2.9.1 Part of polyethylene chain (from Ward et al., 2005)

The different properties in polyethylene are due to the fact that polyethylene can have different types and degrees of side branches:

- High density polyethylene (HDPE) consists of mostly linear chains of polyethylene.
- Low density polyethylene (LDPE) contains both short and long branches of polyethylene.

- Ultra high molecular weight polyethylene (UHMWPE) exhibits extremely long chains of polyethylene.

The most immediate difference caused by short branches is the density. In the presence of both long and short branches, molecular chains cannot pack closely together and hence in the solid state produce low density polyethylene, which also has lower crystallinity. Long branches affect the melt properties and increase entanglements, thus modifying the processability of the polymer.

Crosslinked polymers consist of continuous networks. They may be lightly crosslinked, producing flexible products (e.g. vulcanised rubbers) or highly crosslinked, producing rigid materials (e.g. thermosets). These systems are insoluble and infusible, so they must be shaped prior to crosslinking. More specialised materials include thermoplastic elastomers (or rubbers) and crosslinked thermoplastics.

Polyethylene is produced by chain polymerisation, which may be represented as follows:



In equation (2.9.1), n is the number of molecules reacting together, which is described as the degree of polymerisation. $\text{CH}_2=\text{CH}_2$ is the chemical formula of ethylene, or ethene, the monomer from which polyethylene is produced. In ethylene, each carbon is linked to two hydrogen atoms, so it is said to be *unsaturated*, which means that it contains a double bond between the two carbons. Polymerisation proceeds via breaking of a double bond in the presence of an initiator (free radical, anionic, cationic or heterogeneous), which enables individual repeat units to join together to form a chain.

2.9.2 POLY(METHYL METHACRYLATE) (PMMA)

Polymethyl methacrylate (PMMA) is a thermoplastic acrylic resin (Figure 2.9.2) formed by polymerization of methyl methacrylate, and its molecular formula is $(C_5O_2H_8)_n$ (Myer, 2002).

Figure 2.9.2 has been removed due to the Copyright restrictions

Figure 2.9.2 Polymethyl methacrylate (PMMA) (from Smith and Javad, 2006)

PMMA was initially the polymer of choice for artificial cornea (Chapoy and Lally, 2008) and it was indeed the first synthetic polymer used in KPRO materials (Chirila, 2001). It is still used now a days as an optic and as skirt in keratoprosthesis devices since it is optically clear, but it is not permeable and does not promote epithelialization (Xie *et al.*, 2001).

On the other hand, PMMA is biologically inert, transparent, and easy to fabricate and can be manufactured to a broad range of optical powers (Guo, 2001).

However, the success of the PMMA keratoprosthesis has been plagued by problems including extrusion, glaucoma and opaque fibrous membrane formation (Patel *et al.*, 2006).

2.9.3 POLY(2-HYDROXYETHYL METHACRYLATE) (PHEMA)

Poly(2-hydroxyethyl methacrylate) (PHEMA) (Figure 2.9.3) has the molecular formula $(C_6H_{10}O_3)_n$ and forms a hydrogel in water.

Figure 2.9.3 has been removed due to the Copyright restrictions

Figure 9.2.3 Poly(2-hydroxyethyl methacrylate) (PHEMA) (from Ratner, 2004)

PHEMA is a biomaterial with a record of ocular tolerance in applications such as contact lenses and intraocular lenses (Chirila, 2001). PHEMA has been used for the optic and skirt of KPROs because of its hydrophilicity, flexibility and the ability to change its porosity (porous or non-porous) by altering the water content. Thus, the optic is made of a transparent PHEMA gel to provide a refractive power similar to that of the human cornea. The skirt is made of an opaque high water content PHEMA sponge to encourage bio-integration with host tissue and thus promote retention of the implant. In the AlphaCor Type II device, the optic and the skirt were joined and the permanent bond formed at the molecular level is designed to prevent the down-growth of cells around the optic, which can lead to the formation of retro-prosthetic membranes, one of the major complications historically associated with artificial cornea (Chirila, 2001).

However, the PHEMA optic used in the BioKpro I, Collar-button Dohlman and AlphaCor Type II (see Table 2.10.1) devices does not promote epithelialization and there is evidence that in the thick and central part of the cornea there are insufficient nutrients to maintain a healthy cornea because the PHEMA is not permeable to large molecules (Xie *et al.*, 2001).

2.9.4 POLYTETRAFLUOROETHYLENE (PTFE)

Polytetrafluoroethylene (PTFE) (Figure 9.2.4) has the linear formula $(CF_2CF_2)_n$.

Figure 2.9.4 has been removed due to the Copyright restrictions

Figure 9.2.4 Polytetrafluoroethylene (PTFE) (from Houde et al., 2006)

PTFE is chemically inert and has very high oxygen permeability, good transparency, low refractive indices and high oxidative stability. The advantage of this polymer is that the porosity and pore size can be modified (Sweeney, 2006) and it promotes bio-integration of corneal tissue (Xie *et al.*, 2001). The disadvantage of PTFE is that epithelialization is not possible. PTFE has been used as the skirt on the BioKPROs I – III (Table 2.10.1).

ProplastTM is a composite of polytetrafluoroethylene (PTFE, TeflonTM) and vitreous carbon. ProplastTM skirt was incorporated in human patients using the Cardona nut-and-bolt Kpro by Girard (1993) for the first time, but fibroblast invasion into the ProplastTM, glaucoma and retinal detachment occurred.

Gore-TexTM is another form of porous PTFE, known as an expanded Polytetrafluoroethylene (ePTFE), which has been used as skirt material by Legeais in his BioKPRO, which was reported successful in clinical trials in human patients and is presently marketed in Europe (Hicks *et al.*, 1997; Chirila, 2001). However, ePTFE 200 μ m thick with 50 μ m pores showed that collagen filled the pores and the opaque material became translucent, but not sufficiently transparent to be used as an optic (Hicks *et al.*, 1997).

ProplastTM and Gore-TexTM (or ePTFE) have been compared in animal trials. ePTFE was found to be the most satisfactory in terms of biocompatibility with host tissue, but in some cases Gore-TexTM had become encapsulated with host tissue. ProplastTM presented

inflammatory response, giant foreign body cells and fibrovascular invasion (Hicks *et al.*, 1997).

2.9.5 POLYETHYLENE TEREPHTHALATE (PET)

Polyethylene terephthalate (PET) is a thermoplastic polymer resin of the polyester family, with a molecular formula of $(C_{10}H_8O_4)_n$ (Figure 3.9.5).

Figure 2.9.5 has been removed due to the Copyright restrictions

Figure 9.2.5 Polyethylene terephthalate (PET) (from Fakirov, 2002)

PET has been used as skirt in KPRO designs since it promotes bio-integration of corneal tissue; however it does not promote epithelialization.

Pintucci *et al.* (1995) used a flexible polyethylene terephthalate (DacronTM) as a skirt material in their KPRO design implanted in humans in a manner similar to the OOKP technique (section 2.10.2, page 66), with the skirt fixed to the corneal surface and covered with buccal mucosa. The optic was made of PMMA. The optic core-and-skirt junction presented some fixing problems related to the dissimilarity of the two materials, and 10% extruded in clinical trials.

2.9.6 HIGH DENSITY POLYETHYLENE (HDPE)

High density polyethylene (HDPE) is a polyethylene which consists of mostly linear chains (Figure 2.9.6). Therefore, highly linear polyethylene molecules can be closely packed and result in high density polyethylene, making it highly crystalline (up to 95%).

Figure 2.9.6 has been removed due to the Copyright restrictions

Figure 2.9.6 High density polyethylene (HDPE) (from Ward et al., 2005)

HDPE is a flexible thermoplastic polymer. Thus, HDPE is of particular interest as a biomaterial since it can easily be processed using conventional thermoplastic moulding and extrusion methods due to the fact that linear polymers can be shaped by application of heat (Ward *et al.*, 2005) and the process is reversible provided that chemical degradation does not occur.

2.9.7 ULTRA HIGH MOLECULAR WEIGHT POLYETHYLENE (UHMWPE)

Ultra high molecular weight polyethylene (UHMWPE) is a thermoplastic polymer with extremely long chains of polyethylene (Figure 2.9.1), which are aligned in the same direction and have a molecular weight between 2 and 6 million. Each chain is bonded to the others through van der Waals bonds between the molecules. The longer chains help to transfer load to the polymer bonds by strengthening intermolecular interactions, so that the UHMWPE can support high tensile loads, making this polymer very tough, with high impact strength. UHMWPE has a high resistance to chemicals and UV radiation, and is non-toxic.

UHMWPE has over 40 years of clinical history as a successful biomaterial for use in hip, knee, and most recently (since the 1980s), for spine implants (Kurtz, 2004). UHMWPE is widely used as a biomaterial due to its excellent mechanical properties, including resistance to wear and impact. Most interesting is that a variety of synthetic implants made of UHMWPE have been used in ophthalmology (Allan, 1999).

2.9.8 POLYETHER ETHER KETONE (PEEK)

Polyether ether ketone (PEEK) is a thermoplastic polymer and an aromatic polyether (Sakamoto, 2003), consisting of repeating monomers of two ether groups and a ketone group (Figure 2.9.7).

Figure 2.9.7 has been removed due to the Copyright restrictions

Figure 2.9.7 Polyether ether ketone (PEEK) (from Sakamoto, 2003)

An ether group contains an oxygen atom connected to two (substituted) alkyl (general formula C_nH_{2n+1}) or aryl (simple aromatic ring) groups, with general formula R-O-R'. A ketone group contains a carbonyl group (O=C) linked to two other carbon atoms, and it can be generally represented by the chemical formula $R_1(CO)R_2$.

Because of the symmetry of the benzene rings along the polymer backbone, PEEK has high mechanical strength and from the characteristic of almost linear chemical structure, the polymer has a crystalline phase (Sakamoto, 2003). PEEK is a semi-crystalline material, with excellent mechanical properties (Table 3.2.3) maintained to high temperatures. It exhibits two glass transition temperatures at around 140 °C and around 275 °C, depending on cure cycle and formulation.

PEEK has high resistance to chemicals, electricity and temperature, and excellent dimensional stability and large processing capabilities (Sakamoto, 2003).

PEEK film is an opaque (brown) material, which presents two distinctive sides:

- 1) **Bright side**, which is shine/glossy and smoother.
- 2) **Matt side**, which is slightly rough and lacking highlights or gloss.

PEEK is considered an advanced biomaterial used in medical implants. A great emphasis on the physiochemical and micro-morphology of the surfaces on PEEK implant has been investigated to produce an hydroxyapatite-like surface after the immobilisation of calcium ions. Also, the effects of the surface modification of PEEK implants and models have been assessed on their *in vivo* performance.

PEEK has been used as biomaterial due to its relative inertness, and hydroxyapatite (HA) and tricalcium phosphate (TCP) have been blended into sintered PEEK. It has also been used in spinal implants as a radiolucent alternative to metallic biomaterials in the spine (Kurtz and Devine, 2007).

PEEK biomaterials research has also focused on compatibility of the polymer with bioactive materials, including hydroxyapatite (HA), either as composite filler, or as a surface coating (Yu *et al.*, 2005; Fan *et al.*, 2004; Tan *et al.*, 2003; Abu Bakar *et al.*, 2003; Ha *et al.*, 1997). This material can be engineered today with a wide range of physical, mechanical, and surface properties, depending on their implant application (Kurtz and Devine, 2007).

2.9.9 APATITES

Apatites are groups of phosphate minerals. Phosphate minerals are those minerals that contain the tetrahedral coordinated phosphate (PO_4^{3-}) anion along with the freely substituting arsenate (AsO_4^{3-}) and vanadate (VO_4^{3-}). Also, chlorine (Cl^-), fluorine (F^-), and hydroxyl (OH^-) anions also fit into the crystal structure (Cruz *et al.*, 2005). Therefore, apatites are compounds that contain a divalent metal cation (primarily Ca^{2+} , Sr^{2+} , Ba^{2+} , Cd^{2+} , and Pb^{2+}), a phosphate (PO_4^{3-}) and a monovalent anion (OH^- , F^- , Cl^- , and Br^-). The calcium derivatives are by far the most abundant (Greenwood and Earnshaw, 1997).

Calcium phosphate is a compound of a family of minerals containing calcium ions (Ca^{2+}) together with orthophosphates (PO_4^{3-}) (Kingston *et al.*, 2003). Calcium orthophosphates are minerals of biological origin and are the most important inorganic constituent of hard tissue in vertebrate (Lowenstam and Weiner, 1989; Vallet-Regi and Gonzalez-Calbet, 2004). In the form of a non-stoichiometric, ion-substituted and calcium deficient hydroxyapatite (known also as biological apatite), calcium phosphates are present in bones, teeth, deer antlers and tendons of mammals (Dorozhkin, 2009). Apatite is an important biological mineral found in teeth and bones of vertebrates (Nickel, 1995).

Hydroxyapatite (HA) is referred to as an apatite with a high concentration of OH^- ions in the crystal. The formulae of HA is $\text{Ca}_5(\text{PO}_4)_3(\text{OH})$, usually written as $\text{Ca}_{10}(\text{PO}_4)_6(\text{OH})_2$ to denote the two molecules of the crystal unit cell.

Calcium phosphate related to the hexagonal hydroxyapatite, $\text{Ca}_{10}(\text{PO}_4)_6(\text{OH})_2$, with small quantities of other elements such as Na^+ , Cl^- and Mg^{2+} substituted into the crystal structure are found in the inorganic part of the tooth enamel of human (Gutierrez-Salazar and Reyes-Gasga, 2003; Tadic *et al.*, 2001). The apatite contained in enamel, dentine and bone mineral is calcium-deficient biologic apatite (Legeros *et al.*, 2003). Dental enamel contains approximately 98% of biological apatite (calcium deficient hydroxyapatite) and 2% of bio-organic compounds and water. Dentine contains approximately 50% of biological apatite, 30% of bio-organic compounds and 20% of water (Nelson, 2009; Dorozhkin, 2009). Interestingly, the Ca/P molar ratio of dental enamel is 1.63 and the Ca/P

molar ratio of dentine is 1.61 (Legeros, 1991; Dacusi *et al.*, 1997).

In biological apatites (as in tooth and bone) the OH^- or PO_4^{3-} ions can be replaced by carbonate, CO_3^{2-} . It crystallizes in a hexagonal crystal system. The substitution of the carbonate group occurs either in the PO site (for the B type apatite substitution), or in the OH site (for the A type of apatite substitution) (Jokanovic *et al.*, 2006; Tadic *et al.*, 2001).

Additionally, the chemical composition of many calcium orthophosphates includes hydrogen, either as part of an acidic orthophosphate anion (HPO_4^{2-} or H_2PO_4^-), hydroxide ($\text{Ca}_{10}(\text{PO}_4)_6(\text{OH})_2$) and/or incorporated water ($\text{CaHPO}_4 \cdot 2\text{H}_2\text{O}$). Different combinations of CaO and P_2O_5 (both in the presence of water and without it) provide a large variety of calcium phosphates, which are differentiated by the type of the phosphate anion: ortho- (PO_4^{3-}), meta- (PO_3^-), pyro- ($\text{P}_2\text{O}_7^{4-}$) and poly- ($(\text{PO}_3)_n^{n-}$). In the case of multi-charged anions (orthophosphates and pyrophosphates), calcium phosphates are also differentiated by the number of hydrogen ions attached to the anion, for instance, mono- ($\text{Ca}(\text{H}_2\text{PO}_4)_2$), di- (CaHPO_4), tri- ($\text{Ca}_3(\text{PO}_4)_2$) and tetra- ($\text{Ca}_2\text{P}_2\text{O}_7$) calcium phosphates (Legeros, 1991; Elliot, 1994, Amjad, 1997; Dorozhkin, 2009).

The atomic arrangement of calcium orthophosphates is built up around a network of orthophosphate (PO_4) groups, which provides stability to the structure. The majority of calcium orthophosphates are soluble in water and insoluble in alkaline solutions (Dorozhkin, 2009). However, the calcium phosphates that can be precipitated from aqueous solutions will be discussed in detail in this thesis.

Calcium phosphates can be prepared by precipitation from supersaturated aqueous of calcium and phosphate-containing salts (Hofmann *et al.*, 2007). Synthetic calcium phosphates are used as implant materials due to their biocompatibility, bonding ability, and their similarity to the mineral phase of bone (Gutierrez-Salazar and Reyes-Gasga, 2003; Hofmann *et al.*, 2007).

Therefore, calcium phosphates can be used as biomaterials due to the excellent biocompatibility (Ginebra *et al.*, 2004; Cai and Tang, 2008) since their chemical similarity

to the mineral component of bones and teeth (Vallet-Regi and Gonzalez-Calbet, 2004; Weiner and Wagner, 1998; Dorozhkin, 2007; Dorozhkin, 2009). Moreover, calcium phosphates are non-toxic, not recognized as foreign materials in the body and, most importantly, exhibit bioactive behaviour and integrate into living tissue (Dorozhkin, 2009). The calcium phosphates that can be precipitated from aqueous solutions are listed in Table 2.9.1 together with their Ca/P molar ratio and their chemical formula.

Table 2.9.1 Calcium phosphate compounds that can be deposited from aqueous solutions (data from Dorozhkin, 2007; Dorozhkin, 2009)

Calcium Phosphate Compounds	Chemical formula	Ca/P molar ratio
Hydroxyapatite (HA)	$\text{Ca}_{10}(\text{PO}_4)_6(\text{OH})_2$	1.67
Calcium-deficient hydroxyapatite (CDHA)	$\text{Ca}_9(\text{HPO}_4)(\text{PO}_4)_5(\text{OH})$	1.5
Calcium-deficient hydroxyapatite (CDHA)	$\text{Ca}_{10-x}(\text{HPO}_4)_x(\text{PO}_4)_{6-x}(\text{OH})_{2-x}$ ($x=1$ when $\text{Ca/P}=1.5$)	$1.5 > 1.67$
Mono-calcium phosphate monohydrate (MCPM)	$\text{Ca}(\text{H}_2\text{PO}_4)_2 \cdot \text{H}_2\text{O}$	0.5
Di-calcium phosphate dihydrate (DCPD)	$\text{CaHPO}_4 \cdot \text{H}_2\text{O}$	1.0
Octa-calcium phosphate (OCP)	$\text{Ca}_8(\text{HPO}_4)_2(\text{PO}_4)_4 \cdot 5\text{H}_2\text{O}$	1.33

The hydroxyapatite (HA) structure was described as aggregation of $\text{Ca}_9(\text{PO}_4)_6$ clusters in 1964 (Kay *et al.*, 1964; Treboux *et al.*, 2000). This hexagonal structure of HA ($\text{Ca}_{10}(\text{PO}_4)_6(\text{OH})_2$) is a more common one for biomedical applications (Elliot, 1994; Mathew and Takagi, 2001; Hughes and Rakovan, 2002; White and Dong, 2003) since it can be formed from precipitated solutions such as Simulated Body Fluids (SBFs). In fact, the precipitates are generally non-stoichiometric, suggesting intermediate formation of precursor phases (Dorozhkin, 2009). The surface of freshly precipitated HA is composed of a structured hydrated layer containing easily exchangeable mobile ionic species (Cazalbou *et al.*, 2004). Usually unsintered HA is poorly crystalline and often non-stoichiometric, resembling calcium deficient hydroxyapatite (CDHA).

Interestingly, pure HA never occurs in biological systems. However, due to the chemical similarities to bone and teeth mineral, HA is widely used as a coating on orthopedic, dental implants (Hench, 1991; Suchanek and Yoshimura, 1998; Hench, 1998; Willmann, 1999; Ong and Chan, 1999; Sun *et al.*, 2001; Geesink, 2002) and other diverse biomedical implants (Aoki, 1991; de Groot *et al.*, 1998; Gross and Berndt, 2002; Ferraz *et al.*, 2004; Damien and Revell, 2004; Barinov and Komlev, 2008). HA particles can also be implanted (Mangano *et al.*, 2008).

Moreover, HA has been used for a long time in liquid chromatography of nucleic acids, proteins and other biological compounds (Dickinson, 1956; Bernardi, 1965; Doonan, 2004; Jungbauer *et al.*, 2004; Smith and Gingrich, 2005; Yoshitake *et al.*, 2006; Xia *et al.*, 2008; Brand *et al.*, 2008) and for drug delivery purposes (Liu *et al.*, 2005; Palazzo *et al.*, 2005) due to its similarity to biological apatite.

Calcium-deficient hydroxyapatites (CDHA) have a variety of Ca/P molar ratios and this has been explained through various models: Surface adsorption, lattice substitution and intercrystalline mixtures of HA and octa-calcium phosphate (OCP) (Rodriguez-Lorenzo, 2005). Due to a lack of stoichiometry, CDHA usually contains other ions (Rey *et al.*, 2006). The extent depends on the counter-ions of the chemicals used for preparation (Na^+ , Cl^-).

CDHA may be considered as HA with some ions missing (Brown and Martin, 1999; Zahn and Hochrein, 2008). The more calcium is deficient, the more disorder and imperfections are in the CDHA structure (Honghui *et al.*, 2007). According to the chemical formula of CDHA (Table 2.9.1), there are vacancies of Ca^{2+} (mainly on Ca sites) and OH^- ions in crystal structure of this compound (Mortier *et al.*, 1989; Jeanjean *et al.*, 1996; Brown and Martin, 1999; Wilson *et al.*, 2003; Wilson *et al.*, 2005; Zahn and Hochrein, 2008). However, the vacancies of orthophosphate ions are not known, for instance in CDHA, a portion of PO_4^{3-} ions is either protonated (as HPO_4^{2-}) or substituted by other ions (CO_3^{2-}) (Ivanova *et al.*, 2001).

Therefore, in CDHA: Ca^{2+} can be substituted by Na^+ , K^+ , Mg^{2+} , Sr^{2+} , the PO_4^{3-} by CO_3^{2-} , the HPO_4^{2-} by CO_3^{2-} and OH^- by F^- , Cl^- , CO_3^{2-} plus some water forming biological apatite, which is the main inorganic part of animal and human calcifications (Legeros, 1991; Rey *et al.*, 2006; O'Neill, 2007). Thus, CDHA is a very promising compound for industrial manufacturing of artificial bone and teeth substitutes as well other artificial compounds (Tsuchida *et al.*, 2008).

Mono-calcium phosphate monohydrate (MCPM) is a highly acidic compound, which due to its acidity is not found in biological calcification. In addition, pure MCPM is not biocompatible (Koster *et al.*, 1977; Williams, 1999). Despite this, MCPM can be used as a component of self-hardening calcium orthophosphate cements in the medical field (Bermudez *et al.*, 1994; Bermudez *et al.*, 1994; Driessens *et al.*, 1994; Huan and Chang, 2009).

Di-calcium phosphate dihydrate (DCPD) can be precipitated from aqueous solutions (Arsic *et al.*, 2004; Qiu and Orme, 2008). DCPD is mostly found in calcification in humans due to the pathological lesions (Legeros, 1991; Legreos, 2001; Becker *et al.*, 2004; O'Neill, 2007). DCPD has been studied as an intermediate in bone mineralization and dissolution of enamel in acid (dental acidity) (Legeros, 1991; Legeros, 2001; O'Neill, 2007). Moreover, DCPD may be used in calcium orthophosphates cements and in tooth remineralisation in the medical field (Bermudez *et al.*, 1994; Kurashina *et al.*, 1997; Driessens *et al.*, 1998; Takagi *et al.*, 1998; Yamamoto *et al.*, 1998).

Octa-calcium phosphate (OCP) is usually found in unstable intermediate compounds during the precipitation of the calcium phosphates in aqueous solutions (Legeros, 1985; Bigi *et al.*, 1999; Nakahira *et al.*, 2001; Shelton *et al.*, 2006). OCP is of great biological importance because it is one of the stable components of human dental and urinary calculi (Schroeder, 1969; Legeros, 1974; Chow and Eanes, 2001). OCP plays an important role *in vivo* in the formation of apatitic biominerals. In the medical field, OCP is used for bone defect as implantable filler (Kamakura *et al.*, 1999; Kamakura *et al.*, 2001; Sargolzaei-Aval *et al.*, 2004; Suzuki *et al.*, 2006; Suzuki *et al.*, 2008; Kikawa *et al.*, 2009).

To conclude calcium hydroxyapatite (CaHA) is a biocompatible material because it contains Ca^{2+} , PO_4^{3-} and OH^- ions; the ions that human tissue has in relatively high percentage (Jokanovic *et al.*, 2006). However, most synthetic apatites differ from stoichiometric apatite as well as from biogenetic carbonate hydroxyapatite (CHA) by their composition and particularly their CO_3^{2-} content (Hofmann *et al.*, 2007). A common feature of bioactive materials is that their surfaces develop a biologically active carbonate hydroxyapatite layer after implantation. For a material to be bioactive *in vivo*, it must have the ability of induce CHA formation on its surface *in vitro* (Ni and Wang, 2002).

2.9.10 SIMULATED BODY FLUID (SBF)

1.5 SBF was used in this study as a treatment to produce Ca/P layer on the surface of the polymers to make them bioactive, before implantation. While it is important to perform the material tests in conditions which replace or simulate the body environment this was not the primary purpose for the use of 1.5 SBF in this study. It should, however, be noted that since SBF has an ion concentration and pH which is close to that of the human blood serum (Renke-Gluszko and Fray, 2004), its characteristics are similar to those of the aqueous humour fluid in tears which resembles blood plasma in composition, but contains less protein and glucose and more lactic acid and ascorbic acid (Tiffany *et al.*, 1989; Nagyova and Tiffany, 1999).

Simulated Body Fluids (SBFs) are acellular solutions suitable to study the bioactivity behaviour of a material *in vitro* on the basis that the ion concentration in SBF is similar to that of human blood plasma. The first SBF was developed by Kokubo and his colleagues in 1987, in order to perform *in vitro* simulation of *in vivo* conditions (Kokubo *et al.*, 1987). It was designed to explore *in vitro* bioactivity of different materials intended for implants as a preliminary analysis. Since then this technique has been widely used to evaluate the potential of materials, coatings and surgical implant devices to predict the bone bonding ability. This means that the *in vivo* bone bioactivity of materials may be predicted by examining apatite formation on its surface after being immersed in SBF for a period of time (Kokubo and Takadama, 2006).

The history of the SBF was summarised by Kokubo and his group recently (Kokubo and Takadama, 2006), where the interaction between the ability to form apatite on different materials soaked in SBF and their *in vivo* bone bioactivities were reported from the first time SBF was used through to the latest formulations. This review included the different approaches to produce biomaterials up to the development of novel bioactive materials based on the formation of apatite on their surfaces.

Various Simulated Body Fluids (SBFs) have been used to assess the bioactivity of artificial materials *in vitro* (Chan *et al.*, 2004; Juhasz *et al.*, 2008). The materials are exposed to a SBF to evaluate its bioactivity and to analyse its evolution over the time (Auclair-Daigle *et al.*, 2005). The evaluation is assessed by examining the ability to form apatite from the solution, and the evolution is assessed by testing structure, chemistry and mechanical adhesion of the coatings on the surface (Gu *et al.*, 2003).

Simulated Body Fluids (SBFs) have been used *in vitro* to study apatite formation or apatite precipitation on the surfaces of different types of biomaterials, such as metals, polymers, ceramics and composites (Kokubo *et al.*, 1990; Kokubo *et al.*, 1991; Huang *et al.*, 1997; Tanahashi and Matsuda, 1997; Kawashita *et al.*, 2003; Jonasova *et al.*, 2002; Oyane *et al.*, 2005; Muller and Muller, 2006; Kokubo and Takadama, 2006).

The apatite layer formed on the materials surfaces after being exposed to SBF could define its bioactivity in the process of biomineralisation. Therefore, the formation of the calcium phosphate deposits that occur on the surface of materials soaked in SBF is used to predict the bioactivity of a material. The process of producing minerals from living organisms to modify or restore functionally the existing tissues is known as biomineralisation. By definition, a bioactive material is “a material that elicits a specific biological response at the interface of the material, which results in the formation of a bond between the tissue and the materials” (Hench, 1998) (see detail discussion in sections 2.8, and 2.13). Thus, a material may be considered bioactive is it reacts with or affects cells or tissues in the human body. Hence, the *in vitro* deposition of calcium and phosphate formed on the surface of a material as layers or coatings of apatite is a potential biomaterial.

Apatite is a form of calcium phosphate, known as hydroxyapatite, $\text{Ca}_5(\text{PO}_4)_3\text{OH}$; fluorapatite, $\text{Ca}_5(\text{PO}_4)_3\text{F}$; and chlorapatite, $\text{Ca}_5(\text{PO}_4)_3\text{Cl}$, depending on the high concentration of hydroxide (OH^-), fluorine (F^-), or chlorine (Cl^-) ions, respectively. Calcium phosphates can also be prepared by precipitation from supersaturated aqueous of calcium and phosphate-containing salts (Hofmann *et al.*, 2007), such SBFs.

Recently, Kokubo and his colleagues (2006) reviewed the SBF method for the two decades since SBF was first developed, and they insisted that SBF could be used to assess bioactivity, and that the formation of apatite on a material immersed in SBF is a proof of its bioactivity and can be used to predict its bone bonding ability *in vivo*; those statements are in agreement with Ohtsuki *et al.* (1992), Kawashita *et al.* (2003), Renke-Gluszko and Fray (2004), and Auclair-Daigle *et al.* (2005). Slightly contradictory, Oyane *et al.* (2003) assessed the conventional SBF and developed a revised SBF for *in vitro* bioactivity assessment of artificial materials and for biomimetic production of bone-like apatite, on the basis of the finding that a large amount of calcium and magnesium ions present in the SBF is bound to proteins and hence apatite formation did not arise. More recently, Bohner and Lemaitre (2009) published an interesting paper arguing that a SBF method is insufficient evidence to test the bioactivity of a material and concluded that such an assumption needs improvement; the SBF ion concentration is not identical to the body fluids in humans and the test is usually not conducted in the appropriate conditions, for example, an adequate partial pressure since human serum is in equilibrium with a CO_2 partial pressure of 0.05 atm. This lack of correlation between *in vitro* and *in vivo* bioactivity results, which has been commented on by Ohura *et al.* (1996), Walsh *et al.* (2003), Apelt *et al.* (2004); Chan *et al.* (2004), Theiss *et al.* (2005) and Juhasz *et al.* (2008) require to be further investigated until consistent results are obtained.

Many attempts have been made to produce apatite-polymer composites in a biomimetic manner since apatite nucleation could be formed on organic polymers due to the presence of functional groups. The polymers are then immersed in SBF for the further growth of apatite (Kawashita *et al.*, 2003). Despite all experimental trials, the ability to form apatite on polymers is still poor. However, over a decade ago Tanahashi and Matsuda (1997) demonstrated that carboxyl groups ($-\text{COOH}$) were effective to nucleate apatite in self-assembled monolayers. Thus, since then, it has been believed that polymers with

certain functional groups such as carboxyl could form apatite on their surfaces when immersed in SBF.

Basically, the biomimetic process of the apatite layer formation on polymers occurs in two stages. During the first stage, the polymer is subjected to a severe alkaline solution; for instance, highly concentrated NaOH, and then immersed in SBF at 37 °C, to induce the apatite nuclei formation on the polymer surface. In the second stage, the SBF solution, in which the polymer is immersed, is renewed with a fresh SBF solution, to make the apatite nuclei grow and with time cover the polymer surface. The apatite coating thickness depends on the SBF immersion time of the second stage. The adhesion properties of the coatings may depend on the polymer type (Renke-Gluszko and Fray, 2004).

The apatite nuclei induction time is usually from 1 to 3 days for the majority of the polymers reported in the literature: Polyethylene terephthalate (PET), polymethyl methacrylate (PMMA), polyether sulfone (PESF), polyethylene (PE), polyamide 6, or poly(tetrafluorethylene) (PTFE) (Kokubo, 1996; Huang *et al.*, 1997; Kokubo, 1998; Kim *et al.*, 1999; Kawashita *et al.*, 2003). The apatite deposition on the polymer may occur on day 1 of the SBF immersion of the second stage; however, it has been reported that it mostly happens after day 3 and could grow to form a thick apatite layer after 15 to 30 days of incubation in SBF. Kawashita *et al.* (2003) have reported that carboxyl group-containing polymers gels in SBF can form apatite on the fibres. Huang *et al.* (1997) used SBF to investigate the apatite formed on Bioglass®-reinforced high density polyethylene composite, to mention few examples from literature.

In the last decade, different strengths of SBF have often been used *in vitro* to aid apatite formation or precipitation on surfaces of different types of biomaterials, such as metals, polymers and ceramics (Kokubo *et al.*, 1990 and 1991; Janasova *et al.*, 2002; Oyane *et al.*, 2005; Yu *et al.*, 2005; Muller and Muller, 2006; Huang *et al.*, 2007). The modifications of SBFs have shown that it is possible to obtain thicker carbonated apatite layers and also the formation of homogeneous apatites. It is believed that a concentrated SBF could be used to accelerate the SBF coating processes. For instance, Kim *et al.* (1999) have used 0.75-2.00 SBF on polyethylene terephthalate (PET) to study the apatite formed. All these results have demonstrated positive results testing the bioactivity *in vitro* on

materials.

As mentioned early, NaOH induces the formation of apatite nuclei (calcium phosphate) on the polymeric film surfaces. On the other hand, any potential released Na^+ might cause external alkalization that triggers an inflammatory response and leads to cell death (Jonasova *et al.*, 2002). Therefore, the lower the concentration of NaOH, the less harmful it would be for the patient. The apatite nuclei formed initiate the deposition of calcium and phosphate ions from the surrounding fluid (Kokubo *et al.*, 1991). Thus apatite nuclei stimulate the growth of carbonate hydroxyapatite (CHA) layers when immersed in SBFs producing bioactive material. Kim *et al.* (2000) suggested that the bioactivity of the apatite-polymer depends on the structure and composition of the formed apatite.

Finally, the aim for the artificial materials is to be implanted in the human body to support or restore the normal functionality in a specific area. For instance, an artificial cornea implant may replace the cornea functionality including its metabolic process. Therefore, it is extremely important to perform the material tests in conditions which replace or simulate the body environment. SBF offers such conditions to a certain extend, due to its ion concentration being close to the human blood serum, typically at temperature of 37 °C and a PH of 7.4. Thus, SBF is proposed to be used in order to predict material behaviour through the apatite layer formation on the material surface (Renke-Gluszko and Fray, 2004).

2.10 ARTIFICIAL CORNEA IMPLANTS

Commonly, there are two procedures to replace the damaged cornea using an artificial device:

The keratoprosthesis (KPRO), which consists of a clear central optic and a sewing skirt to anchor the implant.

The Osteo-odonto-keratoprosthesis (OOKP) is a KPRO device with a tooth dentin based skirt and a PMMA optic.

First, KPROs are described in general followed by detailed discussion of OOKP.

2.10.1 KERATOPROSTHESIS (KPRO)

In the instance of failure of cornea transplant from donor eyes, an opaque cornea can be replaced with an artificial cornea, keratoprosthesis, (KPRO) (Refojo, 2005). KPRO is required for patients with bilateral corneal blindness who suffer from tear deficiency, chemical burns, trachoma, vascularization, Stevens-Johnson syndrome, ocular cicatricial pemphigoid, or uncontrollable intraocular pressure. Patients with these conditions cannot be treated with penetrating keratoplasty (PK) (Hicks *et al.*, 1997; Legeais and Renard, 1998; Kim *et al.*, 2002; Falcinelli *et al.*, 2005).

KPRO is also advised for the treatment of severe corneal opacities not suitable for PK procedure (Falcinelli *et al.*, 2005). Patients with severe ocular surface diseases, successive graft failures and paediatric patients with congenital corneal opacities are not recommended to undergo a PK procedure (Moffatt *et al.*, 2005); thus, KPRO might be an alternative for these patients. On the other hand, some patients cannot undergo PK with donor tissue due to disease severity, religious or ethical objection to the use donor tissue, failed past donor tissue transplants, or where measures required to prevent graft rejections are medically contraindicated (IPAC, 2004). Therefore, the best alternative at the moment for the majority of these patients is a keratoprosthesis (KPRO) intervention.

Generally, there are two types of cornea replacement designs:

Central optic-and-skirt keratoprosthesis (Figure 2.10.1), which consists of a clear central optic and an annular porous surround, or skirt, designed to provide tissue integration between the prosthesis and the recipient cornea (Albon, 2003; Hicks *et al.*, 2005; Myung *et al.*, 2007).

Figure 2.10.1 has been removed due to the Copyright restrictions

Figure 2.10.1 Central optic-and-skirt keratoprosthesis (from Ilhan-Sarar, 2005)

Collar-button keratoprosthesis, which holds the optical cylinder of the prosthesis to the recipient cornea by means of front and back plastic plates (Figure 2.10.2). PMMA is the most commonly used material in cornea replacements (Refojo, 2005).

Figure 2.10.2 has been removed due to the Copyright restrictions

Figure 2.10.2 Collar-button keratoprosthesis (from Dohlman and Harissi-Dagher, 2007)

The different designs of KPRO vary mainly in their skirt (Myung *et al.*, 2008), while the optical is basically the same being PMMA. Various KPRO models have been used in a few countries for small number of patients with varying degrees of success. The Strampelli, Cardona and Dohlman KPROs have become the most commonly used models, which involve a rigid polymethylmethacrylate (PMMA) optic (Hicks *et al.*, 2000; Guo, 2001) with an anchoring surround with a front plate and a back plate. There are currently two totally synthetic KPROs and a semi-synthetic KPRO available commercially:

The Legeais BioKPRO III, which uses a skirt of porous polytetrafluoroethylene (PTFE). The device (Figure 2.10.3) consists of a central 5 mm clear silicone optic chemically bonded to a 10 mm opaque fluorocarbon PTFE porous skirt (Hollick *et al.*, 2006).

Figure 2.10.3 has been removed due to the Copyright restrictions

Figure 2.10.3 The Legeais BioKpro III before implantation (from Hollick et al., 2006)

AlphaCor (previously known as the Chirila KPRO, Figure 2.10.4), which uses a porous polyhydroxyethylmethacrylate (PHEMA) (Chirila *et al.*, 1995).

Figure 2.10.4 has been removed due to the Copyright restrictions

Figure 2.10.4 AphaCor™ keratoprosthesis (from Chirila et al., 1995)

Osteo-odonto-keratoprosthesis (OOKP), a semi-synthetic KRPO (Figure 2.10.5), uses an autologous tooth as a form of biological hydroxyapatite (Viitala *et al.*, 2009) as a skirt and an optical cylinder (Figures 2.10.5 and 2.10.6). Further details on this approach are given in section 2.10.2.

Figure 2.10.5 has been removed due to the Copyright restrictions

Figure 2.10.5 Schematic representation of the tooth lamina and optical cylinder of the OOKP design (from Tan et al., 2005)

Figure 2.10.6 has been removed due to the Copyright restrictions

Figure 2.10.6 Dentil lamina used a skirt in the OOKP (from Liu et al., 2007)

Table 2.10.1 summaries the KPRO most recognized designs, whose developments and modifications are further detailed, including the results in human trials.

Table 2.10.1 Keratoprosthesis used in human clinical trials (data from Cardona, 1962; Strampelli, 1963; Cardona, 1969; Dohlman and Doane, 1994; Legeais et al., 1997; Legeais and Renard, 1998; Hicks et al., 2000, Crawford et al., 2002; Allan, 2002; Albon, 2003; Falcinelli et al., 2005; Bleckmann and Holak, 2006; Hollick et al., 2006; Viitala et al. 2009)

Author	KPRO design	Optic Material	Skirt	Results	Complication
Strampelli (1963)	OOKP	PMMA	Tooth surrounded by buccal mucosa sutured to cornea	17/85 retained the KPRO but poor aseptic eyes	Glaucoma, membrane formation, extrusion
Falcinelli (2005)	Strampelli modified OOKP	PMMA	Osteodental lamina and mucous epithelium	Rate unknown: 108 excluded and 40 retained of 153	Extrusion, glaucoma
Cardona (1962, 1969)	Central optic and skirt	Acrylic PMMA	Intra-lamellar plate Attached by screws	17/31 retained the KPRO and vision was improved	Membrane formation, glaucoma, extrusion
Dohlman (1994)	Collar button	PMMA	PMMA	6/13 KPRO were retained and vision was improved	Aqueous leakage, extrusion, membrane formation, retinal detachment, 2/13 removed
Chirila (2000)	AlphaCor Type I	PHEMA	PHEMA Attached by PIN	KPRO removed and PK	Conjunctivitis
Chirila (2002)	AlphaCor Type II	PHEMA	PHEMA	28/38 retained the KPRO and uncomplicated post-surgery	Aqueous leakage, membrane formation
Legeais (1997)	BioKPRO I	PMMA Lens removal	PTFE Attached by clips	47/73 retained the KPRO and 34/73 improved vision	Extrusion, membrane formation, glaucoma
Legeais (1998)	BioKPRO II	PDMS coated PVP	PTFE Chemically fused	11/13 KPRO clinically stable and 7/13 improved vision	No epithelial coverage, membrane formation, necrosis, extrusion
Legeais (2001)	BioKPRO III	PDMS coated PVP	PTFE Chemically fused	1/7 retained the KPRO and improved vision	Extrusion, membrane formation

The Strampelli, Cardona and Dohlman KPROs have been the implants mostly used in Europe. These models have been implanted in humans and there are plenty of published results from their trials, which will be discussed later. There are also two completely synthetic KPROs: the Legeais BioKPRO III and AlphaCor (previously known as the Chirila KPRO). These devices recently have been implanted into patients and the published outcomes are detailed in this section.

The Strampelli osteo-odonto-keratoprosthesis (OOKP) replaces the cornea with a PMMA optical cylinder glued to a biological support (haptic) made by human living tissue (ie, the autologous osteodental lamina) (Falcinelli *et al.*, 2005). The Strampelli OOKP remains the KPRO of choice for end-stage corneal blindness not amenable to penetrating keratoplasty (PK), its rigid optical cylinder gives excellent image resolution and quality (Moffatt *et al.*, 2005).

Early British followers of the Strampelli technique reported poor retention results (Casey, 1999). Falcinelli modified this technique and it was re-introduced into Britain in 1996 (Liu *et al.*, 1998). The Falcinelli OOKP is capable of providing acceptable results, particularly for patients with corneal blindness untreated by other approaches (Parel and Sweeney, 2005). Published results from clinical trails using a modified OOKP (Falcinelli *et al.*, 1987; Falcinelli *et al.*, 1993; Falcinelli *et al.*, 1999) suggest good long term retention (85% in 18 years) with 75% of patients seeing 6/12 or better (Liu *et al.*, 1998; Parel and Sweeney, 2005).

The modified OOKP provides satisfactory long-term anatomical and functional results mainly because the OOKP is an autograft made of living human tissue, the haptic is made of dentine, an avascular hard tissue with a slow metabolic exchange. All these biological properties prevent retro-prosthetic membrane formation and infections and provide protection and nutrition to the underlying bone (Ricci *et al.*, 1992; Falcinelli *et al.*, 2005).

However, the Falcinelli OOKP implant failure is related to poor tissue integration, which would appear to be significantly less than for the BioKPRO III and AlphaCor devices (Viitala *et al.*, 2009). Also the OOKP requires the extraction of at least one of the

patient's teeth which has disadvantages compared with using synthetic materials (Falcinelli *et al.*, 2005).

The Cardona KPRO is a combined intra-lamellar/perforating KPRO with a transparent central perforating cylinder and a holding lamellar plate. A later design known as a „nut-and-bolt“ KPRO consists of an external cosmetic contact lens of coated PMMA and a PMMA cylinder, which screwed into the contact lens and also into the PMMA nut that is placed against the endothelium (Cardona, 1991; Hicks *et al.*, 1997). This device reduces evaporation, has a thicker supporting tissue. It also has a covered junction between the cylinder and the host stroma, and no need for donor corneal tissue.

Hicks *et al* (1997) explained that the Cardona KPRO design reduces extrusion because the front plate, which is fixed to the corneal surface, is also buried. Cardona KPRO designs reinforced with donor sclera, autologous tissue (i.e. lid skin) or synthetic materials have been developed by others (Chilaris and Liaricos, 1973; Cardona and DeVoe, 1977; Cardona, 1983; Girard, 1983) and their outcomes include serious complications such as retro-prosthetic formation and glaucoma. However, of 31 patients, 22 improved their independence level, 17 achieved 6/60 visual acuity, 5 maintained 6/12 visual acuity, and the best outcome was 6/6 in 1 patient. Cardona KPROs modified with a nylon skirt, a Dacron™ skirt, a PMMA flange, and a modified nut-and-bolt arrangement with Dacron™ reinforcement have all presented serious problems (Rao *et al.*, 1979; Aquavella *et al.*, 1982; Cardona, 1983; Girard, 1983). Cardona described in detail his latest KPRO with good average results and pointed out that it was a more less invasive surgery (Cardona, 1991).

The Dohlman KPRO is a „collar-button“ of PMMA. The anterior plate has a short stem which pierces a donor corneal button, and a back plate is either threaded onto it or glued. Initial results from 1974 were disappointing, due to „melting“ of the surrounding corneal stroma, causing complications such as aqueous leakage, exposure, extrusion and retinal detachment. Ulceration could be avoided if cyanoacrylate glue were used to prevent the epithelium and tears from getting under the anterior plate (Hicks *et al.*, 1997).

There are two types of Dohlman's latest designs:

Type I is used in eyes with good tear and blinking conditions.

Type II has an added anterior nub for through-the-lid placement in end-stage dry eye (Yaghouti and Dohlman, 1999).

These modified devices are simple, minimum swelling of the tissue around the prosthesis is achieved and repair of necrosis is relatively easy (Dohlman and Doane, 1994). In a recent report, 91.1% of Dohlman KPROs were retained, although glaucoma shunting was performed in 60.4% of the patients (Dohlman *et al.*, 1996).

AlphaCor is a synthetic cornea implant made from PHEMA that has a peripheral region with interconnecting pores allowing bio-integration with surrounding corneal tissue. The surgery is performed in two stages. In stage I, the PHEMA cornea is placed within a lamellar corneal pocket with tissue posterior to the optic, which is removed at the time of implantation. In stage II, the tissue anterior to the optic is removed. The porous skirt remains enclosed with corneal stromal tissue, both (skirt and stroma tissue) bio-integrate due to the cellular colonization of the skirt and collagen deposition (Hicks *et al.*, 2005).

More than 150 AlphaCor devices have been implanted into human recipients. In a follow-up of 40 patients 30% exhibited complications associated with poor tissue integration. Of 14 extruded cases, 5 presented complications related to the optic (calcification caused by topical medication or fungal invasion of the optic), of which 3 developed stromal leakage and breakdown. Also, 8 were removed due to melting of corneal tissue anterior to the device skirt and 1 due to a retro-prosthetic membrane (Hicks *et al.*, 2005). Importantly, this device can be replaced with a donor graft in the event of the development of significant complication. Moffatt *et al.* (2005) concluded that the AlphaCor devices, despite the different designs available, has yet to show that it is clinically superior and further evaluation and development is required.

Legeais developed a KPRO made of a porous PTFE skirt and a PMMA optic (Legeais *et al.*, 1991; Legeais *et al.*, 1992; Legeais *et al.*, 1993) and his modified devices are known as BioKPROs I, II and III:

The BioKPRO I had four pieces: a PMMA optic, a PTFE skirt, PMMA fixation clips and a PMMA sealing ring (Hollick *et al.*, 2006). Thus, the optic made of PMMA was attached by clips to a supporting skirt of a biocolonizable expanded PTFE. The crystalline lens was removed in all patients because of the thickness of the central optic. Visual acuity was improved in half of the patients, but a high rate of implant extrusion had occurred, and other severe problems such as retroprosthetic membrane formation, leakage and endophthalmitis.

The BioKPRO II has only 2 fused pieces: a soft optic and a skirt. The optic was a soft polydimethylsiloxane (PDMS) copolymer coated with polyvinylpyrrolidone (PVP), and the skirt was white opaque of hydrophobic fluorocarbon haptic (PTFE). The optic was chemically fused with the supporting colonisable skirt instead of the clips that formed the mechanical junction between the optic and the skirt. The dimensions of the new optic were close to those of the human cornea. Also, the biocolonisation was faster due to the modification of the optic support, but the optic and junction were not covered by epithelial cells (Legeais and Renard, 1998). This device was successful in human clinical trials (Legeais *et al.*, 1997; Legeais and Renard, 1998), and is presently marketed in Europe (Chirila, 2001), available from France Chirurgie Industries (FCI) SA, Paris, France as the BioKPsil.

However, in clinical series of patients implanted with BioKPROs I and II failure was up to 40% within 1 year, with retraction of the surface tissue over the haptic element, retroprosthesis membrane formation, infection, or aqueous leakage, and in many cases the implant was removed.

The BioKPRO III (FCI Ophthalmics, Marshfield Hills, MA, USA) has two fused pieces (a silicone optic and a PTFE skirt) similar to the BioKPRO II, but the optic was smaller and the skirt larger. The porous material used as the skirt surround for tissue integration was made of opaque polytetrafluoroethylene (PTFE), which is a synthetic

element of the device that can be produced fairly simply. Trials of BioKPRO III have been in progress at Moorfield Eye Hospital in London since January 2001 and visual acuity, visual field, device retention and incidence of adverse events will be published after 10 years (Allan, 2002). Although, Hollick *et al.* (2006) recently reported results of BioKpro III implanted in seven patients: only one was successful at 5 years with improved vision of 6/12, but presented mucus accumulation on the optic, in six cases extrusions occurred, retro-prosthetic membranes in three, and inflammation in one patient.

2.10.2 OSTEO-ODONTO-KERATOPROSTHESIS (OOKP)

One of the major complications in the KPROs is the poor integration of the KPRO with surrounding tissue, especially with the stroma in the host cornea. Many attempts have been made to overcome this problem, for instance to use a skirt with autologous tissue, such as tooth, bone or cartilage (Temprano, 1993; Liu *et al.*, 2005; Michael *et al.*, 2008) with hydroxyapatite. These were however still not successful (Allan, 2002), for instance, the Osteo-odonto-keratoprosthesis (OOKP) which used a tooth base-lamina, resulted in 30-75% progressive glaucoma, 10% retinal detachment and limited vision (Bleckmann and Holak, 2006).

To date, there are no KPROs that fulfill all the optimal requirements, i.e. are not to be rejected by the immune system of the patient, are completely inert but biologically functional, with long term stability and clarity, easy to maintain, with reasonable cost for the device, surgery and post-surgery, and also easy to implant. However, results of the OOKP have shown a good success over a long time as the implant is retained. Thus, the principle of the OOKP is still valid but needs to be improved upon. Actually, the Osteo-odonto-keratoprosthesis (OOKP) is a standard technique for surgery for visual rehabilitation in corneal blind patients at the end-stage of ocular surface diseases and trauma (as mentioned earlier) not treatable with penetrating keratoplasty (KP).

Hille *et al.* (2006) published a special article summarising the protocol of the OOKP procedure including indications and contraindications, patient selection criteria, postoperative treatment and complications. This protocol contains in detail the modified

Strampelli's OOKP procedure by Falcinelli's group and their results in a series of 234 patients who underwent for OOKP with follow-up at 5, 10 and up to 20 years.

The OOKP technique was pioneered in the early 1960s by Strampelli, who chose a tooth as the skirt material. The Strampelli procedure is very complex and the surgery involves stages over a period of months, however, the outcome of his technique was fairly successful because the reproduction of mucosal epithelium was limited by the contact with the alveolar dental ligament, reducing the membrane formation and extrusion (Ricci *et al.*, 1992). The Strampelli OOKP was then modified by Falcenelli's group over the years, but it is still based on the same principle as the original Strampelli OOKP. The OOKP basic principle is the use of a tooth with the root and surrounding alveolar bone (Figure 2.10.7) to form a plate (skirt) as a holder for the optical cylinder made of PMMA.

Figure 2.10.7 has been removed due to the Copyright restrictions

Figure 2.10.7 Schematic representation of cross section of a normal tooth (from Shah, 2009)

In the OOKP (Figure 2.10.8), the PMMA optical cylinder is glued to the host cornea with cement. Therefore, the optical cylinder becomes the central part of the OOKP lamina (Figures 2.10.5 and 2.10.6). The dentine is joined to the alveolar bone by the dentoalveolar ligament. The OOKP lamina is secured and fixed to the cornea by the surrounding periosteum, a dense membrane composed of fibrous connective tissue that coats bones, and also the OOKP lamina is fixed and sewn to the sclera surface with sutures. Finally, a thick buccal mucous membrane graft is placed on the OOKP device except on the top of the optic cylinder in order to protect and cover the device (Hille *et al.*, 2006). This buccal mucous graft also supplies the alveolar living bone with nutrients making it bioactive and restoring part of the metabolic process of the cornea.

Figure 2.10.8 has been removed due to the Copyright restrictions

Figure 2.10.8 Schematic representation of the cross section of an OOKP device (from Liu et al., 2008)

The OOKP surgery is performed in two stages (I and II) separated by 1 year:

In stage I, a circular flap of buccal mucosa from the cheek is sutured over the cornea and sclera. The flap is removed when it is about 2 mm thick. A crown tooth is harvested and with it alveolar dental ligament. The tooth root and surrounding bone is sectioned to obtain a lamina with dentine on one side and bone on the other. A hole is drilled through the dentine to place a PMMA optical cylinder. The assembled device (osteo-odonto lamina) is placed in a lower eyelid subcutaneous pocket to acquire a soft tissue covering (Hicks *et al.*, 1997; Liu *et al.*, 1998; Falcinelli, 2005; Liu *et al.*, 2008).

In stage II, up to 1 year later, the osteo-odonto lamina is removed from its subcutaneous pocket and the excess soft tissue is cleaned from the bone surface, therefore, no soft tissue remains on the dentine surface. The buccal mucosal flap is opened to uncover the cornea. A small hole is trephined for one end of the optical cylinder and the other end passes through a hole in the buccal mucosa. Incisions are then made to extract the lens. The lamina is inserted in the corneal hole and sutured onto the cornea and sclera. The eye is re-inflated with filtered air. Finally, the mucosal flap is replaced (Hicks *et al.*, 1997; Liu *et al.*, 1998; Falcinelli, 2005; Liu *et al.*, 2008).

The Stampelli OOKP technique was modified by the Falcinelli group and this modified OOKP surgery is still one of the most successful procedures for KPROs in terms of retention of the implant for patients with corneal blindness untreatable by other surgical procedures.

The disadvantages of the OOKP certainly are the long term surgery, and that it is usually not performed in both eyes at the same time. The complication of degree varies and mostly depends on the pre-conditions of the patient's eyes, for instance indications including dry eye, chemical burns, glaucoma pre-surgery, and failed keratoplasty. However, the most common complications in the OOKP procedure are glaucoma (an ocular condition in which the fluid pressure inside the eye is too high due to slow fluid drainage from the eye), haemorrhage into the vitreous, endophthalmitis (inflammation of the internal tissues in the eye), retinal detachment, alteration of the mucus, infection of the lamina in the pocket, membrane formation (retro-prosthetic membrane), corneal

perforation, expulsion of the optic cylinder, absorption of lamina, expulsion of the prosthesis, optic cylinder instability, and rupture of the sclera (Chirila, 2001; Hille *et al.*, 2006; Bleckmann and Holak, 2006; Chirila *et al.*, 2007). There are only a few centres in the world for OOKP surgery due to the complexity of the medical intervention. In the UK, OOKP is carried out at the Sussex Eye Hospital in Brighton, which has been the national referral centre for the OOKP medical procedure since 1996 (Liu *et al.*, 2008).

2.11 PRESENT COMPLICATIONS OF ARTIFICIAL CORNEA DESIGNS

The most common complications of KPROs are the inadequate integration between the skirt of the artificial implant and host tissue, specially the sclera; and between the cylindrical optic and its skirt (Hicks *et al.*, 1997; Legeais and Renard, 1998; Kim *et al.*, 2002; Albon, 2003; Meek, 2008). Therefore, the fixation methods and the bio integration of the skirt in the artificial cornea must be evaluated and improved, without compromising the mechanical strength of the KPRO.

Legeais and Renard (1998) addressed that the poor integration between the artificial implant and host cornea, results in infection and/or inflammation and eventual extrusion. Albon (2003) added that a poor interface seal between optic and skirt, leads to epithelial down-growth and aqueous leakage. Hicks *et al.* (1997) and Albon (2003) stated that a retro-corneal membrane can be formed behind the optic and leads to extrusion of the optic. Refojo (2005) reported faulty tissue-prosthesis interface, epithelium down growth, retro corneal membranes, tissue ulceration and infections around the prosthesis as the common problems associated with central optic-and-skirt keratoprosthesis. Albon (2003) outlined similar problems and added some cases of glaucoma have been found.

Certainly, the interfaces between the optic and the skirt of the KPROs, which are joined by using either different glues or sewing procedures with threads, constitute very risky sites, where epithelial down growth, leakage and infection are prone to occur. The same risks can also be present in the interface between the KPRO and the host sclera. Meek (2008) explained that rigid components on KPROs can produce mechanical stress in the cornea causing ulceration on the surface of the KPRO or opacification of the cylinder

optical interface. Kim *et al.* (2002) and Albon (2003) have reported low biocompatibility in KPRO devices, and the result is an inability of recipient cells (epithelial cells and keratocytes) to colonise the optics, which leads to inflammation, retro-prosthetic membrane formation, tissue breakdown, leakage and eventual implant extrusion. Undoubtedly, all surgery which involves full or partial replacement of part of the body is highly complex and causes inflammation. In particular in the case of KPROs, intraocular inflammation and glaucoma are definitely the results of an extremely complex medical procedure, which is predisposed to retro-prosthetic membrane formation.

On the other hand, the available KPROs are not covered with a layer that can protect the implant itself, the optic from the external environment; therefore extrusion and infection are prone to occur. The natural cornea and sclera are protected from these normal surroundings with an epithelial layer. Thus, the KPROs must somehow allow to solve this problem, for instance to allow coating the KPRO with an artificial epithelial surface without interfering with the clearness of the optic.

To overcome the main problem of the KPROs, the poor integration of the KPRO with its surrounding tissue, the tissue must be autologous, following the principle of the OOKP, and address the subsequent complications. It would therefore be very important to consider an ideal artificial cornea and evaluate the feasibility in a more realistic approach.

CHAPTER 3

MATERIALS AND METHODS

3.1 INTRODUCTION

Polymer-based materials are preferentially used for the skirts (scleral part) of artificial cornea (KPRO) because clinically it is easier to implant a prosthesis with a flexible polymeric skirt than an implant with a rigid skirt such as the tooth lamina from the OOKP (Osteo-odonto-keratoprosthesis) design. Secondly, the mechanical compatibility is closer between the sclera and polymers compared to sclera versus tooth enamel. Moreover, it is desirable that polymers for KPRO skirt are both biocompatible and bioactive to interact with the metabolic activity of the cornea.

Possible materials include high-density polyethylene (HDPE), ultra high molecular weight polyethylene (UHMWPE) and polyether ether ketone (PEEK). These were pre-treated with different concentration of sodium hydroxyl (NaOH) solutions for 48 hours followed by soaking in 1.5 Simulated Body Fluid (SBF) for up to 30 days to stimulate the growth of apatite and to accelerate calcium and phosphate depositions on the pre-treated substrate forming an apatite layer.

Apatite layers can be formed on the polymers by using a suitable treatment in 1.5 SBF to produce Ca/P layer on its surface before implantation, potentially rendering these polymers bioactive. To this end, a NaOH pre-treatment may be necessary to activate functional groups (OH⁻) that can act as potential nuclei on the polymer surface for the apatite deposition during the 1.5 SBF treatment.

In this chapter, the materials used are described with a summary of the physical properties, as well as the production of the HDPE and UHMWPE films. The preparation of

the NaOH and SBF solutions are detailed. Also, the immersion of HDPE, PEEK and UHMWPE films in 1M, 5M or 10M NaOH pre-treatments and the incubation in the 1.5 SBF treatments are described. Finally, the characterisation techniques to study the morphology and the composition of the layers deposited on the films are described in detail in order to assess *in vitro* bioactivity of the layers.

3.2 MATERIALS

3.2.1 HIGH DENSITY POLYETHYLENE (HDPE)

The high density polyethylene (HDPE M30053S) was supplied as granules by Saudi Basic Industries Corporation (SABIC- Europe Ltd, Belgium). The physical properties are given in Table 3.2.1.

Table 3.2.1 Physical properties of HDPE (data from SABIC- Europe Ltd. Belgium)

Polymer Properties			Test Methods
Density	953	kg m ⁻³	ISO 1183
Melt flow rate (MFR)	4.0 – 10.5	g/10 min	ISO 1133
Melt volume rate (MVR)	5.3 - 14	ml/10 min	ISO 1133
Mechanical Properties			
Tensile test			ISO 527-2
stress at yield	25	MPa	
stress at break	31	MPa	
strain at break	>200	%	
tensile modulus	1100	MPa	
Creep modulus			ISO 899
after 1 hour	500	MPa	
after 1000 hours	250	MPa	
Izod impact notched			ISO 180/A
at 23 °C	5	kJ m ⁻²	
at -30 °C	5	kJ m ⁻²	
Hardness Shore D	61	-	ISO 868
Thermal properties			
Heat deflection temperature			ISO 75-2
at 0.45 MPa (HDT/B)	81	°C	
Vicat softening temperature			ISO 306
at 10 N (VST/A)	124	°C	
DSC test			DIN 53765
Melting point	132	°C	
Enthalpy change	203	J g ⁻¹	

3.2.2 ULTRA HIGH MOLECULAR WEIGHT POLYETHYLENE (UHMWPE)

The ultra high molecular weight polyethylene (UHMWPE 1900) was supplied as powder by Himont, USA. The physical properties given by the supplier are shown in Table 3.2.2.

Table 3.2.2 Physical properties of UHMWPE (data from Himont, USA)

Polymer Properties		Test Methods	
Physical Properties			
Density	930	kg m ⁻³	ASTM D792
Mechanical Properties			
Tensile and compression tests			
strength at yield	3,100 psi	(21 MPa)	ASTM D638
tensile impact	800 ft lb in ⁻²	(1,700 kJ m ⁻²)	ASTMD1822
elongation at break	300 %		ASTM D638
shear strength	3,500 psi	(24 MPa)	ASTM D732
Izod impact strength			
at 23 °C	no break		ASTM D256
Hardness Shore D at 23 °C	62-66	-	ASTM D785
Thermal properties			
Heat deflection temperature			ASTM D648
at 1.8MPa (264 psi)	47 °C		
at 0.45 MPa (66 psi)	80 °C		
Vicat softening temperature	124 °C		ASTMD1525
DSC test			
Melting point	135-138 °C		ASTM D789
Enthalpy change	200 J g ⁻¹		ASTMD7696

3.2.3 POLYETHER ETHER KETONE (PEEK)

The polyether ether ketone (PEEK) was supplied by Invibio Ltd. Lancashire, UK as films. The PEEK film presents two distinctive sides (bright and matt). The physical properties are given in Table 3.2.3.

Table 3.2.3 Physical properties of PEEK (data from Invibio Ltd. Lancashire, UK)

Polymer Properties			Test Methods
Physical Properties			
Density	1310	kg m ⁻³	ASTM D792
Water absorption, 24 hrs	0.10	%	ASTM D750
Mechanical Properties			
Tensile and compression tests			
tensile strength	16,000 psi	(110 MPa)	ASTM D638
tensile modulus	500,000 psi	(3450 MPa)	ASTM D638
tensile elongation at break	20 %		ASTM D638
flexural strength	25,000 psi	(170 MPa)	ASTM D790
flexural modulus	600,000 psi	(4140 MPa)	ASTM D790
compressive strength	20,000 psi	(140 MPa)	ASTM D695
compressive modulus	500,000 psi	(3450 MPa)	ASTM D695
Hardness (Rockwell)	M100	-	ASTM D785
Izod impact notched	1.0	ft lb in ⁻¹	(54 J m ⁻¹) ASTM D256
Thermal properties			
Heat deflection temperature			ASTM D648
at 264 psi (1.8 MPa)	160	°C	
DSC test			
Melting temperature	340	°C	ASTMD3418
Maximum operating temperature	249	°C	

3.2.4 SODIUM HYDROXIDE (NAOH)

Sodium hydroxide (NaOH) is a caustic metallic base. Sodium hydroxide is a white solid, available in pellets, flakes, granules and as a 50% saturated solution. Anhydrous (100%, solid) sodium hydroxide has a chemical formula of NaOH and a molecular weight of 40.00. Sodium hydroxide forms a strong alkaline solution when dissolved in a solvent such as water; it is very soluble in water with liberation of heat, the reaction is exothermic.

The sodium hydroxide (NaOH) was supplied by Aldrich as anhydrous pellets reagent grade $\geq 98\%$, CAS No. 1310-73-2, Cat. No. S5881, F.W. 40, ECC No. 215-185-5, EC label WGK1. The physical and chemical properties of the NaOH pellets are summarised in Table 3.2.4.

Table 3.2.4 Physical and chemical properties of NaOH

Properties	
Molecular weight	40.00
Odour	Odourless
Specific gravity (water = 1.0) at 25 °C	2.13
Solubility in water at 0 °C	29.6 %
pH (5% solution)	14
Boiling point	1390 °C
Melting point	318 °C

For these experiments, 750 mL of 10M NaOH was prepared by dissolving 300 g of NaOH pellets in 500 mL ultra purified water in a 1000 mL volumetric flask with magnetic stirring in a fume cupboard. When all the pellets were dissolved and the solution was at room temperature, 250 mL of ultra purified water was added to complete the total volume of the solution to 750 mL. Then, 500 mL of 10M NaOH solution were poured into another volumetric flask and closed with a glass lid and left in a fume cupboard for further use. From the remaining 250 mL 10M NaOH, 200 mL was diluted with 200 mL of ultra purified water to make 400 mL of 5M NaOH, and poured into a new flask with a lid, the

flask was then swirled to mix the solution, and kept in the fume cupboard. The final 50 mL of the 10M NaOH were used to make 1M NaOH solution by adding ultra purified water until 500 mL was reached, and poured into a new flask, closed with a lid, swirled and kept in a fume cupboard for further use.

3.2.5 SIMULATED BODY FLUID (SBF)

Simulated Body Fluid (SBF) with ion concentrations 1.5 times those of SBF developed by Kokubo *et al.* (1990) was prepared by dissolving reagent-grade NaCl, NaOHCO₃, KCl, K₂HPO₄·3H₂O, MgCl₂·6H₂O, CaCl₂·2H₂O, Na₂SO₄ and (CH₂OH)₃CNH₂, as shown in Table 3.2.5, in 750mL of ultra purified water and buffered with 1M HCl to pH 7.20 at 37 °C. Care was taken to ensure that each reagent had completely dissolved prior to adding the following reagent as described in Kokubo and Takadama (2006). Ultra high purified water was added to bring up the total volume of the solution to 1000 mL. The 1.5 SBF solution was poured into a plastic bottle and stored at 4 °C for 3 days to ensure that no precipitation occurred, indicating that the SBF was in the appropriate condition to be used. The ions concentration in human blood plasma and 1.0 and 1.5 SBF are shown in Table 3.2.6.

1.5 SBF was used in this study as a treatment to produce Ca/P layer on the surface of the polymers to make them bioactive, before implantation; not to evaluate bioactivity (Tiffany *et al.*, 1989; Renke-Gluszko and Fray, 2004). Thus, the 1.5 SBF solution was part of the process to form a HA layer. A supersaturated concentration, rather the normal SBF, was used to accelerate the precipitation of HA. Note, however, that this study was not intended to develop a material which triggers bone bonding ability, thus, normal SBF was not used.

Table 3.2.5 Reagent grade chemicals to prepare 1 litre of 1.5 SBF

Order	Chemical	Technical information	
1	NaCl	Sodium chloride	11.994 g
		Aldrich 99+% A.C.S. Reagent, Cat.No.22,351-4, ECC No.231-598-3, CAS No. 7647-14-5, Lot. No. TN08028JN	
2	NaHCO ₃	Sodium hydrogen carbonate	0.525 g
		Aldrich 99.7+% ACS. Reagent, Cat.No.23,652-7, F.W.84.01, Lot. No. 69170	
3	KCl	Potassium chloride	0.336 g
		Aldrich 99+% ACS. Reagent, Cat.No.20,800-0, CAS No. 7447-40-7, Lot. No. 74735	
4	K ₂ HPO ₄ ·3H ₂ O	Dipotassium hydrogen phosphate	0.342 g
		Aldrich 99+% (dipotassium hydrogen phosphate), Cat.No.22,131-7, F.W.228.23, Lot. No. 69459	
5	MgCl ₂ ·6H ₂ O	Magnesium chloride hexahydrate	0.458 g
		Aldrich 99+% ACS. Reagent, Cat.No.24,696-4, CAS No. 7791-18-6, Lot. No. 69354	
6	1M HCl	Hydrochloric acid aqueous solution	50mL
		HCl solution 98.91g 37% HCl (BDH) diluted to 1L in vol.	
7	CaCl ₂ ·2H ₂ O	Calcium chloride dehydrate	0.552 g
		Aldrich 98+% ACS. Reagent, Cat.No.22,350-6, F.W.147.02	
8	Na ₂ SO ₄	Sodium sulfate	0.0257 g
		Aldrich powder 99+% ACS. Reagent, Cat.No.23,859-7, ECC No.231-820-9, CAS No. 7757-82-6	
9	(CH ₂ OH) ₃ CNH ₂	Tris-(hydroxymethyl) amino methane	9.086 g
		Aldrich 99+% ACS. Reag. Cat.No.25,285-9.CAS No.77861	

Table 3.2.6 Ion concentration of SBF and human blood plasma (Kokubo et al., 1990; Kokubo and Takadama, 2006)

Ion	SBF (mM)	1.5 SBF (mM)	Human Blood Plasma (mM)
Na ⁺	142.00	213.00	142.00
K ⁺	5.00	7.50	5.00
Mg ⁺	1.50	2.25	1.50
Ca ⁺	2.50	3.75	0.50
Cl ⁻	147.80	221.70	103.00
HCO ³⁻	4.20	6.30	27.00
HPO ₄ ²⁻	1.00	1.50	1.00
SO ₄ ²⁻	0.50	0.75	2.50

3.3 METHODS TO PRODUCE THE BIOACTIVE LAYERS

The coating procedure using Simulated Body Fluid (SBF) is shown in Figure 3.3.1 along with the characterisation techniques.

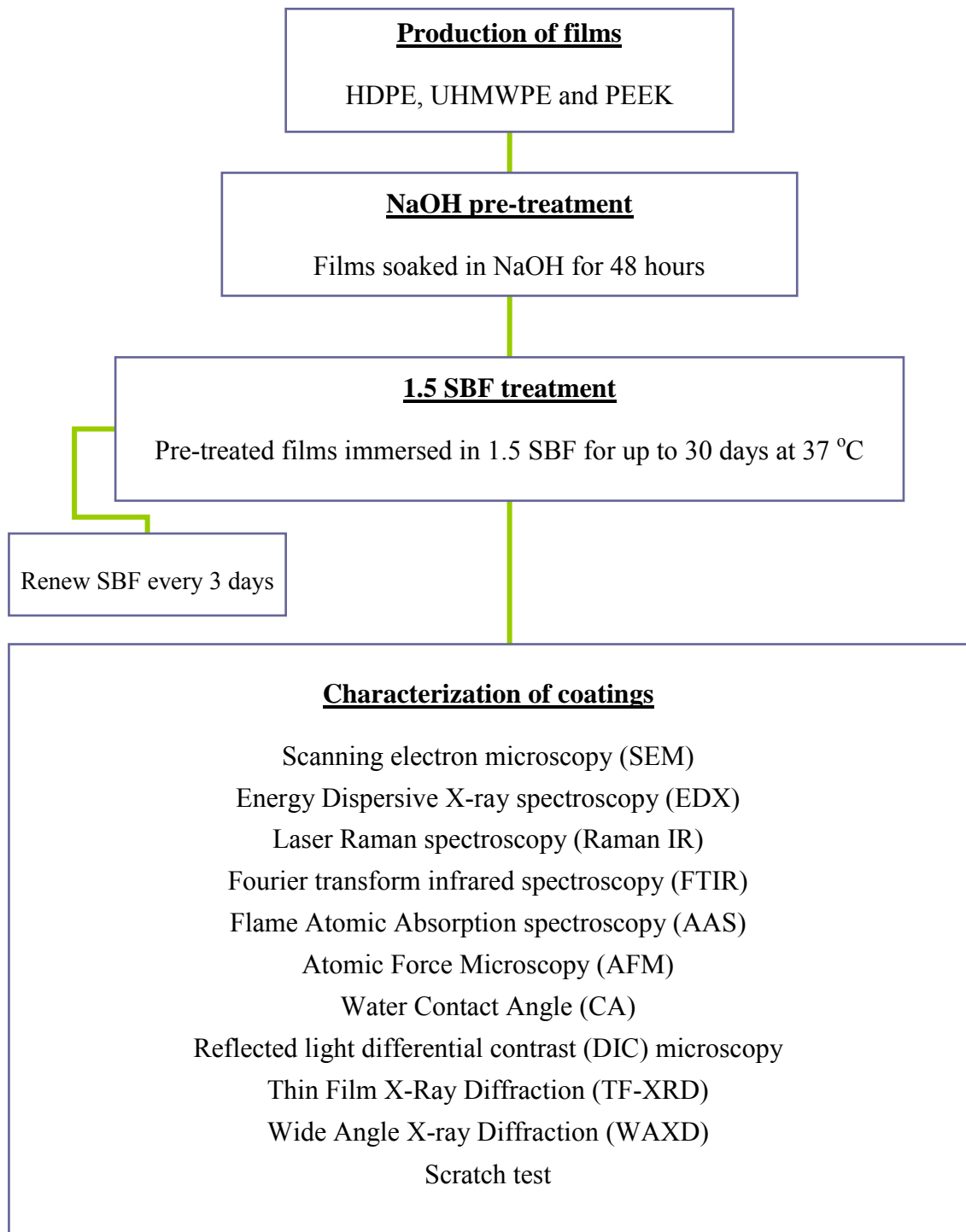


Figure 3.3.1 Experimental coating procedures and tests

The procedure shown in Figure 3.3.1 was applied in two separate batches of experiments. Details of the materials used, the treatment methods and the analysis techniques used for each batch are summarised in table 3.3.1.

Table 3.3.1 Experimental procedure and tests for batch I and batch II.

	Batches	
	I	II
Materials	HDPE PEEK UHMWPE	PEEK UHMWPE
NaOH pre-treatment	1M 5M 10M	5M 10M
1.5 SBF treatment	0, 1, 3, 7 and 15-18 days	0, 3, 7, 15 and 30 days
Characterisation techniques	SEM EDX IR FTIR TF-XRD	SEM EDX AAS AFM CA DIC WAXD Scratch test

3.3.1 PRODUCTION OF HDPE, UHMWPE AND PEEK FILMS

A hydraulic press, Rondol Benchtop Hot Press (Rondol Technology Ltd., Stone, UK), was used to produce HDPE and UHMWPE films. Small amounts of granules or powder were placed between two polyimide films and two aluminium sheets, which then were placed between the platens of the hot press. The polyimide films were used as release

films to avoid contamination of the polymeric films from the aluminium sheets. The plates were placed within the platens preheated at 180 °C, and left for 3 min for the HDPE granules and 10 min for UHMWPE powder to ensure complete melting within the sample and the release of air bubbles from the melt. Pressures of 10 kN and 20 kN were applied for 3 min and 10 min for HDPE and UHMWPE respectively. The platens still under pressure were then water cooled until a temperature of 80-100 °C was reached. The cooling was stopped, the pressure released and the film removed from the press.

A S10316/95 Mackey Bowley hydraulic thermal press (Mackey Bowley International Ltd, Norfolk, Kent, UK), was used to produce a second batch of UHMWPE films. 25 g of UHMWPE powder were placed between two polished copper plates of dimensions of 255 x 255 x 2 mm, separated by four spacers. The plates were placed within the temperature-controlled platens of a hydraulic press; the platens being pre-heated to 140 °C. A pressure of 10 kN was applied for 10-15 min, the final pressure of 20 kN was applied for 25-30 min. After this, the pressure was released and the plates were left in the press to cool down cold using water until the platens reached 70 °C. The plates were removed from the press and the film was taken from the plates.

The thicknesses of the first batch of HDPE, UHMWPE and PEEK films were 0.06, 0.26 and 0.09 mm, respectively. These were cut to discs 6 mm in diameter using a punch. They were soaked in ethanol for 10 min, washed with ultra high purified water and dried overnight at room temperature. The water had been purified up to 18ΩM using USF ELGA DI water de-ionising equipment.

The thickness of second batch of UHMWPE and PEEK film were 0.26 mm and 0.09 mm, respectively. PEEK and UHMWPE films were then cut to 20 x 50 mm stripes and cleaned with a damp ethanol cloth and then soaked in 0.1vol% benzalkonium chloride solution for 30 min, then rinsed with ultra pure water and dried overnight at 37 °C.

3.3.2 NAOH PRE-TREATMENTS

The HDPE, UHMWPE and PEEK dried samples from the first batch were immersed in 1M, 5M or 10M NaOH solutions for 48 hours at 37 °C. First, 100 mL polyethylene bottles and their lids were washed with ethanol, rinsed with ultra high purified water and dried at 37 °C overnight. Secondly, each bottle with its lid was labelled and 10 samples of HDPE, UHMWPE and PEEK film were put in the respective bottle in a fume cupboard, and approximately 100 mL of 1M NaOH, 5M NaOH or 10M NaOH were poured into each bottle. The bottles were closed and shaken manually to assure the samples did not stick to each other. Finally, the bottles were left in an oven at 37 °C for 48 hours. Manual agitation was done every 6-8 hours. After 48 hours, all samples were carefully taken out and rinsed with ultra high purified water and placed in labelled Petri dishes previously washed with ethanol and rinsed with ultra high purified water. The Petri dishes were left overnight without a cover to allow the samples to dry at room temperature. After the samples were dried, 2 samples from each Petri dish were taken out and placed in new Petri dishes labelled according to the NaOH concentration and polymer film for further characterization analysis. The remaining samples were subjected to 1.5 SBF treatments.

The UHMWPE and PEEK dried samples from the second batch were soaked in 5M or 10M NaOH solutions for 48 hours at 37 °C. 132 Sterilin tubes 30 mL universal container with leak free cap (Sterilin Ltd., London, UK) were used to incubate the samples for the NaOH pre-treatment. Firstly, 120 rectangular samples and 30 circular samples of UHMWPE and PEEK were placed in the Sterilin tubes and in a fume cupboard, approximately 25 mL of 5M NaOH or 10M NaOH were poured into each Sterilin tube. Then, all the Sterilin tubes were left in the oven at 37 °C for 48 hours. Manual agitation was done twice daily. After 48 hours the samples were removed and rinsed with ultra high purified water. The samples were replaced in the Sterilin tubes previously washed with ethanol and rinsed with ultra high purified water. The Sterilin tubes were left in the oven at 37 °C overnight without a cap to dry the pre-treated samples.

3.3.3 1.5 SBF TREATMENT

The first batch of NaOH pre-treated samples (HDPE, UHMWPE and PEEK) along with a set of samples not subjected to the NaOH pre-treatment were soaked in 1.5 SBF and incubated at 37 °C for 1, 3, 7, 15 or 18 days. Approximately 225 mL of 1.5 SBF were taken from the bottle kept in the fridge, and were heated at 37 °C. Approximately 25 mL of the 1.5 SBF at 37 °C was poured into each Petri dish which contained the samples. The Petri dishes were closed with their covers and incubated in the oven at 37 °C. The Petri dishes were agitated twice daily and the SBF was replaced every 3 days to maintain the SBF concentration.

On days 1, 3, 7, 15 and 18 of the 1.5 SBF treatments, 1 or 2 samples were taken out from the 1.5 SBF solutions in the Petri dishes and rinsed with ultra high purified water. The samples were allowed to dry in Petri dishes previously washed with ethanol, rinsed with ultra high purified water and dried at 37 °C overnight, and used for further characterisation.

The second batch of NaOH pre-treated samples (UHMWPE and PEEK) were soaked in 1.5 SBF and incubated at 37 °C for 3, 7, 15 or 30 days. 3000 mL of 1.5 SBF solution kept in the fridge was poured into a 3000mL conical flask and heated at 37 °C on a hot place. Approximately 25 mL of the 1.5 SBF at 37 °C was poured into each Sterilin tube which contained samples pre-treated with 5M or 10M NaOH. The Sterilin tubes were closed and incubated in the oven at 37 °C. The Sterilin tubes were agitated twice daily and the SBF was replaced every 3 days.

On days 3, 7, 15 and 30 after the 1.5 SBF treatment, 6-8 rectangular samples of UHMWPE and PEEK and 25-30 circular samples of PEEK were removed from the 1.5 SBF solutions in the Sterilin tubes and rinsed with ultra high purified water and placed into the Sterilin tubes previously washed with ethanol and rinsed with ultra high purified water. These Sterilin tubes were left overnight in the oven at 37 °C to dry the samples. When the samples were dry, all Sterilin tubes were closed until further characterisation.

3.4 CHARACTERISATION TECHNIQUES

3.4.1 SCANNING ELECTRON MICROSCOPY (SEM) AND ENERGY DISPERSIVE X-RAY SPECTROSCOPY (EDX).

Scanning electron microscopy (SEM) is a technique that uses an electron beam to form magnified images of specimens. The electron beam is scanned across the surface of the sample and when the electrons strike the sample, a variety of signals are generated (Danilatos, 1988). The detection of specific signals produces an image or an elemental composition of the sample. The signals can be secondary electrons, backscattered electrons and/or X-rays. The secondary electrons are a) emitted from the atoms occupying the surface and produce an image of the surface, b) the result of primary beam electrons interacting with weakly bonded electrons within the specimen, and c) one of the two particles emitted from the specimen, the other one being backscattered electrons. Backscattered electrons are primary beam electrons reflected from the atoms in the sample; the interaction of primary beam with atoms causes shell transitions, which results in the emission of an X-ray (Danilatos, 1988). The detection and measurement of the energy by a X-ray detector gives the elemental composition of the sample, known as Energy Dispersive X-ray spectroscopy (EDX).

The samples must be conductive otherwise an electron charge will build up. Non-conductive specimens are coated with carbon or gold (Suzuki, 2002). Carbon is usually used for X-ray analysis and gold for high resolution imaging (Danilatos, 1988).

The morphology of the samples was studied using a JEOL JSM 6300 field emission scanning electron microscope (SEM) at an accelerating voltage of 5keV and a working distance of 15 mm. The samples were secured onto specimen holders by conductive carbon cement and coated with a thin layer of carbon. Fifteen specimens (1, 5 and 10M NaOH and times 0, 1, 3, 7 and 15 day SBF incubation) for each polymer film (PEEK, HDPE and UHMWPE) were measured at 5 specific areas, taking 3 points randomly on each area to allow the calculation of means and standard deviations. The main elemental composition of the layers was determined using energy dispersive X-ray spectroscopy (EDX), the Ca/P molar ratio was then calculated and averaged.

Secondly, the thickness of the apatite layer was also obtained using the shadowing technique under EDX. A strip cut from each polymer samples (PEEK, HDPE and UHMWPE) treated with 1.5 SBF for 18 days was placed transversally on the carbon base holders, and then coated with a layer of carbon. The shadowing technique was applied since the surface of the coating was uneven, and from the image produced it was possible to measure the minimum and maximum thickness of the coating. Basically this technique is an exaggeration of the specimen dimensions by accumulation of shown materials, which in this case, was mainly Ca^{2+} , PO_4^{3-} and OH^- (Suzuki, 2002).

Finally, the dispersion and area covered of the deposited layers were assessed from the micrographs and image analysis performed.

A similar procedure was also used for batch II with non-treated specimens and PEEK and UHMWPE samples pre-treated with 5M or 10M NaOH for 48 hours, carefully rinsed off with high purified water and then immersed in 1.5 SBF treatments for up to 30 days to study the morphology of the deposited layers on the films and to determine its elemental composition, mainly calcium (Ca) and phosphorous (P) deposited on the layers of the films. The SEM and EDX scans were taken after 3, 7, 15 and 30 days of 1.5 SBF treatment. Each specimen was tested in triplicate for the SEM and EDX experiments. The samples used for the SEM were coated with gold rather than with carbon used for the first series since the carbon coating was no longer available. Therefore, the samples used for EDX were not coated considering that golden and phosphorous peaks overlap. The SEM employed was a Hitachi S-4700 with acceleration voltages of 5–10 kV and equipped with a field emission gun and an EDX spectrometer. The calcium (Ca), phosphorus (P) amounts were obtained from the EDX experiments and the Ca/P molar ratio was calculated.

Therefore, the aim of the SEM was to study the morphology and to assess the growth and dispersion of the apatite deposited on the surface of the films non pre-treated with NaOH and immersed in 1.5 SBF, and pre-treated with NaOH followed by 1.5 SBF. The aim of EDX was to determine the presence of calcium (Ca) and phosphorous (P) quantitatively from the apatite deposition of the layers and then to calculate the Ca/P molar ratio.

3.4.2 LASER RAMAN SPECTROSCOPY

Raman spectroscopy is a technique used to study vibrational, rotational, and other low-frequency modes in a system. Therefore, molecules in compounds can be identified since vibrational information is specific for the chemical bonds within the molecules. The scattering process may occur either elastically (Rayleigh scattering), or inelastically (Raman scattering). Thus, Raman spectroscopy measures the wavelength and intensity of inelastically scattered light from molecules (Gardiner, 1989). The laser light interacts with phonons, which are macroscopic vibrational modes, or other excitations on the system, making the photons shift up or down. This shift in energy from the molecular vibrations gives information about the phonon modes in the system. Consequently, the Raman shift corresponds to the energy difference between the incident light and scattered photon (Gardiner, 1989). The mechanism of Raman scattering is different from that of infrared absorption, and Raman and IR spectra provide complementary information (Matousek and Parker, 2006).

Generally, a sample is illuminated with a laser beam. Light reflected from the illuminated spot is collected using a lens and sent to a monochromator (Gardiner, 1989). Wavelengths close to the laser line, due to the Rayleigh scattering, are filtered out while the rest of the collected light is dispersed onto a CCD (charge-coupled device) detector. A graph of number of photons detected (Raman intensity) versus Raman shift from the incident laser energy gives the Raman spectrum (Matousek and Parker, 2006).

In these studies, the vibrations, C=C and CH₂, and the ionic groups, CO₃²⁻ (carbonate) and PO₄³⁻ (phosphate), from the treated HDPE, UHMWPE and PEEK films were detected using a Nicolet Amelga Raman spectrometer (Thermo Fisher Scientific, Madison Wisconsin, USA). The microscope has a CCD Detector of Andor DV420 Open Electrode. The Raman spectra were stimulated by laser light at 785 nm wavelength. The spectra were obtained in the ranges of 1800 to 400 cm⁻¹ and 4000 to 400 cm⁻¹, averaging 256 scans at 2.0 s exposure time and 4 cm⁻¹ resolution.

3.4.3 FOURIER TRANSFORM INFRARED SPECTROSCOPY (FTIR)

Fourier Transform Infrared spectroscopy (FTIR) is an absorption technique used to identify chemical bonds and molecular structure of compounds. The FTIR is based on the interferometer designed by Michelson and a mathematical procedure developed by Fourier that converts response from the time to the frequency domain (Crompton, 2008).

Infrared (IR) radiation is electromagnetic radiation in the wavelengths between the visible and microwave regions of the electromagnetic spectrum. The IR region can be divided into 3 smaller regions: near-IR (14000-4000 cm^{-1}), mid-IR (4000-400 cm^{-1}) and far-IR (400-20 cm^{-1}). Changes in fundamental vibrational levels of most molecules occur in the mid-IR. Therefore, the spectra in these studies were obtained in the mid-IR region.

Infrared energy is emitted from a source, this beam passes through an aperture which controls the amount of energy presented to the samples (and, ultimately, to the detector). The beam enters the interferometer where the encoding takes place. The resulting interferogram signal then exits the interferometer. The beam passes through the sample. Some of the infrared radiation is absorbed by the sample and some of it passes through (transmitted). The absorbed frequencies of energy are characteristic of the sample since the frequency of vibration is determined mainly by the masses of the atoms and the strength of the bond between them, which is only slightly altered by other atoms in the vicinity (George and McIntyre, 1987). The IR beam finally passes to the detector to measure the interferogram signal. The measured signal is digitalized and sent to the computer where the Fourier transformation takes place. Thus, the resulting spectrum represents the molecular absorption and transmission, creating a molecular “fingerprint” of the sample. The absorption peaks represent the frequencies of vibrations between the bonds of the atoms of the materials (Crompton, 2008). In addition, the heights of the peaks in the spectrum indicate the relative amount of the materials present.

The ionic groups, CO_3^{2-} (carbonate), PO_4^{3-} (phosphate), and OH^- (hydroxyl) from the treated HDPE, UHMWPE and PEEK films were detected using a Nicolet 8700 FTIR spectrophotometer (Thermo Electron Corporation, UK). The spectra were obtained in the range between 4000 and 500 cm^{-1} , averaging 128 scans at 4 cm^{-1} resolution.

3.4.4 ATOMIC ABSORPTION SPECTROSCOPY (AAS)

Atomic absorption spectroscopy (AAS) is an analytical technique used to determine the concentration of a particular element in a specimen, usually metals, such as calcium (Ca). This technique can analyse the concentration of the particular element in a solution. The principle is based on detecting elements by means of atomic absorption since metals absorb light at specific wavelengths (Zybin *et al.*, 2005; Skoog *et al.*, 2007). Thus, the metal ions in a solution can be converted into atomic state using a flame. The light absorbed is measured against a standard curve of the specific metal (L'vov, 2005).

The solution is usually turned into a gas in the form of an atomic gas. Firstly, the solution is evaporated using a flame, which can be quantified as an input and as a remainder at the other side of the detector; this first step is known as a desolvation (drying or evaporation of the liquid solvent). Secondly, the solid specimen vaporises into a gas, so it is a vaporization step, known as ashing. Thirdly, the compounds present in the specimen are broken into free atoms, known as an atomisation process (L'vov, 1997; Axner, 2000).

Therefore, the amount of energy, the power, put into the flame is known, and the amount of energy remaining at the other side of the detector can then be measured; then, it is possible to calculate how many of these transitions occurred, and the signal obtained is proportional to the concentration of the particular element that has been measured (Sperling and Welz, 1999; Skoog *et al.*, 2007).

In fact, the atomic absorption technique (AAS) that uses a flame is not always referred as AAS, despite being one of the methods of the atomic absorption spectroscopy. It is called flame atomic absorption spectroscopy (FAAS), but to make it less complicated, AAS is used in this thesis to refer to the flame absorption technique. This flame AAS uses a solution which contains the element that needs to be quantified, so the solution is sucked into an „L“ shape tube, and then aerosolised, and finally it is mixed with combustible gas, acetylene (C₂H₂) and nitrous oxide (N₂O). The mixture is then ignited in a flame (Broekaert, 1998). The temperature of the flame can range from 2000 °C up to 3000 °C.

The atoms are reduced to the free state, meaning that the atoms are no longer excited as in their normal state. This process occurs during the combustion. Thus, the unexcited atoms absorb light at characteristic wavelengths (Broekaert, 1998; Axner, 2000).

To study the release of calcium from the specimens, after being pre-treated with 5M or 10M NaOH and immersed in SBF treatment for 30 days, the PEEK and UHMWPE specimens were immersed in plastic tubes with 25 mL of ultra purified water at 37 °C for 3 and 7 days. Total Ca on the samples was determined by immersing a separate set of samples in 0.6M HCl for 24 hours. The calcium concentration (Ca) in homogenised aliquots of the water solution after 3 and 7 days, and the 0.6M HCl solution were measured using flame atomic absorption spectrometry with a nitrous oxide (N₂O) and acetylene (C₂H₂) flame on a Thermo Fischer iCE 3000 Series spectrometer. Calibration standards were gravimetrically diluted from Merck CertiPur 1000 mg/l Aluminium Standard Solution. Measurement results represent the mean of three repeats. Combined calibration and measurement uncertainties are less than 1%.

Thermo Fischer iCE 3000 Series Atomic Absorption Spectrophotometer used in these studies functioned by:

- 1) The solution extracted from the tubes which contains the polymeric samples was aspirated through a flame in order to convert the calcium to its atomic form,
- 2) Light from a hollow cathode lamp, which contains calcium, was passed across the flame and the atoms absorbed the light (atomic absorption) and went to an excited state,
- 3) The reduction of the intensity of the light beam during the atomic absorption were measured, and is directly proportional to the concentration of the calcium atomic species,
- 4) Finally the light absorbance of the calcium obtained from the samples were compared the light absorbance of the calcium standards calibration.

The aim of the AAS tests was to calculate the initial amount of calcium (Ca) deposited on the surface of the specimens, after being pre-treated with NaOH and treated with 1.5 SBF for 30 days, and then to study the release of Ca in water for 1 week.

3.4.5 ATOMIC FORCE MICROSCOPY (AFM)

Atomic force microscopy (AFM) is a method that measures the surface topography of a substrate on a scale from 0.1 to 100 microns. This technique involves scanning a sample by using a probe, or tip, with a radius of 20 nm. The sharp tip is automatically scanned over the sample surface with a feedback mechanism that measures surface-tip interactions on the scale of nanoNewtons force. The feedback mechanism enables the piezo-electric scanners to maintain the tip at a constant force (to obtain height information), or height (to obtain force information), producing a topographic image of the surface (Roiter and Minko, 2005). Tips are typically made from Si_3N_4 or Si, and extend down from the end of a cantilever. The AFM head uses an optical detection system in which the tip is attached to the cantilever. A diode laser is focused onto the back of a cantilever. As the tip scans the surface of the sample, moving up and down with the contour of the surface, the laser beam is deflected off the attached cantilever into a dual element photodiode. The photodetector measures the difference in light intensities between the upper and the lower photodetectors, and then converts this to a voltage. Feedback from the photodiode difference signal, through software control from the computer, enables the tip to maintain either a constant force or constant height above the sample. In the constant force mode the piezo- electric transducer monitors real time height deviation. In the constant height mode the deflection force on the samples is recorded (Wilson *et al.*, 2006).

The force between the tip and the sample surface is very small, usually less than 10^{-9} N; typical forces between tip and sample range from 10^{-11} to 10^{-6} N. For covalently bonded atoms the force is of the order of 10^{-9} N at separation of approximately 0.01 nm. Typical spring constants are between 0.001 to 100 Nm^{-1} , and motions from microns to approximately 0.01 nm are measured by the deflection sensor (Meyer *et al.*, 1992). Typically, the deflection is measured using a laser spot reflected from the top surface of the cantilever into an array of photodiodes (Martin *et al.*, 1987). Thus, non-destructive imaging is possible with these small forces (Meyer *et al.*, 1988; Meyer and Amer, 1988).

A variety of forces can be sensed by atomic force microscopy. Moreover, the AFM is also capable of producing images in other modes rather than the basic one described in the previous paragraph, thus the AFM can be operated in a number of modes, depending on the application (Wilson *et al.*, 2006). According to the interaction of the tip and the

sample surface, the AFM can be classified as Contact Mode (repulsive mode), Non-contact Mode (attractive mode) and Tapping Mode (Martin *et al.*, 1987).

In the contact (repulsive) mode, the instrument lightly touches the tip at the end of a leaf sprint (or cantilever) to the sample. Thus, the force on the tip is repulsive with a mean value of 10^{-9} N. This force is produced by pushing the cantilever against the sample surface with the piezo-electric positioning element. The deflection of the cantilever is sensed and compared in a direct current (DC) feedback amplifier to some desired value of deflection. If the measured deflection is different from the desired value of the feedback the amplifier applies voltage to the piezoelectric element to raise or lower the sample relative to the cantilever to restore the desired value of deflection. The voltage that the feedback amplifier applies to the piezo is a measure of the height of features on the sample surface. It is displayed as the lateral position of the sample (Hong-Qiang, 1997). As a raster-scan drags the tip over the sample, the detection apparatus measures the vertical deflection of the cantilever, which indicates the local sample height. Thus, in contact mode the AFM measures the hard-shape repulsion forces between the tip and the sample (Dagani, 2007).

In the non-contact (attractive) mode, the AFM derives topographic images from measures of attractive forces; the tip does not touch the sample (Baselt, 1993). The distances between the tip and the sample surface are greater than 1nm between the tip and the sample surface; hence van der Waals, electrostatic, magnetic or capillary forces produce images of topography, whereas in the contact mode, ionic repulsion forces take the leading role (Meyer, 1992).

In the tapping mode, the tip is placed in contact with the surface to provide high resolution and then by lifting the tip off the surface to avoid dragging the tip across the surface (Hong-Qiang, 1997). Therefore, the tip oscillates above the sample surface, and data may be collected from interactions with surface topography, stiffness, and adhesion (Baselt, 1993). Thus, it results in an expanded number of image contrast methods compared to the basic AFM.

Other less commonly used modes include magnetic force, electrical force, and pulsed force. In the magnetic force mode, a magnetic tip is used to make visualizations of magnetic domains on the sample. In the electrical force mode, a charged tip locates and

records variations in surface charge. In the pulsed force mode, the sample oscillates underneath the tip, and several pseudo force-distance curves are generated. This allows the separation of sample topography, stiffness and adhesion values, producing three different images (Dagani, 2007; Roiter and Minko, 2005).

The AFM provides a three-dimensional surface profile, and the samples viewed by AFM do not require any special coating. However, the AFM can only display images of a maximum height in the order of micrometres and a maximum scanning area of $150 \text{ nm} \times 150 \text{ nm}$ (Giessibl, 2003).

In these studies, surface topography/roughness of the non-treated PEEK (bright and matt sides) and UHMWPE films and 5M or 10M NaOH pre-treated PEEK (bright and matt sides) and UHMWPE specimens was assessed using Atomic Force Microscopy (AFM, MultiMode IV, Veeco). $5 \times 5 \text{ }\mu\text{m}$, $25 \times 25 \text{ }\mu\text{m}$ and $45 \times 45 \text{ }\mu\text{m}$ -sized images were recorded using contact mode (scan rate of 1 Hz). The roughness parameter R_a – arithmetical mean deviation (ISO/DIN 25178-2) – was evaluated in two different ways:

- 1) five random lines were placed across the whole scanned surface giving line profiles, with R_a calculated directly for those lines and averaged, and

- 2) NanoScope software (Veeco) was used to calculate R_a from the whole recorded image.

Therefore, the aim of the AFM experiments was to evaluate the influence of the NaOH pre-treatments on the surface of the films and to observe any changes in their topography after the NaOH pre-treatments.

3.4.6 WATER CONTACT ANGLE (CA)

The contact angle (CA) is a quantitative measure of the wettability of a solid by a liquid. The contact angle is the angle formed by the solid surface and the tangent line to the upper surface at the end point. Thus, the contact angle is determined by drawing a tangent at the contact where the liquid and the solid intersect. For instance, if the liquid used is

water, the solid is defined as hydrophilic or hydrophobic. The solid is hydrophilic when it has a high affinity for water, so the droplet (water drop) spreads on the surface of the solid and the contact angle is between 0° and 30° . The solid is considered hydrophobic when the water is not spread and instead forms a spherical cap at equilibrium on the surface of the solid and the contact angle is larger than 90° (Kowk and Neumann, 1999; Israelachvili, 2004).

Also it is possible to analysis the drop shape in order to determine the surface energy. The surface energy refers to the interaction between the cohesion and adhesion forces, so the surface energy can be measured. A hydrophobic solid, which presents a large contact angle, has poor wettability and poor adhesiveness, and hence it has low surface free energy. A hydrophilic solid, where the contact angle is small, has better wettability, better adhesiveness, and higher surface energy (De-Gennes, 1985; Tadmor, 2004;).

The physical properties between the solid and the liquid such as wettability, affinity, adhesiveness and repellency can be determined by means of the contact angles (Tadmor, 2004; Israelachvili, 2004).

To assess the wettability of PEEK and UHMWPE films, both before and after surface modifications with 5 or 10M NaOH, water contact angle measurements were performed, following the sessile drop method using a KSV Cam100 Contact Angle System (Lot-Oriel, UK). Prior to each measurement, the samples were rinsed with ultra pure water and dried with compressed air. Approximately 5 μ l of ultra pure water was placed on the specimen surfaces using a manual syringe. The drop shape was recorded for 30 sec with 0.5 sec intervals. The measurements were carried out in triplicate on samples which were not incubated in SBF. The main interest was to look at the wettability and determine if the 5M and 10M NaOH pre-treatments had modified the surface of the films, either increasing or decreasing wettability, which will have an effect on the subsequent 1.5 SBF treatments.

Therefore, the aim of the CA was to assess the wettability of the materials, before and after surface modifications with 5M or 10M NaOH.

3.4.7 REFLECTED LIGHT DIFFERENTIAL CONTRAST MICROSCOPY (DIC)

Reflected light differential contrast (DIC) microscopy is used to examine opaque specimens, which are not highly reflective and do not absorb or transmit any significant light (the incident light). The uneven surfaces on the specimen can make optical path differences, which can be converted by reflected light DIC microscopy into amplitude or intensity changes creating a topographical profile. This profile is a 3D image of the surface geometry, which gives distinctive raised and lowered areas on the surface of the specimen (van Munster *et al.*, 1998; Ishiwata *et al.*, 2005).

In the DIC microscope, light is reflected from the specimen, separated by fraction of a micrometer (the shear distance). Thus their resulting image consists of these two superimposed components, because their separation is too small to be resolved by the microscope. However, each point (e.g. pixel) in the image originates from two closely spaced and overlapping Airy disks originating from adjacent points on the specimen, and each disk has an intensity that corresponds to its respective optical path difference produced by the specimen. Therefore, image contrast is known as the differential since it is a function of the optical path gradient across the specimen surface, with steeper gradients producing greater contrast (Ishiwata *et al.*, 2005).

The method to establish the reflected light DIC is to use a Nomarski prism, which is attached to a mobile carriage within a rectangular frame (slider) that fits into the microscope nosepiece base, above the revolving objective turret (Nomarski, 1955; Francon, 1961). Thus, the Nomarski prism is translated back and forth laterally across the microscope optical axis. The formation of the final image in difference contrast microscopy is the results of interference between two different wavefronts that reach the image plane slightly out of phase with each other, giving an algebraic summation of the intensities to the image plane (van Munster *et al.*, 1998).

A Nikon reflected light DIC microscope with Nomarski prism was used to measure the area of the apatite deposited on the 5M or 10M NaOH pre-treated PEEK (bright and matt) and UHMWPE films treated with 1.5 SBF treatments on 3, 7, 15 and 30 days. The test was conducted in duplicate, so two identical samples of each sample were measured under the DIC microscope. The images were recorded in black and white.

3.4.8 THIN FILM X-RAY DIFFRACTION (TF-XRD) AND WIDE ANGLE X-RAY DIFFRACTION (WAXD)

Thin film X-ray diffraction (TF-XRD) is an analytical technique which reveals information about the crystal structure and preferred orientation of coatings anchored on thin films. X-rays are electromagnetic radiation with wavelengths between 0.01 nm and 10 nm, similar to the interatomic distances in a crystal. Therefore, crystal structures diffract X-rays. Thus, the structural arrangement of atoms and molecules in materials can be probed since the wavelength of X-rays is comparable to the size of atoms (Warren, 1990; Drenth, 1994; Als-Nielsen and McMorrow, 2001).

Basically, X-rays interact with the electrons in atoms. When X-ray photons collide with electrons, some photons from the incident beam will be deflected away from their original direction of travel. In the elastic scattering process (Thomson Scattering) the wavelengths of these scattered X-rays do not change, that is, the X-ray photons do not lose any energy and only momentum is transferred in the scattering process. Thus, the X-rays measured in diffraction are the elastically scattered X-rays, which carry information about the electron distribution in materials. On the other hand, during the inelastic scattering process (Compton Scattering), X-rays transfer some of their energy to the electrons and the scattered X-rays will have different wavelengths to the incident X-rays (Brumberger, 1993; Drenth, 1994; Als-Nielsen and McMorrow, 2001).

The diffraction pattern allows the distribution of atoms in materials to be deduced since the diffracted waves consist of sharp peaks with the same symmetry as the distribution of atoms. Thus, the peaks in an X-ray diffraction pattern are directly related to the interatomic distances (Brumberger, 1993; Drenth, 1994).

Thin film diffraction refers to a collection of XRD technique used to characterise thin films sample grown on substrates. Thin film diffraction methods such as hard X-rays (short wavelength X-ray i.e. 1 keV – 120 keV) can penetrate through the outer layers of the sample and measure the properties of both the film and the substrate (Warren, 1990). However, a major interest is to identify the coating, therefore, the scattering angle should be as low as possible not to penetrate the film or substrate. It is common to use 1° to 5°, depending on the XRD equipment (Als-Nielsen and McMorrow, 2001).

The crystalline phase composition of these samples was examined using a Siemens D5000 diffractometer in detector scan mode with a thin film analyser. Samples were aligned at 3° to the incident beam. A step size of 0.02° (2θ) and a scan time of 5 seconds were used. Data was collected from 20° to 40° on the surfaces of the HDPE, UHMWPE and PEEK specimens pre-treated with 1, 5 or 10M NaOH and treated in 1.5 SBF for 15 days.

For the second batch of specimens, PEEK and UHMWPE pre-treated with 5 or 10M NaOH and immersed in 1.5 SBF for 15 and 30 days, a Standard transmission wide-angle X-ray diffraction (WAXD) was carried out at room temperature using a Philips X'Pert Pro - PAN analytical instrument using Nickel Filter CuK_α -radiation ($\lambda = 0.15418$ nm). The voltage power was 40 kV and emission current was 40 mA. The scan range was selected to be in between 30° and 40° with a step size of 0.0084° and counting time of 20.480 sec per step. All specimens were tested in triplicate.

Therefore, the aim of the TF-XRD and WAXD tests was to examine the crystalline phase composition of the apatite deposited on the polymer films during the immersion time in the 1.5 SBF treatment after and before of being pre-treated with NaOH.

3.4.9 SCRATCH TEST

The Scratch test is a method of assessing the adhesion of the coatings. The adhesion of the coating to the polymer film is a property that can be determined as the interfacial forces between the two surfaces (the coating and the substrate). This technique generally uses a scratch with a sharp tip on a selected area of the coating. The material of the tip is commonly either diamond or a hard metal. The tip is drawn linearly across the coated surface under constant, increasing or progressive load until the coating starts to fail at a certain critical load. The critical loads can be detected precisely using an acoustic sensor attached to the load arm and some have a built-in optical microscope to collect observations. The adhesive properties can then be quantified using the critical load data. Scratch testers can also measure the applied force, the friction force (the tangential force) and the penetration depth. These parameters and the acoustic emission results provide the adhesion properties of the coatings (Long *et al.*, 2002; Liu *et al.*, 2003; Liu *et al.*, 2005).

In the basic scratch tests the diamond tip is moved by the scratch tester (a pen shaped device) within a radius of 50 to 200 μm across the coated surface of the polymeric film at a constant speed while an increasing normal force is applied at constant loading rate (Liu *et al.*, 2005). Therefore, the scratch test introduces stresses to the interface between the coating and the substrate, which results in a delaminating or chipping (cohesive failure) of the coating. The normal force at which the first failure of the coating is detected is known as the critical load (Liu *et al.*, 2003).

The failure in the scratch tester can be divided into three categories according to the failure type: 1) Cracking, 2) Chipping (cohesive failure), and 3) elimination (adhesive failure). A load cell is used to measure the change in friction or acoustic emission. Thus, the intensity of the acoustic emission is dependant on the type of coating failure during the adhesion test. Therefore, it is important to determine the coating failure after the scratch test using an optical microscope (Long *et al.*, 2002; Liu *et al.*, 2003; Liu *et al.*, 2005).

The scratch test was performed by Dr. T. Liskiewicz in the Chemistry Department of Leeds University using a nanoindenter with a maximum depth of 1500 nm. Also, the hardness and the elastic modulus by nano-indentation were measured. Scratches were produced in duplicate for each coating by linearly increasing the load on a 50 μm -radius spherical diamond stylus with a scanning speed of 20 $\mu\text{m s}^{-1}$ and at loading rates of 0.49, 1.60 or 7.3 N mm^{-1} to reach final loads of 0.9, 3.0 or 1.8 N, respectively.

The samples analysed by the above procedure were PEEK bright side, PEEK matt side and UHMWPE pre-treated with 5M or 10M NaOH and treated with 1.5 SBF for 30 days.

Therefore, the aim of the scratch test was to assess to adhesion of the apatite layers on the polymer substrate in order to deduce their mechanical stability.

3.4.10 STATISTICAL ANALYSIS

All experimental results presented in the following chapter of this thesis have been derived from at least three repetitions per test, and in some cases of up to 15, in order to estimate a representative value. Thus, all results are given as the mean of the measurements taken, together with the respective standard deviations. No additional formal pre-processing, such as removal of outliers, was performed.

While the mean represents an estimate of the expected value of the measurement, the standard deviation is the square root of an unbiased estimator of the variance of the population from which the measurements are drawn, assuming that the measurements are taken from independent, identically distributed samples.

Thus, the standard deviation provides a measure of confidence of the estimate of the expected value. It tends to be smaller as the number of measurements increases, which reflect the greater confidence of the mean values as more measurements were taken (i.e. 15 measurements were taken by each sample in the EDX; and 3 measurements were taken per specimen in the AAS).

For two groups of measurements (e.g. treated and non-treated) with different mean values, a small standard deviation indicates a greater confidence that the difference in the results is statistically representative.

CHAPTER 4

RESULTS

4.1 INTRODUCTION

The skirt of an artificial cornea must integrate the implant to the host sclera to prevent implant extrusion, a major cause of failure of current artificial corneal devices. Thus, it is highly desirable to encourage the response of the cornea to the implant by using a more bioactive material. The most important criterion for a polymer to be bioactive *in vivo* is to have the ability to induce apatite deposition on its surface *in vitro*. Apart from inducing the apatite formation, it is essential to stimulate the growth of apatite and to accelerate the SBF coating process.

A pre-treatment with 1, 5 or 10M NaOH followed by treatment with 1.5 SBF have been applied to HDPE, UHMWPE and PEEK films, to increase their bioactivity. The layers have been studied by using different techniques: Scanning Electron Microscopy (SEM), Energy Dispersive X-ray spectroscopy (EDX), Laser Raman spectroscopy (Raman IR), Fourier Transform Infrared spectroscopy (FTIR), flame Atomic Absorption spectroscopy (AAS), Atomic Force Microscopy (AFM), water Contact Angle (CA), reflected light Differential Contrast (DIC) microscopy, Thin Film X-Ray Diffraction (TF-XRD) and Wide-angle X-ray Diffraction (WAXD), to assess their bioactivity and their mechanical properties, as well to gain a better understanding of the apatite nucleation and growth on the polymer surfaces. It is also important to look at the effect caused by NaOH to the films and to determine the most suitable NaOH pre-treatment for the further treatment in 1.5 SBF.

This chapter presents the results of the *in vitro* assessment of the layers for the skirt materials.

4.2 WATER CONTACT ANGLE (CA)

Figure 4.2.1 shows the water contact angle (CA) of PEEK on both sides (bright and matt) and UHMWPE films before and after pre-treatment with 5M or 10M NaOH for 48 hours. Figure 4.2.2 shows the pictures of the CA of PEEK and UHMWPE (non-treated and NaOH pre-treated) films. Overall, the water contact angle decreases with the concentration of NaOH. For PEEK, the water contact angle decreased with the concentration of NaOH pre-treatment, for both sides of such polymer, demonstrating that the NaOH treatment increased the wettability on PEEK. In contrast, no significant differences in water CA were found for UHMWPE. Interestingly, non-treated samples have similar water CA.

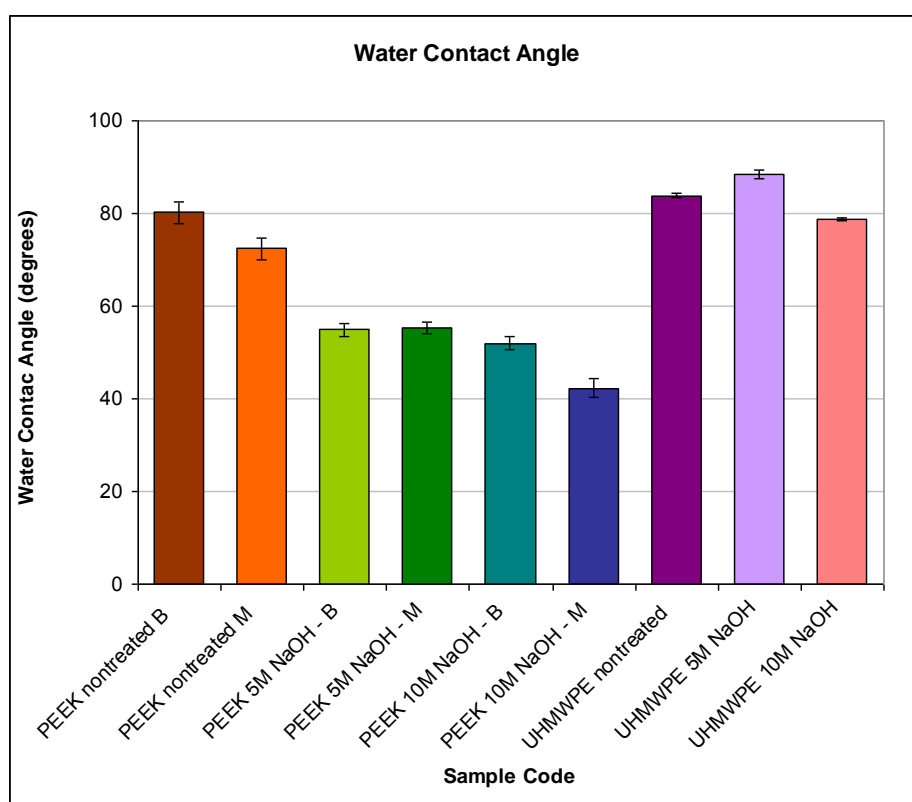


Figure 4.2.1 Averaged water contact angle and the Standard Deviation (error bar) of the non-treated films, PEEK (bright and matt sides) and UHMWPE, and 5M or 10M NaOH pre-treated samples, PEEK (bright and matt sides) and UHMWPE (B= bright, M= matt)

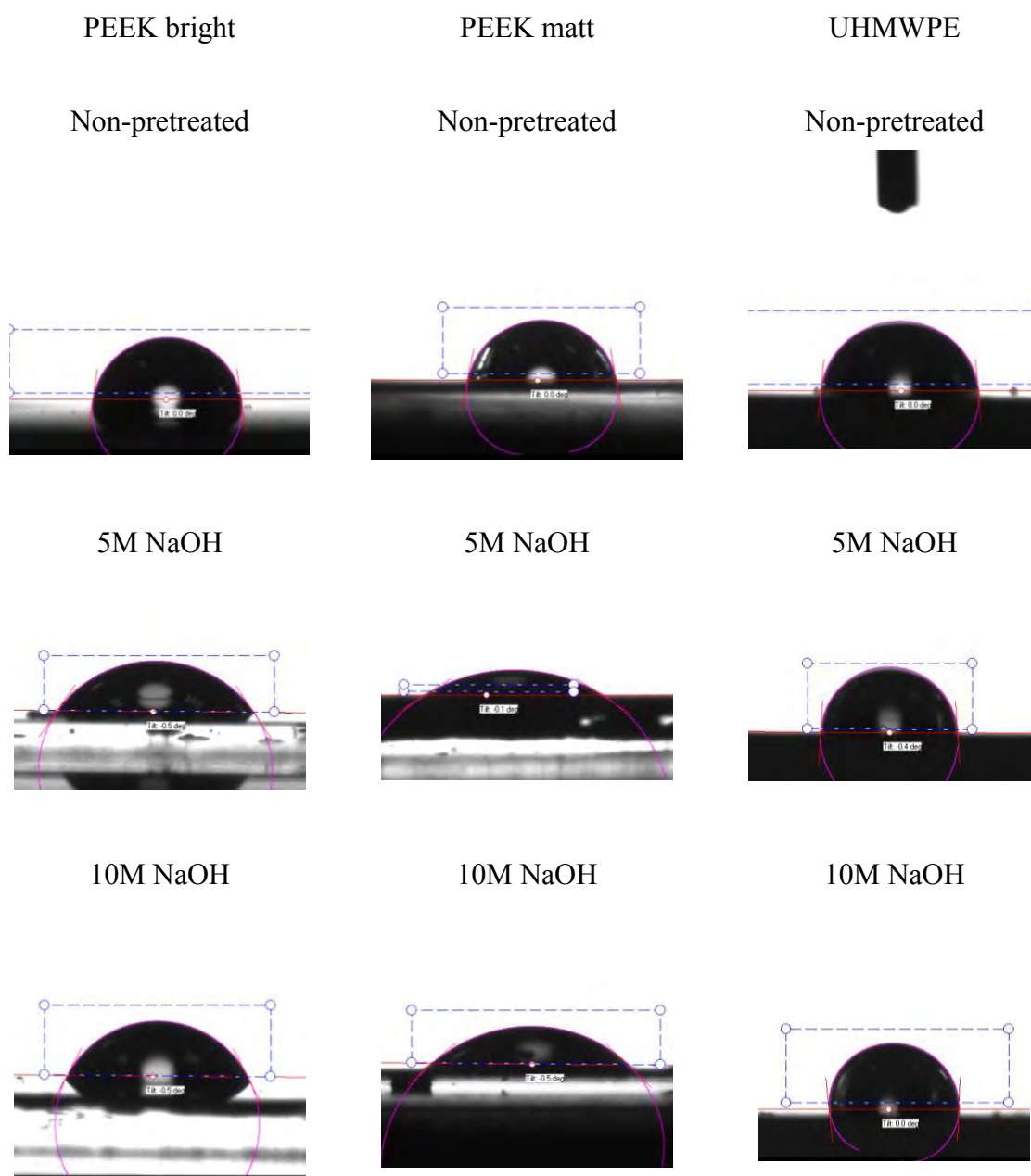


Figure 4.2.2 Pictures of the water contact angle of the non-treated films, PEEK (bright and matt sides) and UHMWPE and 5M or 10M NaOH pre-treated PEEK (bright and matt sides) and UHMWPE

4.3 ATOMIC FORCE MICROSCOPY (AFM)

Results of surface topography and corresponding roughness (R_a) data of the non-treated and NaOH pre-treated PEEK (bright and matt) and UHMWPE specimens as measured by AFM are presented in Tables 4.3.1 and 4.3.2 respectively. The R_a was evaluated in two different ways: a) five random lines were placed across the whole scanned surface giving line profiles, with calculated R_a directly for those lines and averaged and b) software (NanoScope – Veeco) was used to calculate R_a from the whole recorded image. Therefore, the R_a results are different for the whole image compared to the line profile values (Figure 4.3.1).

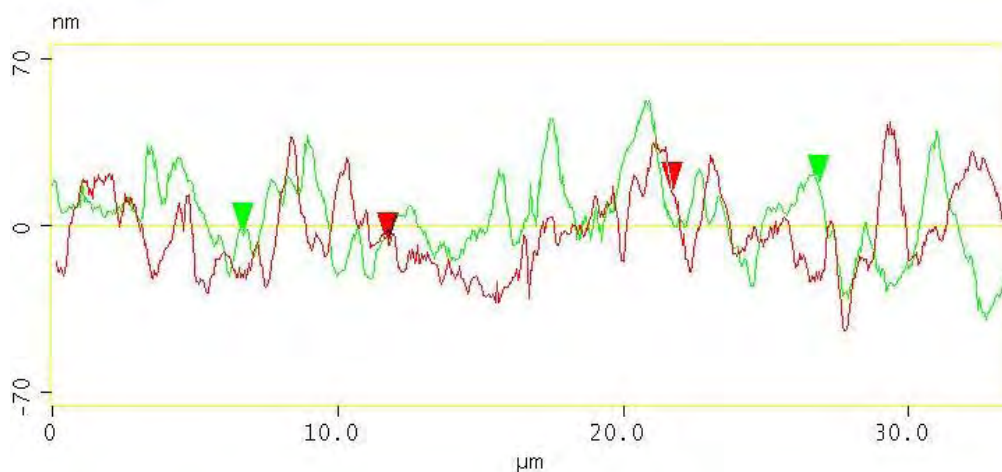


Figure 4.3.1 Example of Atomic Force Microscope (AFM) line profiles of PEEK (matt) pre-treated with 5M NaOH using a scan size of 25 microns (μm). The profiles for two different lines are shown (red, green), with arrows indicating the analysis range.

R_a values obtained from the AFM micrographs demonstrate that R_a was not strongly affected by the NaOH treatment on PEEK (bright side) since R_a slightly increased after the pre-treatment. On the contrary, R_a decreased for PEEK (matt surface) and UHMWPE, particularly after treatment with 10M NaOH. A similar trend could be observed when using R_a deduced from the AFM line profiles. It should be noted that the vertical scale on the AFM scans is set automatically; therefore there is a factor of over 20 between the maximum and minimum vertical scales.

Table 4.3.1 Roughness (R_a) in nanometres (nm) from the Atomic Force Microscope (AFM) using scan sizes of 25 x 25 or 5 x 5 microns (μm) of PEEK (bright and matt) non-treated samples and pre-treated samples with NaOH (B= bright, M= matt, S.D.= standard deviation)

Scan size	R_a from the whole image				R_a from line profiles			
	25x25 μm		5x5 μm		25x25 μm		5x5 μm	
Ra units	nm	S.D.	nm	S.D.	nm	S.D.	nm	S.D.
PEEK B	4.37	2.06	1.00	1.40	13.23	1.74	5.56	2.11
PEEK B 5M NaOH	14.07	1.81	8.35	1.61	8.64	2.09	4.54	1.70
PEEK B 10M NaOH	13.85	2.11	7.22	1.37	15.06	1.58	4.08	2.10
PEEK M	18.43	2.26	13.69	1.34	17.38	1.73	11.38	1.98
PEEK M 5M NaOH	17.59	1.36	18.17	1.62	21.78	1.87	13.40	1.96
PEEK M 10M NaOH	13.51	1.38	7.86	1.83	13.70	2.23	5.51	1.64

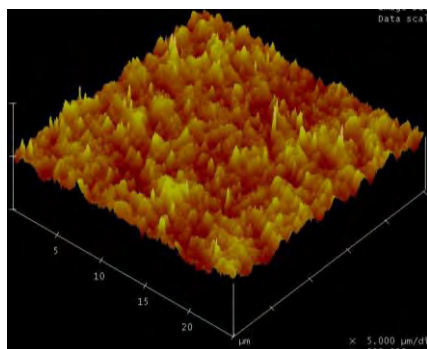
Table 4.3.2 Roughness (R_a) in nanometres (nm) from the Atomic Force Microscope (AFM) using scan sizes of 45 x 45, 25 x 25 or 5 x 5 microns (μm) of UHMWPE(UH) non-treated samples and pre-treated samples with 5M or 10M NaOH (S.D = Standard Deviation)

Scan size	R_a from the whole image			R_a from line profiles		
	45 x 45 μm	25 x 25 μm	5 x 5 μm	45 x 45 μm	25 x 25 μm	5 x 5 μm
R_a units	nm	nm	nm	nm	nm	nm
UHMWPE	123.43	129.98	74.64	83.12	88.33	15.62
S.D.	1.32	1.86	1.56	1.50	1.91	2.20
UHMWPE 5M NaOH	114.32	59.48	14.90	50.26	91.26	12.10
S.D.	1.61	1.41	1.87	1.80	1.45	2.13
UHMWPE 10M NaOH	64.22	65.09	13.12	73.36	32.86	5.86
S.D.	1.71	1.41	2.18	1.67	1.98	1.57

Figures 4.3.2-4.3.4 show the topographical micrographs of the non-treated and NaOH pre-treated PEEK (bright and matt) and UHMWPE specimens. The bright side of non-treated PEEK is less spiky compared to the matt side of PEEK, which appears to be rough and with lots of sharp peaks. The surface of the bright side of PEEK was slightly more affected by the NaOH pre-treatments as the spiky patterns seem to be more appearing compared to the non-treated PEEK bright. On the other hand, the topography surfaces for PEEK (matt side) and UHMWPE seem to be slightly flatter in comparison to the non-treated specimens, especially after pre-treatment with 10M NaOH. In general, there are noticeable changes in topography of the specimens after the NaOH pre-treatments, which are also present in the R_a values.

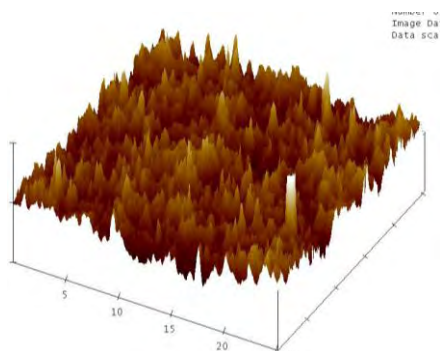
25 x 25 μm

PEEK Bright



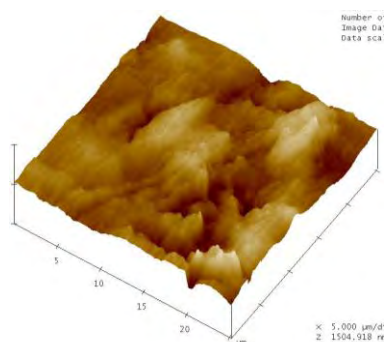
x=5 μm /div
z=300 μm /div

PEEK Matt



x=5 μm /div
z=150 μm /div

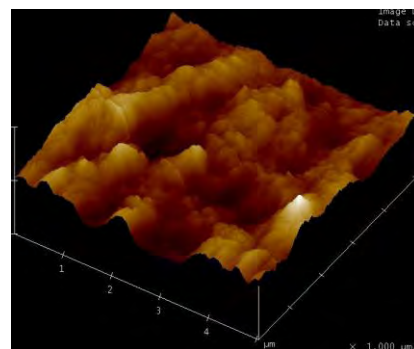
UHMWPE



x=5 μm /div
z=1505 μm /div

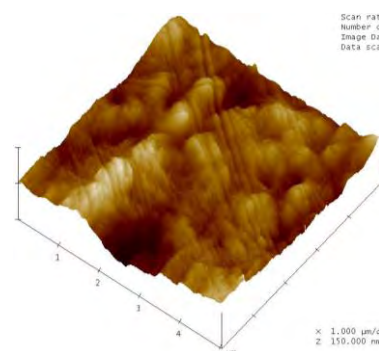
5 x 5 μm

PEEK Bright



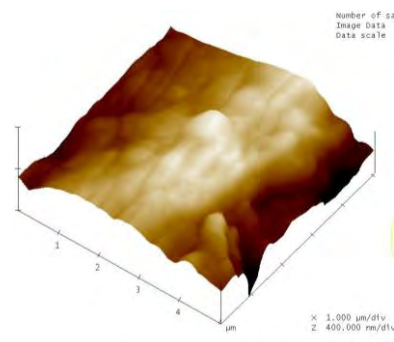
x=1 μm /div
z=150 μm /div

PEEK Matt



x=1 μm /div
z=150 μm /div

UHMWPE



x=1 μm /div
z=400 μm /div

Figure 4.3.2 3D topography from the Atomic Force Microscope (AFM) using scan sizes of 25 x 25 and 5 x 5 μm of the non-treated PEEK and UHMWPE films

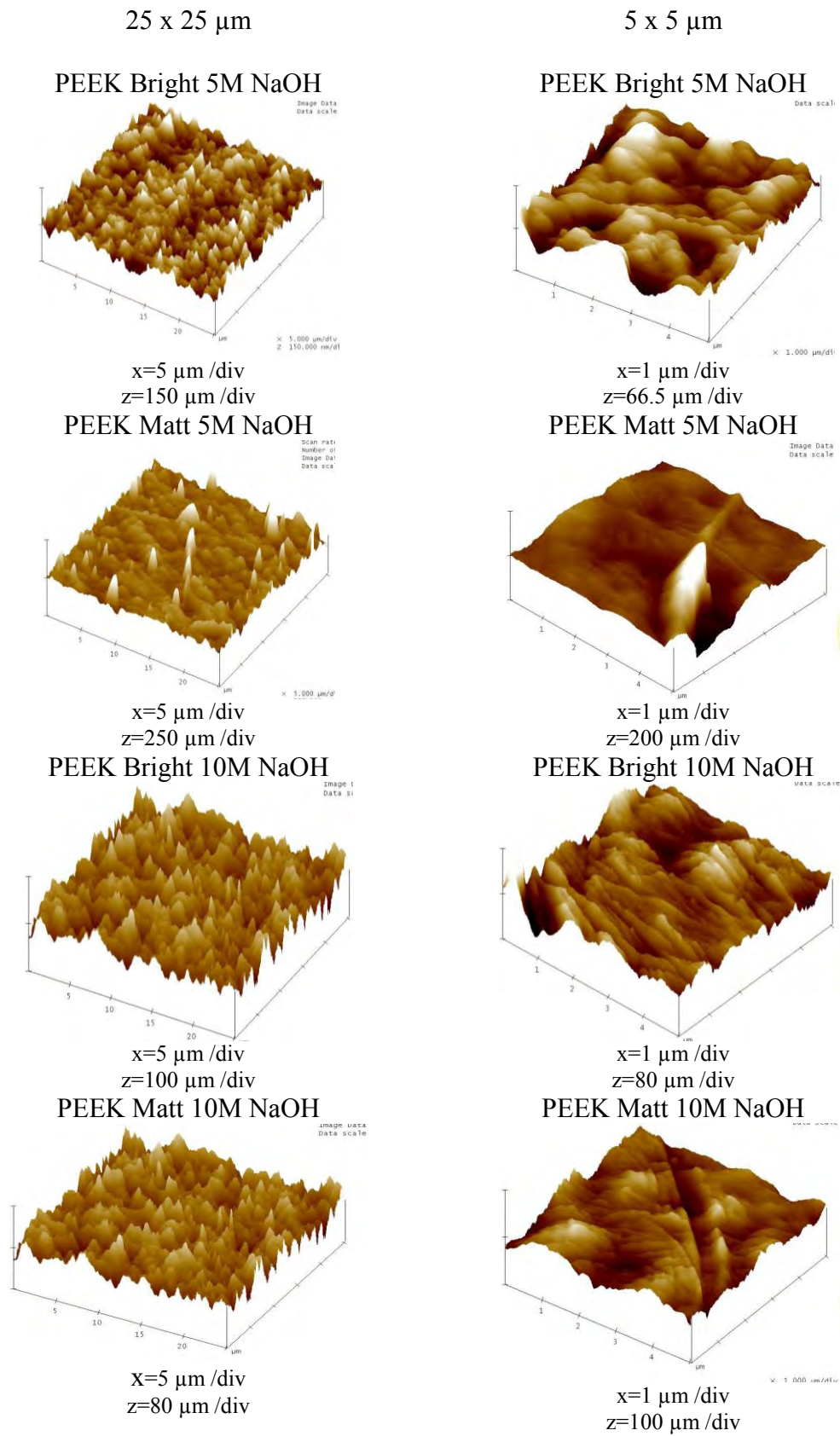


Figure 4.3.3 3D topography from the Atomic Force Microscope (AFM) using scan sizes of 25 x 25 and 5 x 5 μm of the 5 or 10M NaOH pre-treated PEEK (bright and matt)

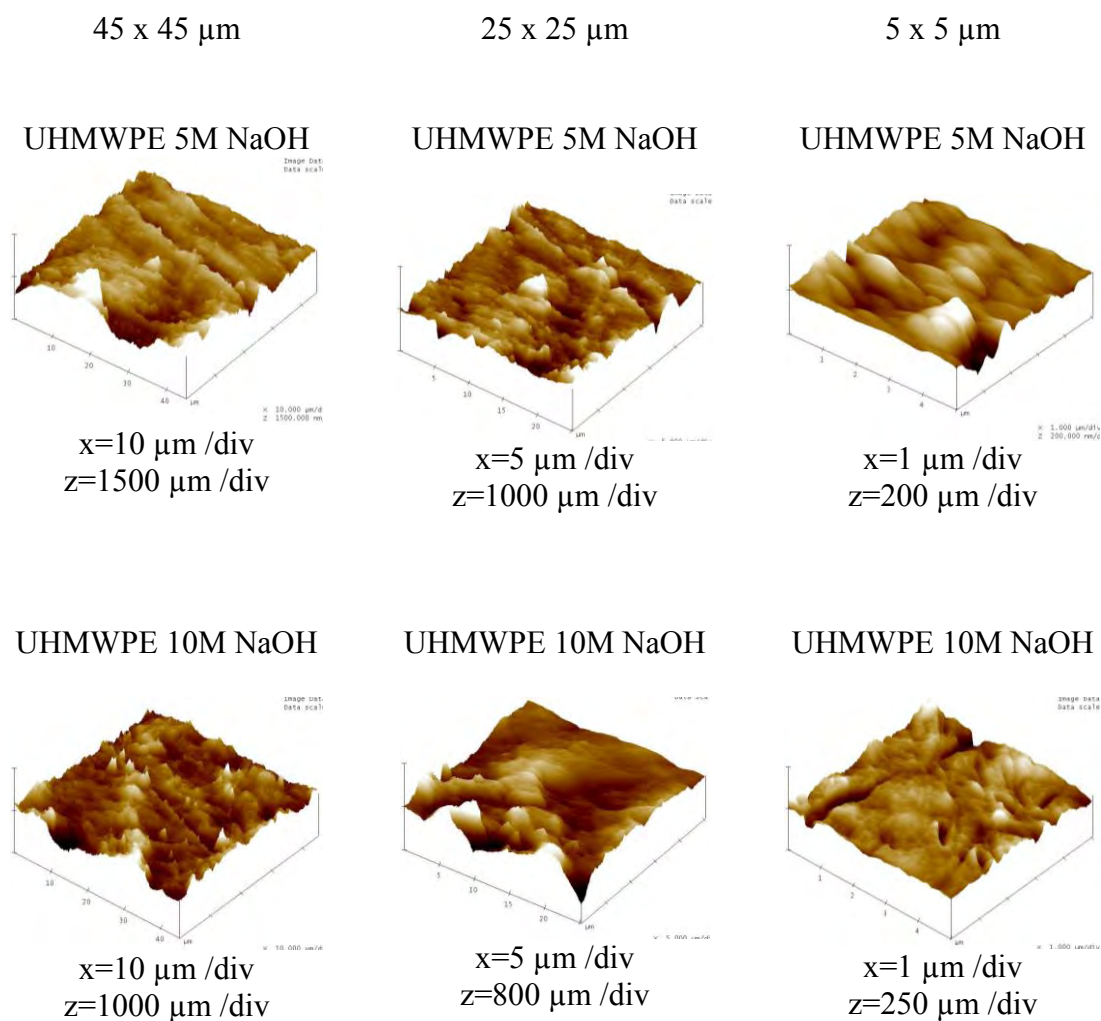


Figure 4.3.4 3D topography from the Atomic Force Microscope (AFM) using scan sizes of 45 x 45, 25 x 25 and 5 x 5 microns (μm) of the 5M or 10M NaOH pre-treated UHMWPE films

4.4 SCANNING ELECTRON MICROSCOPY (SEM)

4.4.1 INITIAL SCREENING OF POLYMERS WITH NaOH ACTIVATION

Apatite formation on the polymers (PEEK, HDPE and UHMWPE) films after 1M, 5M or 10M NaOH pre-treatment, are shown in the SEM micrographs in Figures 4.4.1 to 4.4.3. In these figures the word ‘spectrum’ indicates the location where an EDX spectrum was taken; these spectra are shown in section 4.5. For the PEEK films, pre-treated with different concentrations of NaOH solution and immersed in 1.5 SBF for up to 15 days, an apatite layer was first formed on the surface of the PEEK films on day 3 when the PEEK film was pre-treated with 10M NaOH, on day 7 when 5M NaOH pre-treatment was used, and on day 15 after 1M NaOH pre-treatment (Figure 4.4.1). A similar dependence was found for apatite formation on HDPE films; however the apatite growth seemed to proceed faster. On HDPE films, apatite was found on day 1 with 10M NaOH pre-treatment, on day 3 when 5M NaOH was used and on day 7 after 1M NaOH pre-treatment (Figure 4.4.2). On the UHMWPE films, apatite attached to the surface on day 3 for both 10M and 5M NaOH pre-treatments, and on day 7 when 1M NaOH pre-treatment was used (Figure 4.4.3). In the early stages of the treatment in 1.5 SBF after the NaOH pre-treatment, calcium phosphate clusters initiate and then grow forming a thin and porous layer on the polymer film. As the immersion time in 1.5 SBF progresses, additional nucleation and growth occurred producing a more consolidated apatite layer (Figures 4.4.1 – 4.4.4), followed by a second layer above the initial compacted layer, with the appearance of ‘snow balls’, since the apatite depositions on the last days in the SBF treatment produce larger apatite particles (Figure 4.4.4). Another observation is the appearance of cracks on the initial calcium phosphate layer with the increase in 1.5 SBF time, which are very prominent on PEEK pre-treated with 1M or 5M NaOH and incubated for 15 days in 1.5 SBF (Figure 4.4.1), and also on UHMWPE pre-treated with 5M NaOH and soaked in 1.5 SBF for 7 days (Figure 4.4.3). However, these cracks are probably the results of drying the films for electron microscopy.

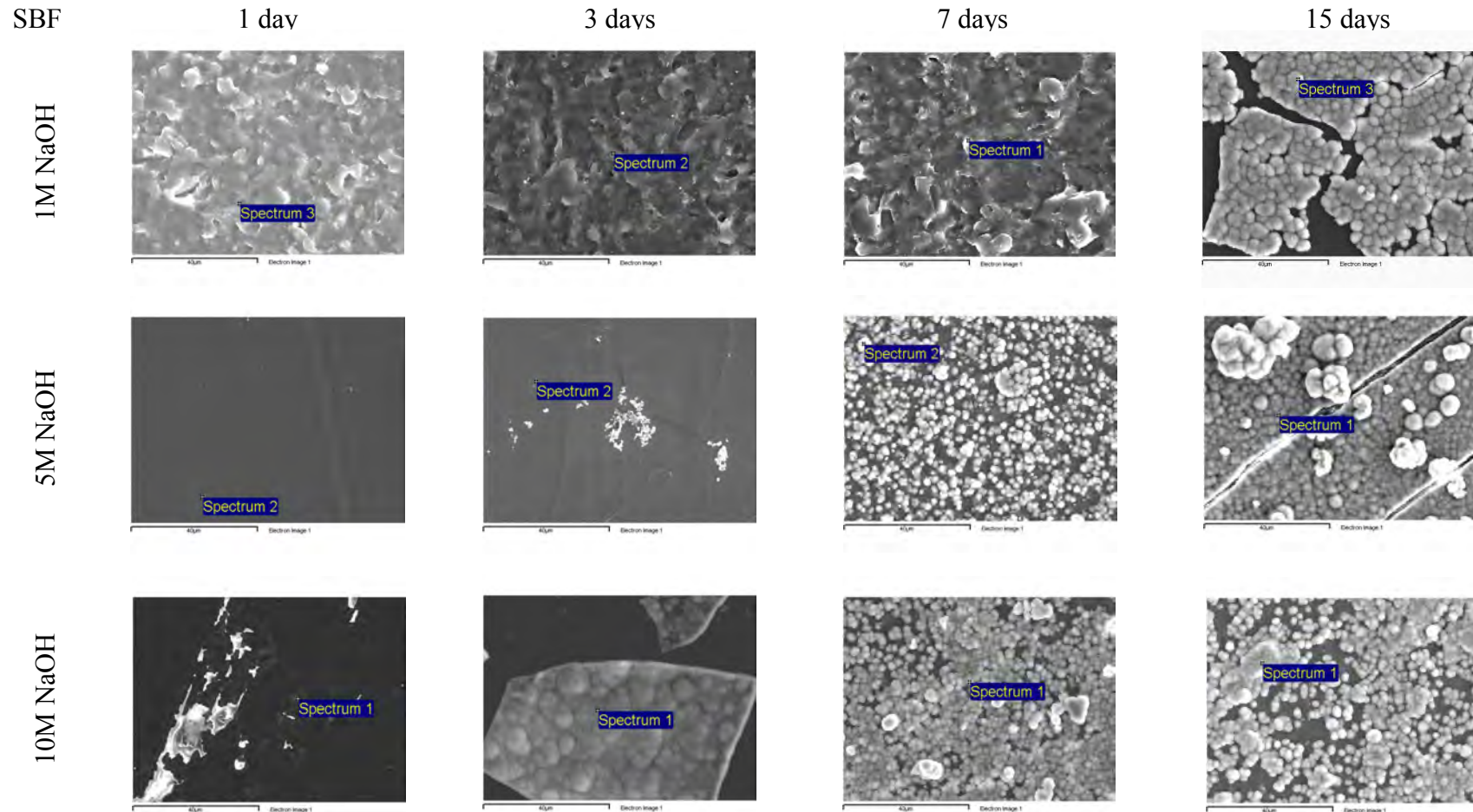


Figure 4.4.1 SEM micrographs of the PEEK films pre-treated with 1, 5 and 10M NaOH and soaked in 1.5 SBF for 1,3, 7 and 15 days. (Scale bars= 40 μ m)

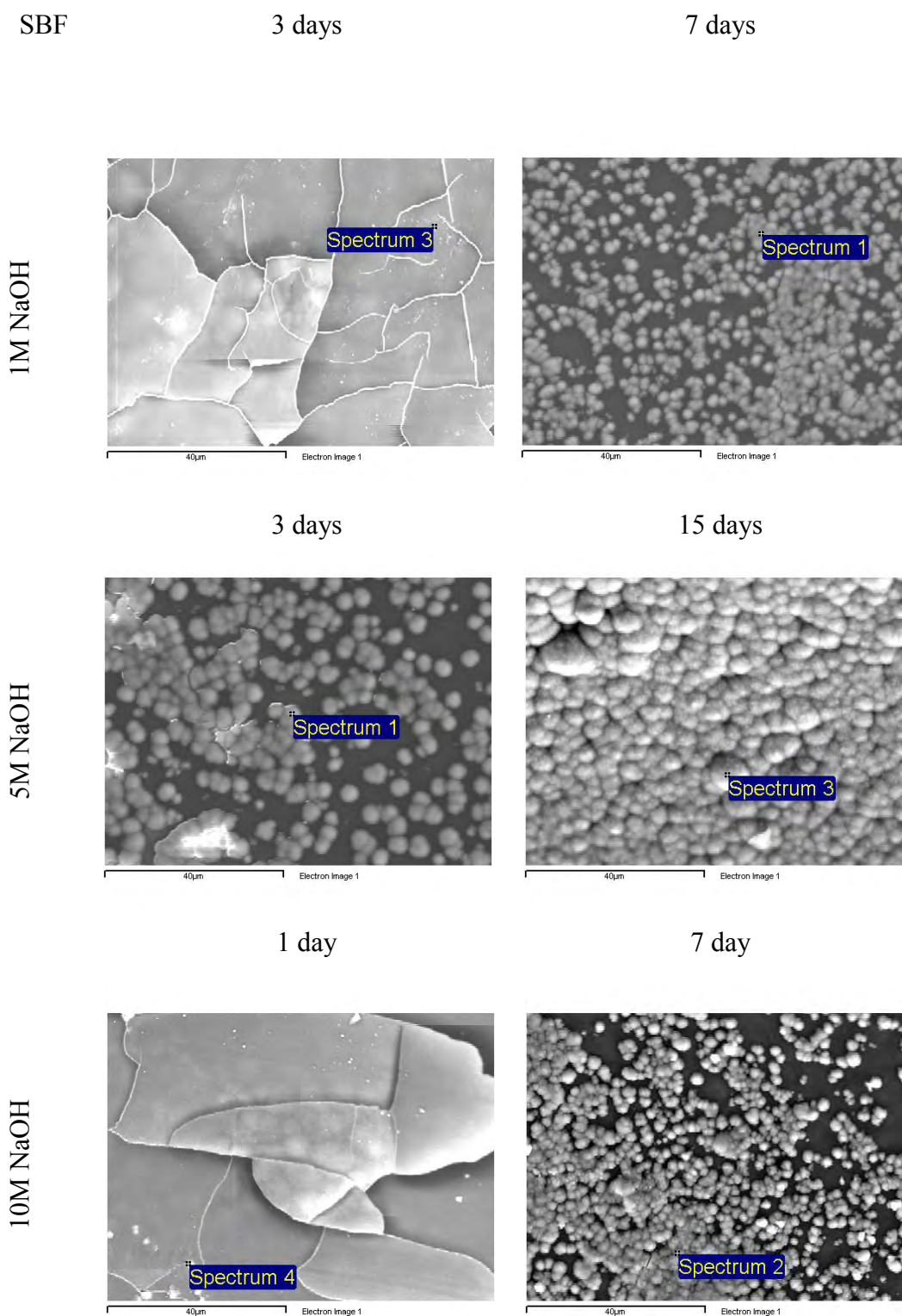


Figure 4.4.2 SEM micrographs of the HDPE films pre-treated with 1M NaOH and 1.5 SBF for 3 and 7 days (top); HDPE films in 5M NaOH and 1.5 SBF for 3 and 15 days (middle); and HDPE films in 10M NaOH and 1.5 SBF for 1 and 7 days (bottom). (Scale bars=40 µm)

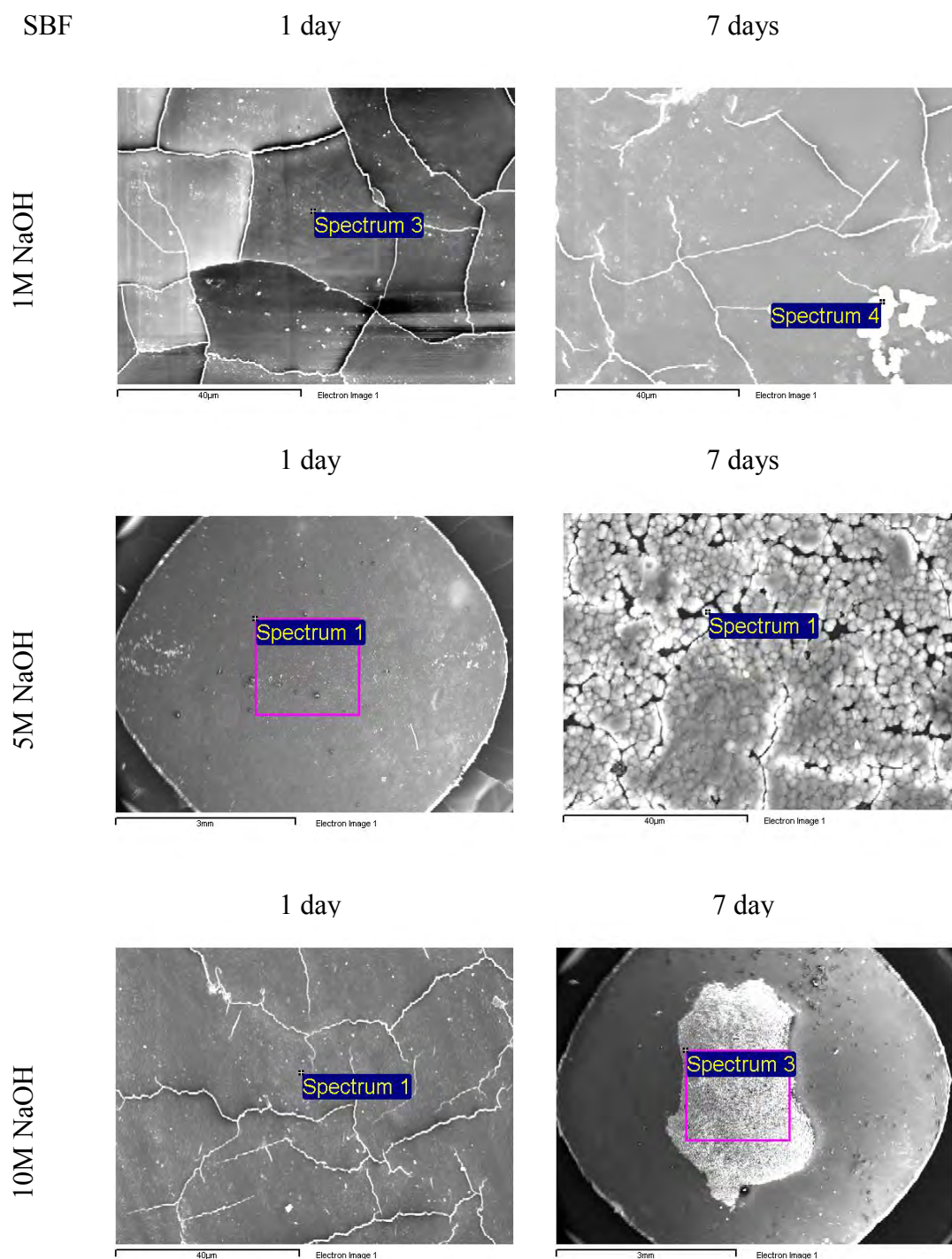


Figure 4.4.3 SEM micrographs of the UHMWPE films pre-treated with 1, 5, and 10M NaOH and soaked in 1.5 SBF for 1 day and 7 days. (Scale bars= 40 µm for 1M NaOH for at 1 day and 7 days, 5M NaOH at 7 days and 10M NaOH at 1 day. Scale bars= 3 mm for 5M NaOH at 1 day and 10M NaOH at 7 days)

As seen in Figures 4.4.1 to 4.4.3, for all pre-treated polymers (HDPE, UHMWPE and PEEK) immersion in 1.5 SBF treatments initially resulted in the formation of individual agglomerates, which were typically less than 5 μm across. With increasing immersion time in 1.5 SBF, further apatite deposition resulted in growth of these agglomerates, producing continuous, thicker and more compact coatings. These layers contain spherical aggregates with diameters up to 8-10 μm (Figure 4.4.4), consisting of nanoparticles of apatite crystallites, which are characteristic for coatings precipitated from 1.5 SBF treatment. Figure 4.4.4 shows the spectra from the shadowing technique under EDX of the cross section of the polymer film pre-treated with 5M NaOH and soaked in 1.5 SBF for 18 days, which was used to measure the thickness of the aggregate layers presented in the calcium phosphate deposited layer.

In contrast, films that had not been pre-treated with NaOH, showed no calcium phosphate deposition, even after immersion for 18 days in 1.5 SBF.

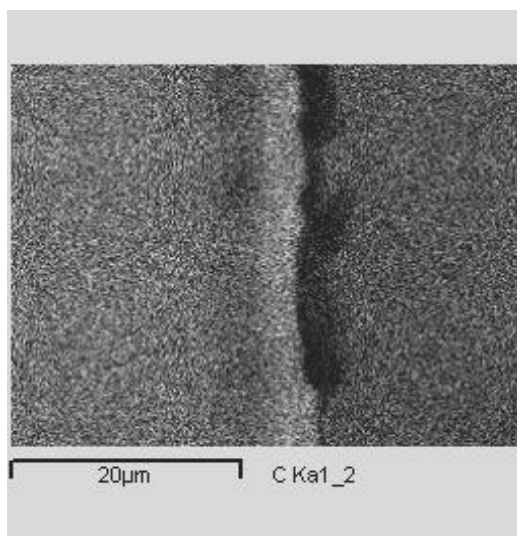


Figure 4.4.4 Spectra of the shadowing technique under EDX of the cross section of the polymer film pre-treated with NaOH and soaked in 1.5 SBF for 18 days. Dark shadow represents the thickness of the apatite layer. (Scale bar= 20 μm)

4.4.2 ASSESSMENT OF ACTIVATION OF PEEK AND UHMWPE WITH HIGH NaOH CONCENTRATION AND PROTRACTED SBF INCUBATION

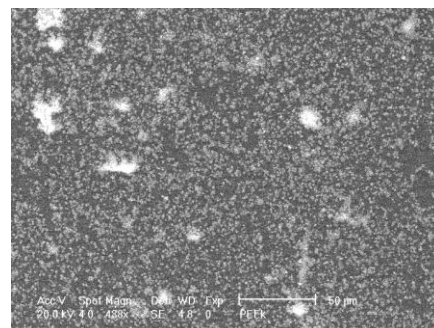
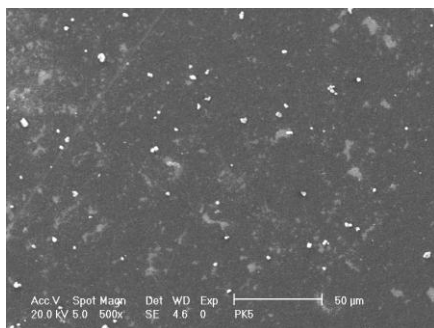
The second series study also showed that an apatite layer was deposited on PEEK and UHMWPE after 5M or 10M NaOH pre-treatment and subsequent immersion in 1.5 SBF for up to 30 days. This is almost double the time compared with the previous set of results, in which the pre-treated films were soaked in 1.5 SBF for up to 15-18 days. It is important to mention that the PEEK film has a bright side and a matt side; therefore, SEM was performed on both sides, which has not been done in the previous set of results. Figure 4.4.5 shows the SEM scans of both sides of PEEK pre-treated with 5M NaOH and soaked in 1.5 SBF treatment for up to 30 days. An apatite layer appeared on both surfaces of the PEEK films on day 3 of the SBF treatment, slightly more appearing on the matt side than on the bright side, and a second apatite layer started to form after day 15 and growth continuously until day 30. Also, some cracks were noticed after day 15 in the SBF treatment, with more cracks observed on the matt side (Figure 4.4.5). Figure 4.4.6 shows the SEM scans of PEEK films on both sides after being pre-treated with 10M NaOH and immersed in 1.5 SBF for 30 days. A similar tendency was found on 10M NaOH pre-treated PEEK films compared with the 5M NaOH pre-treated PEEK films (Figure 4.4.5); yet the second layer of apatite appeared earlier, at day 7 rather than day 15, as well as the presence of cracks. Thus, the growth of apatite seemed to proceed faster on PEEK films pre-treated with the higher concentration of NaOH (Figure 4.4.6). Figure 4.4.7 shows the SEM scans of UHMWPE films pre-treated with 5M or 10M NaOH and soaked in 1.5 SBF for up to 30 days. A similar behaviour to that found on the PEEK samples could be observed for the case of UHMWPE: as the strength of the NaOH pre-treatment increases, from 5M to 10M NaOH, a faster nucleation and growth of apatite occurred. Apatite growth also increased with the immersion time in the 1.5 SBF treatment. The cracks were more predominant on the UHMWPE films pre-treated with 10M NaOH compared with the 5M NaOH pre-treatment (Figure 4.4.7).

1.5 SBF

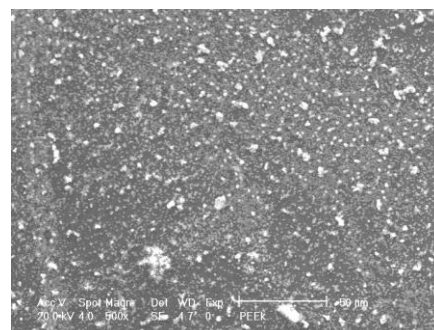
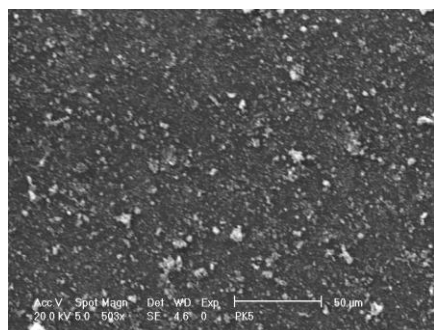
5M NaOH pre-treated PEEK
Bright side

5M NaOH pre-treated PEEK
Matt side

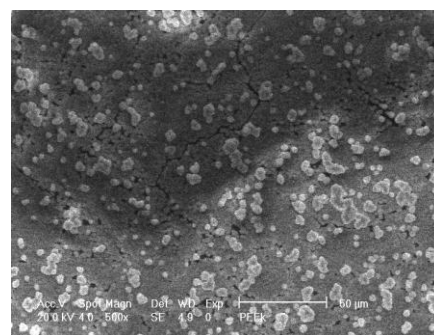
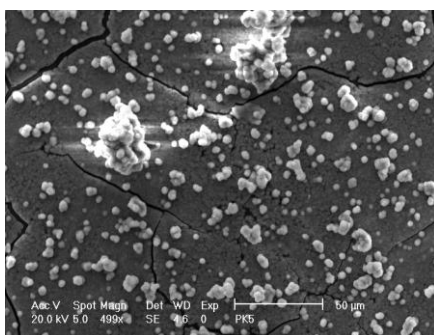
3 days



7 days



15 days



30 days

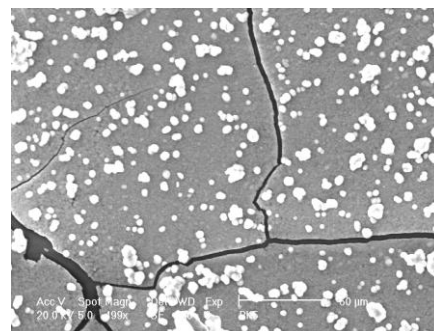
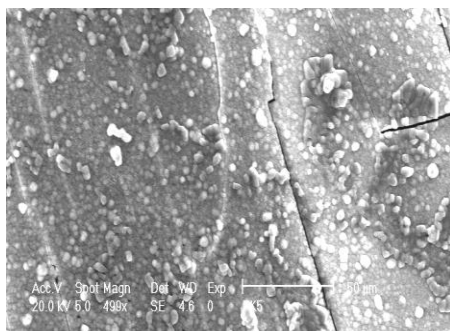


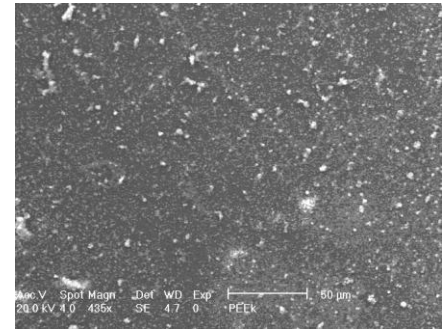
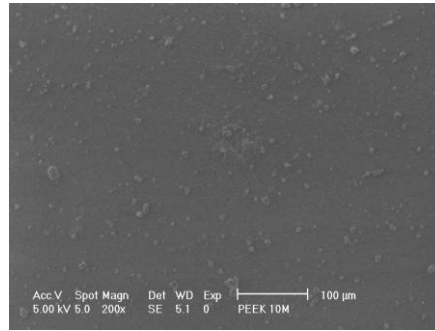
Figure 4.4.5 SEM micrographs of the PEEK films on the bright and matt sides pre-treated with 5M NaOH and soaked in 1.5 SBF for up to 30 days. (Scale bars= 50 μm)

1.5 SBF

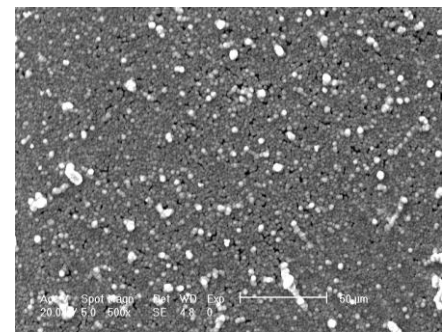
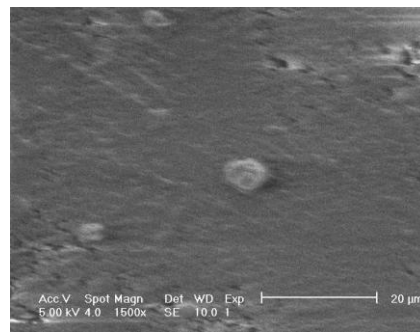
10M NaOH pre-treated PEEK
Bright side

10M NaOH pre-treated PEEK
Matt side

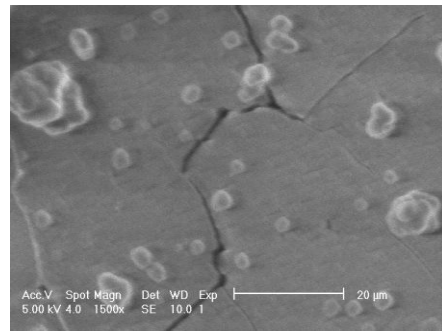
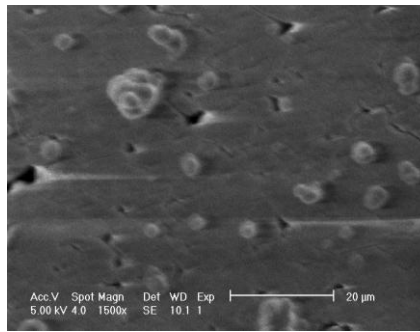
3 days



7 days



15 days



30 days

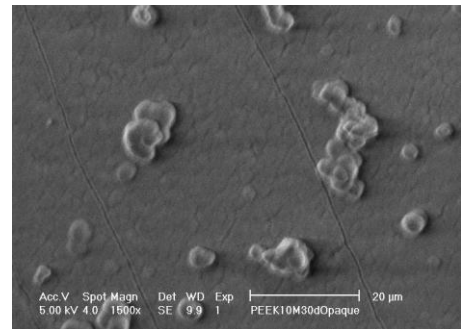
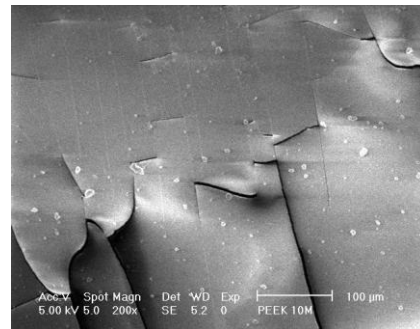
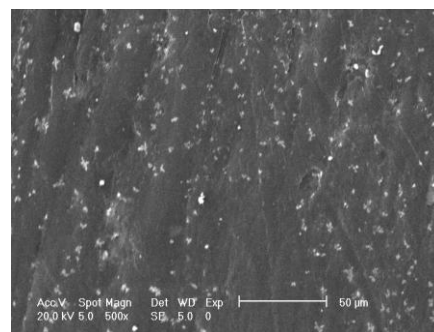
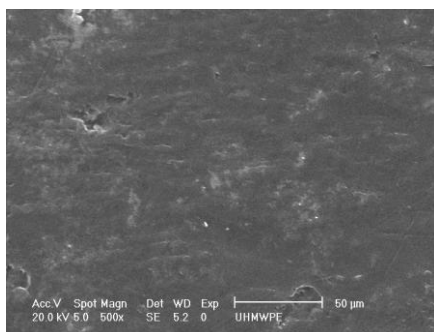


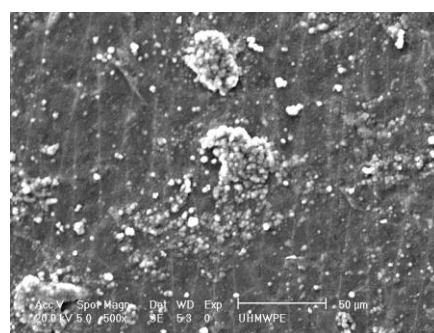
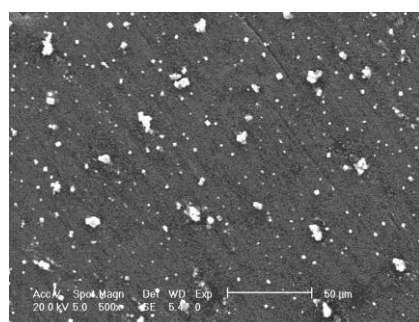
Figure 4.4.6 SEM micrographs of the PEEK films on the bright and matt sides pre-treated with 10M NaOH and soaked in 1.5 SBF for up to 30 days. (Scale bars= 20 μm for PEEK bright at 7 and 15 days and PEEK matt at 15 and 30 days. Scale bars= 50 μm for PEEK matt side at 3 and 7 days. Scale bars= 100 μm for PEEK bright side at 3 and 30 days)

1.5 SBF 5M NaOH pre-treated UHMWPE 10M NaOH pre-treated UHMWPE

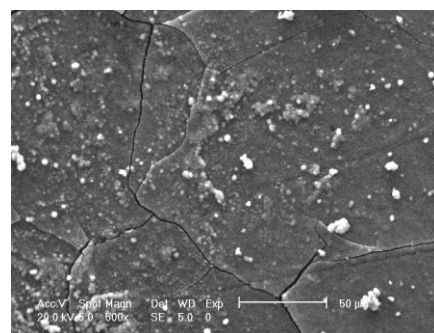
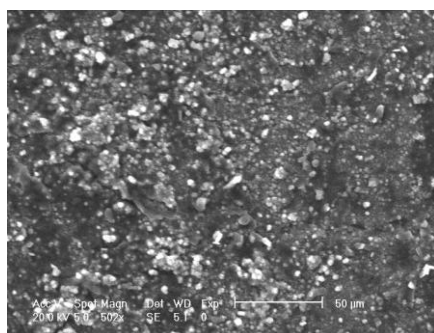
3 days



7 days



15 days



30 days

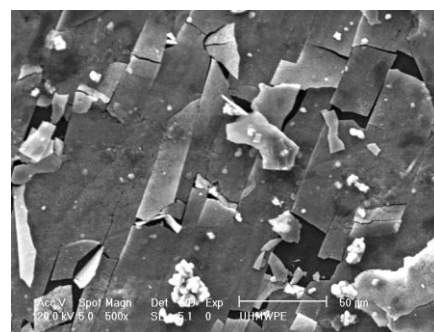
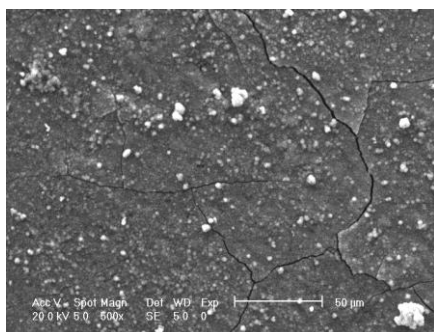


Figure 4.4.7 SEM micrographs of the UHMWPE films pre-treated with 5 or 10M NaOH and soaked in 1.5 SBF for up to 30 days. (Scale bars= 50 μm)

4.5 ENERGY DISPERSIVE X-RAY SPECTROSCOPY (EDX)

4.5.1 INITIAL SCREENING OF POLYMERS WITH NaOH ACTIVATION

Energy Dispersive X-ray (EDX) spectra of PEEK, HDPE and UHMWPE pre-treated with 1M, 5M or 10M of NaOH solutions and soaked in 1.5 SBF for up to 15 days showed similar trends (Figures 4.5.1 to 4.5.3). Calcium (Ca) and phosphorous (P) with small fractions of magnesium (Mg) and sodium (Na) were found, indicating that these deposits are crystalline apatite. Magnesium (Mg^{2+}) and sodium (Na^+) ions can substitute for calcium (Ca^{2+}) ions in apatites, which is in agreement with the composition of biological apatites from human bones and teeth which are non-stoichiometric with trace components such as magnesium (Mg^{2+}), sodium (Na^+), carbonate (CO_3^{2-}), phosphate (HPO_4^{2-}), fluorine (F^-) or chloride (Cl^-).

The prominent peaks of Calcium (Ca) and phosphorous (P) were found on all polymers, PEEK, HDPE and UHMWPE, after different times during the 1.5 SBF treatments, previously pre-treated with different NaOH solutions, as shown in the EDX spectra in Figures 4.5.1 to 4.5.3, respectively.

The increasing height of these peaks implies a strong dependence on the concentration of the NaOH pre-treatment and also on the immersion time in the 1.5 SBF treatments, as shown particularly in the EDX spectrum of PEEK in Figure 4.5.1, as well in the case of HDPE displayed on the EDX scan in Figure 4.5.2. However, this dependence is less evident in the case of UHMWPE shown on the EDX spectrum in Figure 4.5.3. For example, on PEEK films pre-treated with different strengths of NaOH solution and immersed in 1.5 SBF for up to 15 days, the calcium (Ca) and phosphorous (P) peaks appeared first on the EDX spectrum on day 3 when the film was pre-treated with 10M NaOH, on day 7 when 5M and 10M NaOH pre-treatments were used, and on day 15 after 1M NaOH pre-treatment (Figure 4.5.1). A similar pattern was present on HDPE films, but occurring slightly earlier, with the calcium (Ca) and phosphorous (P) peaks identified first on day 1 when HDPE was pre-treated with 10M NaOH, on day 3 when 5M NaOH solution was used, and on day 7 when the film was subjected to 1M NaOH (Figure 4.5.2). In the case of UHMWPE, calcium (Ca) and phosphorous (P) peaks emerged until day 7 after all

NaOH pre-treatments, 1M, 5M and 10M (Figure 4.5.3). This could indicate that the calcium (Ca) and phosphorous (P) peaks appearance may depend on the structure of the polymer as well as on the concentration of the NaOH pre-treatment used and on the immersion time in 1.5 SBF treatments.

The average Ca/P molar ratio was obtained from the EDX of the layer precipitated on PEEK, HDPE and UHMWPE films, pre-treated with 1M, 5M or 10 M NaOH aqueous solution and immersed in 1.5 SBF for 3, 7 and 15 days was 1.19, 1.26-1.35, and 1.33-1.44, respectively. It should be noted that the Ca/P ratio increased with immersion time in 1.5 SBF treatments. The Ca/P molar ratio was very similar for all polymers pre-treated with different concentration of NaOH solution and treated with 1.5 SBF, the major variation of the Ca/P molar ratio was found from the immersion days in the 1.5 SBF. Thus, it seems that the Ca/P is not strongly related to the type of polymer. The increase of the Ca/P was found more directly proportional to the time of exposure of the polymers in the 1.5 SBF treatment.

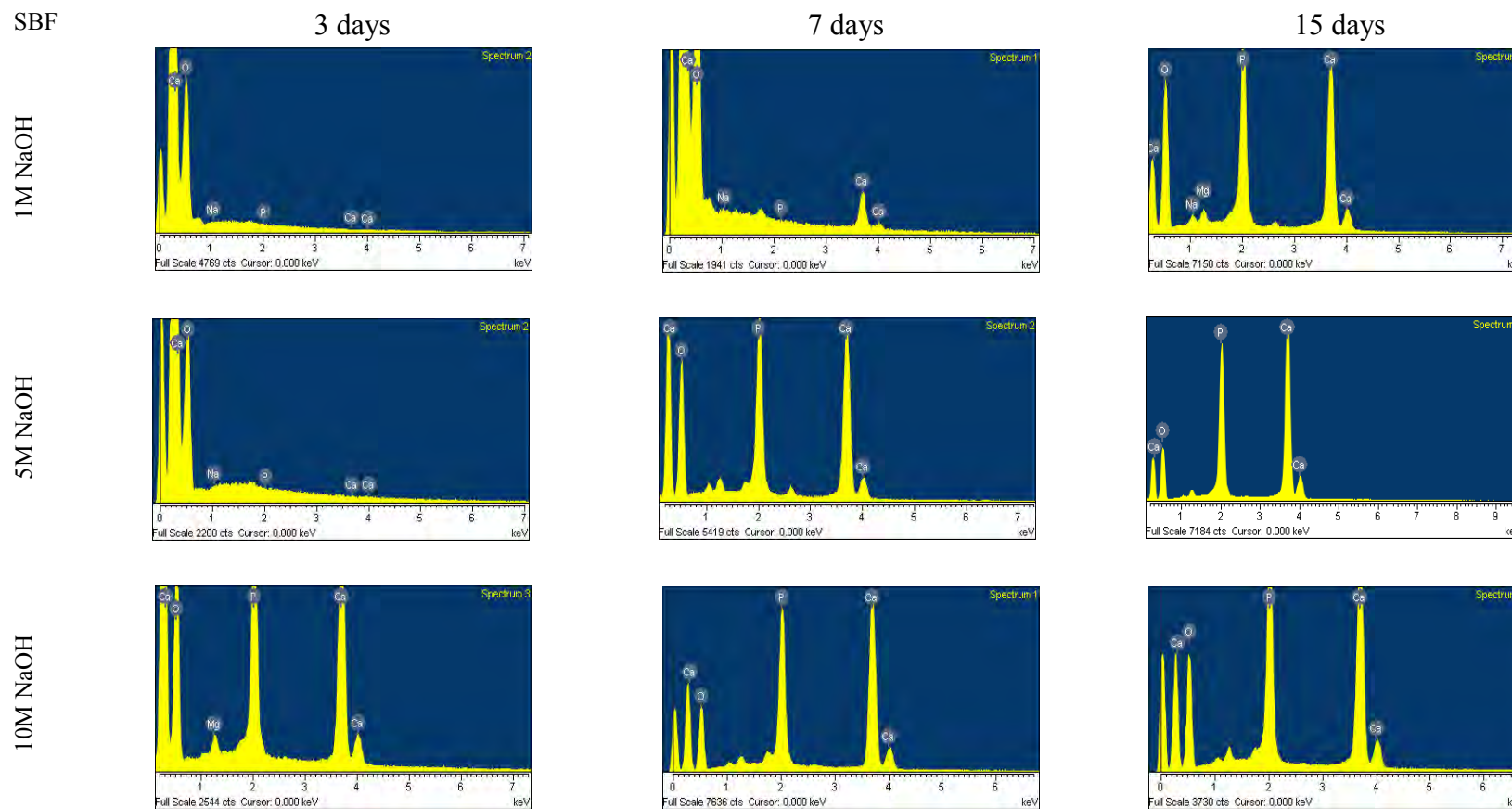


Figure 4.5.1 EDX spectra of PEEK pre-treated with 1, 5, and 10M NaOH and soaked in 1.5 SBF for 3, 7 and 15 days

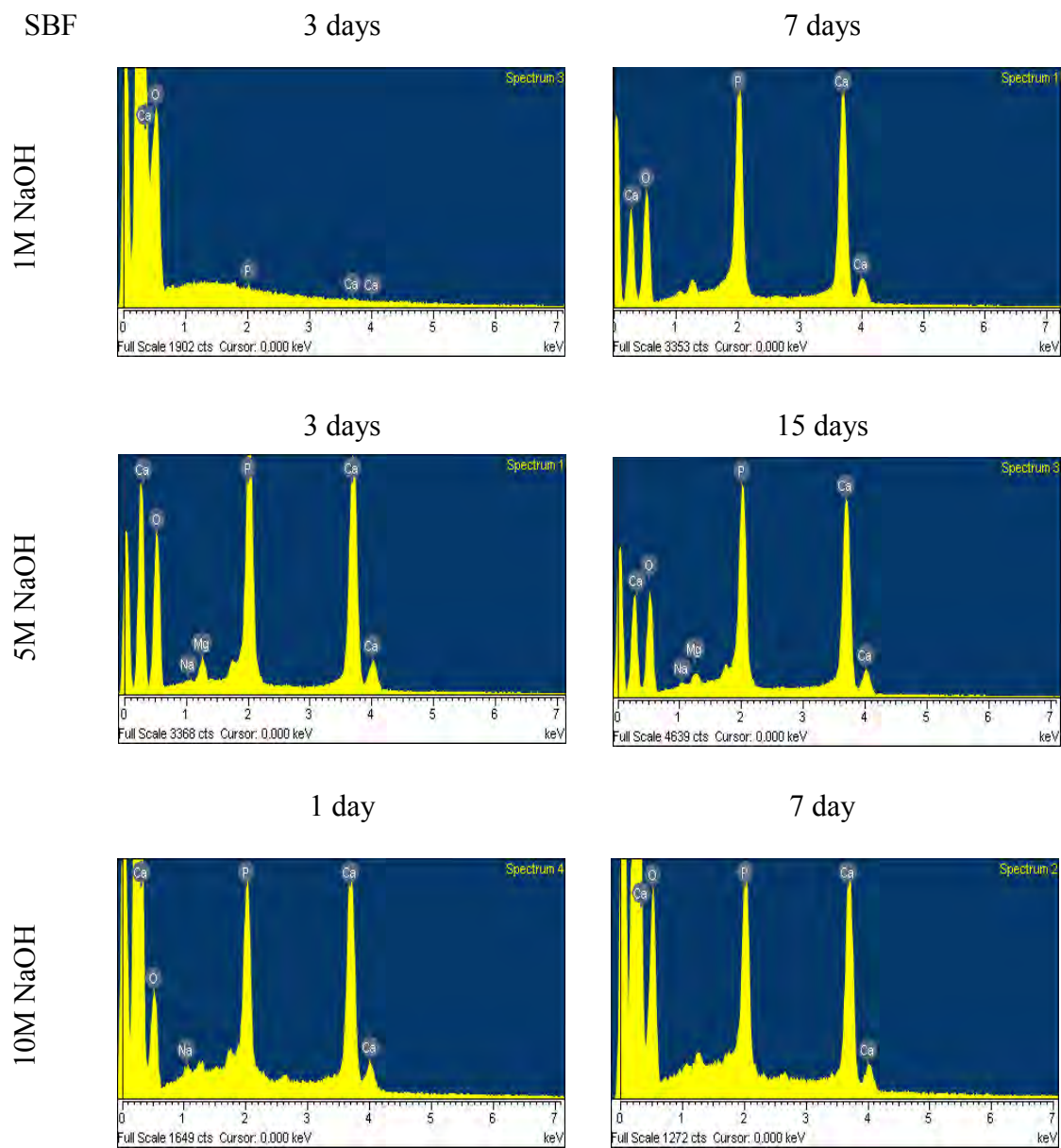


Figure 4.5.2 EDX spectra of HDPE pre-treated with 1M NaOH and soaked in 1.5 SBF for 3 and 7 days (top); HDPE with 5M NaOH and 1.5 SBF for 3 and 15 days (middle); and HDPE with 10M NaOH and 1.5 SBF for 1 and 7 days (bottom)

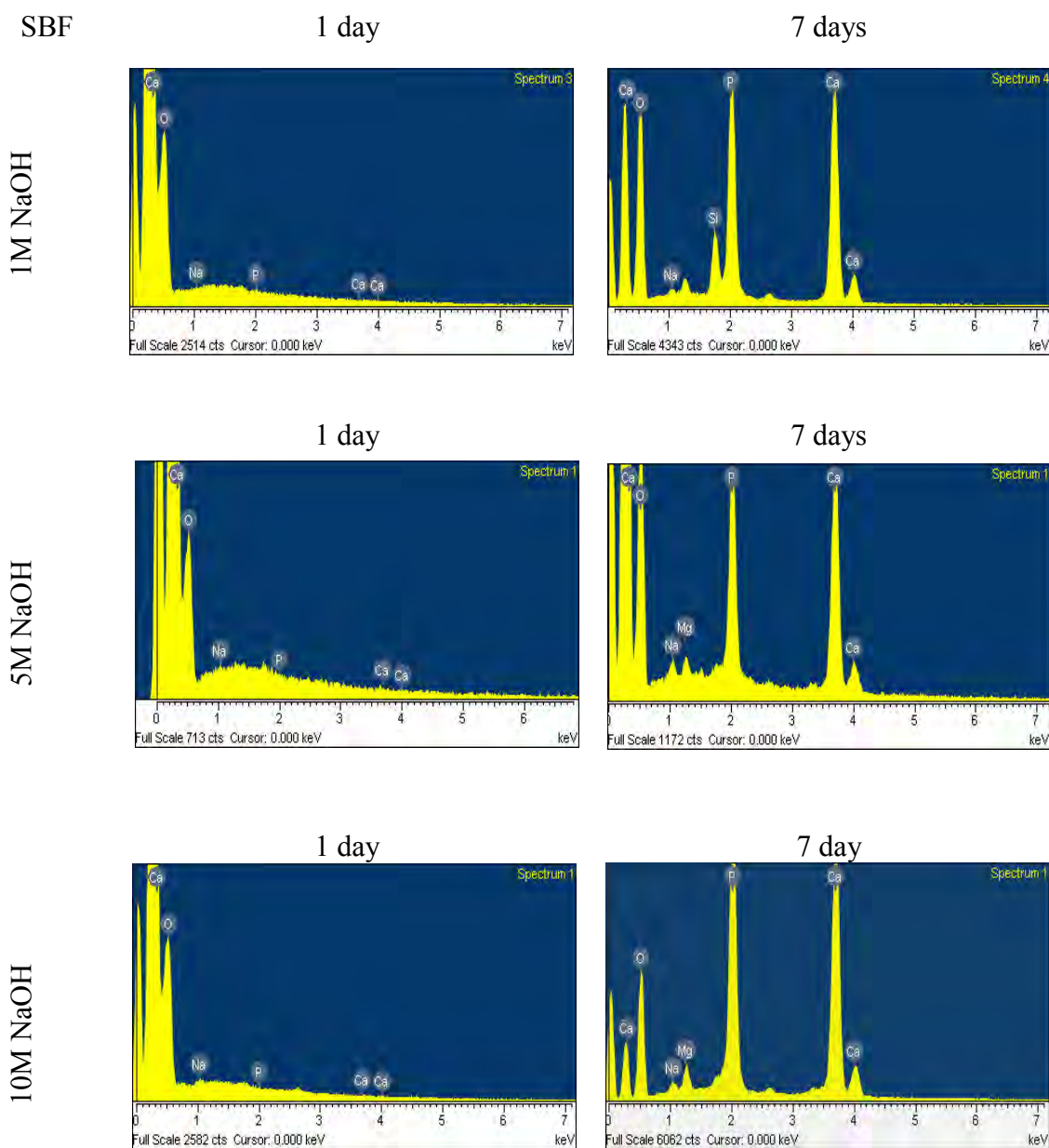


Figure 4.5.3 EDX spectra of UHMWPE pre-treated with 1, 5, and 10M NaOH and soaked in 1.5 SBF for 1 and 7 days

4.5.2 ASSESSMENT OF ACTIVATION OF PEEK AND UHMWPE WITH HIGH NaOH CONCENTRATION AND PROTRACTED SBF INCUBATION

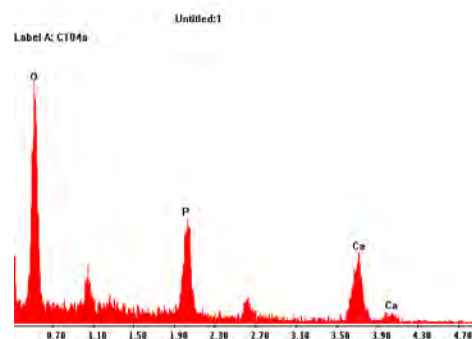
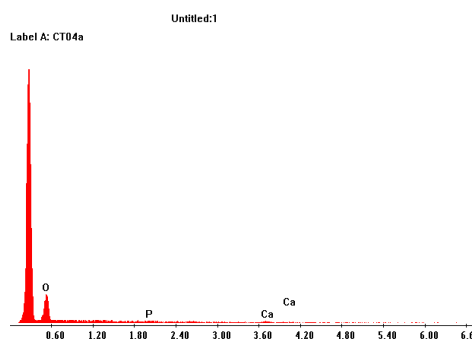
Films of PEEK and UHMWPE were treated for longer periods in 1.5 SBF compared with the previous set of EDX scans (Figures 4.5.1 to 4.5.3). Therefore, Figures 4.5.4 to 4.5.6 show EDX spectra of PEEK (bright and matt surfaces) and UHMWPE films pre-treated with 5M or 10M NaOH and 1.5 SBF for up to 30 days. The apatite layer appeared on both surfaces of the PEEK films after 3 days in SBF, with the matt side apparently somewhat more favourable for apatite deposition than the bright side, both for 5 and 10M NaOH-treated samples. Growth continued until day 30, proceeding faster on PEEK pre-treated with the higher concentration of NaOH. Independent of concentration, however cracking appeared after day 15 in SBF, which was more pronounced on the matt side. Similar behaviour was observed for the UHMWPE structures; i.e. nucleation and growth of apatite occurred faster as the strength of the NaOH pre-treatment increased from 5M to 10M NaOH, as well as with the immersion time used for the 1.5 SBF treatment. It was found that NaOH pre-treatments impart sites on the polymers for the deposition and growth of apatite deposited from the SBF treatments. The control films that were not pre-treated with NaOH showed no deposition or growth of apatite even after 30 days in 1.5 SBF.

1.5 SBF

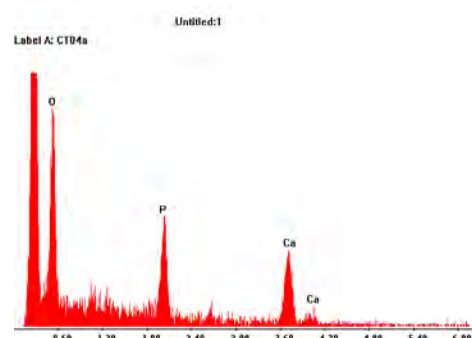
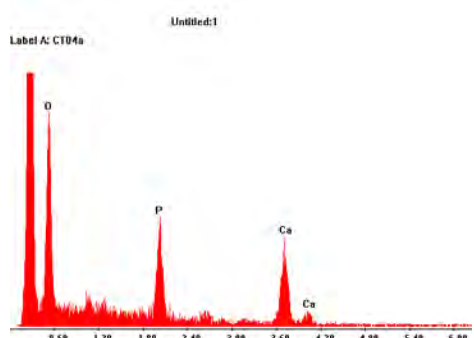
5M NaOH pre-treated PEEK
Bright side

5M NaOH pre-treated PEEK
Matt side

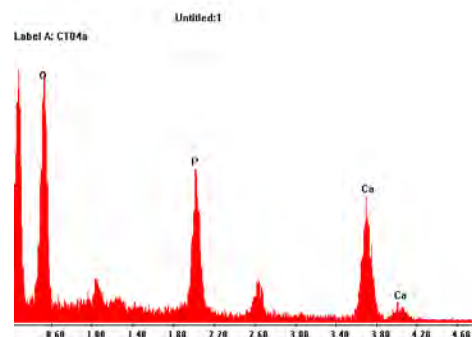
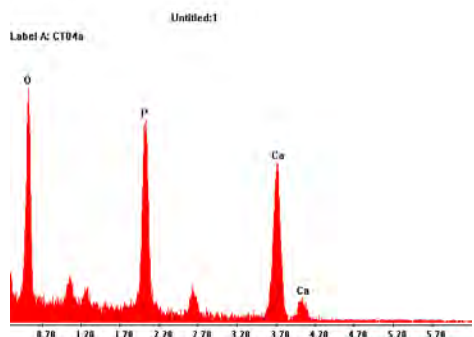
3 days



7 days



15 days



30 days

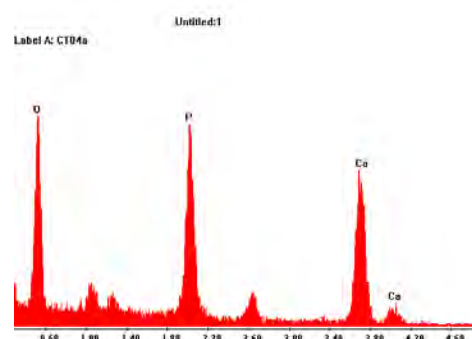
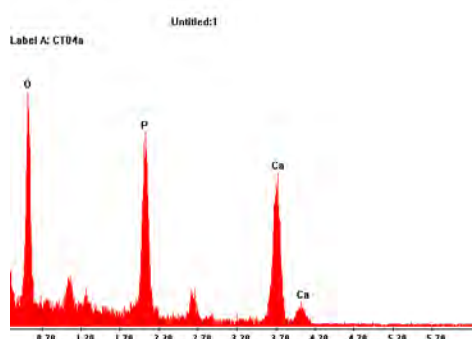


Figure 4.5.4 EDX spectra of the bright and matt sides of PEEK pre-treated with 5M NaOH and soaked in 1.5 SBF for 3, 7, 15 and 30 days

1.5 SBF 10M NaOH pre-treated PEEK 10M NaOH pre-treated PEEK
 Bright side Matt side

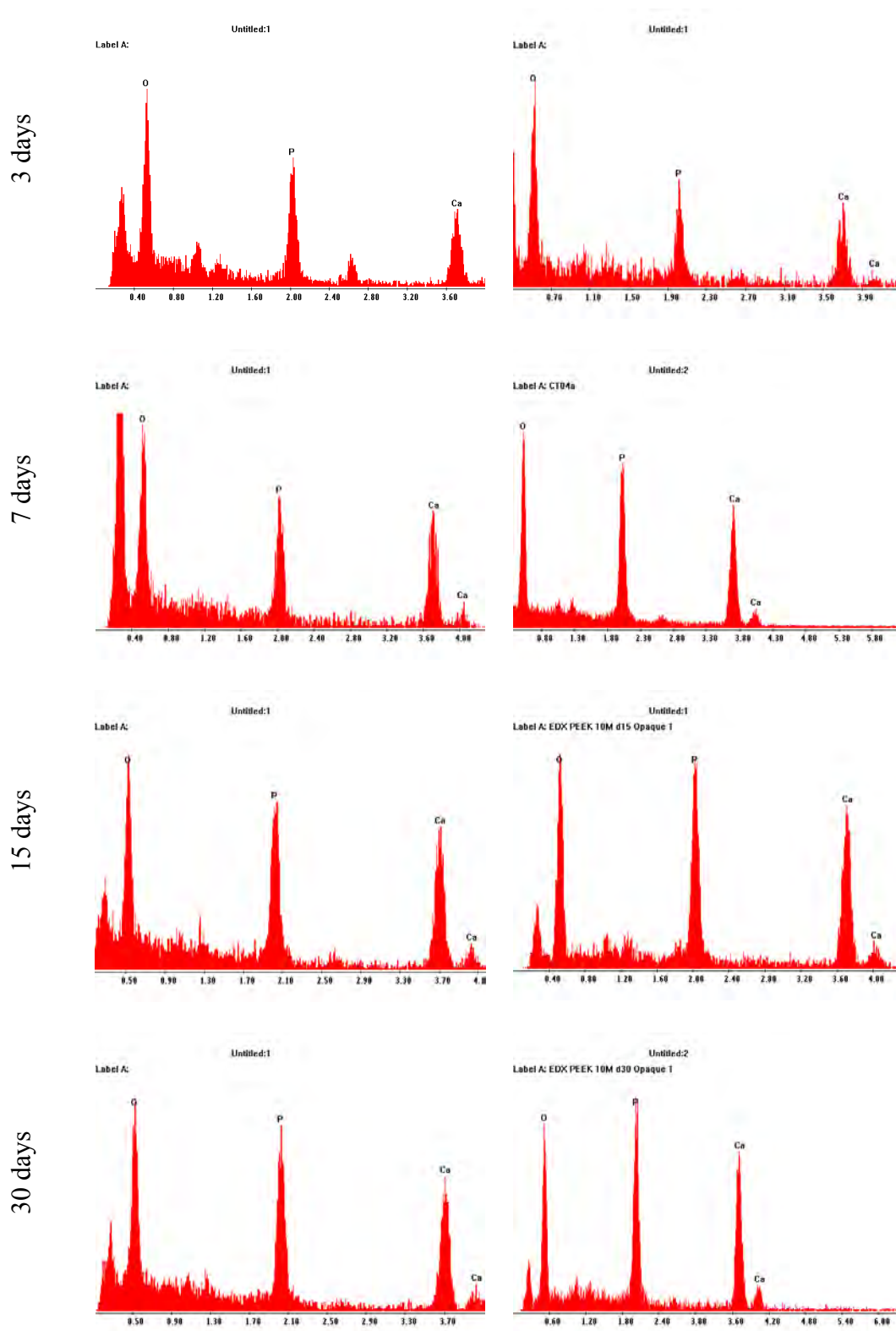


Figure 4.5.5 EDX spectra of the bright and matt sides of PEEK pre-treated with 10M NaOH and soaked in 1.5 SBF for 3, 7, 15 and 30 days

1.5 SBF 5M NaOH pre-treated UHMWPE 10M NaOH pre-treated UHMWPE

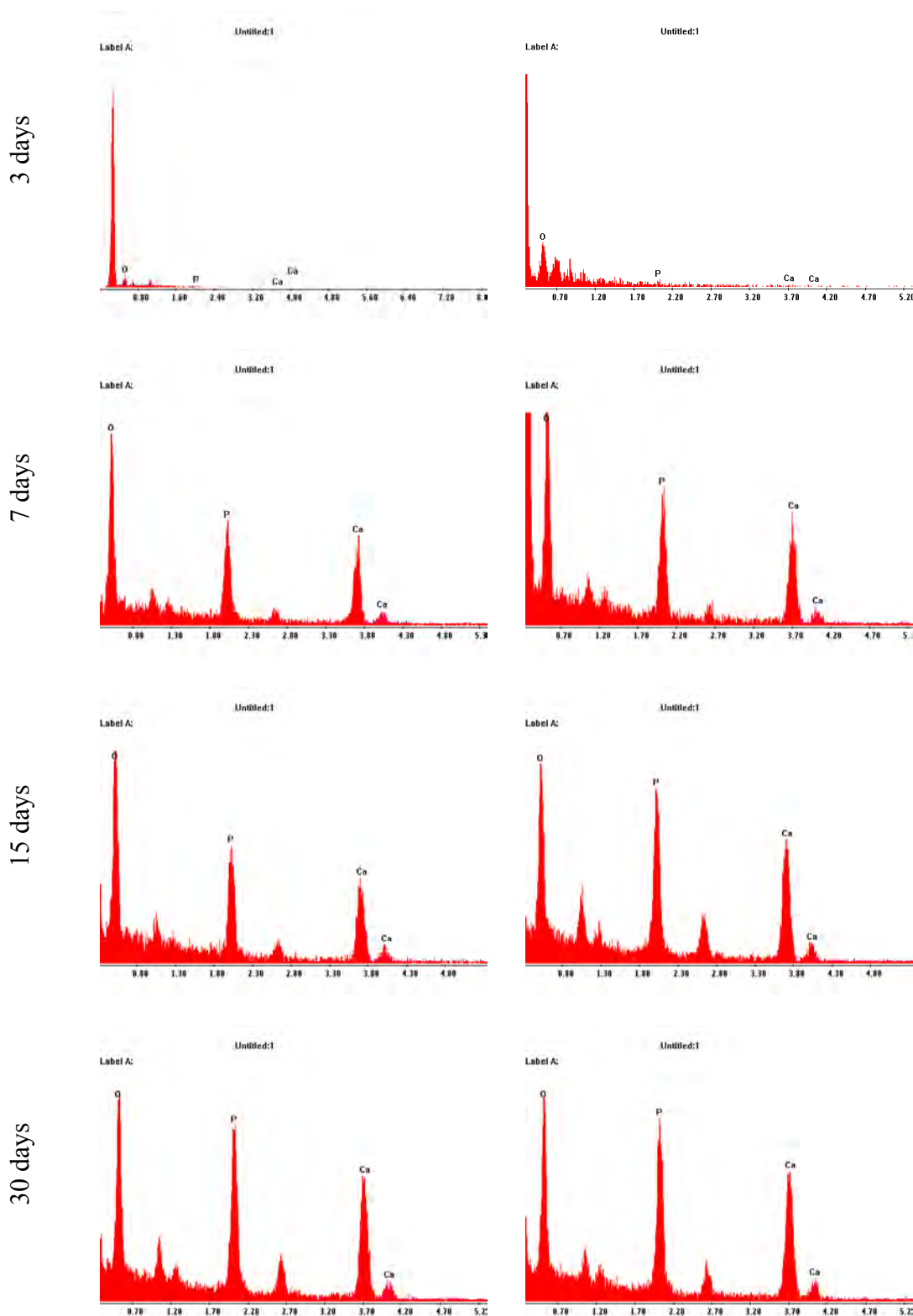


Figure 4.5.6 EDX spectra of UHMWPE pre-treated with 5M or 10M NaOH and soaked in 1.5 SBF for 3, 7, 15 and 30 days

For this second set of experiments, the average calcium (Ca) and phosphorous (P) content found using EDX to analyse the deposited layers on PEEK and UHMWPE films pre-treated NaOH and immersed in 1.5 SBF are shown in Figure 4.5.7. The Ca and P content increased both with the NaOH concentration used during the pre-treatment as well as with the immersion time in 1.5 SBF, for both polymers – i.e. PEEK and UHMWPE. Also, more Ca and P was deposited on the matt PEEK side compared to the bright side.

The Ca/P molar ratio (Figure 4.5.8) in the deposited layers was not strongly affected by the NaOH concentrations for all polymers (Table 4.5.1). Indeed, the Ca/P molar ratio increased from 0.74 (day 3) to 1.58 (day 30) on PEEK (bright side) treated with 5 M NaOH compared to from 1.27 to 1.60 for PEEK (matt side). Thus, the Ca/P molar ratio at the end of day 30 is similar (1.58 and 1.60) for both sides of PEEK.

The PEEK surfaces differences were even less noticeable when pre-treating the polymer films with 10M NaOH. For instance, on day 3, the Ca/P ratios were 1.37 and 1.40 and on day 30, 1.64 and 1.67 for the bright and matt sides of PEEK films pre-treated with 10M NaOH, respectively. For UHMWPE samples, Ca/P increased from 1.42 and 1.49 to 1.61 and 1.64 from day 7 to day 30 in the 1.5 SBF pre-treated with 5M and 10M NaOH, respectively.

The most remarkable difference found in the Ca/P molar ratio of HDPE, PEEK and UHMWPE was due to the immersion time in the 1.5 SBF rather than in the higher concentration of the NaOH pre-treatment. Thus, it seems that above 5M NaOH pre-treatments the effect on increased the Ca/P molar ratio and the acceleration of the apatite deposition on the polymers is nullified. Moreover, it seems that the Ca/P is not strongly dependent on the type of the polymer. The increase of the Ca/P was found directly related to the time of exposure of the polymers in the 1.5 SBF treatment.

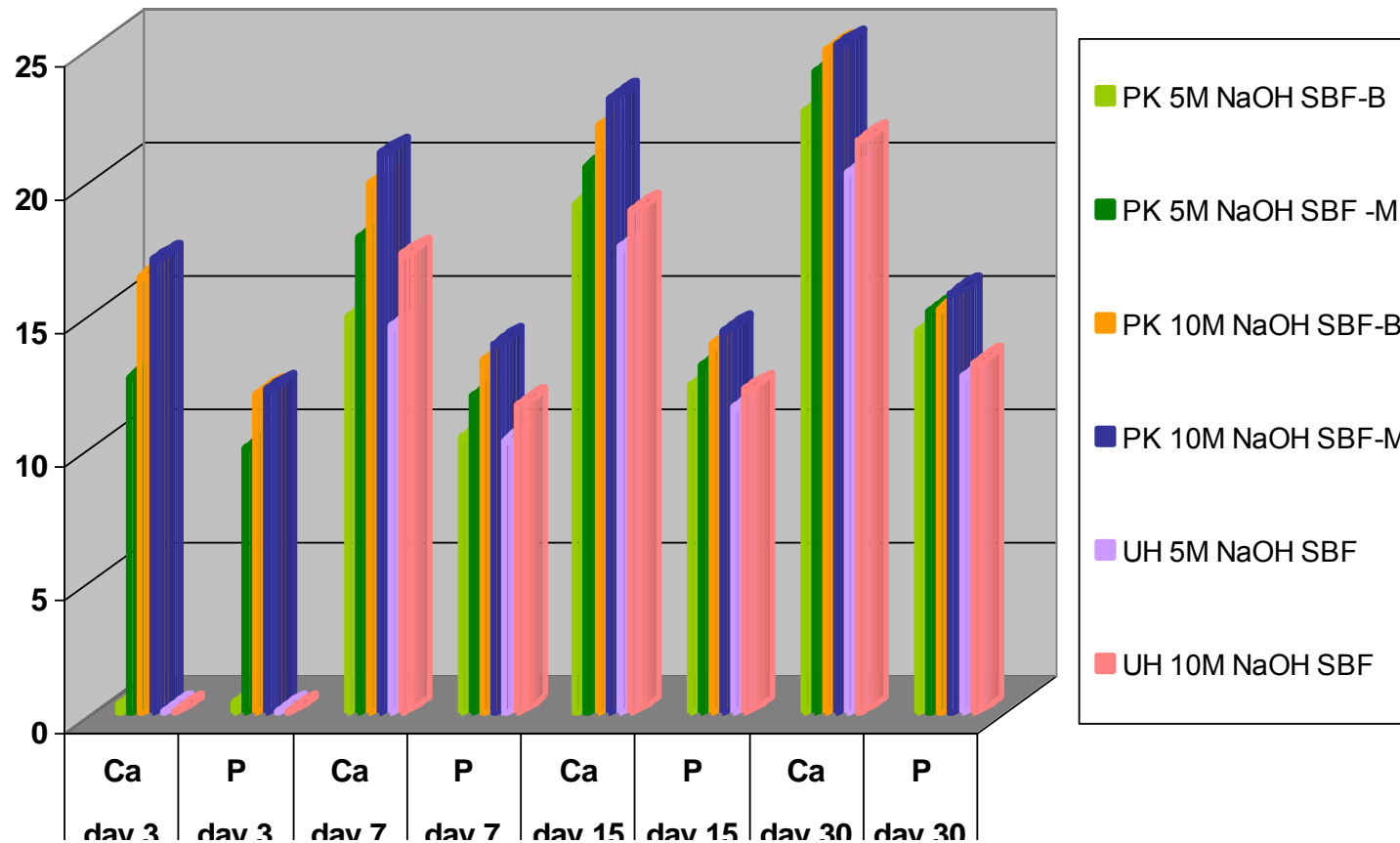


Figure 4.5.7 Average calcium (Ca) and phosphorous (P) in atomic % deposited on PEEK (PK) and UHMWPE (UH) films pre-treated with 5M or 10 M NaOH and immersed in 1.5 SBF for 3, 7, 15 and 30 day, obtained from the EDX test (B= bright, M= matt)

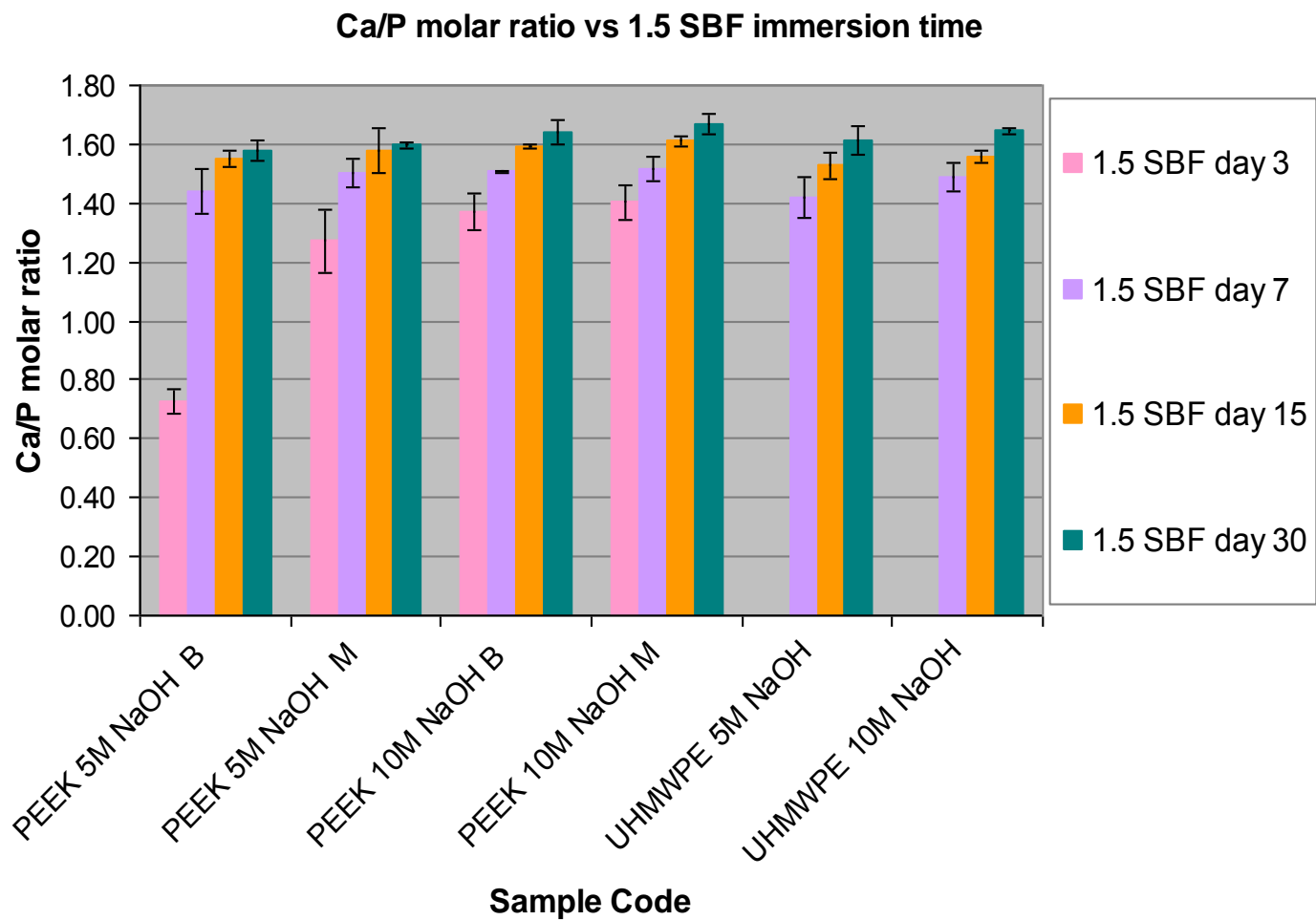


Figure 4.5.8 Average Ca/P molar ratio of PEEK and UHMWPE films pre-treated with 5M or 10M NaOH and immersed in 1.5 SBF for 3, 7, 15 and 30 days, obtained from the EDX test (B= bright, M= matt) (bar error=standard deviation)

Table 4.5.1 The average calcium (Ca) phosphorous (P) and Ca/P molar ratio from the EDX of PEEK and UHMWPE films pre-treated with 5M or 10M NaOH and immersed in 1.5 SBF for 3, 7, 15 and 30 days (S.D = standard deviation)

1.5 SBF	Day 3			Day 7			Day 15			Day 30		
	Ca	P	Ca:P	Ca	P	Ca:P	Ca	P	Ca:P	Ca	P	Ca:P
PEEK 5M NaOH Bright												
Average	0.23	0.32	0.73	14.77	10.26	1.44	19.03	12.25	1.55	22.54	14.28	1.58
S.D.	0.02	0.19	0.04	0.56	0.18	0.08	0.31	0.02	0.03	0.20	0.31	0.03
PEEK 5M NaOH Matt												
Average	12.57	9.89	1.27	17.75	11.83	1.50	20.47	12.97	1.58	24.01	15.03	1.60
S.D.	0.45	0.84	0.10	0.55	0.65	0.05	0.24	0.47	0.07	0.20	0.05	0.01
PEEK 10M NaOH Bright												
Average	16.33	11.91	1.37	19.82	13.15	1.51	21.94	13.79	1.59	24.82	15.12	1.64
S.D.	0.57	0.21	0.06	0.12	0.06	0.01	0.05	0.03	0.01	0.20	0.26	0.04
PEEK 10M NaOH Matt												
Average	16.95	12.08	1.40	20.95	13.80	1.52	23.00	14.27	1.61	26.21	15.71	1.67
S.D.	0.49	0.19	0.06	0.03	0.40	0.04	0.17	1.49	0.02	0.12	0.24	0.03
UHMWPE 5M NaOH												
Average	0.00	0.00	-	14.45	10.20	1.42	17.43	11.40	1.53	20.24	12.55	1.61
S.D.	0.00	0.00	-	0.42	0.23	0.07	0.15	0.28	0.04	0.13	0.34	0.05
UHMWPE 10M NaOH												
Average	0.00	0.00	-	17.15	11.50	1.49	18.81	12.08	1.56	21.44	13.04	1.64
S.D.	0.00	0.00	-	0.64	0.07	0.05	0.18	0.06	0.02	0.08	0.06	0.01

4.6 LASER RAMAN SPECTROSCOPY

The high-density polyethylene (HDPE) and ultra high molecular weight polyethylene (UHMWPE) films were characterized with Raman spectroscopy. Figures 4.6.1 and 4.6.2 show Raman spectra of HDPE and UHMWPE films, non-treated as well as exposed to 5M NaOH and immersed in 1.5 SBF for 18 days, respectively. The characteristic peaks of the HDPE and UHMWPE are located in three zones. The features present at 1040-1150 cm^{-1} are due to the C-C stretching vibrations, those observed at 1250-1350 cm^{-1} are CH_2 twisting vibrations, and peaks at 1390-1550 cm^{-1} are attributed to CH_2 bending vibrations.

In addition to the features mentioned on the previous paragraph, the spectrum of HDPE samples, which had been pre-treated with 5M NaOH and immersed in 1.5 SBF for 18 days (Figure 4.6.1), displayed two small peaks, which are not present in the spectra for the non-treated HDPE films (Figure 4.6.1). The peak at 873.0 cm^{-1} was assigned to carbonate ions, which occupies one of the sites in carbonated apatite due to the ν_2 vibrational mode (Rehman and Bonfield, 1997; Legeros *et al.*, 1987), whereas the peak at 962.1 cm^{-1} most likely represents a phosphate ν_1 band, which often is observed in hydroxyapatite and carbonated apatites (Rehman and Bonfield, 1997).

The spectra of the UHMWPE pre-treated with 5M NaOH solution and immersed in 1.5 SBF for 18 days (Figure 4.6.2) exhibits three peaks, which are not observed in the non-treated UHMWPE spectra (Figure 4.6.2). The peaks at 873.4 and 961.6 cm^{-1} result from carbonate and phosphate ions, respectively. The peak at 1470.8 cm^{-1} corresponds to carbonate ions, occupying the second site in carbonated apatite due to the ν_1 band (Rehman and Bonfield, 1997). This feature is known to depend on the maturation and formation of apatite crystals. Thus, it is interesting to note that it is not observed in the corresponding (pre-treated) HDPE spectra, possibly due to the fact that less apatite formed on NaOH-treated HDPE when compared to UHMWPE samples.

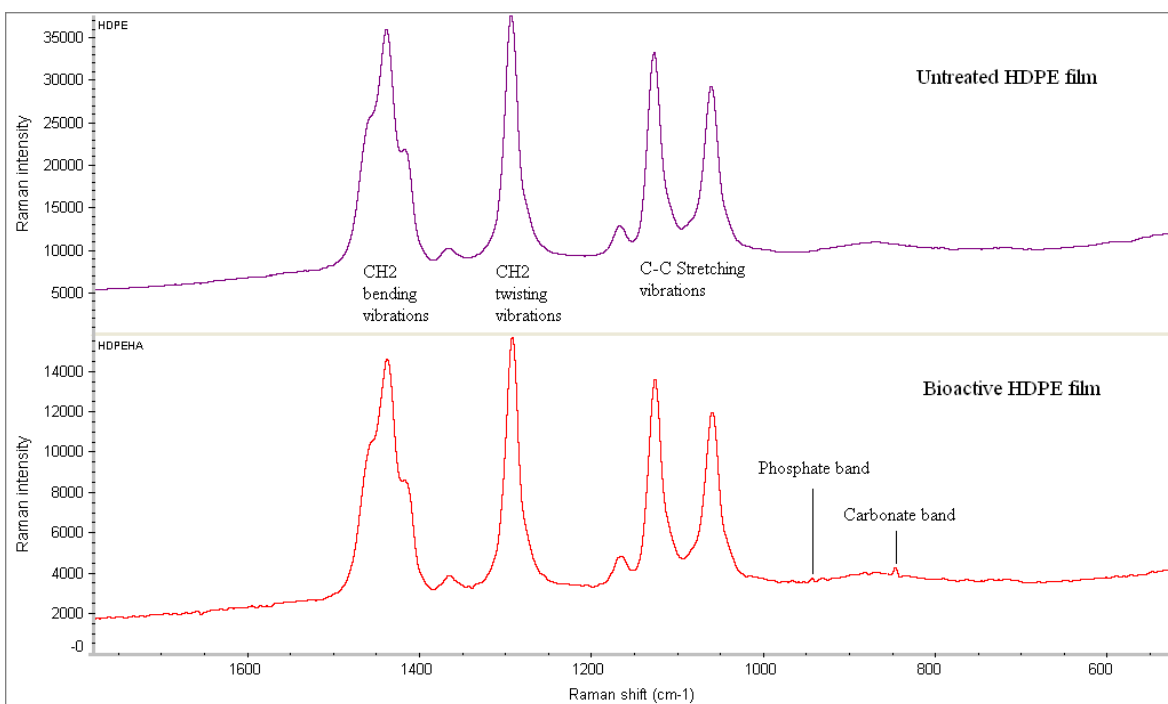


Figure 4.6.1 Raman spectra of non-treated HDPE (top) and HDPE pre-treated with 5M NaOH and soaked in 1.5 SBF for 18 days (bottom)

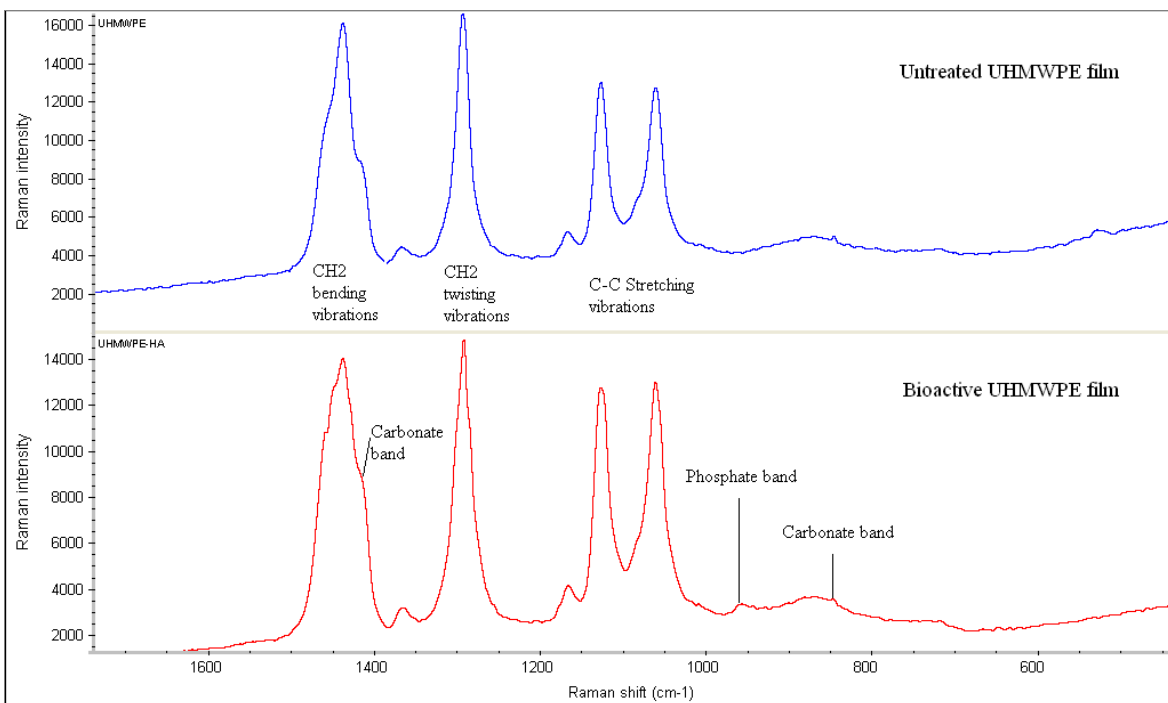


Figure 4.6.2 Raman spectra of non-treated UHMWPE (top) and UHMWPE pre-treated with 5M NaOH and soaked in SBF for 18 days (bottom)

Figure 4.6.3 shows Raman spectra of the apatite scraped from all polymers, high-density polyethylene (HDPE), ultra high molecular weight polyethylene (UHMWPE) and polyether ether ketone (PEEK) films pre-treated with 5M NaOH and immersed in 1.5 SBF treatments for 18 days. The apatite was scraped off all three materials and combined to produce sufficient materials for spectra to be obtained. The peaks at 2880 cm^{-1} and 1440 cm^{-1} are assigned to the $\nu_s\text{CO}_3$ vibration (Petra *et al.*, 2005; Hofmann *et al.*, 2007) and the $\nu_3\text{CO}_3$ band (Ha *et al.*, 1997), respectively. Peaks at 1076 cm^{-1} and 1130 cm^{-1} , as well as the shoulder at 1170 cm^{-1} , are attributed to the P-O asymmetric stretching mode, also reported by Ning *et al.* (2004). The shoulder-like appearance of the 1076 cm^{-1} feature may origin from some overlap with the 1070 cm^{-1} vibration, which corresponds to the $\text{CO}_3^{2-}\nu_1$ band (Penel *et al.*, 1998). Finally, the peaks at, 2850 cm^{-1} may be related to the H-C-O functional group from the polymeric films, and 1290 cm^{-1} to P-O (phosphate region).

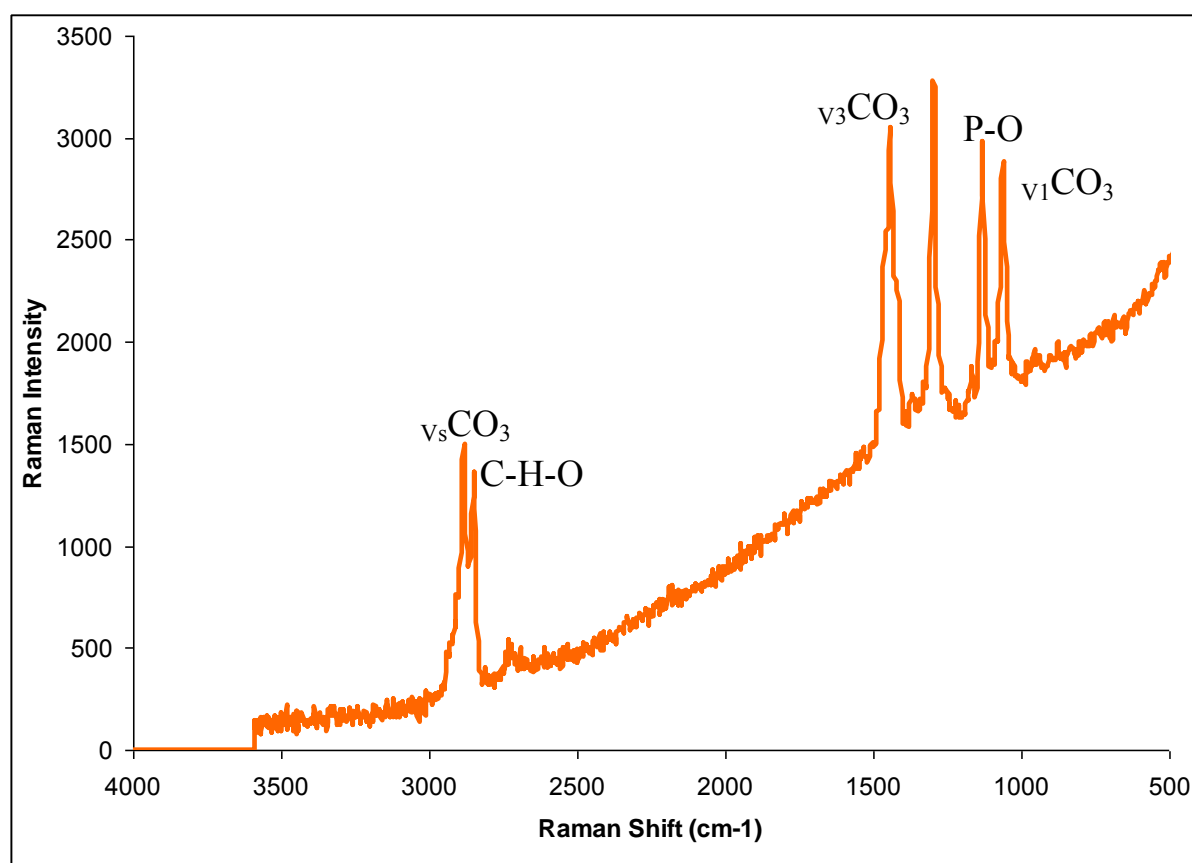


Figure 4.6.3 Raman spectrum of the layer scraped from PEEK, HDPE and UHMWPE pre-treated with 5M NaOH then the immersed in SBF for 18 days

4.7 FOURIER TRANSFORM INFRARED SPECTROSCOPY (FTIR)

FTIR spectra of non-treated HDPE films and those exposed to 5M NaOH and immersed in 1.5 SBF for 18 days, are shown in Figure 4.7.1. Characteristic HDPE features are found, which are in agreement with spectra reported in the literature (Muller and Muller, 2006; Pandey *et al.*, 2006). The intense peaks at 2920 cm^{-1} and 2850 cm^{-1} correspond to asymmetric and symmetric CH_2 stretching vibrations, respectively; those at 1558 cm^{-1} and 1471 cm^{-1} result from the C-H bending deformation, the less pronounced feature at 1371 cm^{-1} can be assigned to the C-H symmetric deformation of terminal methyl group and the intense peak at 720 cm^{-1} originates from C-H rocking deformation. The spectrum of the treated HDPE sample with 5M NaOH and SBF immersion shows a very small peak at 3210 cm^{-1} , which is probably due to the OH groups of the apatite; a strong peak at 1600 cm^{-1} is likely due to CO_3 band, which overlaps possibly with the C-H vibration of the polymer, a broad doublet at about 1468 and 1425 cm^{-1} is assigned to CO_3 absorption in precipitated apatites (Elliot, 1994); features at 1039 cm^{-1} and 728 cm^{-1} are most likely due to structural and P-O bond of the phosphate groups (Pandey *et al.*, 2006). It is worth noticing in the case of treated HDPE in 5M NaOH and SBF, that the characteristic polymer bands tend to weaken when apatite forms, which may illustrate the formation of apatite from carbonate and phosphate.

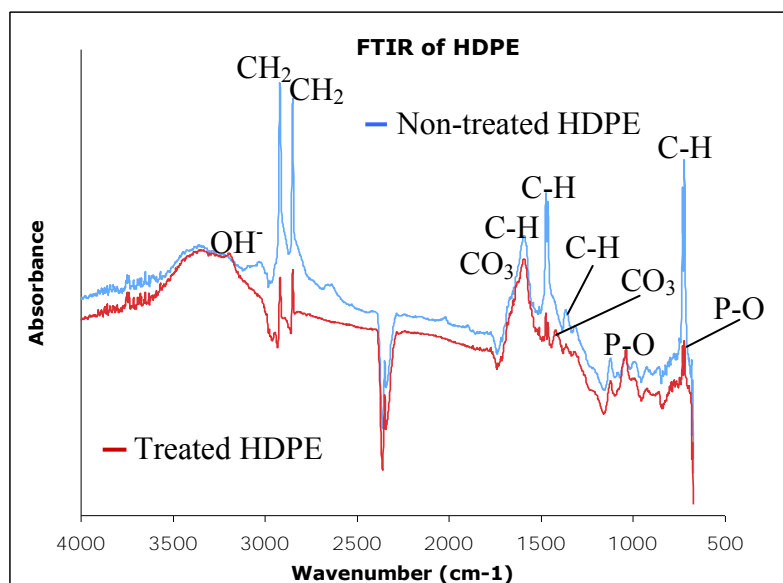


Figure 4.7.1 FTIR of non-treated HDPE and pre-treated HDPE with 5M NaOH after immersion in SBF for 18 days

Similar observations as was the case for the FTIR of HDPE (Figure 4.7.1) can be made for UHMWPE non-treated and pre-treated with 5M NaOH and 1.5 SBF for 18 days (Figure 4.7.2). Strong characteristic peaks resulting from the UHMWPE film are present at 2920 and 2850 cm^{-1} . These bands correspond to asymmetric and symmetric CH_2 stretching vibrations, respectively, whereas the features at 1471 and 720 cm^{-1} are due to the C-H bending and rocking deformations, respectively. Treated UHMWPE shows, in addition to the polyethylene features (which, again weaken for treated samples with NaOH solution and 1.5 SBF solution), peaks at 1030 cm^{-1} and 1440 cm^{-1} , which we assigned to structural and P-O bonds of the phosphate groups and, respectively, CO_3 absorption in precipitated apatites.

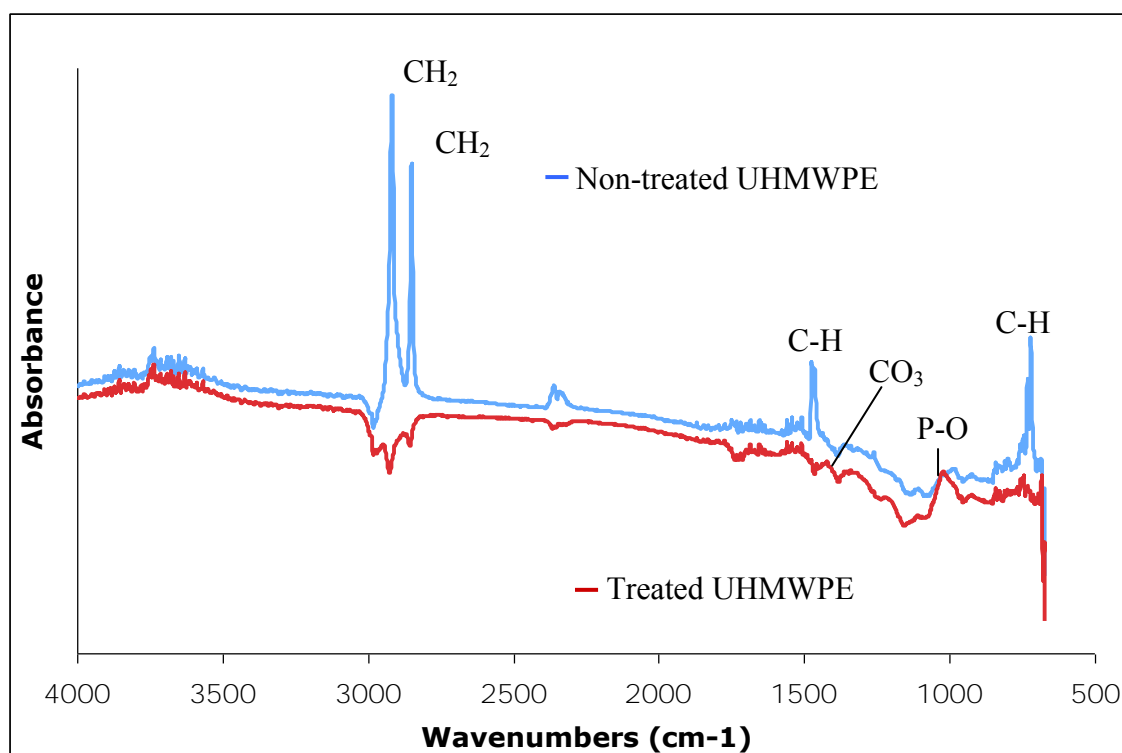


Figure 4.7.2 FTIR of non-treated UHMWPE and pre-treated UHMWPE with 5M NaOH after immersion in SBF for 18 days

Figure 4.7.3 shows the IR spectra of corresponding PEEK films, non-treated PEEK samples, and treated PEEK samples with 5M NaOH solution and 1.5 SBF treatments for 18 days. In the spectrum of the non-treated PEEK specimen, all the characteristic bands are present (diphenyl ketone bands at 1650, 1490 and 928 cm^{-1} ; aryether band at 1230 cm^{-1} , C-O-C stretching vibration of diaryl groups at 1190 and 1160 cm^{-1} (Simonin and Liao, 2000), three features at 1310, 1280 and 1010 cm^{-1} typical of sulphonyl groups, used as solvents in the polymerization process; as well as a peak at 1600 cm^{-1} that is related to C=C in the benzene ring in PEEK). Interestingly, in the spectra of treated PEEK with 5M NaOH and 1.5 SBF solutions, some shift in these characteristic polymer bands can be observed, in addition to peaks originating from apatite. However, identification of all apatite peaks was challenging, as the spectra of PEEK itself is very complex.

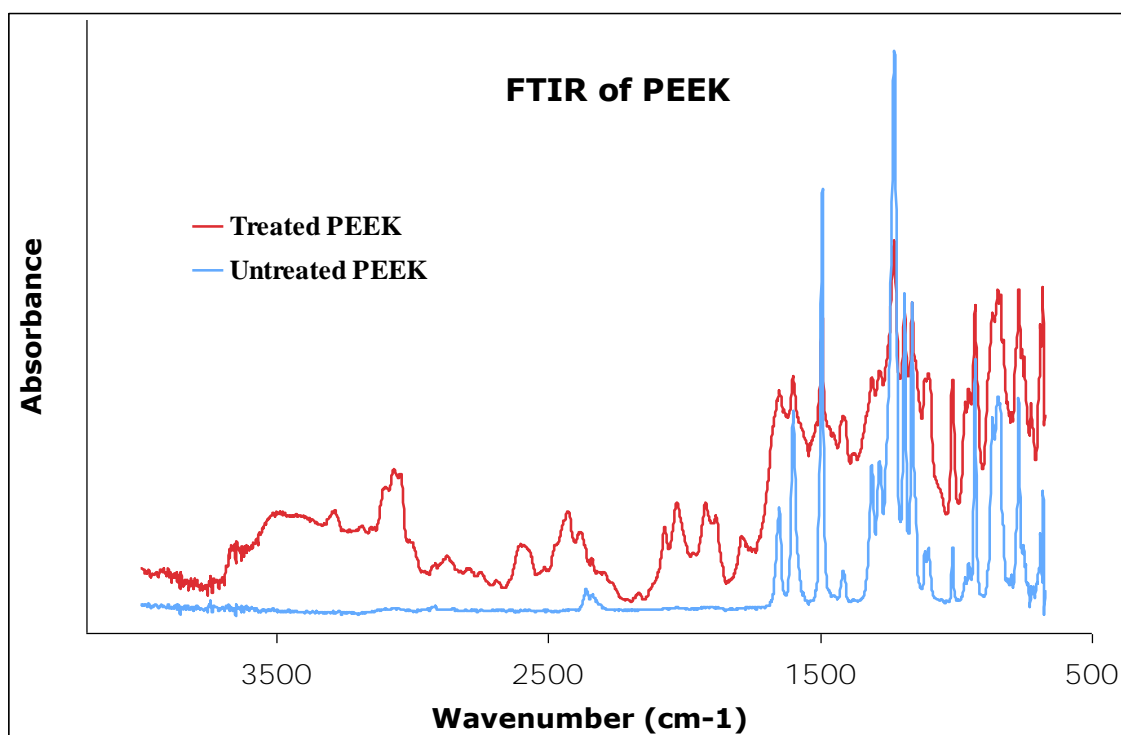


Figure 4.7.3 FTIR of non-treated PEEK and pre-treated PEEK with 5M NaOH after immersion in SBF for 18 days

4.8 REFLECTED LIGHT DIFFERENTIAL CONTRAST (DIC) MICROSCOPY

Table 4.8.1 lists the averaged area of the deposited layers and percentage of area/image area from the reflected light Differential Contrast (DIC) microscope pictures of PEEK (bright and matt sides) and UHMWPE films pre-treated with 5M or 10M NaOH and incubated in 1.5 SBF treatments for 3, 7, 15 and 30 days. Overall, the area of the apatite deposition on the matt surface of PEEK films is always greater than on the PEEK bright surface for both 5 and 10M NaOH-treated samples independent of the immersion time in SBF, even though the area increases with the immersion time for both sides of PEEK. Area and percentage of area covered in the image continued until day 30 of the SBF treatment, with higher values on PEEK pre-treated with higher concentration of NaOH (Figures 4.8.1 and 4.8.2). A similar characteristic was observed for the UHMWPE specimens (Figure 4.8.3), where the area increased with the strength of NaOH, from 5M to 10M. In agreement with the SEM micrographs, it was found that the apatite area increased both with the NaOH concentration used for the pre-treatments as well as the immersion time in 1.5 SBF, for PEEK and UHMWPE. Interestingly, the areas and the percentage of the area/image at the end of day 30 are similar (around 42%) on both PEEK surfaces pre-treated with 5 or 10M NaOH. In the case of UHMWPE, a difference of the area and area/image was found at the end of the SBF treatment on day 30 when the films has been pre-treated with 5M or 10M NaOH, showing a more favourable response for the higher concentration of NaOH.

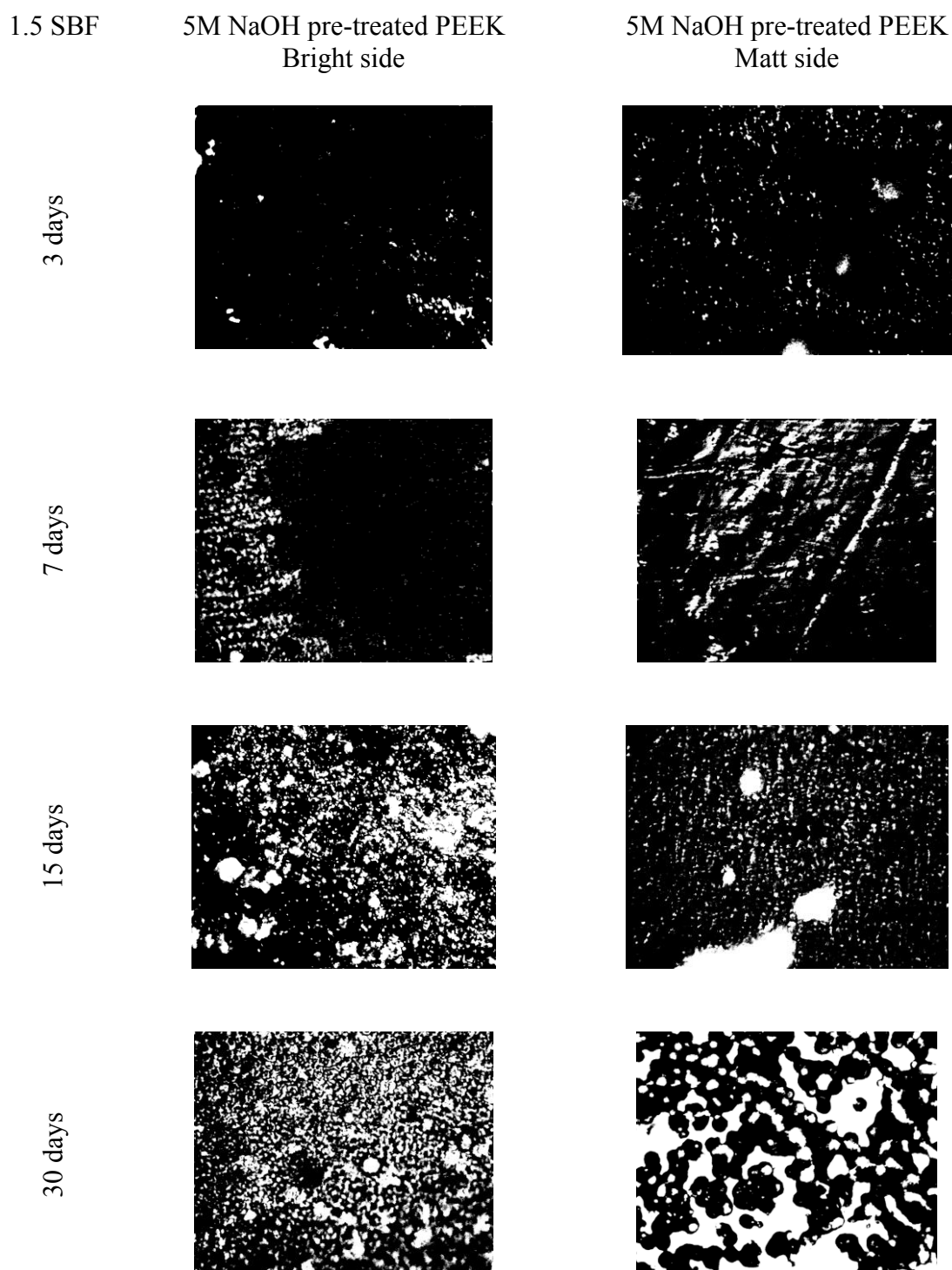


Figure 4.8.1 Reflected light Differential Contrast (DIC) microscope images of PEEK (bright and matt sides) films pre-treated with 5M NaOH and incubated in 1.5 SBF treatments for 3, 7, 15 and 30 days

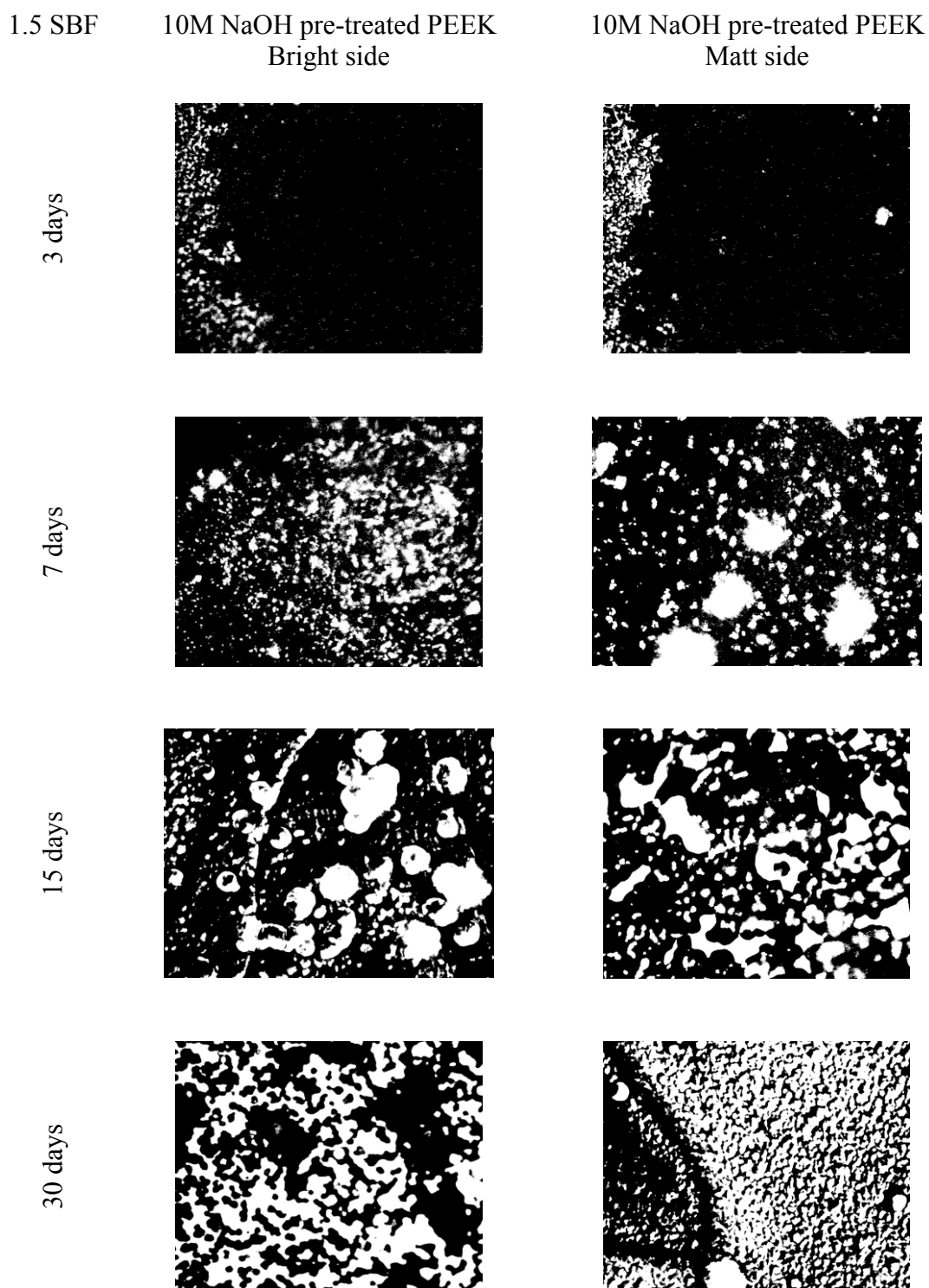


Figure 4.8.2 Reflected light Differential Contrast (DIC) microscope images of PEEK (bright and matt sides) films pre-treated with 10M NaOH and incubated in 1.5 SBF treatments for 3, 7, 15 and 30 days

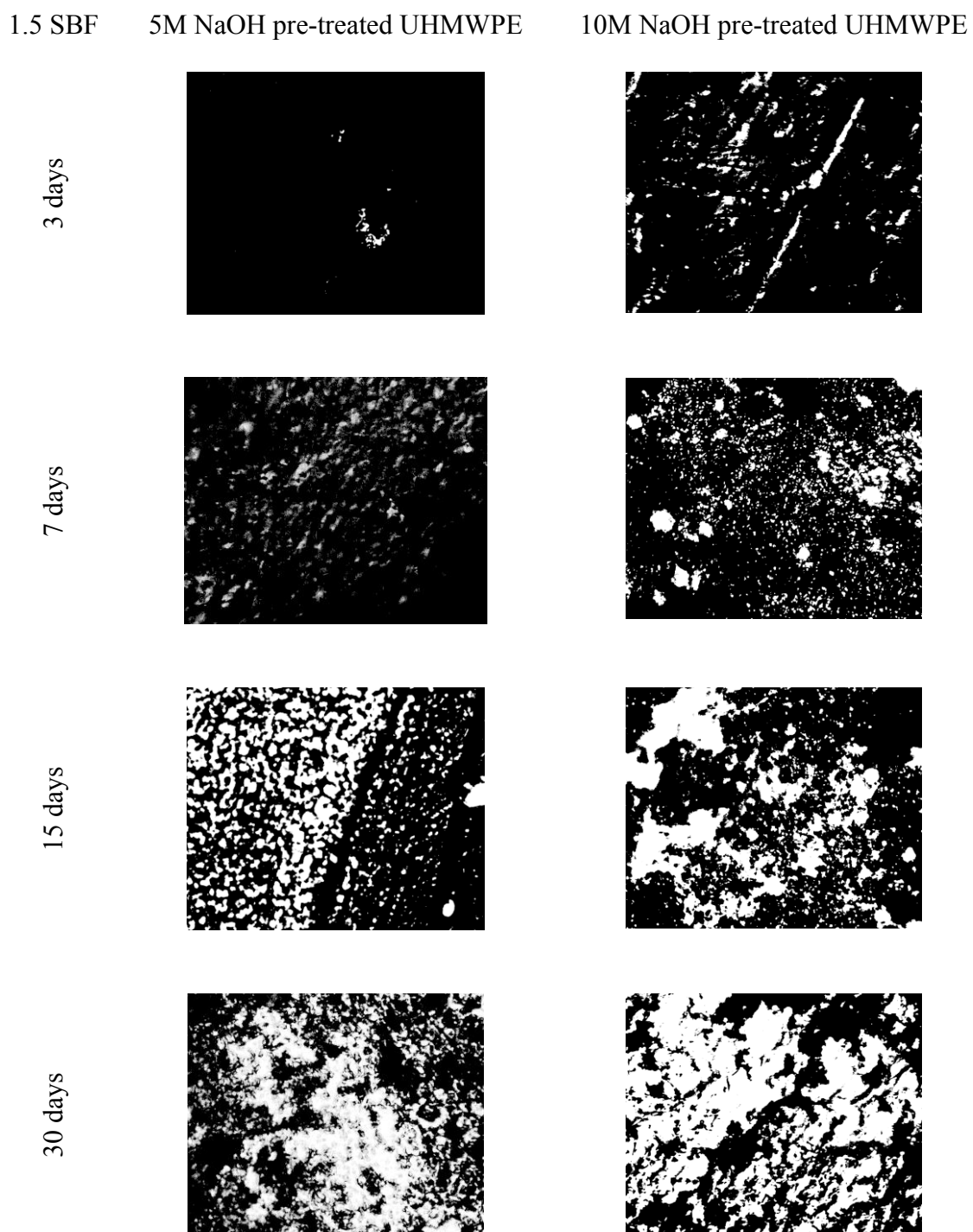


Figure 4.8.3 Reflected light Differential Contrast (DIC) microscope images of UHMWPE films pre-treated with 5M or 10M NaOH and incubated in 1.5 SBF treatments for 3, 7, 15 and 30 days

Table 4.8.1 Percentage of area/image area from the reflected light Differential Contrast (DIC) microscope pictures of PEEK (bright and matt sides) and UHMWPE films pre-treated with 5M or 10M NaOH and incubated in 1.5 SBF treatments for 3, 7, 15 and 30 days (B= bright, M= matt, S.D.= standard deviation)

1.5 SBF	Day 3	Day 7	Day 15	Day 30
	Area/Image Area (%)	Area/Image Area (%)	Area/Image Area (%)	Area/Image Area (%)
PEEK 5M NaOH - B				
Average	1.42	6.50	27.38	37.81
S.D.	0.41	0.37	0.36	2.60
PEEK 10M NaOH - B				
Average	4.17	22.35	31.12	42.95
S.D.	0.14	0.62	2.88	1.16
PEEK 5M NaOH - M				
Average	2.40	11.03	30.63	40.24
S.D.	0.42	0.13	0.76	1.71
PEEK 10M NaOH - M				
Average	5.65	26.25	32.70	46.99
S.D.	0.18	4.56	1.23	3.80
UHMWPE 5M NaOH				
Average	0.42	6.39	29.54	35.35
S.D.	0.09	0.06	0.88	0.53
UHMWPE 10M NaOH				
Average	4.93	16.15	31.38	52.33
S.D.	2.18	0.22	0.88	0.25

4.9 THIN FILM X-RAY DIFFRACTION (TF-XRD) AND WIDE-ANGLE X-RAY DIFFRACTION (WAXD)

The thin film X-ray (TF-XRD) patterns of the HDPE, PEEK and UHMWPE samples pre-treated with 1, 5 or 10M NaOH followed by 1.5 SBF treatment for 15 days contained the typical peaks of the polymers and some peaks of the adhesive used to secure the samples on the holder. These results showed no indication of any layer on the polymers probably due to the angle permitted by diffractometer, which greater than 3° , and perhaps the deposited layer was too thin to be detected by these X-rays.

Despite the lack of results from TF-XRD, further structural information was obtained from wide-angle X-ray diffraction (WAXD). The WAXD patterns of PEEK and UHMWPE treated only with 1.5 SBF for 15 and 30 days (these films were not pre-treated with any NaOH pre-treatments) are shown in Figures 4.9.1 and 4.9.2. The respective WAXD patterns of PEEK and UHMWPE before and after 5 or 10M NaOH pre-treatments and SBF treatments for 15 and 30 days are shown in Figures 4.9.3 to 4.9.6 respectively. Reassuringly, diffraction peaks corresponding to the respective polymer (PEEK and UHMWPE) as well as features typical for HA were observed. Indeed, the broad peaks between 18° and 31° were attributed to the (001), (110), (113), (200) and (213) diffractions from the polymers, and the features at 11° and between 25° and 35° to HA, albeit of somewhat of good crystallinity (Weng *et al.*, 1997; Reis *et al.*, 2003). In general, there is no explicit evidence of diffraction peaks other than HA, which indicates that the deposited layers on PEEK and UHMWPE was HA or carbonate hydroxyapatite (peaks 11° to 35°). The relative intensities of apatite (HA or CDHA) peaks (002), (112), (211) or (300), as observed from the Figures 4.10.3 to 4.10.6, increases with the concentration of NaOH from 5M to 10M.

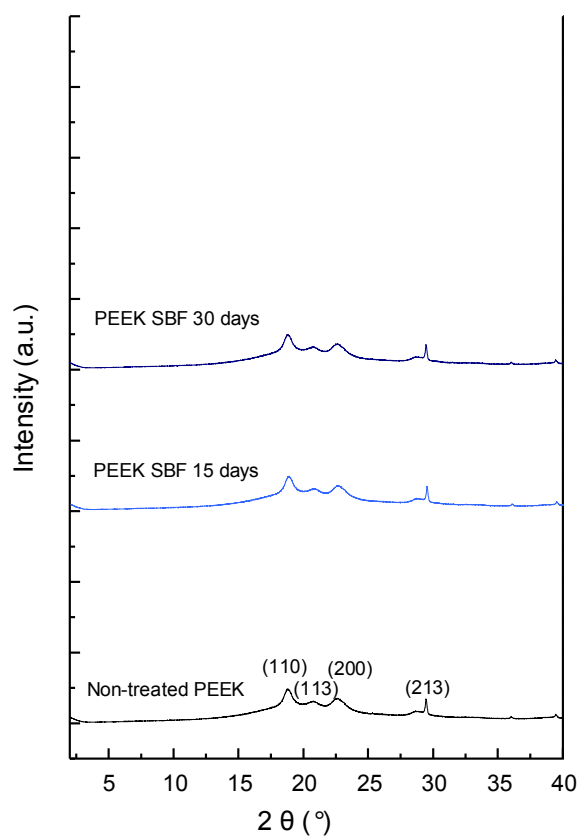


Figure 4.9.1 WAXD patterns of non-treated PEEK and PEEK treated only with 1.5 SBF for 15 and 30 days

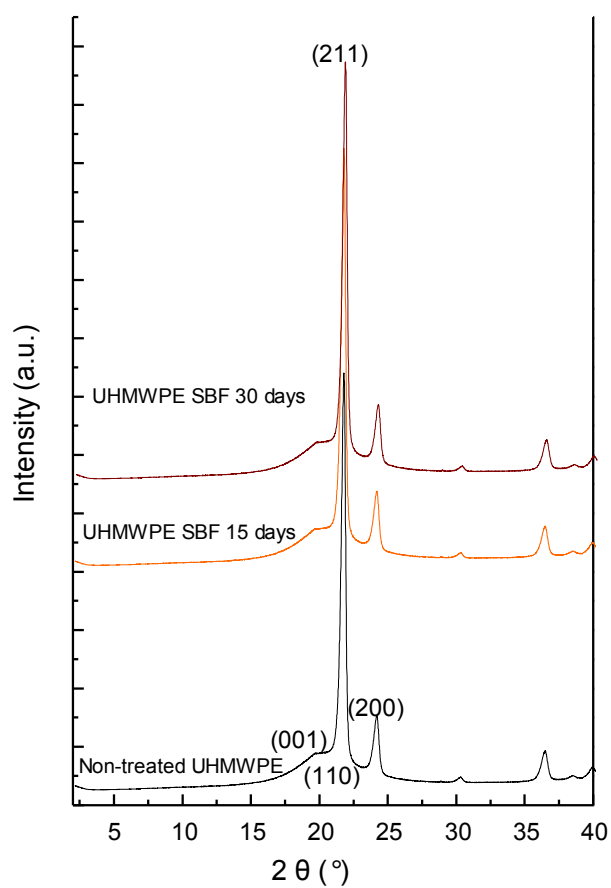


Figure 4.9.2 WAXD patterns of non-treated UHMWPE and UHMWPE treated only with 1.5 SBF for 15 and 30 days

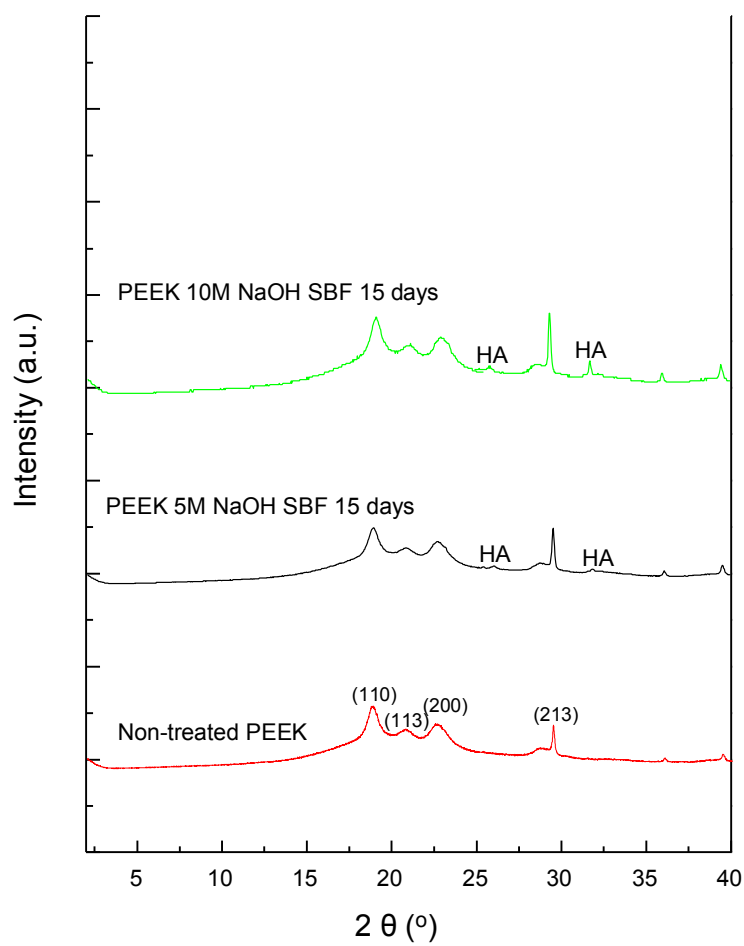


Figure 4.9.3 WAXD patterns of non-treated PEEK and PEEK pre-treated with 5M or 10M NaOH followed by 1.5 SBF for 15 days

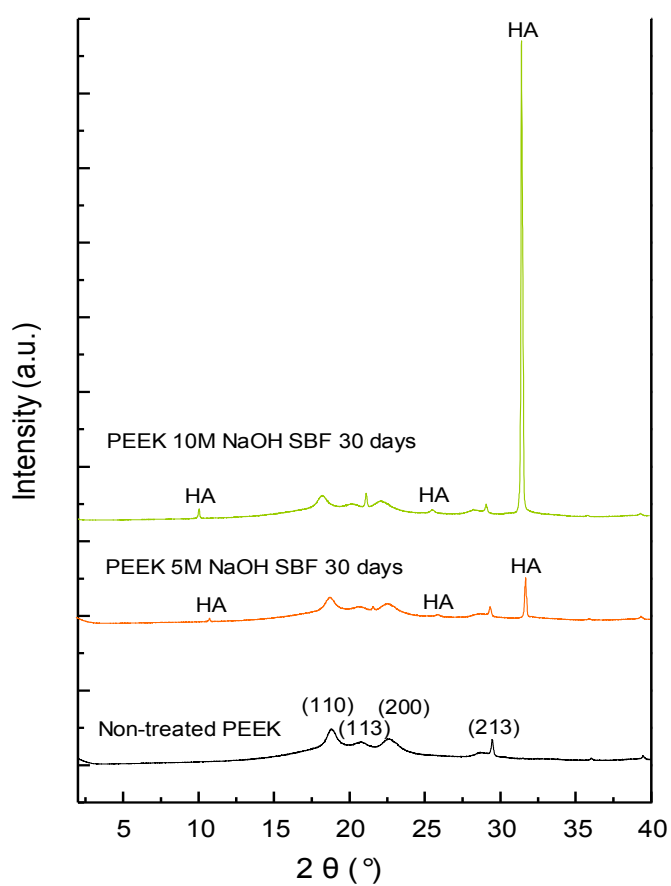


Figure 4.9.4 WAXD patterns of non-treated PEEK and PEEK pre-treated with 5M or 10M NaOH followed by 1.5 SBF for 30 days

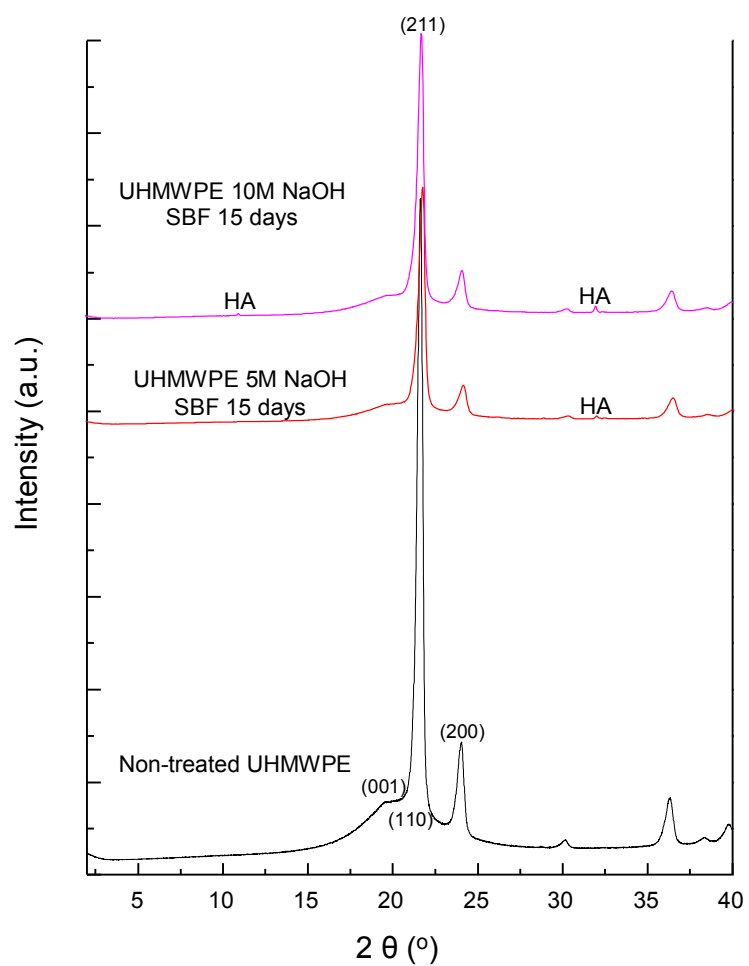


Figure 4.9.5 WAXD patterns of non-treated UHMWPE and UHMWPE pre-treated with 5M or 10M NaOH followed by 1.5 SBF for 15 days

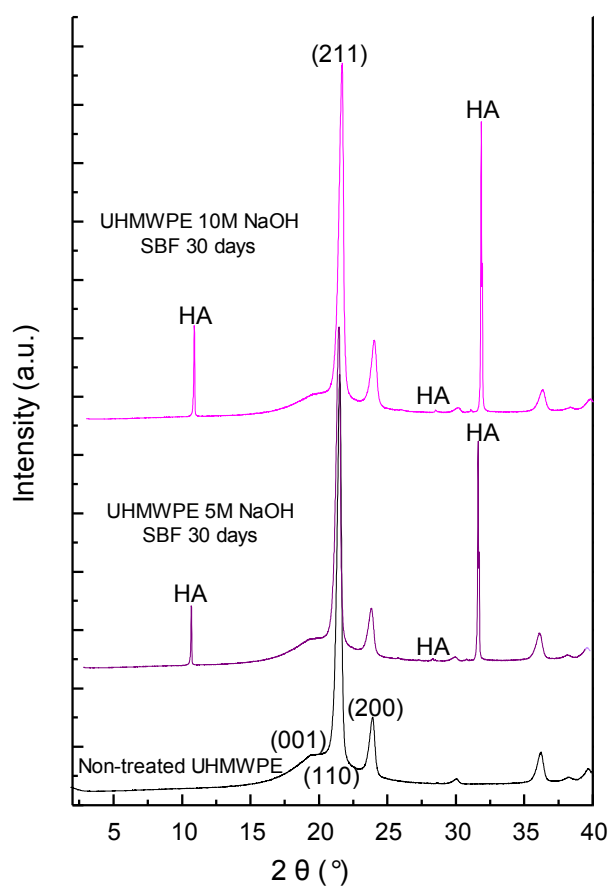


Figure 4.9.6 WAXD patterns of non-treated UHMWPE and UHMWPE pre-treated with 5M or 10M NaOH followed by 1.5 SBF for 30 days

4.10 SCRATCH TEST

A Micro-Materials nanoindenter was used to test PEEK (bright and matt) and UHMWPE pre-treated with 5M or 10M NaOH followed by 1.5 SBF for 30 days. The coatings were too thick, few tens of μm , for adhesion measurements with this nanoindenter as the maximal depth it could reach was 1.5 μm . Instead, the hardness and elastic modulus of the specimens were intended to be measured by simple nano-indentations. However, the results were inconsistent and not reasonable due to the fact that the deposit layers were not homogeneous, thus a rigid diamond indenter was too stiff to use for soft/flexible materials. Consequently, the specimens with thinner deposited layers such as 5M or 10M NaOH pre-treated PEEK and UHMWPE incubated only for 15 days in SBF were also subjected to this technique but the results were also inconsistent. Thus, it seems that the coatings were perhaps too fragile to be characterized with a rigid diamond indenter.

4.11 ATOMIC ABSORPTION SPECTROSCOPY (AAS)

Table 4.11.1 summarises the total amount of calcium (Ca) present in the samples after the NaOH pre-treatments followed by 1.5 SBF treatment for 30 days to investigate the amount of the Ca formed during the SBF treatment; and the Ca released during water immersion for 3 and 7 days.

On the whole, it was found that more calcium was initially deposited on samples pre-treated with 10M NaOH compared with 5M NaOH for both the PEEK and UHMWPE polymers. However, the Ca formed was then released again within 3 days of immersion in water, with UHMWPE yielding slightly more (>10%) than PEEK (<8%) compared with the total calcium initially present for both polymers; and from PEEK films, Ca could be extracted for 4 more days. Interestingly, for UHMWPE, it appears that after 7 days immersion there is less Ca present in the parent solution, indicating that Ca may have re-precipitated on these polymers. This implies that for PEEK the release of calcium continues after day 3 in water whereas for UHMWPE the calcium release seems to be stable.

Table 4.11.1 Total (Ca) present in the samples after the NaOH pre-treatments followed by 1.5 SBF for 30 days and the Ca released in water of PEEK and UHMWPE after pre-treated with 5M or 10M NaOH and 1.5 SBF for 30 days. (S.D = standard deviation)

	Total Ca on the samples	Total Ca in parent solution (μg)	
	Before immersion in water	Immersion time in water	
Samples:	($\mu\text{g} \pm \text{S.D.}$)	Day 3	Day 7
PEEK 5M NaOH 1.5 SBF	1747.58 \pm 0.53	132.50	235.86
PEEK 10M NaOH 1.5 SBF	2697.83 \pm 0.58	169.12	370.66
UHMWPE 5M NaOH 1.5 SBF	1773.30 \pm 0.12	186.14	157.34
UHMWPE 10M NaOH 1.5SBF	1933.65 \pm 0.14	287.82	264.74

CHAPTER 5

DISCUSSION

5.1 INTRODUCTION

The main aim of this research was to increase the bioactivity of polymer materials which may be suitable for the design of the skirt section of implants for artificial corneas. Polyether ether ketone (PEEK), high-density polyethylene (HDPE) and ultra-high molecular weight polyethylene (UHMWPE) films were investigated.

The results obtained show that apatite was formed on the surfaces of HDPE, PEEK and UHMWPE films which were pre-treated with highly concentrated NaOH and subsequently immersed in 1.5 SBF. This method can therefore render these thin films bioactive, making them potential skirt materials if they are to be integrated in the artificial corneal implants.

In order to gain a better understanding of apatite nucleation and growth on polymer surfaces, the apatite formed on PEEK, HDPE and UHMWPE films from 1.5 SBF treatments with different concentrations of NaOH pre-treatments was studied, with the ultimate objective of improving ophthalmic biomaterials for keratoprotheses (KPRO).

In this chapter, the effectiveness of NaOH and the influence of immersion time in SBF are discussed in order to determine the optimum concentration of NaOH for stimulating the apatite deposition from the SBF treatment and the most effective incubation time in SBF according to the apatite phase formed. The apatite formation is also examined to establish the phases required to get hydroxyapatite (HA). Finally, the results obtained from the different analysis are compared.

5.2 EFFECTIVENESS OF NAOH PRE-TREATMENT

An apatite layer was formed within a short period of time on HDPE, PEEK and UHMWPE films after pre-treatment with different concentrations of NaOH followed by immersion in 1.5 SBF treatments for up to 30 days. This finding was corroborated by Fourier transform infrared spectroscopy (FTIR) and Raman spectroscopy, combined with scanning electron microscopy (SEM) and energy dispersive X-ray spectroscopy (EDX) analysis, and further supported by the wide-angle X-ray diffraction (WAXD) data. This apatite layer is expected to respond in a similar way to the apatite found in dentine, enamel and bone in teeth, from which the dentil lamina used in the osteo-odonto-keratoprosthesis (OOKP) is made, containing mostly dentine. The OOKP has demonstrated good retention of the implant due to its non-rejection issue from the host eye because the patient's own tooth is used to make the skirt of this semi-artificial cornea implant. The apatite is the bioactive material in the skirt since it contains carbonate and phosphate ions, promoting potentially good *in vitro* test and *in vivo* bioactivity on polymer films.

No apatite was deposited on any of the polymer films by the SBF treatment unless they were pre-treated in NaOH. This finding was confirmed by X-ray diffraction (WAXD) patterns when the polymer films were treated with 1.5 B SBF for 30 days without pre-treatment and no apatite peaks such as hydroxyapatite (HA) or calcium deficient hydroxyapatite (CDHA) were found.

Pre-treatment of the surface with NaOH aids the formation of potential apatite nuclei on polymeric surfaces. The nuclei formed initiate the deposition of calcium and phosphate ions from the surrounding fluid (Kokubo and Takadama, 2006) and stimulate the growth of the apatite coating when immersed in 1.5 strength SBF. Thus, NaOH pre-treatment imparts surface function sites (chemical re-activation of functional groups (e.g OH-) that act as potential nuclei) on the polymers for the formation and growth of apatite deposited from the SBF treatments, as previously reported on different substrates (Kokubo *et al.*, 1990; Kokubo *et al.*, 1991; Janasova *et al.*, 2002; Oyane *et al.*, 2005a and b; Muller and Muller, 2006). In fact, results from various groups have demonstrated the need for NaOH pre-treatment. Janasova *et al.* (2002), for example, used SBF to form an apatite layer on the surface of NaOH-treated titanium. Similarly, Oyane *et al.* (2005 and 2005) reported apatite growth on NaOH-treated poly(ϵ -caprolactone (PCL) and on O₂ plasma-

treated PCL. Neither could Filmon *et al.* (2002) detect any deposition of calcium-phosphorous (CaP) phases on poly-hydroxyethyl methacrylate (PHEMA) in SBF unless the PHEMA was previously modified with carboxymethyl. Grassmann and Lobmann (2004) reported similar results to Filmon *et al.* (2002), concluding that CaCO_3 enhanced CaP coating on polyacrylamide. Tanahashi and Matsuda (1997) have detailed the influence of functional groups on apatite formation on self-assembled monolayers (SAMs) in SBF. Yu *et al.* (2005) concluded that PEEK was an inert material in SBF and did not induce CHA (carbonate hydroxyapatite) formation, unless PEEK was reinforced with hydroxyapatite.

In agreement with these previous reports and others (Kokubo *et al.*, 1990; Kokubo *et al.*, 1991; Muller and Muller, 2006), it was found in this study that the NaOH pre-treatment provides favourable sites for nucleation and the growth of apatite. In fact, on all NaOH pre-treated HDPE, UHMWPE and PEEK samples an apatite layer formed over time. This finding is in strong contrast to polymer films that were simply immersed in 1.5 SBF without exposure to NaOH, in which case no apatite growth was observed, as has also been observed by others (Ha *et al.*, 1997; Yu *et al.*, 2005).

In addition, Stancu *et al.* (2004) and Chirila *et al.* (2007) reported no calcification on phosphated polymers such as PHEMA and mono-acryloyloxyethyl (MAEP), suggesting that phosphate groups inhibit the CaP phase growth because calcium ions were double-bonded by phosphate groups from the polymers rather than from the SBF medium, suppressing the deposition of CaP since no further nucleation and crystallization occurred to form hydroxyapatite, despite using NaOH to produce functional groups.

A strong dependency of apatite growth and NaOH-concentration was found in the WAXD and SEM analysis and from the reflected light differential contract microscopy (DIC). Overall, the area and the percentage area/image of the apatite deposited on all polymers increased with the strength of NaOH, from 5M to 10M. When utilizing NaOH-solutions at low concentration (e.g. 1M) for the pre-treatment, apatite deposition occurred only after 7 days in 1.5 SBF incubation for pre-treated HDPE and UHMWPE, and after 15 days for pre-treated PEEK. With 5M NaOH pre-treatments, HDPE and UHMWPE showed apatite in 3 days and PEEK on day 7 after 1.5 SBF soaking. With higher NaOH-concentration (10M NaOH), HDPE pre-treated films showed apatite already by day 1 after 1.5 SBF immersion, while PEEK and UHMWPE pre-treated exhibited apatite formation

after 3 days in 1.5 SBF. As expected from the WAXD patterns, the relative intensities of apatite peaks increases with NaOH strength, suggesting that the higher concentrations of NaOH pre-treatment favoured apatite nucleation. It is apparent that at NaOH concentrations of 5M or 10M the pre-treatment lead to similar apatite deposition.

In agreement with the SEM results in this study, it was found from EDX and WAXD that the calcium (Ca) and phosphorous (P) content increased both with the NaOH concentration used during the pre-treatment as well as with the immersion time in 1.5 SBF, for all the polymers tested, HDPE, UHMWPE and PEEK.

Beneficially, the Ca/P molar ratio in the deposited layers was relatively unaffected by the NaOH concentrations for all structures. Indeed, the Ca/P molar ratio increased from 0.74 (day 3) to 1.58 (day 30) on PEEK (bright surface) treated with 5 M NaOH and, similarly from 1.27 (day 3) to 1.60 (day 30) for PEEK (matt side). Thus, the Ca/P ratio at the end of day 30 is of a similar value (1.60) on both PEEK surfaces. The differences between the PEEK surfaces were even less pronounced when treating the polymer films with 10M NaOH. For instance on day 3, the Ca/P was 1.37 (bright) and 1.40 (matt) and on day 30, 1.64 (bright) and 1.67 (matt) for such PEEK films. For UHMWPE, the Ca/P ratio increased from 1.42 (5M) and 1.49 (10M) to 1.61 (5M) and 1.64 (10M) from day 7 to day 30 in the 1.5 SBF pre-treated with 5M and 10M NaOH, respectively. From these observations it is evident that 5M NaOH treatment is sufficient to get apatite deposition on PEEK and UHMWPE when subsequently immersed in 1.5 SBF for 7, 15 or 30 days. However, it may be that the 10M NaOH pre-treatment accelerates the calcium and phosphorous nucleation at the beginning of the SBF treatments.

Figure 5.2.1 illustrates that the PEEK water contact angle (CA) decreased as the concentration increased from 5M to 10M NaOH. This was observed independent of which surface was analysed, indicating that the NaOH increased the wettability of this polymer. In strong contrast, no major dependence on NaOH concentration used in this pre-treatment was found in the CA for UHMWPE, although CA decreases slightly when 10M NaOH is used on UHMWPE. Thus, 10M NaOH increased the wettability of the PEEK and UHMWPE, and 5M NaOH increased the wettability only on both PEEK surfaces. However, the roughness values (R_a) as obtained from the AFM micrographs seemed relatively unaffected by the NaOH for PEEK (bright side), indeed, if anything R_a increased. Controversially, R_a appeared to decrease for PEEK (matt surface) and

UHMWPE, especially after treatment with 10M NaOH, as was also shown in the topographical micrographs, where changes in topography are visible. A similar trend was observed when R_a was deduced from the AFM line profiles compared with R_a from the whole image. Moreover, UHMWPE has about 30 times higher roughness compared with PEEK, and the similar water contact angle (CA) values of UHMWPE films (non-treated, 5M and 10M NaOH) might indicate that the high roughness of UHMWPE masks the beneficial effects of NaOH pre-treatments in terms of increasing the wettability (Figure 5.2.1).

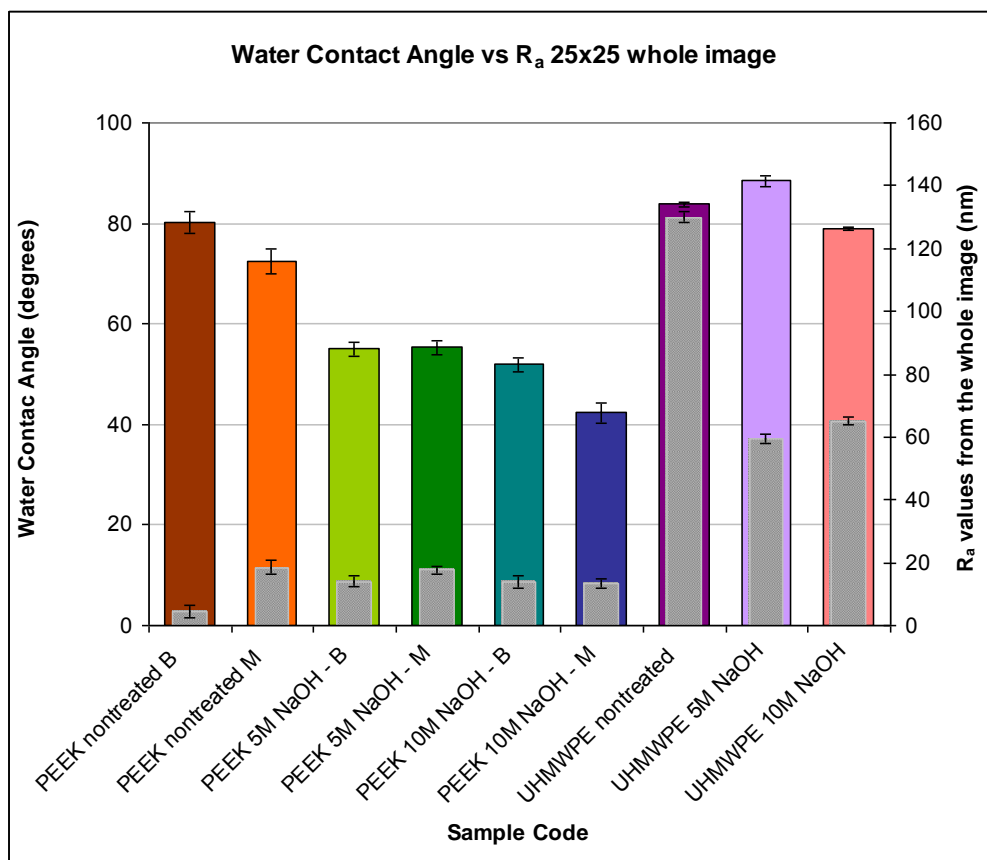


Figure 5.2.1 Water contact angle (CA, coloured bars) vs. R_a from the whole image (scan size = 25 x 25 μm) (grey bars) of non-treated and treated PEEK (bright and matt) and UHMWPE specimens. (B= bright, M= matt, error bar= standard deviation)

Interestingly, the NaOH pre-treatment appears to modify the surface topography and the surface chemistry of the polymers, which determine the apatite formation from the SBF treatment on the polymers. This is demonstrated in Figure 5.2.2 which shows that the

Ca/P molar ratios obtained after the immersion in the SBF for 30 days were strongly affected by the surface modifications resulting from NaOH pre-treatment.

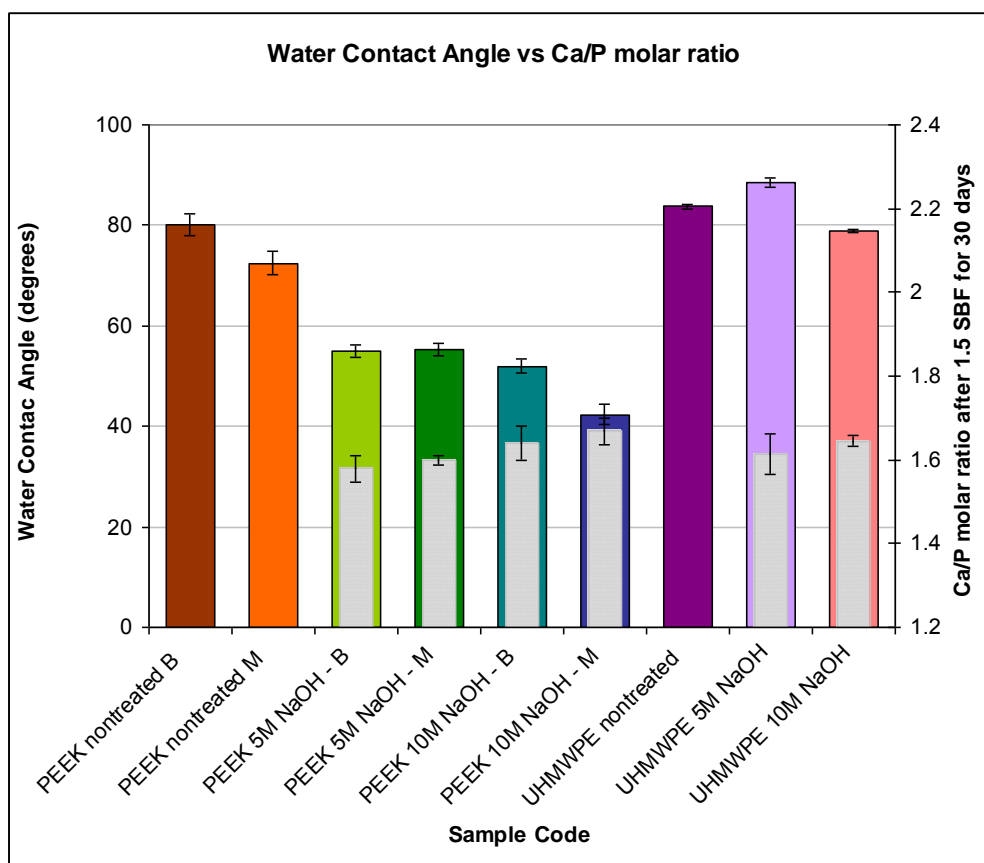


Figure 5.2.2 Water contact angle (CA, coloured bars) vs. Ca/P from EDX (grey bars) of non-treated and treated PEEK (bright and matt) and UHMWPE specimens. (B= bright, M= matt, error bar= standard deviation)

The favourable effect of NaOH -impairing functional sites on the HDPE, UHMWPE and PEEK polymers for the deposition and growth of apatite from the SBF treatments may at least in part be attributed to an increased wettability of the polymer films after such treatment, as well as to the modified topography. Independent of the polymer used, the apatite growth is unaffected by the concentration of NaOH pre-treatment if this is at least 5M NaOH. The resulting Ca/P molar ratios were similar to those found in dentine (Ca/P= 1.61) and enamel (Ca/P=1.63) (Legeros, 1991; Daculsi *et al.*, 1997). The apatite formation from the SBF during different immersion time is discussed in the following sections.

5.3 INFLUENCE OF THE IMMERSION TIME IN SBF

In addition to the NaOH concentration, immersion time in SBF was found to affect apatite formation. With increasing immersion time, further apatite nucleation and growth was observed, resulting in a thicker and more compact apatite layer. The apatite layer was deposited from the SBF treatments within a short period of time on the surfaces of NaOH pre-treated HDPE, UHMWPE and PEEK. This result was supported by wide-angle X-ray diffraction (WAXD), as well by Raman spectroscopy and FTIR, in conjunction with the SEM and EDX analysis.

Interestingly, various pathways to obtain an apatite coating from different SBF have been investigated on a variety of materials. Kawashita *et al.* (2003) showed that carboxyl group-containing polymer gels in SBF can form apatite on fibres, and Huang *et al.* (1997) used SBF-K9 to investigate the bioactivity on a Bioglass®-reinforced high density polyethylene composite and demonstrated the formation of a biologically-active carbonate hydroxyapatite (CHA) layer on the composite surface after immersion in SBF, showing that *in vitro* bioactivity could be obtained in a composite. Use of slightly modified SBF has been reported to result in thicker carbonated apatite layers and/or the formation of homogeneous apatites. For instance, Muller and Muller (2006) have modified SBF with a different HCO_3^- on NaOH-treated titanium, and Kim *et al.* (1999) have used 0.75-2.00 strength SBF to study the apatite formed on polyethylene terephthalate (PET). Accordingly, 1.5 SBF is often used to accelerate the apatite coating process and most importantly as a treatment to produce Ca/P layer on materials before implantation.

As confirmed by the SEM and EDX analysis here, the apatite layer developed earlier on HDPE (1-3 days in SBF) than on PEEK (3-7 days in SBF) and UHMWPE (7 days in SBF). Gradual nucleation and growth of apatite occurred with the prolongation of immersion time in 1.5 SBF treatments, as previously reported on different substrates (Kokubo *et al.*, 1990; Kokubo *et al.*, 1991; Janasova *et al.*, 2002; Oyane *et al.*, 2005a and b; Muller and Muller, 2006). Moreover, the area and the percentage area of the image of the apatite growth with immersion time in SBF for the NaOH pre-treated specimens, is confirmed by the reflected light Differential Contrast microscopy (DIC) analysis. It was found that the Ca and P amounts increased both with the immersion time in 1.5 SBF as well as with the NaOH concentration, for all polymers as deduced from the EDX results.

Thus, for all NaOH pre-treated polymers (HDPE, UHMWPE and PEEK) immersion in 1.5 SBF treatments initially resulted in the formation of individual agglomerates, which were typically less than 5 μm across. With increasing immersion time in 1.5 SBF, further apatite deposition led to growth of these agglomerates, producing continuous, thicker and more compact coatings. These layers contain spherical aggregates with diameters up to 8-10 μm , consisting of nanoparticles of apatite crystallites, which are characteristic for coatings precipitated from 1.5 SBF treatment.

It was noticed that the results from the SEM and DIC techniques demonstrated the same tendency: the apatite increased with the immersion time in 1.5 SBF. However, there is a slight discrepancy in the SEM micrograph and DIC microscope images, which can be attributed to the differences in the SEM and DIC in terms of the sample area analysed. In the SEM the micrographs profile was in μm and in the DIC microscope the profile was in mm. The apatite layer was not homogeneously distributed over the sample especially in the early days (1-3) of the 1.5 SBF treatments. The SEM is an electron microscope and the DIC is an optical microscope.

In addition to the features mentioned above, the Raman spectra of NaOH pre-treated HDPE, PEEK and UHMWPE demonstrated that carbonate and phosphate bands were present after 15-18 days in the 1.5 SBF incubation. These bands are associated with hydroxyapatite and carbonated apatites (Legeros *et al.*, 1987; Elliot, 1994; Rehman and Bonfield, 1997; Ha *et al.*, 1997; Penel *et al.*, 1998; Ning *et al.*, 2004; Petra *et al.*, 2005; Hofmann *et al.*, 2007). It is worth mentioning that the characteristic peaks of the polymers (Simonin and Liao, 2000) were shifted and/or weakened by apatite formation, as also confirmed by the FTIR spectra, as the polymer signals were reduced by the overlying apatite signals.

Further information was also obtained from WAXD spectra. The diffraction peaks observed in the WAXD patterns of polymers pre-treated with NaOH and immersed in 1.5 SBF for 15 and 30 days are attributed to calcium phosphates (e.g. calcium deficient hydroxyapatite –CDHA- or octa-calcium phosphate –OCP-) and to apatite, indeed to hydroxyapatite (HA) and/or carbonate hydroxyapatite (CHA). These results are in agreement with those of Fang *et al.* (2007) and Wang and Bonfield (2001). The intensity of the HA peaks increases substantially from day 15 to day 30 in the SBF treatments although the increase due to different concentrations of NaOH is less strong, suggesting that the

longer period of time in contact with the 1.5 SBF favoured the growth of HA on PEEK and UHMWPE structures. Reassuringly, that longer period in SBF lead to thicker apatite layers on the treated polymers.

Consequently, apatite (HA and/or CDHA) layers were formed on HDPE, PEEK and UHMWPE after incubation in 1.5 SBF treatments previously pre-treated with different NaOH strengths. The apatite growth is increased by the immersion time in SBF and concentration of NaOH. This is discussed in the next section.

5.4 APATITE FORMATION

This apatite layer is expected to enhance the *in vitro* bioactivity of polymeric objects, illustrating the potential for use of such synthetic materials as artificial cornea designs.

However, it is critical to keep in mind that the bioactivity of the apatite-polymer depends on the structure and composition of the formed apatite (Kim *et al.*, 2000). As a consequence, on polymer surfaces, an apatite coating has been investigated and various phases have been demonstrated. Varma *et al.* (1999) have produced a porous calcium deficient hydroxyapatite (CDHA) coating on $\text{Ca}(\text{OH})_2$ treated phosphorylated chitosan films. Choong *et al.* (2004) studied both *in vitro* and *in vivo* the effect on the processes of calcium phosphate coatings deposited on PCL from SBF. It should be noted that Choong *et al.* (2004) did not identify the CaP phases they produced; they commented that the coatings were structurally similar to hydroxyapatite.

Carbonate and phosphate were found on the apatite produced on the NaOH pre-treated films, as evidenced by FTIR and Raman spectroscopy and also reported by Legeros *et al.* (2003). Good integration of carbonate and phosphate in the apatite phase is suggested by the fact that due to CH_2 vibration of the HDPE, PEEK and UHMWPE polymeric substrates the polymer bands weakened considerably for pre-treated films with a long immersion time in 1.5 SBF.

The Ca/P atomic ratio of stoichiometric apatite $\text{Ca}_{10}(\text{PO}_4)_6(\text{OH})_2$ is 1.67 (Dorozhkin, 2009). The Ca/P of calcium-deficient hydroxyapatite (CDHA) is $1.5 > 1.67$ (Dorozhkin, 2007) and the Ca/P of octa-calcium phosphate (OCP) is 1.33 (Dorozhkin,

2007; Dorozhkin, 2009). The average Ca/P molar ratio of the NaOH pre-treated polymer films after 3, 7 and 15 days in 1.5 SBF immersion was 1.19, 1.26-1.35, and 1.33-1.44, respectively, which indicates that calcium-deficient apatite (Chirila *et al.*, 2007) with gradually increasing Ca was produced in this study.

Varma *et al.* (1999) used SBF on Ca(OH)_2 treated phosphorylated chitosan films to produce a porous calcium deficient hydroxyapatite coating with a Ca/P of 1.34. They also reported that the Ca/P ratio increased with the SBF immersion time. Kim *et al.* (1999) describe a Ca/P of 1.45 using 1.5 SBF on PET. When an apatite is deposited from an aqueous solution, some sites for PO_4^{3-} ions are often substituted by HPO_4^{2-} and CO_3^{2-} ions. As a consequence, vacancies are produced in the Ca^{2+} sites. A substitution of CO_3^{2-} for PO_4^{3-} results in one P and half a Ca deficiencies originating in a Ca/P ratio above 1.67, while one HPO_4^{2-} substituted for PO_4^{3-} results in half Ca deficiency resulting in a Ca/P ratio lower than 1.67 (Kim *et al.*, 2000). Accordingly, the Ca/P ratio of apatite could be the less than the stoichiometric phase, in cases where more CO_3^{2-} ions occupy HPO_4^{2-} instead of PO_4^{3-} sites.

Additionally, various authors (Kim *et al.*, 1999; Varma *et al.*, 1999; Kim *et al.*, 2000; Chirila *et al.*, 2007) have reported a Ca/P lower than 1.67 in similar experiments claiming that they produced calcium-deficient apatite. In the WAXD patterns in this study, there is no explicit evidence of diffraction peaks other than those for HA or CDHA, which indicates that the deposited layers on PEEK and UHMWPE were HA and/or CDHA after 15 and 30 days immersed in 1.5 SBF previously pre-treated in NaOH. Accordingly, the Ca/P increases approximately from 1.45 to 1.67, indicating the change of phase of the apatite from CDHA to HA with immersion time in SBF until the stoichiometric phase of apatite was produced on both PEEK and UHMWPE.

In conclusion, it should be noted that calcium-deficient apatite was produced on the NaOH pre-treated HDPE, PEEK and UHMWPE films subsequently immersed in 1.5 SBF up to 15 days, and that hydroxyapatite was produced when the pre-treated films were incubated in SBF for a longer period of time, from 15 to 30 days.

Further analysis of the hydrophilicity, the topographical changes and the values of R_a at the later stages of the treatment during immersion in 1.5 SBF should be conducted to provide additional information on the changes associated with the development of apatite

layers. In addition, more fundamental studies including detailed statistical analysis are required to fully elucidate the influence of surface roughness, surface chemistry on the wettability and apatite formation of artificial sclera materials.

5.5 APPLICATION FOR SKIRT MATERIALS IN CORNEAL IMPLANTS

HDPE, PEEK and UHMWPE were selected for this study. UHMWPE has a clinical history as a successful biomaterial for hip, knee, spine (Kurtz, 2004) and ophthalmologic implants (Allan, 1999). PEEK is also used in medical implants in the orthopaedic, cardiovascular and dental fields (Roeder *et al.*, 2009) and it has been shown to produce hydroxyapatite-like surfaces (Ha *et al.*, 1997; Abu-Bakar *et al.*, 2003; Tan *et al.*, 2003; Fan *et al.*, 2004; Yu *et al.*, 2005). In addition, PEEK can be engineered with a wide range of physical, mechanical and surface properties (Kurtz and Devine, 2007). HDPE is of particular interest as a biomaterial since it can easily be processed and has already demonstrated its biocompatibility when hydroxyapatite particles have been incorporated (Bonfield *et al.*, 1984).

Thus, HDPE, PEEK and UHMWPE are promising candidates to tackle at least some of the problems with current keratoprosthesis (KPRO) technologies. However, the bioactivity of these polymers has to be significantly improved for them to be used as skirt materials for artificial corneal implants. This bioactivity may be achieved through a suitable “coating”.

Consequently, apatite was formed on their surfaces, when pre-treating HDPE, PEEK and UHMWPE with highly concentrated NaOH and by subsequent immersion in 1.5 Simulated Body Fluid (SBF), which renders such thin-film structures bioactive, making them promising skirt materials if they are to be integrated into artificial corneal implants.

Ideally, the calcium deficient apatite (CDHA) and/or hydroxyapatite (HA) apatite layer contained phosphate and carbonate ions, promoting potentially good *in vivo* bioactivity on polymeric films since it has been proven in this study that they are bioactive *in vitro*.

Most beneficially, the HA and CDHA formed is very close to the apatite found in teeth, from which the lamina of the osteo-odonto-keratoprosthesis (OOKP) is made, a

design that promotes excellent long-term retention results (Falcinelli *et al.*, 2005; Liu *et al.*, 2007) but requires the donation of one of the patient's teeth. Furthermore, it is clinically easier to implant a prosthesis with a polymeric skirt than one with a rigid skirt, such as a OOKP.

Furthermore, it is expected for mechanical compatibility to be improved between the sclera and polymers compared to the sclera and tooth dentine.

Thus, this present study clearly demonstrates that apatite layers can form on the surfaces of HDPE, PEEK and UHMWPE, provided that these polymers are pre-treated with NaOH followed by immersion in 1.5 SBF. This finding is important as it is the presence of apatite that provides the skirts used in OOKPs with good bioactivity since it contains carbonate and phosphate ions, resulting in possible retention of the implant *in vivo*. Considering this, it can be expected that the layers formed on the treated HDPE, PEEK and UHMWPE films will respond similar to the apatite found in dentine, enamel and bone of teeth, from which the dentil lamina of the osteo-odonto-keratoprosthesis (OOKP) are fabricated (Falcinelli *et al.*, 2005; Liu *et al.*, 2007). This promises good *in vitro* and *in vivo* bioactivity of such HDPE, PEEK and UHMWPE films. In this context it is interesting to note that the apatite layer produced on the treated HDPE, PEEK and UHMWPE films is slightly Ca deficient (compared to hydroxyapatite), similar to the apatite contained in dentine, enamel and bone mineral (Legeros *et al.*, 2003) (the Ca/P molar ratio of dentine is 1.61; whilst the one of dental enamel is 1.63 (Legeros, 1991; Daculsi *et al.*). To further validate the feasibility of this approach, cell culture studies have to be performed on treated materials, PEEK and UHMWPE films. Fibroblast growth studies on the NaOH pre-treated specimens immersed in 1.5 SBF for 15 and 30 days have recently started, the results of which will be quantified in terms of cell attachment and proliferation.

CHAPTER 6

CONCLUSIONS AND FUTURE WORK

6.1 CONCLUSIONS

Apatite layers were formed within 1, 3 and 7 days on high-density polyethylene (HDPE), polyether ether ketone (PEEK), and ultra-high molecular weight polyethylene (UHMWPE) films after 1, 5 or 10M NaOH pre-treatment followed by incubation in 1.5 Simulated Body Fluid (SBF) for up to 30 days; which promises to render such thin films bioactive since the common characteristic of the bioactive materials *in vitro* is to produce a Ca/P layer of biological apatite – a necessity if they are to be integrated into artificial cornea implants.

The apatite nucleation and growth are affected by the immersion time in 1.5 SBF and by the concentration of NaOH (control films that were not treated in NaOH showed no apatite formation after 1.5 SBF immersions). The Ca/P molar ratio of the apatite deposited on the polymers increased with NaOH strength and with SBF incubation time.

Immersion in NaOH (before the subsequent SBF incubation step) resulted in improved wettability, which increased with the NaOH. In addition, the NaOH treatment led to some changes in the topography (i.e. increase/decrease of roughness) of the polymer surfaces. Thus, the favourable effect of NaOH on apatite formation may be attributed to an increased wettability of the polymer films after such treatment, as well as a modified topography. Effectively, the resulting modifications of the surface topography and surface chemistry determine apatite formation on the polymers.

In the NaOH pre-treated specimens the apatite layer developed earlier on HDPE (1-3 days in SBF) than on PEEK (3-7 days in SBF) and UHMWPE (7 days in SBF). Increase in the immersion time in SBF enhanced the deposition of the apatite layer, which was thick and compact. For all polymers, immersion in SBF initially resulted in the formation of

individual agglomerates, which were typically less than 5 μm across on polymer surface, indicating the development of apatite nucleating points on the polymer surfaces. With increasing immersion time in SBF, further apatite deposition resulted in growth of these agglomerates, producing a continuous, thicker and more compact layer. These layers contained spherical aggregates with diameters up to 8-10 μm , consisting of nanoparticles of apatite crystallites, which are characteristic for apatite coatings precipitated from SBF solutions.

Independent of the polymer used, the apatite growth is affected below 5M NaOH by the concentration of NaOH pre-treatment. Evidently, 5M NaOH treatment could be sufficient to enhance the deposition of apatite on HDPE, PEEK and UHMWPE when subsequently immersed in 1.5 SBF for 7, 15 or 30 days. On the other hand, 10M NaOH treatments resulted in a more rapid formation of the apatite layer compared with lower molarity pre-treatment solutions. Additionally, more Ca was initially deposited on samples with 10M NaOH compared with 5M NaOH for all polymer structures.

Desirably, the calcium-deficient apatite (CDHA) and/or hydroxyapatite (HA) apatite layer contained phosphate and carbonate ions, potentially promoting good *in vitro* bioactivity on polymeric films. The Ca/P molar ratio increases from ~ 1.45 to 1.67 with increased SBF immersion time (7-15 to 15-30 days), indicating a change of phase of the apatite from calcium deficient apatite (CDHA) to hydroxyapatite (HA); which can be expected to be highly bioactive and having a good crystallinity.

Most beneficially is that the calcium deficient apatite (CDHA) formed with Ca/P $1.50 > 1.67$ is very close to the apatite found in dentine ($\text{Ca/P}_{\text{dentine}} = 1.61$) and enamel ($\text{Ca/P}_{\text{enamel}} = 1.63$), which is mainly composed of calcium-phosphate related to hydroxyapatite (HA). Dentine and enamel are the bioactive materials used to make the lamina of the semi-synthetic artificial cornea implant, the osteo-odonto-keratoprosthesis (OOKP), a design that demonstrated good long-term retention results due to its non-rejection properties from the host eye because the patient's own tooth is used to make the skirt of the cornea implant, although it does require the donation of one of the patient's teeth.

In addition to the above findings, the inorganic layers were found to be chemically stable as the calcium deposited on the films did not dissolve fully when immersed in water for one week.

6.2 FUTURE WORK

The research detailed in this thesis has demonstrated the potential of bioactive polymer materials to be used as the skirt for an artificial corneal implant. To further validate the feasibility of this approach, the next step is to culture cells on the treated materials. Thus, fibroblast growth studies on the NaOH pre-treated specimens immersed in 1.5 SBF for 30 days have recently started at Moorfields Eye Hospital, London and results of this cell culture study will be quantified in terms of attachment and proliferation.

While the characterisation tests used in this thesis have shown that apatite layers developed on the polymers, these results can be validated further using the follow-on tests described below.

Since the results from the scratch test were inconclusive, it is recommended that further work be carried out to investigate the adhesion of the deposited layers on the samples pre-treated with 5 or 10M NaOH followed by immersion in 1.5 SBF for 7, 15 and 30 days using nanoindenter with a different depth (e.g. <1500 nm).

The data obtained from the flame atomic absorption spectroscopy (AAS) was conclusive and very interesting. The test should be repeated with the immersion time in water extended to more than 7 days, until the calcium (Ca) release would be stable.

The water contact angles (CA) were determined on the films after and before the NaOH pre-treatment and the results were very interesting. Therefore, it would be also important to analyse the hydrophilicity of the films after immersion in 1.5 SBF using the same technique.

The roughness value (R_a) and the topography of the films were performance with Atomic Force Microscopy (AFM) to analyse the effects of the pre-treatment, and these results were conclusive. Thus, it would be advised to do this test also after the immersion in 1.5 SBF to analyse the topographical changes and the values of R_a through time.

Additionally, the carbonate, phosphates and hydroxyl ionic groups were determined using Laser Raman spectroscopy and Fourier transform infrared spectroscopy (FTIR) in the first batch on the samples treated in 1.5 SBF for 15-18 days. The results showed peaks which were slightly flatted, and it was possible to conclude the presence of phosphate and carbonate groups on the apatite deposition. However, it would be relevant to apply these

two tests for samples treated in 1.5 SBF for longer time (e.g. 30 days) to confirm the presence of any ionic groups.

Apart from the tests already done during this research either for the batch I or batch II, additional analysis techniques to characterise the apatite layer and to determine the fundamental changes in the surface chemistry of the polymers upon NaOH pre-treatment could be applied. X-ray photoelectron spectroscopy (XPS) is a very sensitive surface technique that could confirm and clarify some of the findings which resulted from the other characterisation techniques used in this research. It could be carried out before and after the NaOH pre-treatment and SBF treatment, allowing further characterisation, such as a) the chemical inertness/stability of UHMWPE against NaOH treatment since the CA for non-treated and treated samples were very similar, with the possibility that the high roughness of the UHMWPE could mask the beneficial effects of the NaOH treatment (e.g. increasing wettability), b) the differences in chemical composition between the bright and matt PEEK surfaces.

During the course of this research, the solid and compact films, despite being flexible, were bioactive after the procedure proposed from this work. However, the skirt materials for the corneal implants should be porous, which is required for proper fixation *in vivo*. Further work toward porous HDPE, PEEK and UHMWPE films is therefore necessary in future studies. The porosity of the skirt material should be improved to allow fibroblast in-growth and collagen deposition to provide the adequate anchorage of the skirt into the sclera.

Finally, the corneal implant design should be investigated in the future to address aspects such as aesthetics, cost and implant procedure.

REFERENCES

- Abou-Neel E A, Mizoguchi T, Ito M, Bitar M, Salih V, Knowles J C. In vitro bioactivity and gene expression by cells cultured on titanium dioxide doped phosphate-based glasses. *Biomaterials* **2007**, *28*, 2967-77.
- Abu-Bakar M S, Cheng M H W, Tang S M, Yu S C, Liao K, Tan C T. Tensile properties, tension-tension fatigue and biological response of polyetheretherketone-hydroxyapatite composites for load-bearing orthopaedic implants. *Biomaterials* **2003**, *24*, 2245-2250.
- AET, Aging eye Times. What is Dry Eye? *Dry Eyes* **2006**, 1.
- Albon J. Corneal transplantation and the artificial cornea. *J. Mechanics in Medicine and Biology* **2003**, *3*, 96-106.
- Allan B. Closer to nature: new biomaterials and tissue engineering in ophthalmology. *Br. J. Ophthalmology* **1999**, *83*, 1235-1240.
- Allan B. Trial of a new artificial cornea (the Legeais BioKPRO III) at Moorfields Eye Hospital. Moorfields Eye Hospital NHS Foundation Trust. *National Research Register Document* no. N0141127510, London **2002**, 3.
- Als-Nielsen J, McMorro D. Modern X-ray physics & new developments. In: Barsoukov E., MacDonald J R. Editors., *Elements of Modern X-ray Physics*, John Wiley & Sons, Ltd., London, UK, **2001**.
- Amjad, Z. Calcium phosphates. In: Amjad Z. Editor. *Calcium phosphates in biological and industrial systems*. Kluwer Academic Publishers, Boston, MA, USA, **1997**, 529.
- Aoki H. Science and medical applications of hydroxyapatite; JAAS: Tokyo, Japan, **1991**, 245.
- Apelt D, Theiss F, El-Warrak A O, Zlinszky K, Bettschart-Wolfisberger R, Bohner M In vivo behavior of three different injectable hydraulic calcium phosphate cements, *Biomaterials* **2004**, *25*, 1439-1451.
- Aquavella J V, Rao G N, Brown A C, Harros J K. Keratoprosthesis. *Ophthalmology* **1982**, *89*, 655-660.
- Arsic J, Kaminski D, Poodt P, Vlieg E. Liquid ordering at the brushite-{010}-water interface. *Physics Review B* **2004**, *69*, 245406.
- Auclair-Daigle C, Bureau M N, Legoux J G, Yahia L H. Bioactive hydroxyapatite coatings on polymer composites for orthopedic implants. *J. Biomedical Materials Research* **2005**, *37A*, 398-408.
- Axner O. Laser Spectrometric Techniques in Analytical Atomic Spectrometry. In: Meyers R A, Editor. *Encyclopaedia of Analytical Chemistry*. John Wiley & Sons, Inc., New York, **2000**, 9506-9595.

- Barinov S M, Komlev V S. *Calcium phosphate based bioceramics for bone tissue engineering*, Materials Science Foundations, Trans Tech Publ.: Switzerland, **2008**, 48, 170.
- Baselt D. Subfibrillar structure of type I collagen observed by atomic force microscopy. *Biophysical Journal* **1993**, 65, 2644-2655.
- Becker A, Epple M, Müller K M, Schmitz I. A comparative study of clinically well characterized human atherosclerotic plaques with histological, chemical, and ultra structural methods. *J. Inorganic Biochemistry* **2004**, 98, 2032-2038.
- Bermúdez O, Boltong M G, Driessens F C M, Planell J A. Development of some calcium phosphate cements from combinations of α -TCP, MCPM and CaO. *J. Materials Science: Materials in Medicine* **1994**, 5, 160-163.
- Bermúdez O, Boltong M G, Driessens F C M, Planell J A. Optimization of a calcium orthophosphate cement formulation occurring in the combination of monocalcium phosphate monohydrate with calcium oxide. *J. Materials Science: Materials in Medicine* **1994**, 5, 67-71.
- Bernardi G. Chromatography of nucleic acids on hydroxyapatite. *Nature* **1965**, 206, 779-783.
- Bigi A, Boanini E, Borghi M, Cojazzi G, Panzavolta S, Roveri N. Synthesis and hydrolysis of octacalcium phosphate: effect of sodium polyacrylate. *J. Inorganic Biochemistry* **1999**, 75, 145-151.
- Biswell R. Cornea. In Vaughan D, Asbury T, Riordan-Eva P, Editors, *General Ophthalmology*. Prentice-Hall International, London, **1995**, 138-145.
- Bleckmann H, Holak S. Preliminary results after implantations of four AlphaCor artificial corneas. *Graefe's Archive for Clinical and Experimental Ophthalmology* **2006**, 244, 502-506.
- Bohner M, Lemaître J. Can bioactivity be tested in vitro with SBF solution? *Biomaterials* **2009**, 30, 2175-2179.
- Bonfield W, Bowman J A, Grynepas M D. Prosthesis comprising composite material. *UK Patent* 2, 085, 461B, **1984**.
- Brand M, Rampalli S, Chaturvedi C P, Dilworth F J. Analysis of epigenetic modifications of chromatin at specific gene loci by native chromatin immunoprecipitation of nucleosomes isolated using hydroxyapatite chromatography. *Nature Protocols* **2008**, 3, 398-409.
- Broekaert A C. Analytical Atomic Spectrometry with Flames. In: Weinheim Editor. *Analytical Atomic Spectrometry with Flames and Plasmas*. Wiley-VCH, Berlin, Germany **1998**, 1-17.
- Brown P W, Martin R I. An analysis of hydroxyapatite surface layer formation. *J. Physical Chemistry B* **1999**, 103, 1671-1675.
- Brumberger H. SAXS techniques. In: Brumberger H. Editor. *Modern Aspects of Small-Angle Scattering*, Kluwer Academic Publishers, London, UK, **1993**.
- Cai Y, Tang R. Calcium phosphate nanoparticles in biomineralization and biomaterials. *J. Materials Chemistry* **2008**, 18, 3775-3787.
- Cao W, Hench L L. Bioactive materials. *Ceramics International* **1996**, 22, 493-507.

- Cardona H, DeVoe A G. Prosthokeratoplasty. Transactions Am. Academy of Ophthalmology and Otolaryngology **1977**, 83, 271-280.
- Cardona H. Keratoprosthesis. *Am. J. Ophthalmology* **1962**, 54, 284-294.
- Cardona H. Mushroom transcorneal keratoprosthesis. *Am. J. Ophthalmology* **1969**, 68, 604-612.
- Cardona H. Prosthokeratoplasty. *Cornea* **1983**, 2, 179-182.
- Cardona H. The Cardona keratoprosthesis: 40 years experience. *Refractive and Corneal Surgery* **1991**, 7, 468-471.
- Casey T A. Osteo-odontokeratoprosthesis. *Br. J. Ophthalmology* **1999**, 83, 126.
- Cazalbou S, Combes C, Eichert D, Rey C. Adaptive physico-chemistry of bio-related calcium phosphates. *J. Materials Chemistry* **2004**, 14, 2148-2153.
- Chan H, Mijares D, Ricci J L. In vitro dissolution of calcium sulfate: evidence of bioactivity. In: *Transactions - seventh world biomaterials congress*, Sydney **2004**; 627.
- Chapoy L L, Lally J M. The property driven innovation of materials for use in ophthalmology. *Key Engineering Materials* **2008**, 380, 149-166.
- Chilaris G, Liaricos S. Fascia of the temporalis muscle in scleral buckling and keratoprosthesis operations. *Am. J. Ophthalmology* **1973**, 76, 35-37.
- Chirila T V, Constable I J, Crawford G J, Russo A V. Method of producing a keratoprosthesis. US patent 5,458,819, 17 October **1995**.
- Chirila T V, Constable I J, Crawford G J, Vijayasekaran S, Thompson D E, Chen Y C, Fletcher W A, Griffin B J. Poly (2-hydroxyethyl methacrylate) sponges as implant materials: in vivo and in vitro evaluation of cellular invasion. *Biomaterials* **1993**, 14, 26-38.
- Chirila T V, Zainuddin, Hill D J T, Whittaker A K, Kemp A., Effect on phosphate functional groups on the calcification capacity of acrylic hydrogels. *Acta Biomaterialia* **2007**, 3, 95-102.
- Chirila T V. An overview of the development of artificial corneas with porous skirts and the use of PHEMA for such an application. *Biomaterials* **2001**, 22, 3311-3317
- Choong C, Triffitt JT, Cui ZF. Polycaprolactone scaffolds for bone tissue engineering: Effects of a calcium phosphate coating layer on osteogenic cells. *Food and Bioproducts Processing* **2004**, 82, 117-125.
- Chow L C, Eanes E D. *Octacalcium phosphate*. In: Chow L C, Eanes E D. Editors, Karger: Basel, Switzerland, **2001**, 167.
- Chrzanowski W, Abou-Neel E, Armitage D, Knowles J, Surface preparation of bioactive Ni-Ti alloy using alkali, thermal treatments and spark oxidation. *J. Materials Science: Materials in Medicine* **2008**, 19, 1553-1557.
- Crawford G J, Hicks C R, Lou X, Vijayasekaran S, Tan D, Mulholland B, Chirila T V, Constable I J. The Chirila keratoprosthesis: phase I human clinical trial. *Ophthalmology* **2002**, 109, 883-889.
- Crompton T R. Fourier Transform Infrared spectroscopy (FTIR) In: Crompton T R. Editor.

- Characterisation of polymer*. Chem. Tec. Publishing Inc., New York, USA, **2008**, 1.
- Cross U, Kinne R, Schmit H J, Strunz V. The response of bone to surface active glass/glass-ceramics. *Critical Research in Biocompatibility* **1988**, 4, 2.
- Cruz F J A L, Minas-da-Piedade M E, Calado J C G. Standard molar enthalpies of formation hydroxyl-, chlor-, and bromapatite. *J. Chemical Thermodynamics* **2005**, 37, 1061-1070.
- Daculsi G, Bouler J M, Legeros R Z. Adaptive crystal formation in normal and pathological calcifications in synthetic calcium phosphate and related biomaterials. *International Reviews in Cytology* **1997**, 172, 129-191.
- Dagani R. Individual Surface Atoms Identified. In: Dagani R. Editor. *Chemical and Engineering News*, American Chemical Society Publishers, New York, USA, **2007**, 13.
- Damien E, Revell P A. Coralline hydroxyapatite bone graft substitute: a review of experimental studies and biomedical applications. *J. Applied Biomaterials and Biomechanics* **2004**, 2, 65-73.
- Danilatos G D. Foundations of environmental scanning electron microscopy. *Advances in Electronics and Electron Physics* **1988**, 71, 109-250.
- de Groot K, Wolke J G C, Jansen J A. Calcium phosphate coatings for medical implants. *Proceedings on the Institution of Mechanical Engineering part H: J. Engineering in Medicine* **1998**, 212, 137-147.
- de Groot K. Bioceramics of Calcium Phosphate. In: CRC Editors. *Bio-ceramics*. CRC Press, Boca Raton, USA, **1983**, 1-32.
- De-Gennes P G. Wetting: statics and dynamics. *Reviews of Modern Physics* **1985**, 57, 827-863.
- Deng C, Li F, Hackett J M, Chaudhry S H, Toll F N, Toye B, Hodge W, Griffith M. Collagen and glycopolymer based hydrogel for potential corneal application. *Acta Biomaterialia* **2010**, 6, 187-194.
- Dickinson W. Chromatography of insulin on calcium phosphate columns. *Nature*, **1956**, 178, 994-995.
- Djordjevic I, Britcher L G, Kumar S. Morphological and surface compositional changes in poly(lactide-co-glycolide) tissue engineering scaffolds upon radio frequency glow discharge plasma treatment. *Applied Surface Science* **2008**, 254, 1929-1935.
- Dohlman C H, Doane M G. Some factors influencing outcome after keratoprosthesis surgery. *Cornea* **1994**, 13, 214-218.
- Dohlman C H, Harissi-Dagher M. The Boston Keratoprosthesis: A New treadles design. *Digital J. of Ophthalmology* **2007**, 13, 3.
- Dohlman C H, Netland P A, Fung W C. Keratoprosthesis update. In: 4th World Congress on the Cornea. *The Castroviejo Society*, Orlando, Florida, USA, **1996**, 36.
- Doonan S. Chromatography on hydroxyapatite. *Methods in Molecular Biology* **2004**, 244, 191-194.
- Dorozhkin S V. Calcium orthophosphates. *J. Materials Science* **2007**, 42, 1061-1095.
- Dorozhkin S V. Nanodimensional and nanocrystalline apatites and other calcium orthophosphates

- in biomedical engineering, biology and medicine. *Materials* **2009**, *2*, 1975-2045.
- Dorozhkin S. V. Calcium orthophosphates in nature, biology and medicine. *Materials* **2009**, *2*, 399-498.
- Drenth J. Crystallography. In: Drenth J. Editor. *Principles of Protein X-ray Crystallography*, Springer, New York, USA, **1994**.
- Driessens F C M, Boltong M G, Bermúdez O, Planell J A, Ginebra M P, Fernández E. Effective formulations for the preparation of calcium phosphate bone cements. *J. Materials Science: Materials in Medicine* **1994**, *5*, 164-170.
- Driessens F C M, Planell J A, Boltong M G, Khairoun I, Ginebra M P. Osteotransductive bone cements. *Proceedings on the Institution of Mechanical Engineering part H: J. Engineering in Medicine* **1998**, *212*, 427-435.
- Edwards A, Prausnitz M R. Fiber Matrix Model of Sclera and Corneal Stroma for Drug Delivery to the Eye. *AIChE Journal* **1998**, *44*, 214-225.
- Elliot J C. Structure and chemistry of the apatites and other calcium orthophosphates. *Studies in Inorganic Chemistry* **1994**, *18*, 389.
- Ellis P. The conjunctiva. In: Mosby C V, Editor. *Ocular Therapeutics and Pharmacology*, 5th edition, St. Luis, **1977**, 128-129.
- EyeMD. Eye Medical Link. Eye Conditions Encyclopaedia. In: www.eyemlindk.com **2006**.
- Fakirov S. Polyethylene terephthalate. In: Wiley-VCH, Editors, *Handbook of Thermoplastic Polyesters*, Wiley-VCH, Weinheim, **2002**, 1223.
- Falcinelli G, Barogi G, Caselli M, Colliardod P, Taloni M. Personal changes and innovations in Strampelli osteo-odonto-keratoprosthesis. *Anales del Instituto Barraquer* **1999**, *29*, 47-48.
- Falcinelli G, Barogi G, Taloni M. Osteo-odonto-keratoprosthesis: present experience and future prospects. *Refractive and Corneal Surgery* **1993**, *9*, 193-194.
- Falcinelli G, Falsini B, Taloni M, Colliardo P, Falcinelli G. Modified osteo-odonto-keratoprosthesis for treatment of corneal blindness. *Archives of Ophthalmology* **2005**, *123*, 1319-1329.
- Falcinelli G, Missioroli A, Petitti V, Pinna C. Osteo-odonto-keratoprosthesis up to date. *Acta XXV Concilium Ophthalmologicum*. Kugler and Ghedini, Rome **1987**, 2772-2776.
- Fan J P, Tsui C P, Tang C Y, Chow C L. Influence of interphase layer on the overall elasto-plastic behaviours of HA/PEEK biocomposite. *Biomaterials* **2004**, *25*, 5363-5373.
- Fang L, Gao P, Leng Y. High strength and bioactive hydroxyapatite nano-particles reinforced ultrahigh molecular weight polyethylene. *Composites B* **2007**, *38*, 345-351.
- Ferraz M P, Monteiro F J, Manuel C M. Hydroxyapatite nanoparticles: a review of preparation methodologies. *J. Applied Biomaterials and Biomechanics* **2004**, *2*, 74-80.
- Filmon R, Grizon F, Basle M F, Chappard D. Effects of negativity charged groups (carboxymethyl) on the calcification of poly(2-hydroxyethyl methacrylate). *Biomaterials* **2002**, *23*, 3053-3059.

- Francon M. Reflected light differential contrast microscopy. In: Francon M, Editor. *Progress in Microscopy*, Pergamum Press, New York, **1961**, 199.
- Fratzl P, Daxer A. Structural transformation of collagen fibrils in corneal stroma during drying: an X-ray scattering study. *Biophysics* **1993**, *64*, 1210-1214.
- Gardiner D J. Raman Spectroscopy. In: Springer-Verlag Editor. *Practical Raman spectroscopy*. Springer-Verlag, New York, USA, **1989**.
- Geesink R G. Osteoconductive coatings for total joint arthroplasty. *Clinical Orthopaedics and Related Research* **2002**, *395*, 53-65.
- George W O, McIntery P S. Analytical chemistry by Infrared Spectroscopy. In: Mowthorpe D J., Editor, *Infrared Spectroscopy*. **1987**.
- Giessibl F J. Advances in atomic force microscopy. *Review Modern Physics* **2003**, *75*, 949-983.
- Ginebra M P; Driessens F C M, Planell J A. Effect of the particle size on the micro and nanostructure features of a calcium phosphate cement: a kinetic analysis. *Biomaterials* **2004**, *25*, 3453-3462.
- Girard L J. Girard keratoprosthesis with flexible skirt: 28 years experience. *Refractive and Corneal Surgery* **1993**, *9*, 194-195.
- Girard L J. Keratoprosthesis. *Cornea* **1983**, *2*, 207-224.
- Grant J T, Briggs D. X-ray Photoelectron Spectroscopy. In: Grant J T, Briggs D. Editors. *Surface Analysis by Auger and X-ray Photoelectron Spectroscopy*. IM Publications, Chichester, UK, **2003**.
- Grassmann O, Lobmann P. Biomimetic nucleation and growth of CaCO₃ in hydrogels incorporating carboxylate groups. *Biomaterials* **2004**, *25*, 277-282.
- Greenwood N N, Earnshaw A. Apatite. In: Butterworths-Heinemann, Editors. *Chemistry of the Elements*, Butterworths-Heinemann, London, **1997**.
- Gross K A, Berndt C C. Biomedical application of apatites. In: Hughes J M, Kohn M, Rakovan J. Editors, *Phosphates: geochemical, geobiological and materials importance*, Series: Reviews in Mineralogy and Geochemistry. Mineralogical Society of America: Washington, D.C., USA, **2002**, *48*, 631-672.
- Gu Y W, Khor K A, Cheang P. In vitro studies of plasma-sprayed hydroxyapatite/Ti-6Al-4V composite coating in simulated body fluid (SBF). *Biomaterials* **2003**, *24*, 1603-1611.
- Guo B. Keratoprosthesis for the treatment of severe bilateral cornea disease. In: Report Technote 27. Alberta Heritage Foundation for Medical Research, Health Technology Assessment Unit, Alberta, Canada, **2001**, *27*, 1-7.
- Gutierrez-Salazar M P, Reyes-Gasga J. Microhardness and chemical composition of human tooth. *Materials Research* **2003**, *6*, 367-373.
- Ha S W, Kirch M, Birchler F, Eckert K L, Mayer J, Wintermantel E. Surface activation of polyetheretherketone (PEEK) and formation of calcium phosphate coatings by precipitation. *J. Materials Science: Materials in Medicine* **1997**, *8*, 683-690.

- Hench L L, Ethridge E C. An artificial approach. In: Hench L L, Ethridge E C., Editors. *Biomaterials: An artificial approach*. Academic Press, New York, **1982**.
- Hench L L, Polak J M. Third-generation of biomedical materials. *Science* **2002**, *295*, 1014-1017.
- Hench L L, Splinter R J, Allen W C, Greenlee T K. Bonding mechanisms at the interface of ceramic prosthetic materials. *J. Biomedical Materials Research* **1972**, *2*, 117-141.
- Hench L L. Bioactive ceramics. In: Ducheyne P and Lemons J, Editors. *Bioceramics: Materials Characteristics Versus In vivo Behaviour*. Annals of New York Academy of Sciences, New York, **1988**, *523*, 54-71.
- Hench L L. Bioceramics. *J. Am. Ceramic Society* **1998**, *81*, 1705-1728.
- Hench L L. Bioceramics: from concept to clinic. *J. Am. Ceramic Society* **1991**, *74*, 1487-1510.
- Hench L L. Biomaterials: A forecast for the future. *Biomaterials* **1998**, *19*, 1419-1423.
- Hench LL. Biomaterials. *Science* **1980**, *208*, 826-831.
- Hicks C R, Crawford G J, Lou X, Tan D T, Snibson G R, Sutton G, Downie N, Werner L, Chirila T V, Constable I J. Keratoprosthesis: Corneal replacement using a synthetic hydrogel cornea AlphaCor device preliminary outcomes and complications. *Eye* **2003**, *17*, 385-392.
- Hicks C R, Crawford G, Chirila T V, Wiffen S, Vijayasekaran S, Lou X, Fitton J, Maley M, Clayton A, Dalton P, Platten S, Ziegelaar B, Hong Y, Russo A, Constable I. Development and clinical assessment of an artificial cornea. *Progress in Retinal and Eye Research* **2000**; *19*, 149-170.
- Hicks C R, Fitton J H, Chirila T V, Crawford G J, Constable I J. Keratoprosthesis: Advancing towards a true artificial cornea. *Survey of Ophthalmology* **1997**, *42*, 175-189.
- Hicks C R, Werner L, Vijayasekaran S, Mamalis N, Apple D J. Histology of AlphaCor skirts: evaluation of biointegration. *Cornea* **2005**, *24*, 933-940.
- Hille K, Hille A, Ruprecht K W. Medium term results in keratoprostheses with biocompatible and biological haptic. *Graefe's Archive for Clinical and Experimental Ophthalmology* **2006**, *244*, 696-704.
- Hodge W G. Anatomy and embryology of the eye. In: Vaughan D, Asbury T and Riordan-Eva P, Editor, *General Ophthalmology*. Prentice-Hall International Inc., London, UK, **1995**, 7.
- Hofmann I, Muller L, Greil P, Muller F A. Precipitation of carbonated calcium phosphate powders form a highly supersaturated simulated body fluid solution. *J. Am. Ceramic Society* **2007**, *90*, 821-824.
- Holak S A, Holak H M, Bleckmann H. AlphaCor™ keratoprosthesis postoperative development of six patients. *Graefe's Archive for Clinical and Experimental Ophthalmology* **2009**, *247*, 535-539.
- Hollick E J, Watson S L, Dart J K G, Luthert P J, Allan B D S. Legeais BioKpro III keratoprosthesis implantation: long term results in seven patients. *Br. J. Ophthalmology* **2006**, *90*, 1146-1151.

- Honghui Z, Hui L, Linghong G. Molecular and crystal structure characterization of calcium-deficient apatite. *Key Engineering Materials* **2007**, 330-332, 119-122.
- Hong-Qiang L. Biological applications of AFM. *Atomic Force Microscopy* **1997**, 729.
- Houde M, Martin J W, Letcher R J, Solomon K R, Muir D C. Biological monitoring of polyfluoroalkyl substances: A review. *Environmental Science and technology* **2006**, 40, 3463–3473.
- Huan Z, Chang J. Novel bioactive composite bone cements based on the β -tricalcium phosphate – monocalcium phosphate monohydrate composite cement system. *Acta Biomaterialia* **2009**, 5, 1253-1264.
- Huang J, Di Silvio L, Wang M, Rehman I, Ohtsuki C, Bonfield W. Evaluation of *in vitro* bioactivity and biocompatibility of Bioglass–reinforced polyethylene composite. *J. Materials Science: Materials in Medicine* **1997**, 8, 809-813.
- Hughes J M, Rakovan J. The crystal structure of apatite, $\text{Ca}_5(\text{PO}_4)_3(\text{F},\text{OH},\text{Cl})$. In: Hughes; Kohn J M, Rakovan J. Editors, *Phosphates: geochemical, geobiological and materials importance*, Series: Reviews in Mineralogy and Geochemistry. Mineralogical Society of America: Washington, D.C., USA, **2002**, 48, 1-12.
- Ilhan-Sarac O, Akpek E K. Current concepts and techniques in keratoprosthesis. *Current Opinion in Ophthalmology* **2005**, 16, 246-250.
- IPAC. Interventional Procedures Advisory Committee, Interventional Procedure Programme, Interventional procedure overview of insertion of a hydrogel synthetic keratoplasty, Synthetic penetration keratoplasty using a synthetic hydrogel cornea, Royal College of Ophthalmology, **2004**.
- Ishiwata H, Itoh M, Yatagai T. A new method of three-dimensional measurement by differential interference contrast microscope. *Optic Communications* **2005**, 260, 117-126.
- Israelachvili J N. *Intermolecular and Surface Forces*, Academic Press, London, UK, **2004**.
- Ivanova T I, Frank-Kamenetskaya O V, Kol'tsov A B, Ugolkov V L. Crystal structure of calcium-deficient carbonated hydroxyapatite thermal decomposition. *J. Solid State Chemistry* **2001**, 160, 340-349.
- James B, Chew C, Bron A. The Cornea. In: Blackwell Science Ltd, Editor, *Lecture notes on Ophthalmology, Anatomy: The Cornea*. Blackwell Science Ltd, London, **2003**.
- Janasova L, Muller F A, Helegrant A, Strad J, Greil P. Hydroxyapatite formation on alkali-treated titanium with different Na^+ in the surface layer. *Biomaterials* **2002**, 23, 3095-3101.
- Jeanjean J, McGrellis S, Rouchaud J C, Fedoroff M, Rondeau A, Perocheau S, Dubis A. A crystallographic study of the sorption of cadmium on calcium hydroxyapatites: incidence of cationic vacancies. *J. Solid State Chemistry* **1996**, 126, 195-201.
- Jokanovic V, Izvonar D, Dramicanin M D, Jokanovic B, Zivojinovic V, Markovic D, Dacic B. Hydrothermal synthesis and nanostructure of carbonated calcium hydroxyapatite. *J. Materials Science: Materials in Medicine* **2006**, 17, 539-546.
- Jonasova L, Muller F A, Helebrant A, Strad J, Greil P. Hydroxyapatite formation on alkali-treated titanium with different content of Na^+ in the surface layer. *Biomaterials* **2002**, 23, 3095-3101.

- Juhasz J A, Best S M, Auffret A D, Bonfield W. Biological control of apatite growth in simulated body fluid and human blood serum. *J. Materials Science: Materials in Medicine* **2008**, *19*, 1823–1829.
- Jungbauer A, Hahn R, Deinhofer K, Luo P. Performance and characterization of a nanophased porous hydroxyapatite for protein chromatography. *Biotechnology and Bioengineering* **2004**, *87*, 364-375.
- Kamakura S, Sasano Y, Homma H, Suzuki O, Kagayama M, Motegi K. Implantation of octacalcium phosphate (OCP) in rat skull defects enhances bone repair. *J. Dental Research* **1999**, *78*, 1682-1687.
- Kamakura S, Sasano Y, Homma H, Suzuki O, Kagayama M, Motegi K. Implantation of octacalcium phosphate nucleates isolated bone formation in rat skull defects. *Oral Diseases* **2001**, *7*, 259-265.
- Kawashita M, Nakao M, Minoda M, Kim H M, Beppu T, Miyamoto T, Kokubo T, Nakamura T. Apatite-forming ability of carboxyl group-containing polymer gels in a simulated body fluid. *Biomaterials* **2003**, *24*, 2477-2484.
- Kay M I, Young R A, Posner A S. Crystal structure of hydroxyapatite. *Nature* **1964**, *204*, 1050-1052.
- Keely F W, Morin J D, Vesely S. Characterisation of Type I collagen from normal human sclera. *Experimental Eye Research* **1984**, *39*, 663–672.
- Kikawa T, Kashimoto O, Imaizumi H, Kokubun S, Suzuki O. Intramembranous bone tissue response to biodegradable octacalcium phosphate implant. *Acta Biomaterialia* **2009**, *5*, 1756.
- Kim H M, Kishimoto K, Miyaji F, Kokubo T, Yao T, Suetsugu Y. Composition and structure of the apatite formed on PET substrates in SBF modified with various ionic activity products. *J. Biomedical Materials Research* **1999**, *46*, 228-235.
- Kim H M, Kishimoto K, Miyaji F, Kokubo T. Composition and structure of the apatite formed on organic polymer in simulated body fluid with high content of carbonate ion. *J. Materials Science: Materials in Medicine* **2000**, *11*, 421-426.
- Kim K M, Lee J L, Wee W R, Lee J H. Seoul-type keratoprosthesis. *Archives of Ophthalmology* **2002**, *120*, 761-766.
- Kingston R E, Chen C A, Rose J K. Calcium phosphate transfection. *Current Protocol Molecular Biology* **2003**, *9*, 1.
- Kiozumi N, Inatomi T, Suzuki T, Sotozono C, Kiohita S. Cultivated corneal epithelial transplantation for ocular surface reconstruction in acute phase of Steven-Johnson syndrome. *Archives of Ophthalmology* **2001**, *119*, 298-300.
- Kokubo T, Hata K, Nakamura T, Yamamuro T. Apatite formation on ceramics, metals and polymers induced by CaPSiO₂ based glass in a simulated body fluid. *Bioceramics* **1991**, *4*, 113-120.
- Kokubo T, Ito D, Shigematsu M, Sakka S, Yamamuro T. Fatigue and life-time of bioactive glass-ceramic A-W containing apatite and wollastonite. *J. Materials Science* **1987**, *22*, 4067–4070.

- Kokubo T, Kushitani H, Sakka S, Kitsugi T, Yamamuro T. Solutions able to reproduce *in vivo* Surface-Structure changes in Bioactive Glass-Ceramic A-W3. *J. Biomedical Materials Research* **1990**, *24*, 721-734.
- Kokubo T, Takadama H. How useful is SBF in predicting *in vivo* bone bioactivity? *Biomaterials* **2006**, *27*, 2907-2915.
- Kokubo T. Apatite formation on surfaces of ceramics, metals and polymers in body environment. *Acta Biomaterialia* **1998**, *46*, 2519-2527.
- Kokubo T. Formation of biologically active bone-like apatite on metals and polymers by a biomimetic process. *Thermochimica Acta* **1996**, *280/281*, 479-490.
- Kokubo T. Preparation of Bioactive Ti and Its Alloys Via Simple Chemical Surface Treatment. *J. Biomedical Materials Research* **1996**, *32*, 409-417.
- Köster K, Heide H, König R. Resorbierbare Calciumphosphatkeramik im Tierexperiment unter Belastung. *Langenbecks Archiv fuer Chirurgie* **1977**, *343*, 173-181.
- Kowk D Y, Neumann A W. Contact angle measurement and contact angle interpretation. *Advances in Colloid and Interference Science* **1999**, *81*, 167-249.
- Kurashina K, Kurita H, Hirano M, Kotani A, Klein C P, de Groot K. *In vivo* study of calcium phosphate cements: implantation of an α -tricalcium phosphate / dicalcium phosphate dibasic / tetracalcium phosphate monoxide cement paste. *Biomaterials* **1997**, *18*, 539-543.
- Kurtz S M, Devine J N. PEEK biomaterials in trauma, orthopedic, and spinal implants. *Biomaterials* **2007**, *28*, 4845-4869.
- Kurtz S M. ultra-high molecular weight polyethylene. In: Academic Pres, Editor, *The UHMWPE handbook: ultra-high molecular weight polyethylene in total joint replacement*, Academic Press, New York, **2004**, 18.
- L'vov B V. Fifty years of atomic absorption spectrometry. *J. Analytical Chemistry* **2005**, *60*, 382.
- L'vov B V. Forty years of electrothermal atomic absorption spectrometry. *Acta Spectrochimica* **1997**, *52 B*, 1239-1245.
- Langley T, Ledford J K. Eyebrows, Eyelids, and the Lacrimal System. In: Lens A, Nemeth S C, Ledford J K. Editors. *Ocular Anatomy and Physiology*, Slack Incorporated, Thorofare, USA, **2007**, *4*, 25-32.
- Lee S D, Hsiue G H, Kao C Y, Chang P C T. Artificial cornea: Surface modification of silicone rubber membrane by graft polymerization of pHEMA via glow discharge. *Biomaterials* **1996**, *17*, 587-595.
- Legeais J M, Drubaix I, Mayer F, Savoldelli M, Renard G A. A second regeneration of biointegrable keratoprosthesis. First human cases. *Investigative Ophthalmology and Visual Science* **1997**, *38*, 131.
- Legeais J M, Renard G, Pouliquen Y. A novel colonisable keratoprosthesis. *Refractive and Corneal Surgery* **1993**, *9*, 205-206.
- Legeais J M, Renard G, Rossi C, Salvodelli M, D'Hermies F, Pouliquen Y. A new fluorocarbon for

keratoprosthesis. *Cornea* **1992**, *11*, 538-545.

Legeais J M, Renard G, Rossi C, Salvodelli M, D'Hermies F, Pouliquen Y. Keratoprosthesis: a comparative study of three different microporous polymers and first application in human eyes. *Investigative Ophthalmology and Visual Science* **1991**, *32*, 778.

Legeais J M, Renard G. A second generation of artificial cornea (Biokpro II). *Biomaterials* **1998**, *19*, 1517-1522.

Legeros R Z, Kijkowska G, Legeros J P, Abergas T, Bleiwas H. CO₃ for OH (type A) and CO₃ for PO₄ (type B) substitutions in precipitated carbonate apatites. *J. Dental Research* **1987**, *66*, 190-198.

Legeros R Z, Lin S, Rohanizadeh R, Mijares D, Legeros J P. Biophasic calcium phosphate Bioceramics: preparation, properties and applications. *J. Materials Science: Materials in Medicine* **2003**, *14*, 201-209.

Legeros R Z. *Calcium phosphates in oral biology and medicine*. In: Karger, Basel. Switzerland, **1991**, 201.

Legeros R Z. Formation and transformation of calcium phosphates: relevance to vascular calcification. *Z Kardiol* **2001**, *90*, Suppl. 3, III116-III125.

Legeros R Z. Preparation of octacalcium phosphate (OCP): a direct fast method. *Calcified Tissue International* **1985**, *37*, 194-197.

Legeros R Z. Variations in the crystalline components of human dental calculus: I. crystallographic and spectroscopic methods of analysis. *J. Dental Research* **1974**, *53*, 45-50.

Leonor L B, Ito A, Onuma K, Reis R L. In vitro bioactivity of Starch thermoplastic/hydroxyapatite composite biomaterials: an in situ using atomic force microscopy. *Biomaterials* **2003**, *24*, 579-585.

Li Y H, Cao L Y, Huang J F, Zeng X R. Characteristics and preparation of nanometer hydroxyapatite in medical science. *J. Clinical Rehabilitation Tissue Engineering Research* **2008**, *12*, 8143-8146.

Liu C, Okera S, Tandon R, Herold J, Hull C, Thorps S. Visual rehabilitation in end-stage inflammatory ocular surface with osteo-odonto-keratoprosthesis: results from the UK. *Br. J. Ophthalmology* **2008**, *92*, 1211-1217.

Liu C, Paul B, Tandon R, Lee E, Fong K, Mavrikakis I, Herold J, Thorp, S, Brittain P, Francis I, Ferrett C, Hull C, Lloyd A, Green D, Franklin V, Tighe B, Fukuda M, Hamada S. The Osteo-Odonto-Keratoprosthesis (OOKP). *Seminars in Ophthalmology* **2005**, *20*, 113-128.

Liu C, Sciscio A, Smith G, Pagliarini S, Herold J. Indications and technique of modern osteo-odonto-keratoprosthesis (OOKP) surgery. *Eye News*. **1998**, *5*, 17-22.

Liu C, Syam P P, Herold J, Thorp S. Modern osteo-odonto-keratoprosthesis (OOKP) surgery. *Royal College of Ophthalmologists Guidelines*, Sussex Eye Hospital, Brighton, UK **2007**.

Liu T Y, Chen S Y, Liu D M, Liou S C. On the study of BSA-loaded calcium-deficient hydroxyapatite nano-carriers for controlled drug delivery. *J. Controlled Release* **2005**, *107*, 112-121

Liu Y, de Groot K, Hunziker E. BMP-2 liberated from biomimetic implant coatings induces and

sustains direct ossification in an ectopic rat model. *Bone* **2005**, *36*, 745-757.

Liu Y, Hunziker E B, Randall N X, de Groot K, Layrolle P. Proteins incorporated into biomimetically prepared calcium phosphate coatings modulate their mechanical strength and dissolution rate. *Biomaterials* **2003**, *24*, 65-70.

Long J D, Xu S, Cai J W, Jiang N, Lu j H, Ostrikov K N, Diong C H. Structure, bonding state and in-vitro study of Ca-P-Ti film deposited on Ti6Al4V by RF magnetron sputtering. *Materials Science and Engineering* **2002**, *20* (1-2), 175-180.

Lowenstam H A. Weiner S. Biomineralization. In: Oxford University Press, Editors. *On biomineralization*, Oxford University Press, New York, USA, **1989**, 324.

Mangano C, Piattelli A, Perrotti V, Iezzi G. Dense hydroxyapatite inserted into postextraction sockets: a histologic and histomorphometric 20-year case report. *J. Periodontology* **2008**, *79*, 929-933.

Marin J E, Wilcoxon J, Adolf D. Critical exponents for the sol-gel transition. *Physical Review* **1987**, *36 A*, 1803-1810.

Martini F H. Sensory Function: Vision. In: Prentice-Hall, Editor, *Fundamentals of Anatomy and Physiology*. Prentice-Hall, New Jersey, **1995**, 562-579.

Mathew M, Takagi S. Structures of biological minerals in dental research. *J. Research at the National Institute of Standards and Technology* **2001**, *106*, 1035-1044.

Matousek P, Parker A W. Bulk Raman Analysis of Pharmaceutical Tablets. *Applied Spectroscopy* **2006**, *60*, 1353-1357.

Maurice D M. The cornea and sclera. In: Davson H., Editor, *The Eye* (3rd edition), Academic Press, New York, **1984**, 1-158.

McBrien N A, Gentle A. Role of the sclera in the development and pathological complications of myopia. *Progress in Retinal and Eye Research* **2003**, *22*, 307-338.

McBrien N A, Morgan I G, Mutti D O. What's hot in Myopia Research-The 12th International Myopia Conference, Australia, July 2008. *Optometry and Vision Science* **2009**, *86*, 1, 2-3.

Meek K M, Fullwood N J. Corneal and scleral collagens – a microscopist's perspective. *Micron* **2001**, *32*, 261-272.

Meek K M. The Cornea and sclera. In: P. Fratzl, Editor, *Collagen Structure and Mechanics*, Springer, New York, **2008**, 359-396.

Merindano-Encima M D, Potau J M, Ruano D, Costa J, Canals M. A comparative study of Bowman's layer in some mammals: Relations with other constituent corneal structure. *European J. of Anatomy* **2002**, *6*, 133-140.

Meyer E, Overney R, Brodbeck D, Howald L, Luthi R, Frommer J, Guntherodt, H J. Friction and wear of Langmuir-Blodgett films observed by friction force microscopy. *Physical Review Letters* **1992**, *69*, 1777-1780.

Meyer G, Amer n M. Novel optical approach to atomic force microscopy. *Applied Physical Review Letters* **1988**, *53*, 1045.

- Meyer H M, Hill D M, Wagener T J, Gao Y, Weaver J H. Electronic structures of the $\text{YBa}_2\text{Cu}_3\text{O}_{7-x}$ surface and its modification by sputtering and adatoms of Ti and Cu. *Physical Review* **1988**, 38 B, 6500-6512.
- Michael R, Charoenrook V, de la Paz M F, Hitzl W, Temprano J, Barraquer R I. Long-term functional and anatomical results of osteo-and osteodonto-keratoprosthesis. *Graefe's Archive for Clinical and Experimental Ophthalmology* (Cornea) **2008**, 246, 1133-1137.
- Moffatt S L, Carwright V A, Stumpf T H. Centennial review of corneal transplantation. *Clinical and Experimental Ophthalmology* **2005**, 33, 642-657.
- Mortier A, Lemaitre J, Rodrique L, Rouxhet P G. Synthesis and thermal behavior of well crystallized calcium-deficient phosphate apatite. *J. Solid State Chemistry* **1989**, 78, 215-219.
- Moulder J F, Stickle W F, Sobol P E, Bomben K D. X-ray Photoelectron Spectroscopy. In: Moulder J F, Stickle W F, Sobol P E, Bomben K D. Editors. *Handbook of X-ray Photoelectron Spectroscopy*. Perkin-Elmer Corp., Eden Prairie, MN, USA, **1992**.
- Muller L, Muller F A. Preparation of SBF with different HCO_3^- content and its influence on the composition of biomimetic apatites. *Acta Biomaterialia* **2006**, 2, 181-189.
- Myer K. Polymethyl methacrylate. In: John Wiley & Sons, Editors. *Handbook of Materials Selection*, John Wiley & Sons, London, UK, **2002**, 341.
- Myung D, Duhamel P-E, Cochran J, Noolandi J, Ta C, Frank C. Development of Hydrogel-based Keratoprostheses: A Materials Perspective. *Biotechnology Progress* **2008**, 24, 735-741.
- Myung D, Koh W, Bakri A, Zhang F, Marshall A, Ko J, Noolandi J, Carrasco M, Cochran J R, Frank C W, Ta C N. Design and fabrication of an artificial cornea based on a photolithographically patterned hydrogel construct. *J. Biomedical Microdevices* **2007**, 9, 911-922.
- Nagyova B, Tiffany J M. Components responsible for the surface tension of human tears. *Current Eye Research* **1999**, 19, 4-11
- Nakahira A, Aoki S, Sakamoto K, Yamaguchi S. Synthesis and evaluation of various layered octacalcium phosphates by wet-chemical processing. *J. Materials Science: Materials in Medicine* **2001**, 12, 793-800.
- NEI. National Eye Institute. Facts about the cornea and corneal disease. NEI health information, National Institutes of Health, USA, **2006**.
- Nelson S J. Bio-mineral in Teeth. In: Saunders W B, Editor, *Wheeler's Dental Anatomy, Physiology and Occlusion*. W. B. Saunders, Philadelphia, PA, USA, **2009**, 368.
- Nemeth S C, Shea C. Conjunctiva, Episclera, and Sclera. In: Lens A, Nemeth S C, Ledford J K. Editors. *Ocular Anatomy and Physiology*, Slack Incorporated, Thorofare, USA, **2007**, 6, 49.
- NHS Trust. Anatomy of the eye. Eye Health. Moorfields Eye Hospital NHS Foundation Trust, London, UK, **2006**.
- Ni J, Wang M. In vitro evaluation of hydroxyapatite reinforced in polyhydroxybutyrate composite. *Materials Science and Engineering C*. **2002**, 20, 101-109.

- Nickel E H. Definition of a mineral. *The Canadian Mineralogist* **1995**, *33*, 689-690.
- Ning C Q, Greish Y, El-Ghannam A. Crystallization behavior of silica-calcium phosphate biocomposites: XRD and FTIR studies. *J. Materials Science: Materials in Medicine*. **2004**, *15*, 1227-1235.
- NLM. National Library of Medicine. *Genetic home reference: Fibroblasts*. Unified Medical Language System, MeSH. U.S.NLM, USA, **2010**, February 28, 1.
- NMP. Nanotechnologies and nano-sciences, knowledge-based multifunctional materials and new production processes and devices. Three-dimensional reconstruction of human corneas by tissue engineering in Sixth Framework Programme Priority, UK, **2003**, 3.
- Nomarski G M. Reflected light differential contrast microscopy. *J. Physique et Radium Paris* **1955**, *16*, 9S.
- O'Neill W C. The fallacy of the calcium – phosphorus product. *Kidney International* 2007, *72*, 792-796.
- Oehr C. Plasma Surface modification on polymers for biomedical use. *Nuclear Instruments and Methods in Physics Research B* **2003**, *208 B*, 40-47.
- Ohtsuki C, Kokubo T, Yamamuro T. Mechanism of apatite formation on CaO-SiO₂-P₂O₅ glasses in a Simulated Body Fluid. *J. Non-Crystal. Solids* **1992**, *143*, 84-92.
- Ohura K, Bohner M, Hardouin P, Lemaitre J, Pasquier G, Flaute B. Resorption of, and bone formation from, new β -tricalcium phosphate-monocalcium phosphate cements: An *in vivo* study. *J. Biomedical Materials Research* **1996**, *30*, 193-200.
- Olsen T W, Aaberg S Y, Geroski D H, Edelhauser H F. Human sclera: thickness and surface area *American Journal of Ophthalmology* **1998**, *125*, 237-241.
- Olver J, Cassady L. The Cornea. In: Blackwell Publishing, Editor. *Ophthalmology at a Glance*. Blackwell Publishing Ltd., Oxford, **2005**, 9, 9-33
- Ong J L, Chan D C N. Hydroxyapatites and their use as coatings in dental implants: a review. *Critical Reviews in Biomedical Engineering* **1999**, *28*, 667-707.
- Oyane A, Kim H M, Furuya T, Kokubo T, Miyazaki T, Nakamura T. Preparation and assessment of revised simulated body fluids. *J. Biomedical Materials Research* **2003**, *65A*, 188–195.
- Oyane A, Uchida M, Choong C, Triffitt J, Jones J, Ito A. A simple surface modification of poly(ϵ -caprolactone) for apatite deposition from simulated body fluid. *Biomaterials* **2005a**, *26*, 2407-2413.
- Oyane A, Uchida M, Yokoyama Y, Choong C, Triffitt J, Jones J. Simple surface modification on polycaprolactone to induce its apatite-forming ability. *J. Biomedical Materials Research* **2005b**, *75A*, 138-145.
- Palazzo B, Sidoti M C, Roveri N, Tampieri A, Sandri M, Bertolazzi L, Galbusera F, Dubini G, Vena P, Contro R. Controlled drug delivery from porous hydroxyapatite grafts: an experimental and theoretical approach. *Materials Science and Engineering C* **2005**, *25*, 207-213.
- Pandey A, Jan E, Aswath P B. Physical and mechanical behaviour of hot rolled HDPE/HA

- composites. *J. Materials Science* **2006**, *41*, 3369-3376.
- Panjwani N. Cornea and Sclera. In: Harding J J., Editor, *Biochemistry of the Eye*, Chapman and Hall, London, **1997**, 16-51.
- Parel J M, Sweeney D. OOKP. *Cornea* **2005**, *24*, 893-894.
- Patel S, Thakar R G, Wong J, McLeod S D, Li S. Control of cell adhesion on poly(methyl methacrylate). *Biomaterials* **2006**, *27*, 2890-2897.
- Penel G, Leroy G, Rey C, Bres E. Micro Raman spectral study of the PO₄ and CO₃ vibrational modes in synthetic and biological apatites. *Calcified Tissue International* **1998**, *63*, 475-481.
- Petra M, Anastassopoulou J, Theologis T, Theophanides T. Synchrotron micro-FT-IR spectroscopic evaluation of normal paediatric human bone. *J. Molecular Structure* **2005**, *733*, 101-110.
- Pino M, Chrzanowski W, Fabel D, Baklar M, Stingelin N, Tanner K E. Apatite Deposition on NaOH-treated PEEK and UHMWPE Films for Sclera Materials in Artificial Cornea Implant. *Advanced Engineering Materials: Advanced Biomaterials* **2010** (in press).
- Pino M, Duckett R A, Ward I M. Single and mixed gas diffusion through polyethylene films. *Polymer* **2005**, *46*, 48882-4890.
- Pino M, Stingelin N, Tanner K E. Nucleation and growth of apatite on NaOH-treated PEEK, HDPE and UHMWPE for artificial cornea materials. *Acta Biomaterialia* **2008**, *4*, 1827-1836.
- Pintucci S, Pintucci F, Cecconi M, Caiaza S. New Dacron tissue colonisable keratoprosthesis: clinical experience. *Br. J. Ophthalmology* **1995**, *79*, 825-829.
- Qiu S R, Orme C A. Dynamics of biomineral formation at the near-molecular level. *Chemical Reviews* **2008**, *108*, 4784-4822.
- Rao G N, Blatt H L, Aquavella J V. Results of keratoprosthesis. *Am. J. Ophthalmology* **1979**, *88*, 190-196.
- Ratner B D, Bryant S J. Biomaterials: Where we have been and where we are going. *Annual Review Biomedical Engineering* **2004**, *6*, 41-75.
- Ratner B D. An introduction to Materials in Medicine. In: Academic Press, Editor. *Biomaterials Science*. Elsevier, London, **2004**.
- Refojo M F. Ophthalmological applications. In: Ratner B D, Hoffman A S, Schoen F J and Lemons J E, Editor, *Biomaterials Science*. London, Elsevier, **2005**, 583-588.
- Rehman I, Bonfield W. Characterization of hydroxyapatite and carbonated apatite by photo acoustic FTIR spectroscopy. *J. Materials Science: Materials in Medicine* **1997**, *8*, 1-4.
- Renke-Gluszko M, Fray M E L. The effect of simulated body fluid on the mechanical properties of multiblock poly(aliphatic/aromatic-ester) copolymers. *Biomaterials* **2004**, *25*, 5191-5198.
- Rey C, Combes C, Drouet C, Sfihi H. Chemical diversity of apatites. *Advanced Science and Technology* **2006**, *49*, 27-36.
- Ricci R, Pecorella I, Ciardi A, Della Roca C, Di Tondo U, Marchi V. Stampelli's osteo-odonto-

- keratoprosthesis: clinical and histological long-term features of three prostheses. *Br. J. Ophthalmology* **1992**, *76*, 232-234.
- Rodríguez-Lorenzo L. Studies on calcium deficient apatites structure by means of MAS-NMR spectroscopy. *J. Materials Science: Materials in Medicine* **2005**, *16*, 393-398.
- Roeder R K, Smith S M., Conrad T L, Yanchak N J, Meriill C H, Converse G L. Porous and bioactive PEEK implants for interbody spinal fusion. *Advanced Materials and Processes* **2009**, *8*, 46-48.
- Roiter Y, Minko S. AFM single molecule experiments and the solid-liquid interface: In situ conformation of absorbed flexible polyelectrolyte chains. *J. Am. Chemical Society*. **2005**, *127*, 15688-15689.
- Ryhänen J. Biocompatibility evaluation of nickel-titanium shape memory alloy. OulunYliopisto, *Oulu University Library*, **2000**.
- Ryu G H, Yang W S, Roh H W, Lee I S, Kim J K, Lee G H, Lee D H, Park B J, Lee M S, Park J C. Plasma surface modification of poly(D,L-lactic-co-glycolic acid)(65/35) film for tissue engineering. *Surface Coating Technology* **2005**, *193*, 60-64.
- Sakamoto W K. Dielectric spectroscopy and thermally stimulated discharge current in PEEK film. *Eclética Química* **2003**, *28*, 49-53.
- Sanchis-Gimeno J A, Herrera M, Lleo-Perez A, Luis M D, Rahhal M S, Martinez-Soriano F. Quantitative Anatomical Difference in central Corneal Thickness Values determined with Scanning-Slit Corneal Topography and Noncontact Specular Microscopy. *Cornea* **2006**, *25*, 203-205.
- Sandeman S R, Faragher R G A, Allan B D S, Liu C, Lloyd AW. Novel materials to enhance keratoprosthesis integration. *Br. J. Ophthalmology* **2000**, *84*, 640-644.
- Sanhermelando M V, Lleó A, Alonso L, Rahhal M S, Hernández Gil de Tejada T, Martínez Soriano F, Sanchis J A G. Repeatability of central corneal thickness and ocular anterior chamber depth measurements with the Orbscan topography system. *Eur. J. Anatomy* **2002**, *6*, 59-64.
- Sargolzaei-Aval F, Sobhani A, Arab M R, Sarani S A, Heydari M H. The efficacy of implant of octacalcium phosphate in combination with bone matrix gelatin (BMG) on bone regeneration in skull defects in rat. *Iranian J. of Medical Sciences* **2004**, *29*, 124-129.
- Schroeder H. Formation and inhibition of dental calculus. *J. Periodontology* **1969**, *40*, 643-646.
- Seah M P, Briggs D. X-ray Photoelectron Spectroscopy. In: Seah M P, Briggs D. Editors. *Practical Surface Analysis by Auger and X-ray Photoelectron Spectroscopy*. Wiley & Sons, Chichester, UK, **1992**, *2*.
- Shah D. Tooth Anatomy. In: *Every Body Co.* Australia, **2009**.
- Shelton R M, Liu Y, Cooper P R, Gbureck U, German M J, Barralet J E. Bone marrow cell gene expression and tissue construct assembly using octacalcium phosphate microscaffolds. *Biomaterials* **2006**, *27*, 2874-2881.
- Simonin L, Liao, H. Characterisation of flame-sprayed PEEK coating by FTIR-ATR, DSC and acoustic microscope. *Macromolecular Materials and Engineering* **2000**, *283*, 153-162.

- Sinha R, Sharma N, Vajpayee R B. Corneal Blindness – Present Status. *Cataract and Refractive Surgery Today* **2005**, October, 59-61.
- Skelton V A, Henderson K, Liu C. Anaesthetic implications of osteo-odonto-keratoprosthesis surgery. *Eur. J. of Anaesthesiology* **2000**, 17, 390-394.
- Skoog D, Holler J, Crouch S. Atomic Absorption Spectroscopy. In: Thompson B. Editor. *Principles of Instrumental Analysis*. Cole, **2007**, 238.
- Smith G P, Gingrich T R. Hydroxyapatite chromatography of phage-display virions. *Biotechniques* **2005**, 39, 879-884.
- Smith W F, Javad H. Polymethyl methacrylate. In: McGraw-Hill, Editor. *Foundation of Materials Science and Engineering*, McGraw-Hill, London, **2006**.
- Sperling M B, Welz B. Atomic Absorption Spectroscopy. In: Weinheim Editor. *Atomic Absorption Spectrometry*, Wiley-VCH, Berlin, Germany **1999**, 527.
- Stancu I C, Filmon R, Cincu C, Marculescu B, Zaharia C, Tourmen Y, Basle M F, Chappard D. Synthesis of methacryloyloxyethyl phosphate copolymers and in vitro calcification capacity. *Biomaterials* **2004**, 25, 205-213.
- Steinert R. Implantable Devices. In: Steinert R., Editor. *Cataract Surgery*. Saunders, **2003**.
- Strampelli B. Osteo-Odontocheratorpostese. *Annali di Ottalmologia e Clinica Oculistica* **1963**, 89, 1039-1044.
- Suchanek W, Yoshimura M. Processing and properties of hydroxyapatite-based biomaterials for use as hard tissue replacement implants. *J. Materials Research* **1998**, 13, 94-117.
- Sun L, Berndt C C, Gross K A, Kucuk A. Review: material fundamentals and clinical performance of plasma sprayed hydroxyapatite coatings. *J. Biomedical Materials Research B Applied Biomaterials* **2001**, 58, 570-592.
- Suzuki E. High-resolution scanning electron microscopy of immunogold-labelled cells by the use of thin plasma coating of osmium. *J. Microscopy* **2002**, 208, 153-157.
- Suzuki O, Imaizumi H, Kamakura S, Katagiri T. Bone regeneration by synthetic octacalcium phosphate and its role in biological mineralization. *Current Medical Chemistry* **2008**, 15, 305-313.
- Suzuki O, Kamakura S, Katagiri T, Nakamura M, Zhao B, Honda Y, Kamijo R. Bone formation enhanced by implanted octacalcium phosphate involving conversion into Ca-deficient hydroxyapatite. *Biomaterials* **2006**, 27, 2671-2681.
- Sweeney D F. The Max Schapero Memorial Award Lecture 2004: Contact lenses on and in the corneal, what the eye needs. *Optometry and Vision Science* **2006**, 83, 133-142.
- Tadic D, Peters F, Epple M. Continuous synthesis of amorphous carbonated apatites. *Biomaterials* **2001**, 23, 2553-2559.
- Tadmor R. Line energy and the relation between advancing, receding and Young contact angles. *Langmuir* **2004**, 20, 7659-7664.
- Takagi S, Chow L C, Ishikawa K. Formation of hydroxyapatite in new calcium phosphate cements.

Biomaterials **1998**, 19, 1593-1599.

Tan D, Tay A, Theng J, Weng L K, Wong R, Liu C. Tooth-in-eye (OOKP) surgery help and regain sight. *Sight Health*, National Dental Centre Singapore **2005**, 1.

Tan K H, Chua C K, Leong K F, Cheah C M, Cheang P, Abu-Bakar S M. Scaffold development using selective laser sintering of polyetheretherketone-hydroxyapatite biocomposite blends. *Biomaterials* **2003**, 24, 3115-3123.

Tanahashi M, Matsuda T. Surface functional group dependence on apatite formation on self-assembled monolayers in a simulated body fluid. *J. Biomedical Materials Research* **1997**, 34, 305-315.

Taylor H. Towards the global elimination of Trachoma. *Nature Medicine* **1999**, 5, 572-576.

Temprano J. Keratoprosthesis with tibial autograft. KPro Abstracts: Proceedings of the first keratoprosthesis study group meeting. *Refractive and Corneal Surgery* **1993**, 9, 192-193.

Theiss F, Apelt D, Brand B, Kutter A, Zlinszky K, Bohner M, Matter S, Frei C, Auer J A, von Rechenberg B. Biocompatibility and resorption of a brushite calcium phosphate cement. *Biomaterials* **2005**, 26, 4383-4394.

Tiffany J M, Winter N, Bliss G. Tear film stability and tear surface tension. *Current Eye Research* **1989**, 8, 507-515.

Treboux G, Layrolle P, Kanzaki N, Onuma K, Ito A. Existence of Posner's cluster in vacuum. *J. Physical Chemistry A* **2000**, 104, 5111-5114

Tsuchida T, Yoshioka T, Sakuma S, Takeguchi T, Ueda W. Synthesis of biogasoline from ethanol over hydroxyapatite catalyst. *Industrial and Engineering Chemical Research* **2008**, 47, 1443-1452.

Vallet-regi M, Gonzalez-Calbet J M. Calcium phosphates as substitution of bone tissues. *Progress in Solid State Chemistry* **2004**, 32, 1-31.

van Munster E B, Winter E K, Aten J A. Measurement-based evaluation of optical pathlength distributions reconstructed from simulated differential interference contrast images. *J. Microscopy* **1998**, 191, 170-176.

Varma H K, Yokogawa Y, Espinosa F F, Kawamoto Y, Nishizawa K, Nagata F. Porous calcium phosphate coating over phosphorylated chitosan film by biomimetic methods. *Biomaterials* **1999**, 20, 879-884.

Vaughan D, Asbury T, Riordan-Eva P. In: Prentice-Hall, Editor. *General Ophthalmology, Glossary of terms relating to the eye*. Prentice-Hall International Inc., London, UK, **1995**.

Viitala R, Franklin V, Gree D, Liu C, Lloyd A, Tighe B. Towards a synthetic osteo-odonto-keratoprosthesis. *Acta Biomaterialia* **2009**, 5, 438-452.

Walsh W R, Morberg P, Yu Y, Haggard W, Sheath P C, Svehla M, Bruce W J M Response of a calcium sulfate bone graft substitute in a confined cancellous defect. *Clinical Orthopaedics and Related Research* **2003**, 406, 228-236.

Wang M, Bonfield W. Chemically coupled hydroxyapatite-polyethylene composites: Structure and properties. *Biomaterials* **2001**, 22, 1311-1320.

- Warren B E. Classic x-ray physics. In: Warren B E. Editor. *X-ray Diffraction*, General Publishing Company, New York, USA, **1990**.
- Watson P G, Young R D. Scleral structure, organisation and disease: A review. *Experimental Eye Research* **2004**, *78*, 609-623.
- Weiner S, Wagner H D. The material bone: structure-mechanical function relations. *Annual Review of Materials Science* **1998**, *28*, 271-298.
- Weng J, Liu Q, Wolke J O C, Chang X, de Groot K. Formation of characteristics of the apatite layer on plasma-sprayed hydroxyapatite coatings in simulated body fluid. *Biomaterials* **1997**, *18*, 1027-35.
- Whitcher J P, Srinivasan M, Upadhyay M P. Corneal blindness: a global perspective. *Bulletin of the World Health Organisation* **2001**, *79*, 214-221.
- White T J, Dong Z L. Structural derivation and crystal chemistry of apatites. *Acta Crystallographica Section B: Structural Science* **2003**, *B59*, 1-16.
- WHO. World Health Organisation. *Bulletin of the World Health Organisation* **2001**, *79*, 214-221.
- WHO. World Health Organisation. The World Health Report 1998: life in the 21st century, Geneva, **1998**, 47.
- Williams D F. Definitions of Biomaterials. *Progress in Biomedical Engineering*. Elsevier, Amsterdam, **1987**, 72.
- Williams D F. On the mechanisms of biocompatibility. *Biomaterials* **2008**, *29*, 2941-2953.
- Williams D F. The Williams Dictionary of Biomaterials. In: University Press Liverpool, Editor, *The Williams Dictionary of Biomaterials*. University Press, Liverpool, **1999**.
- Willmann G. Coating of implants with hydroxyapatite – material connections between bone and metal. *Advanced Engineering Materials* **1999**, *1*, 95-105.
- Wilson R M, Elliott J C, Dowker S E P, Rodriguez-Lorenzo L M. Rietveld refinements and spectroscopic studies of the structure of Ca-deficient apatite. *Biomaterials* **2005**, *26*, 1317-1327.
- Wilson R M; Elliott J C; Dowker S E P. Formate incorporation in the structure of Ca-deficient apatite: Rietveld structure refinement. *J. Solid State Chemistry* **2003**, *174*, 132-140.
- Wilson S D, Li S, Woo H, Dai P, Mook, H A, Frost C D, Komiya S, Ando Y. *Physical Review Letters* **2006**, *96*, 157001.
- Xia Z, Duan X, Locklin R M, Quijano M, Dobson R L, Triffitt J T, Ebetino F H, Russell G R. Evaluation of the relative mineral-binding affinities of clinically-relevant bisphosphonates by using hydroxyapatite-column chromatography and adsorption isotherms combined with mass spectrometric analysis. *Bone* **2008**, *42 (Supp. 1)*, S90-S91.
- Xie R Z, Stretton S, Sweeney D. Artificial Cornea: Towards a Synthetic Onlay for Correction of Refractive Error. *Bioscience Report* **2001**, *21*, 513-536.
- Yaghouti F, Dohlman C H. Innovations in keratoprosthesis: proved and unproved. *Ophthalmology Clinic* **1999**, *39*, 27-36.

Yamamoto H, Niwa S, Hori M, Hattori T, Sawai K, Aoki S, Hirano M, Takeuchi H. Mechanical strength of calcium phosphate cement *in vivo* and *in vitro*. *Biomaterials* **1998**, *19*, 1587-1591.

Yoshitake T, Kobayashi S, Ogawa T, Okuyama T. Hydroxyapatite chromatography of guanidine denatured proteins: 1. Guanidine containing phosphate buffer system. *Chromatography* **2006**, *27*, 19-26.

Yousefpour M, Afshar A, Chen J, Zhang X. Bioactive layer formation on alkaline-acid treated titanium in simulated body fluid. *Materials and Design* **2007**, *28*, 2154-2159.

Yu S, Hariram-Kithva P, Kumar R, Cheang P, Aik-Khor K. *In vitro* apatite formation and its growth kinetics on hydroxyapatite/polyetheretherketone biocomposites. *Biomaterials* **2005**, *26*, 2343-2352.

Zahn D, Hochrein O. On the composition and atomic arrangement of calcium-deficient hydroxyapatite: an *ab-initio* analysis. *J. Solid State Chemistry* **2008**, *181*, 1712-1716.

Zybin A, Koch J, Wizemann H D, Franzke J, Niemax K. Diode laser atomic absorption spectrometry. *Acta Spectrochimica* **2005**, *60 B*, 1-11.